A Numerical Flow Model Of The Taku Glacier, Alaska

Bryan R. Pearce
Liaqat Ali Khan
Mauri S. Pelto
Peter S. Sucsy
Vijay G. Panchang
Maynard Miller

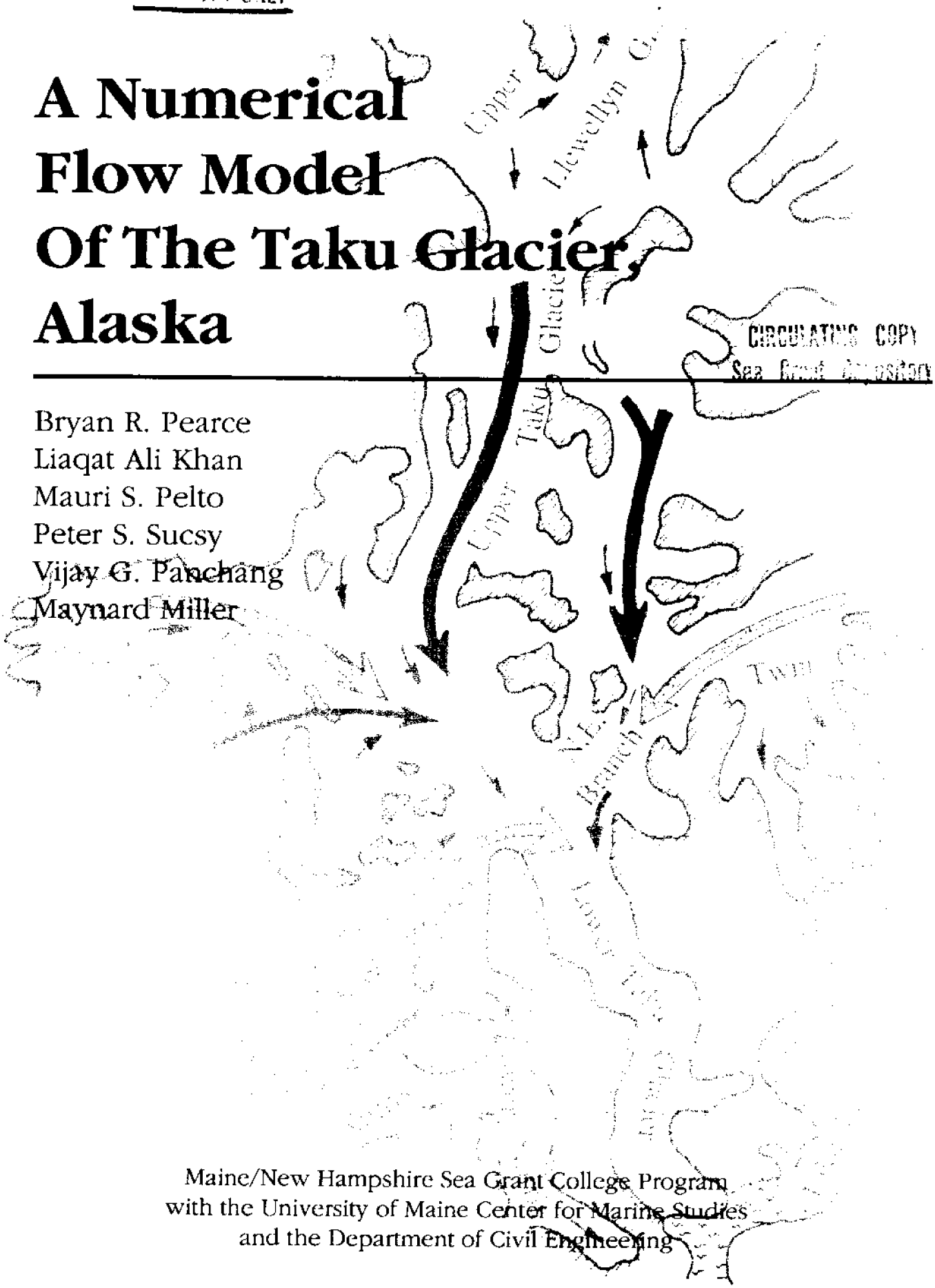

Maine/New Hampshire Sea Grant College Program
with the University of Maine Center for Marine Studies
and the Department of Civil Engineering

TR-MSG-89-1
11/89 300

Published by the Sea Grant College Program at the University of Maine under grant NA89-AA-D-SG020 from the National Sea Grant College Program, National Oceanic and Atmospheric Administration, U.S. Department of Commerce, and with support from the University of Maine's Center for Marine Studies and Department of Civil Engineering.

A NUMERICAL FLOW MODEL OF THE TAKU GLACIER, ALASKA

By

Bryan R. Pearce[1]
Liaqat Ali Khan[2]
Mauri S. Pelto[3]
Peter S. Sucsy[4]
Vijay G. Panchang[4]
Maynard M.Miller[5]

University of Maine
October, 1989

[1] Department of Civil Engineering, Sea Grant College Program, and Center for Marine Studies
University of Maine, Orono, Maine 04473
[2] School of Civil and Environmental Engineering
Cornell University, Ithaca, New York 14853.
[3] Nichols College
Dedham, Massachusetts 01570
[4] Department of Civil Engineering,
University of Maine, Orono, Maine 04473
[5] Juneau Icefield Research Program, Juneau Alaska; Foundation for Glacier and Environmental Research, Seattle, Washington 98109, and Department of Geology, Moscow, Idaho 83843.

A NUMERICAL FLOW MODEL OF THE TAKU GLACIER, ALASKA

A three-dimensional, time-dependent flow model for glaciers has been developed in this study. The starting point of this modelling effort is the hydrodynamic model by Pearce and Cooper (1981). The stability criteria of that hydrodynamic model prevented its application to a highly damped and viscous system, such as glaciers and ice sheets. A partial time centering of velocity in the conventional time-split finite difference scheme of Pearce and Cooper (1981) circumvents this stability problem. An algorithm for the advance and retreat of the terminus has been developed to simulate the response of glaciers to climatic perturbations.

To study the simulation characteristics of this model, numerical experiments were performed. The first experiment compares the computed steady-state surface profile with an analytical solution of Paterson (1972). In the second experiment the vertical velocity profile is compared with an analytical solution of Nye (1965). Kinematic wave propagation in a channel is studied in the third simulation. The final experiment consists of studying the response of a test glacier to sudden increase in surface elevation by 1.0 m and change in mass balance by 0.1 m/year. As a simple application, the model is then applied to the Fedchenko Glacier, Soviet Union to obtain an analysis of the stress gradient terms (Budd,1970).

Kuhn's algorithm (Kuhn, 1979) based on the energy balance at the equilibrium line has been used to incorporate the influence of global warming on the glacier. The analysis indicates that the altitude of the equilibrium line of the Taku Glacier moves up by about 61.0 m per °C rise in temperature. This shift could be off-set, by about 19.0 m, by an increase of accumulation rate of 100 kg/m^2.

As a practical application, the model is applied to the Taku Glacier, south-east Alaska. The model is calibrated by adjusting the friction coefficient and viscosity to reproduce a) surface velocities, b) relative values of bed sliding, and c) the rate of rise of the glacier surface. The model is then used to simulate the flow characteristics of the Taku Glacier, for the present climatic conditions, over a period of 500 years. The glacier appears to approach a steady state in about 450 years.

The glacier terminus continues advancing, for the present climatic conditions, in the next 300 years with an average rate of 20 m/year, and it completely blocks the Taku Inlet. When climatic warming of 2.5 °C per hundred years is assumed, the advance of the Taku Glacier is arrested in about 50 years and it starts retreating in about 100 years. The current global warming scenarios indicate that the terminus of the Taku Glacier will not block the Taku Inlet.

ACKNOWLEDGEMENTS

The research was supported in part by the following organizations: University of Maine, Center for Marine Studies; the Maine Sea Grant College Program, Grant No. NA86AA-D-SG047; the Juneau Icefield Research Program; and the Foundation for Glacier and Environmental Research, Seattle, Washington.

We appreciate the help of Professor Terence J. Hughes, Department of Geological Sciences and Institute of Quaternary Studies and Prof. James L. Fastook, Department of Computer Science for reviewing the manuscript and for offering helpful suggestions.

Dr. K. Blachnitzky, Dr. N. Kersting, and Dr. W. Welsch of Geodetic Institute, University of the Bundeswehr, Neubiberg, F.R.G kindly provided velocity data used in the model comparisons. This report is dedicated to the memory of Dr. Blachnitzky, who died accidently on the icefield during the 1988 season and who will be remembered by us all.

TABLE OF CONTENTS

LIST OF SYMBOLS

A	..Hardness parameter in Glen's flow law
a_I	..Slip angle
c	..Surface wave velocity
$c_b(x,y)$	..Coefficient of bed friction
$c_I(x,y,t)$	..Velocity parameter in x-direction
c_o	..Surface wave velocity in datum state
c_p	..Specific heat of air at constant pressure
$D(x,y,t)$	..Depth of flow
D_o	..Ice thickness at the head of ice sheet
$d_I(x,y,t)$	..Velocity parameter in y-direction
G	..Deviator stress gradient
g	..gravitational acceleration
$H(x,y)$	..Elevation of glacier bed
H_s	..Sensible heat flux
h	..elevation of the equilibrium line
i	..Grid counter in x-direction
j	..Grid counter in y-direction
k	..Counter for time
L	..Half length of ice sheet
m	..Friction law exponent
N	..Number of cosine terms in trial function
n	..Visco-plastic parameter in Glen's Flow Law
R	..Net radiation for atmosphere
R_o	..Long wavedown ward radiation
T	..Variational stress gradient
T_a	..Air temperature
T_s	..Temperature of ice surface
t	..Time
N_H	..Viscosity of fluid in the horizontal

N_V	..Viscosity of fluid in the vertical
Q_x	..Flux in x-direction
Q_y	..Flux in y-direction
$S(x,y)$	..Source or sink term (accumulation or ablation)
S^+	..Mean accumulation rate
S^-	..Mean ablation rate
$U(x,y,t)$	..Vertically averaged x-component of horizontal velocity
U_*	..Friction Velocity
U_w	..Wind velocity
$u(x,y,z,t)$	..Horizontal velocity in x-direction
$u'(x,y,z,t)$	..Galerkin trial function corresponding to u
$u_b(x,y,t)$	..Bed velocity in x-direction
u_s	..Surface velocity in x-direction
$V(x,y,t)$	..Vertically averaged y-component of horizontal velocity
v	..Horizontal velocity in y-direction
$v'(x,y,y,t)$	..Galerkin trial function corresponding to v
$v_b(x,y,t)$	..Bed velocity in y-direction
x	..x-coordinate
y	..y-coordinate
z	..z-coordinate
z_a	..height at which air velocity is measured
z_o	..Surface roughness height
α	..Surface slope
β	..Model parameter
Γ	..Number of ablation days
ε	..Strain
η	..Surface elevation
θ	..Angle
κ	..von-Karman's constant
λ	..Courent number
μ	..Bulk heat transfer coefficient
μ'	..Radiative heat transfer coefficient
ν	..Relative emissivity
Π	..Latent heat of melting of ice

ρ	..Density of ice/air
σ	..Transformed z-coordinate
τ	..Stress
τ_{bx}	..Bed shear stress in x-direction
τ_{by}	..Bed shear stress in y-direction
ϕ	..Atmospheric stability function
φ	..Stefan-Boltzman constant
Ω	..Amplification matrix
ω	..Amplification factor
ϑ	..Volume of cell

LIST OF FIGURES

LIST OF TABLES

1. INTRODUCTION

1.1.0 INTRODUCTION

The National Research Council (1983) listed one high priority that is pertinent to this project: "To identify the regional meteorology and mass exchange of the high mountains bordering the Gulf of Alaska, the result of energy and mass balance studies on mountain glaciers needs to be extended to whole ice-clad mountain ranges". A second high priority to be partially addressed by this research project was stated by the National Science Foundation, Department of Energy, and National Academy of Sciences: "To determine the contribution of Coast Range Alaskan glaciers to global sea level". It has been demonstrated that Alaskan Coast Range glaciers are the primary alpine glacier system contributing meltwater to global oceans (Meier, 1984).

The recent apparent rise in global sea level has been attributed to thermal expansion of sea water and volume loss of alpine glaciers (Barnett, 1983; Meier, 1984). The Coast Range Alaskan glacier system, bordering the Gulf of Alaska, accounts for roughly a third of the total loss in global alpine glacier volume (Meier, 1984). Though the true change of sea level is in doubt, it is evident that Coast Range glaciers lost sufficient volume to raise global sea level by 14 to 19 mm since 1890 (Meier, 1984; Pelto, 1987). Because the average coastal gradient is 1 in 80, this represents an average encroachment by global seas of 1.5 m in the past century, in the absence of other factors. The contribution of Alaskan glaciers to global sea level has not been constant during the past century (Meier, 1984; Miller, 1985). Changes in glacier contribution to sea level have been caused by short-term climatic fluctuations, and by the adjustment of glaciers to the present climate ice regime (Pelto, 1987). It has been postulated that a CO_2-induced climatic warming will cause further extensive retreat of glaciers and ice sheets

(Meier, 1984). Four different projections for the Coast Range region indicate a 3 to 6 °C rise in mean annual temperature (Schlessinger and Mitchell, 1985). What will the effect of this climatic change be on Coast Range glaciers? Could Coast Range glaciers contribute enough water to raise global sea level 25 to 75 mm in the next century, as suggested by Meier (1984)?

In 1982 the Foundation for Glacier and Environmental Research began the North Cascade Glacier-Climate Project. Directed by Dr. Mauri Pelto the goal of this program has been to establish a system for monitoring the mass balance and terminus activity of numerous North Cascade, Washington and Coast Range, Alaskan glaciers. A system is now in place for monitoring the annual balance and terminus activity of forty-seven North Cascade (Pelto, 1987, 1988) and sixty Coast Range glaciers (Pelto, 1987). The next major task is to develop a model that can accurately simulate the behavior of Coast Range glaciers, enabling their future behavior to be predicted, based on mass balance observations.

The Coast Range of southeast Alaska and adjacent British Columbia contains 88,000 km^2 of glacial ice. There are 750 Coast Range glaciers with an area exceeding 15 km^2 comprising 98% of the total Coast Range glacier area. Because of the large size of Coast Range glaciers, the complete response to a mass balance change ranges from several decades to several centuries. For this reason, to successfully model a Coast Range glacier, a long record of mass balance and accompanying velocity fluctuations is required. The Taku Glacier has a sufficiently detailed and lengthy record to be used in a time dependent modeling study. The available data allow estimates of mean annual mass balance at any given point on the glacier to within ±10% (Miller, 1963; Pelto, 1987). Surface elevation is available from USGS topographic maps with an accuracy of ±3m. Bedrock elevation is based on seismic and gravimmetric profiles across the glacier (Prather, 1971; Carlson, 1987).

1.2.0 OBJECTIVES OF THE STUDY

A three-dimensional unsteady free-surface model was developed by Cooper and Pearce(1979), Pearce and Cooper(1981), and Sucsy and Pearce(1986). The model can compute the vertical velocity variation in coastal waters. The characteristics of the fluid are parametarized as viscosity. Considering the similarity of vertical velocity profiles in coastal waters and glaciers, it was recognized that this model could be used for simulating the dynamic characteristics of glaciers. The model constructed by Pearce and Cooper(1981) and further developed by Sucsy and Pearce(1986) is an explicit numerical model, and its computational time step is restricted by two stability criteria. The first is called the Courant condition, which is the usual stability condition for explicit models (Abbott, 1979 and Smith 1979). Because of the particular three-dimensional formulation of this model, a second stability criteria arises. According to the second criterion, the time step is inversely proportional to the kinematic viscosity of the fluid (Pearce and Cooper, 1981). Kinematic viscosity of glacial ice (Ambach and Eisner, 1983) varies from 7.4×10^9 to 15.9×10^9 m^2/s, and the computational time step practically approaches zero for such a viscous fluid. Therefore, appropriate changes in the solution technique were made so that the model could be applied to glaciers.

The primary objectives of this project are as follows:

1. To develop a three-dimensional, time-dependent flow model for temperate glaciers by making appropriate changes in the hydrodynamic model developed by Pearce and Cooper(1981).

2. To ascertain the validity of the model formulation by performing numerical experiments and comparing the model results with analytical solutions.

3. To apply Kuhn's(1981) algorithm to compute the altitudinal shift of the equilibrium line of the Taku Glacier and redistribution of mass balance.

4.To apply the model to the Taku Glacier, calibrate the model with the available field data and study its flow characteristics.

5.To study the response of the Taku Glacier to mass balance perturbations caused by climatic warming.

1.3.0 JUSTIFICATION OF THE STUDY

In the last decade many time-dependent glacier flow models have been developed. Rasmussen and Campbell(1973) and Colebeck and Evans(1973) pointed out that for the effective stresses found in temperate glaciers the Newtonian viscous law was a good approximation to the Glen's flow law for ice (which treats ice as a visco-plastic material). A recent study by Wolff and Doake(1986) also showed the validity of this approximation to the polar ice sheets. As the present model is being primarily developed for the temperate Taku Glacier, it is expected that hydrodynamic models, based on a linear flow law, could be successfully adapted for glaciers. The model is three-dimensional in the sense that vertical variations of horizontal velocity components are computed. Unlike some of the well known models (Budd and Smith, 1982; Budd et al. 1984, Mahaffy, 1976) which can only be applied when basal sliding is small, this model is capable of simulating flows with both very large and very small or no basal sliding. Until now, no three-dimensional "unsteady" flow model for glaciers has been developed. Some of the authors, however, have called their models three-dimensional, even though both the continuity and momentum equations are vertically integrated, thereby eliminating the vertical variations of the flow parameters (Rasmussen and Campbell, 1973; Mahaffy, 1976; Budd and Smith 1982). The model developed in the present study computes velocity as a function of three space dimensions and time, rather than using vertically integrated momentum equations. Thus, this model is probably one of the first three-dimensional models for glaciers and ice sheets. Conceptually, the model can be considered as a combination of two-dimensional flow-line models and models that are two-dimensional in the horizontal plane. Therefore, the development and successful application of the

model to temperate glaciers will represent an important advancement in the development of numerical models for glaciers.

The Taku Glacier is a large and a dynamic temperate glacier in the Juneau Ice field. Though a fairly large volumes of field data has been collected in the last forty years, no numerical model has been tested and applied to it. Therefore, this study will represent a first attempt to study the dynamics of the Taku Glacier with a numerical model. The model will provide information about the spatial and temporal variations of surface profile, ice thickness, vertical and horizontal velocities, advance and retreat of the terminus, as well as the effects of climatic changes on the growth and recession of the glacier. Consequently, this modelling effort may be of help in the planning and management of the ice field, and determining the feasibility of engineering constructions in the adjoining areas. Of particular interest is the proposal by the Alaskan Department of Highways to construct a road just south of the terminus of the Taku Glacier.

1.4.0 OUTLINE OF THE REPORT

This report describes the model development, its applications to simplified cases and to the Taku Glacier. The description of the model is presented in Chapter-2. That chapter also includes a stability analysis for the model. Numerical experiments carried out to ascertain the validity of the model formulation, by comparing with analytical solutions, are described in Chapter-3. Chapter-4 outlines the implications of climatic warming on glaciers and Kuhn's algorithm for the determination of the altitudinal shift of the equilibrium line, so that time dependent mass balance distribution can be estimated. The topographic and meteorological information necessary for the model application are presented in Chapter-5. The application of the model to the Taku Glacier, which includes model calibration and validation, simulation of steady state configurations and flow characteristics, advance/ retreat of glaciers, and response of the glacier to climatic warming, are presented in Chapter-6. The discussions of results are presented in Chapter-7. Finally, a summary of the study and conclusions are presented in Chapter-8.

2. DESCRIPTION OF THE MODEL

2.1.0 INTRODUCTION

Numerical models are tools for simulating physical (or other) processes and they are becoming more sophisticated as both computers and our ability to use them become more sophisticated. These simulations are by nature compromises. The model described below is developed to provide a reasonable solution to the problem of calculating a three-dimensional glacier flow efficiently. To model temperate glaciers in three-spatial dimensions it is assumed that ice can be treated as a highly viscous Newtonian fluid and a linear friction law can be applied at the ice-bed interface. Conventionally, ice is treated in flow models as a visco-plastic material (Paterson, 1980) and the relationship between stress and ice deformation is given by Glen's law, which can be written as:

$$\varepsilon'_{i,j} = A\,\tau^{n-1}\,\tau_{i,j} \qquad (2.1)$$

where $\varepsilon'_{i,j}$ is strain rate component corresponding to the shear stress $\tau_{i,j}$, τ is the effective stress, n is the flow law constant and A is a constant depending on the properties of ice and its temperature. A frequently used value of n is 3. For n=1 this relation represents Newton's law of viscosity. Creep data from laboratory experiments on ice and from field measurements on glaciers point to a gradual change from n=1 for $\tau < 10$ kPa to n=3 for 10 kPa $< \tau <$ 100 kPa, and $n > 3$ for $\tau >$ 100 kPa (Weertman, 1983). Field measurements in temperate glaciers (Colbeck and Evans, 1973) suggests that at the stresses normally found in temperate glaciers, the Newtonian viscous approximation (n= 1) for ice flow is quite

reasonable. For the power law type flow law, Colbeck and Evans(1973) found that n = 1.30 for Blue glacier, Washington. Analysis of data from polar ice sheets by Doake and Wolff(1985) shows that n varied from 0.8 to 1.04 and that n = 1 provides a better simulation of horizontal velocity, while n = 3 gives better results for vertical velocity (Doake and Wolff, 1986). If changes in τ are comparable to the average value of τ over the time span when ϵ' is being measured, ice deforms in regimens of transient creep. Under these conditions, n = 1 gives a better fit than n = 3 to creep data (Weertman, 1985).

The numerical model developed in this study is based on the Navier-Stoke's equations of motion together with the depth-averaged continuity equation. The model uses a functional expansion of horizontal velocities to compute the vertical variation of horizontal velocity without requiring a three-dimensional grid system. The vertical velocity is however, neglected. The Galerkin technique is used to solve the momentum equations. A σ-transform of the vertical coordinate is also made to simplify the integrations that arise from the Galerkin technique. The transformed residual equations are solved by using a "split-time" finite-difference method. The time step of the three-dimensional hydrodynamic model is governed by two stability criteria:

$$\Delta t \leq \frac{\Delta x}{\sqrt{2g\,D}} \tag{2.2a}$$

$$\Delta t \leq \frac{2\,D^2}{N_v\,a_j^2} \tag{2.2b}$$

where

$D(x,y,t)$ is the total depth of flow,
g is the gravitational acceleration,
N_V is the vertical viscosity,
a_J is a model parameter defined later.

Equation(2.2a) is the Courant stability condition applicable to explicit hydrodynamic models and is based on linearized equations that neglect frictional effects. For Δx = 1000 m, and D= 400 m, equation(2.2a) gives $\Delta t \leq 10$ s. The velocity of flow in the Taku Glacier is of the order of 1.0 m/d. Even simulation of glacier dynamics with time steps of hours is considered impractical. Due to the particular formulation of the model, the second stability criterion, equation(2.2b), arises. Viscosity of water is small, so that the first stability criterion governs the model application to coastal waters. The kinematic viscosity of ice in temperate glaciers varies from 7.4 to 15.9 $x10^9$ m^2/s (Ambach and Eisner, 1983). Therefore, the second stability criterion implies unrealistically small Δt. The velocity of flow in glaciers is small compared to the flow of water in a channel. Consequently, numerical simulations over decades or centuries are necessary to observe significant changes.

To circumvent these stability criteria, various numerical schemes were applied so that larger time steps could be used for long term simulation of glaciers. This chapter describes the model and the numerical solution procedure.

2.2.0 MATHEMATICAL MODEL

2.2.1 *Governing Equations*

For constant density the continuity equation can be written as follows (Pearce and Cooper 1981; Cooper and Pearce, 1977; Sucsy and Pearce 1986):

$$\frac{\partial \eta}{\partial t} + \frac{\partial (UD)}{\partial x} + \frac{\partial (VD)}{\partial y} = S \qquad (2.3)$$

where:

$\eta(x,y,t)$ is the surface elevation of the glacier,

$U(x,y,t)$ is the vertically-averaged x-component of the horizontal

velocity,

V(x,y,t) is the vertically-averaged y-components of the horizontal velocity,

S(x,y,t) is source or sink term (accumulation and ablation).

For a linear flow law, the momentum equations correspond to the Navier-Stokes's equations of motion. These equations are:

$$\frac{\partial u}{\partial t} + u\frac{\partial u}{\partial x} + v\frac{\partial u}{\partial y} = -g\frac{\partial \eta}{\partial x} + N_H\left[\frac{\partial^2 u}{\partial x^2} + \frac{\partial^2 u}{\partial y^2}\right] + N_V\left[\frac{\partial^2 u}{\partial z^2}\right] \qquad (2.4a)$$

$$\frac{\partial v}{\partial t} + u\frac{\partial v}{\partial x} + v\frac{\partial v}{\partial y} = -g\frac{\partial \eta}{\partial y} + N_H\left[\frac{\partial^2 v}{\partial x^2} + \frac{\partial^2 v}{\partial y^2}\right] + N_V\left[\frac{\partial^2 v}{\partial z^2}\right] \qquad (2.4b)$$

where:

u(x,y,z,t) is the horizontal velocity along the x axis,
v(x,y,z,t) is the horizontal velocity along the y axis,
N_H is the horizontal viscosity.

Figure 2.1 shows the coordinate system used for these equation and the definition of the variables. In equations(2.4) the vertical pressure distribution is assumed hydrostatic and treats ice mass as a Newtonian viscous fluid. In doing so, ice is considered a homogeneous continuum and ignores phenomena such as formation of crevasses, etc.

In the present formulation of the model, the advective terms in the momentum equations have been neglected because these terms are very small. The local

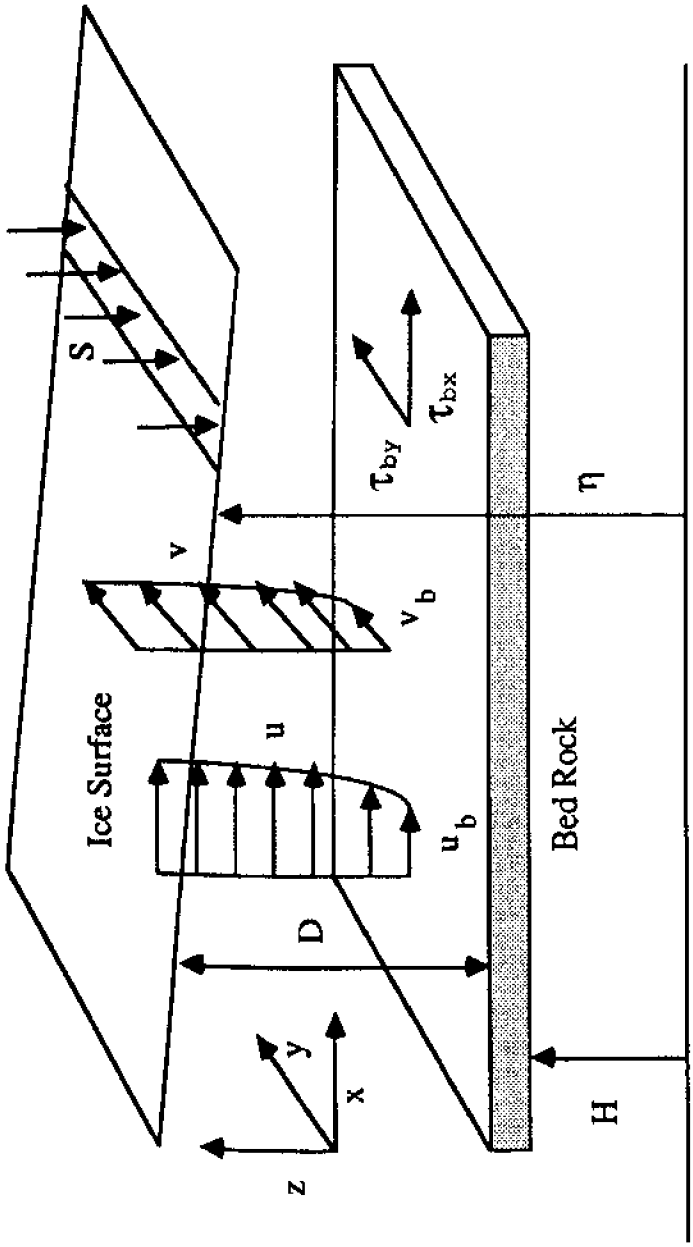

Fig. 2.1: Coordinate System and Definition of Variables

acceleration terms are also small. However, they are retained in this model purely for numerical convenience. This makes the model hyperbolic in nature. Most of the glacier flow models are elliptic (Paterson, 1980; and Hutter, 1983).

2.2.2 Surface and Bed Boundary Conditions

In addition to the governing equations boundary conditions are needed to describe the system. The boundary conditions applicable to the surface and bed are:

$$\frac{\partial u}{\partial z} = 0 \text{ at } z = \eta \tag{2.5a}$$

$$\frac{\partial v}{\partial z} = 0 \text{ at } z = \eta \tag{2.5b}$$

$$\tau_{bx} = -\rho N_V \left[\frac{\partial u}{\partial z}\right] \text{ at } z = H \tag{2.6a}$$

$$\tau_{by} = -\rho N_V \left[\frac{\partial v}{\partial z}\right] \text{ at } z = H \tag{2.6b}$$

where:

H is the glacier bed elevation,
ρ is density of ice,
τ_{bx} is the x-component of bed friction shear stress, and
τ_{by} is the y-component of bed friction shear stress.

Equations(2.5) imply zero shear stress at the ice surface. Assuming that the bed friction varies linearly with the magnitude of the velocity of glacier at bed, τ_{bx} and τ_{by} can be expressed as:

$$\tau_{bx} = -c_b \rho u_b \tag{2.7a}$$

$$\tau_{by} = -c_b \rho v_b \tag{2.7b}$$

where:

c_b is a coefficient of bottom friction,

u_b is the x-component of bed velocity, and

v_b is the y-components of bed velocity.

These equations are obtained by balancing the gravitational force causing the motion of a column of ice to the bed traction opposing the flow under steady state. The model assumes linear friction by taking c_b as constant. Equating τ_{bx} from equations(2.6a) and (2.7a) and τ_{by} from equations(2.6b) and (2.7b) give the following expression for the bed boundary conditions:

$$\frac{\partial u}{\partial z} = \frac{c_b u_b}{N_V} \text{ at } z = H \tag{2.8a}$$

$$\frac{\partial v}{\partial z} = \frac{c_b v_b}{N_V} \text{ at } z = H \tag{2.8b}$$

2.2.3 No-Flow Boundary Condition

Additional boundary conditions are needed at the physical boundaries of the glacier. The no flow boundary condition is applicable where the flow is obstructed by a physical barrier, such as mountains protruding through ice or ice divides created by bed topography and can be expressed as follows:

$$\frac{\partial u}{\partial x} = 0 \qquad (2.9a)$$

$$\frac{\partial v}{\partial y} = 0 \qquad (2.9b)$$

In applying the no-flow boundary condition the location of the flow divide line is assumed to be invariant in time.

2.2.4 Moving Boundary Condition at the Terminus

The boundary condition, applicable at the terminus of the glacier, can be called moving boundary conditions because the terminus is not stationary in time. The configuration of the terminus depends on the supply of ice from the accumulation area, ablation rate, topography of the bed and the physical characteristics of ice (Paterson, 1981). However, no adequate theory has been developed to date for flow of ice in the neighborhood of the the leading edge of the terminus (Hutter, 1983). The fact that the geometry of the terminus depends on the dynamics of the glacier complicates the solution of the flow equations. However, proper specification of this boundary condition is crucial for the simulation of the response and the areal extent of the glacier to climatic perturbations. Nye(1960) first introduced the concept of the "wedge type" boundary condition for simulating the advance/ retreat of terminus of glaciers. Figure 2.2 schematically illustrates the concept of this type of boundary condition. The advance or retreat of the terminus is computed by conserving mass and assuming the depth and flux of ice at the leading edge of the terminus are zero. Subsequent models (Budd and Jenssen, 1975; Bindschadler, 1982) have used the same concept with varying modifications. A two-dimensional version of this concept have been used by Rasmussen and Campbell(1973).

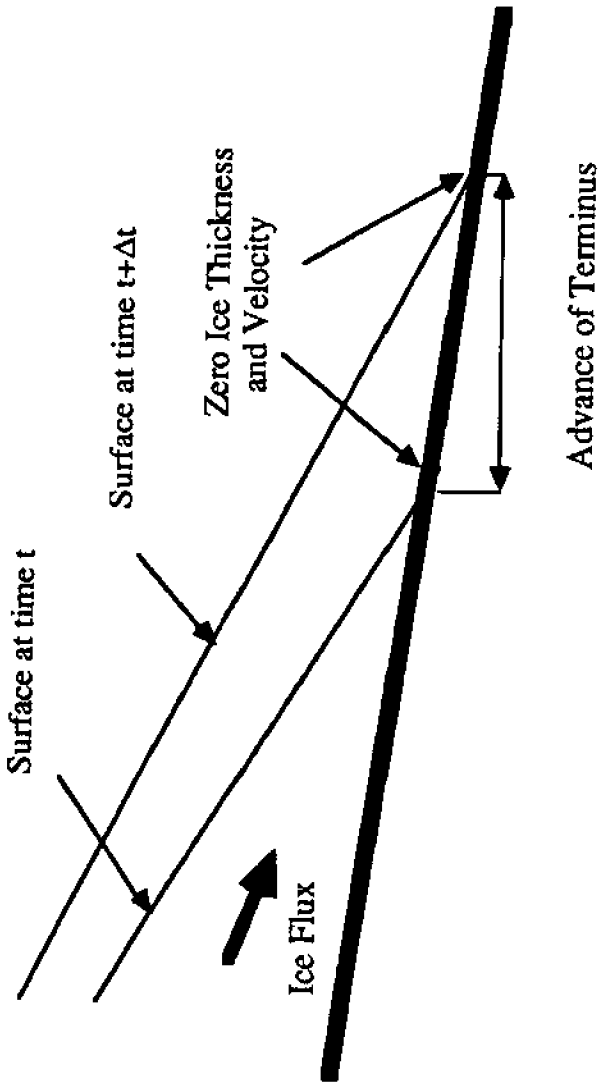

Fig. 2.2: Wedge-Type Moving Boundary Condition

The assumption of zero ice depth is not applicable to the Taku Glacier because the ice thickness of the leading edge of the terminus varies from 200 to 300 m. Therefore, different algorithms for moving boundary conditions were studied. It appears that a boundary condition, similar to the radiation boundary conditions used in hydrodynamics, gives reasonable simulation with non-zero depth and velocity at the terminus. The formulation is such that as the glacier reaches steady state (ablation rate and vertical motion of the terminus cancel one another) the depth of ice approaches zero, similar to the boundary condition generally used in glacier dynamics.

The moving boundary conditions used in this model can be expressed as follows:

$$\left(\frac{\partial \eta}{\partial x}\right)_L = \left(\frac{\partial \eta}{\partial x}\right)_{L-1} \tag{2.10a}$$

$$\left(\frac{\partial \eta}{\partial y}\right)_M = \left(\frac{\partial \eta}{\partial y}\right)_{M-1} \tag{2.10b}$$

where L represents computational grid point in the x-direction at the leading edge of the terminus. Figure 2.3 shows the concept of the moving boundary condition in the x-direction. A consequence of this boundary condition is that mass is allowed to flow into or out of the glacier. Mass is conserved by adding a fictitious grid element until an entire element is either created (advance) or removed (retreat). In integral form this condition can be expressed as:

$$\int_{t_o}^{t} Q_x \, dt \geq \vartheta, \text{ glacier advances in x-direction} \tag{2.11a}$$

$$\int_{t_o}^{t} Q_x \, dt \leq \vartheta, \text{ glacier retreats in x-direction} \tag{2.11b}$$

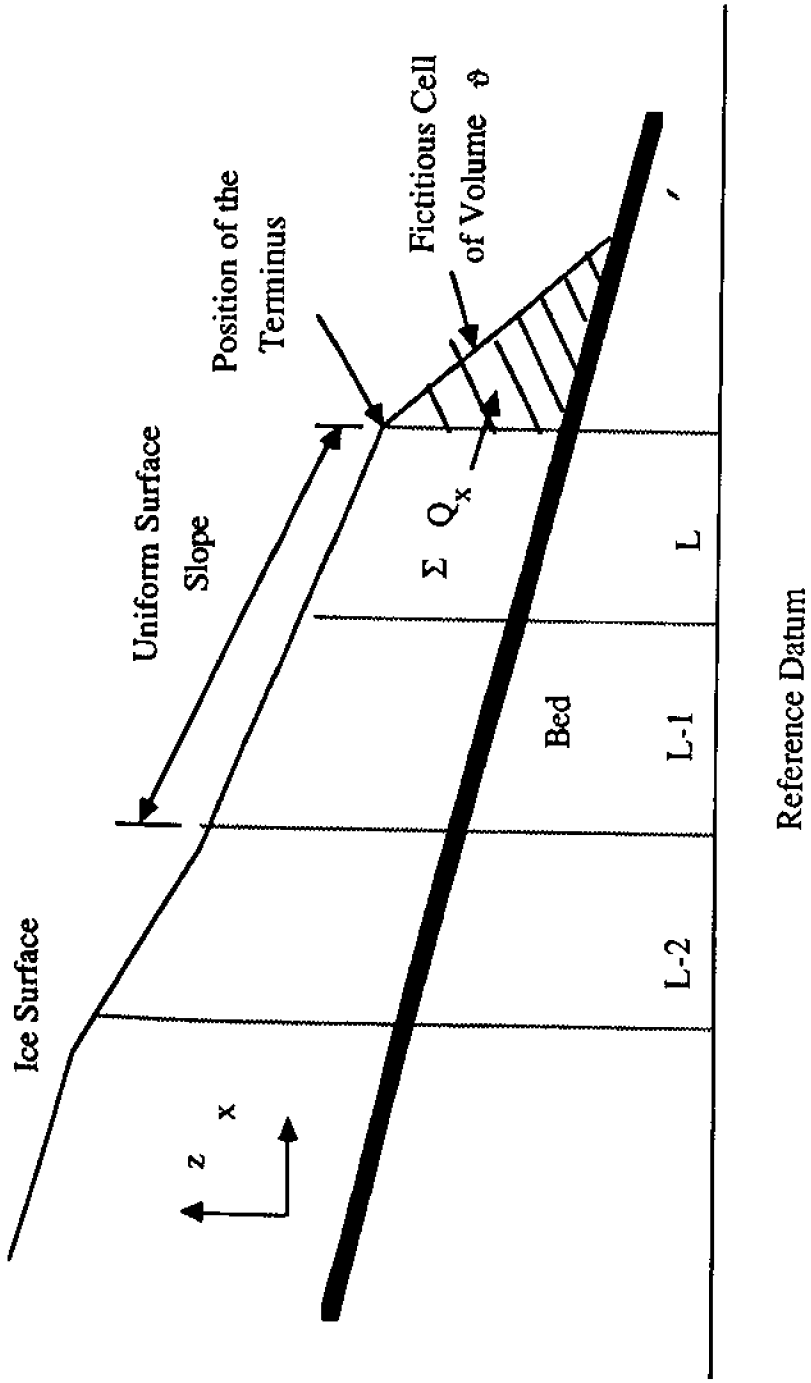
Ice Surface
Uniform Surface Slope
Position of the Terminus
Fictitious Cell of Volume
ΣQ_x
Bed
L
L-1
L-2
z
x
Reference Datum

$$\int_{t_o}^{t} Q_y \, dt \geq \vartheta, \text{ glacier advances in y-direction} \qquad (2.12a)$$

$$\int_{t_o}^{t} Q_y \, dt \leq \vartheta, \text{ glacier retreats in y-direction} \qquad (2.12b)$$

where Q_x is the rate at which mass is flowing into or out of the glacier at the L-th computational cell, t_o is the time at the last time step at which $| Q_x | = 0$, t represents the time over which the integration is performed and, ϑ is the volume of the computational cell to which the glacier will advance or retreat. The volume of the hypothetical cell ϑ is a function of ice thickness at the last computational cell, the bed topography and the grid size. Application of this boundary condition gives a non-zero velocity, i.e. mass flux, at the leading edge of the terminus, and the ice thickness is determined by the supply of ice from the accumulation region.

2.3.0 INITIAL CONDITIONS

To start the computations, initial surface topography and velocity at each computational point are necessary. In the present formulation of the model, initial surface topography is specified and velocity is assumed zero throughout the model domain. Thus these initial conditions can be written as follows:

$$\eta(x,y,t) = \eta_0(x,y) \quad \text{at } t=0 \qquad (2.13a)$$

$$u(x,y,x,t) = 0 \quad \text{at } t=0 \qquad (2.13b)$$

$$v(x,y,z,t) = 0 \quad \text{at } t=0 \qquad (2.13c)$$

As the continuity and momentum equations constitute a system of hyperbolic equations the effects of the assumed initial conditions disappear as the computation advances in time (Smith,1978 and Abbott, 1979).

2.4.0 THE σ-TRANSFORMATION

A transformation of the vertical axis from the interval [H,η] to [0,2] is made to simplify the evaluation of integrals resulting from the application of the Galerkin technique. The Galerkin technique necessitates evaluating single-dimension definite integrals over the entire depth of the glacier with respect to the vertical coordinate. Since the free surface η varies in space and time the integrals would need to be re-evaluated each time η changes significantly. The transformation to a vertical coordinate of domain [0,2] makes it possible to evaluate the integrals in terms of the other model parameters. This transformation is defined by Sucsy and Pearce(1986):

$$\sigma = 2 - \frac{2(\eta - z)}{H+\eta} \qquad (2.14)$$

The transformation is such that the surface and the bed of glacier are fixed at $\sigma = 0$ and $\sigma = 2$ respectively in the transformed coordinate system. This transformation also helps in applying the surface boundary conditions given by equations(2.5). To apply these boundary conditions it is necessary to know the location of the surface, which is not known a priori, as it is a part of the solution process. As the surface is fixed at $\sigma = 2$ in the transformed equations, boundary conditions can thus be applied without actually knowing the location of surface.

2.4.1 Transformation of the Differentials

Let (x', y', z', t') be the old coordinate system and (x, y, σ, t) be the transformed coordinate system. Then the relationships between the first order differentials in the two system can be expressed as follows:

$$\frac{\partial}{\partial x'} = \frac{\partial}{\partial x} + \frac{\partial \sigma}{\partial x}\frac{\partial}{\partial \sigma} \tag{2.15a}$$

$$\frac{\partial}{\partial y'} = \frac{\partial}{\partial y} + \frac{\partial \sigma}{\partial y}\frac{\partial}{\partial \sigma} \tag{2.15b}$$

$$\frac{\partial}{\partial z'} = \frac{\partial \sigma}{\partial z}\frac{\partial}{\partial \sigma} \tag{2.15c}$$

$$\frac{\partial}{\partial t'} = \frac{\partial}{\partial t} + \frac{\partial \sigma}{\partial t}\frac{\partial}{\partial \sigma} \tag{2.15d}$$

Substituting the appropriate differentials of σ from equation(2.14) into equations(2.15) gives the final expressions for transforming the differentials in the (x', y', z', t') to the (x, y, σ, t) coordinate system. These are as follows:

$$\frac{\partial}{\partial x'} = \frac{\partial}{\partial x} + \Gamma_x \frac{\partial}{\partial \sigma} \tag{2.16a}$$

$$\frac{\partial}{\partial y'} = \frac{\partial}{\partial y} + \Gamma_y \frac{\partial}{\partial \sigma} \tag{2.16b}$$

$$\frac{\partial}{\partial z'} = \frac{2}{D}\frac{\partial}{\partial \sigma} \tag{2.16c}$$

$$\frac{\partial}{\partial t'} = \frac{\partial}{\partial t} - \frac{\sigma}{D}\frac{\partial \eta}{\partial t}\frac{\partial}{\partial \sigma} \tag{2.16d}$$

$$\frac{\partial^2}{\partial x'^2} = \frac{\partial^2}{\partial x^2} + \frac{\partial^2 \sigma}{\partial x^2}\frac{\partial}{\partial \sigma} + 2\frac{\partial \sigma}{\partial x}\frac{\partial^2}{\partial x \partial \sigma} + \frac{\partial \sigma}{\partial x}\frac{\partial^2 \sigma}{\partial x \partial \sigma}\frac{\partial}{\partial \sigma} + \left[\frac{\partial \sigma}{\partial x}\right]^2 \frac{\partial^2}{\partial \sigma^2} \tag{2.16e}$$

$$\frac{\partial^2}{\partial y'^2} = \frac{\partial^2}{\partial y^2} + \frac{\partial^2 \sigma}{\partial y^2}\frac{\partial}{\partial \sigma} + 2\frac{\partial \sigma}{\partial y}\frac{\partial^2}{\partial y \partial \sigma} + \frac{\partial \sigma}{\partial y}\frac{\partial^2 \sigma}{\partial y \partial \sigma}\frac{\partial}{\partial \sigma} + \left[\frac{\partial \sigma}{\partial y}\right]^2 \frac{\partial^2}{\partial \sigma^2} \tag{2.16f}$$

$$\frac{\partial^2}{\partial z'^2} = \frac{4}{D^2}\frac{\partial^2}{\partial \sigma^2} \tag{2.16g}$$

where

$$\Gamma_x = \frac{\partial \sigma}{\partial x} = \frac{1}{D}\left[(2-\sigma)\frac{\partial H}{\partial x} - \sigma\frac{\partial \eta}{\partial x}\right] \tag{2.17a}$$

$$\Gamma_y = \frac{\partial \sigma}{\partial y} = \frac{1}{D}\left[(2-\sigma)\frac{\partial H}{\partial y} - \sigma\frac{\partial \eta}{\partial y}\right] \tag{2.17b}$$

where $D = \eta - H$, the total depth of flow.

2.4.2 Momentum Equations

Replacing the differentials in the momentum equations with the appropriate transformed differentials gives the following form of momentum equations in the new coordinate system:

$$\frac{\partial u}{\partial t}+\frac{\sigma}{D}\frac{\partial \eta}{\partial t}\frac{\partial u}{\partial \sigma}+u\left[\frac{\partial u}{\partial x}+\Gamma_x\frac{\partial u}{\partial \sigma}\right]+v\left[\frac{\partial u}{\partial y}+\Gamma_y\frac{\partial u}{\partial \sigma}\right]= \tag{2.18a}$$

$$-g\frac{\partial \eta}{\partial x}+N_H\left[\frac{\partial^2 u}{\partial x^2}+\frac{\partial u}{\partial \sigma}\frac{\partial^2 \sigma}{\partial x^2}+2\frac{\partial \sigma}{\partial x}\frac{\partial^2 u}{\partial \sigma \partial x}+\frac{\partial u}{\partial \sigma}\frac{\partial^2 \sigma}{\partial \sigma \partial x}\frac{\partial \sigma}{\partial x}+\left(\frac{\partial \sigma}{\partial x}\right)^2\frac{\partial^2 u}{\partial \sigma^2}\right]$$

$$+N_H\left[\frac{\partial^2 u}{\partial y^2}+\frac{\partial u}{\partial \sigma}\frac{\partial^2 \sigma}{\partial y^2}+2\frac{\partial \sigma}{\partial y}\frac{\partial^2 u}{\partial \sigma \partial y}+\frac{\partial u}{\partial \sigma}\frac{\partial^2 \sigma}{\partial \sigma \partial y}\frac{\partial \sigma}{\partial y}+\left(\frac{\partial \sigma}{\partial y}\right)^2\frac{\partial^2 u}{\partial \sigma^2}\right]+N_V\left[\frac{4}{D^2}\frac{\partial^2 u}{\partial \sigma^2}\right]$$

$$\frac{\partial v}{\partial t}+\frac{\sigma}{D}\frac{\partial \eta}{\partial t}\frac{\partial v}{\partial \sigma}+u\left[\frac{\partial v}{\partial x}+\Gamma_x\frac{\partial v}{\partial \sigma}\right]+v\left[\frac{\partial v}{\partial y}+\Gamma_y\frac{\partial v}{\partial \sigma}\right]= \tag{2.18b}$$

$$-g\frac{\partial \eta}{\partial y}+N_H\left[\frac{\partial^2 v}{\partial x^2}+\frac{\partial v}{\partial \sigma}\frac{\partial^2 \sigma}{\partial x^2}+2\frac{\partial \sigma}{\partial x}\frac{\partial^2 v}{\partial \sigma \partial x}+\frac{\partial v}{\partial \sigma}\frac{\partial^2 \sigma}{\partial \sigma \partial x}\frac{\partial \sigma}{\partial y}+\left(\frac{\partial \sigma}{\partial x}\right)^2\frac{\partial^2 v}{\partial \sigma^2}\right]$$

$$+N_H\left[\frac{\partial^2 v}{\partial y^2}+\frac{\partial v}{\partial \sigma}\frac{\partial^2 \sigma}{\partial y^2}+2\frac{\partial \sigma}{\partial y}\frac{\partial^2 v}{\partial \sigma \partial y}+\frac{\partial v}{\partial \sigma}\frac{\partial^2 \sigma}{\partial \sigma \partial y}\frac{\partial \sigma}{\partial y}+\left(\frac{\partial \sigma}{\partial y}\right)^2\frac{\partial^2 v}{\partial \sigma^2}\right]+N_V\left[\frac{4}{D^2}\frac{\partial^2 v}{\partial \sigma^2}\right]$$

In equations(2.18) the advective terms have been dropped for simplicity.

2.4.3 Continuity Equation

The continuity equation remains uneffected by the transformation. The vertically averaged velocity components in equation(2.3) are now defined as follows

$$U = \frac{1}{2}\int_0^2 u \, d\sigma \tag{2.19a}$$

$$V = \frac{1}{2}\int_0^2 v \, d\sigma \tag{2.19b}$$

2.3.4 Boundary Conditions

The surface and bed boundary conditions, equations(2.5) and (2.8), when transformed to the σ-coordinate system become:

$$\frac{\partial u}{\partial \sigma} = 0 \quad \text{at } \sigma = 2 \tag{2.20a}$$

$$\frac{\partial v}{\partial \sigma} = 0 \quad \text{at } \sigma = 2 \tag{2.20b}$$

$$\frac{\partial u}{\partial \sigma} = \frac{D\, c_b\, u_b}{2N_v} \quad \text{at } \sigma = 0 \tag{2.21a}$$

$$\frac{\partial v}{\partial \sigma} = \frac{D\, c_b\, v_b}{2N_v} \quad \text{at } \sigma = 0 \tag{2.21b}$$

Boundary conditions defined by equations(2.9) to (2.12) are not effected by this transformation.

2.5.0 THE GALERKIN TECHNIQUE

2.5.1 Trial Functions

To solve the transformed equation of motion together with the boundary conditions, the following trial functions for $u(x,y,\sigma,t)$ and $v(x,y,\sigma,t)$ are assumed:

$$u' = \sum_{I=1}^{N} c_I(x,y,t)\,\mathrm{Cos}\left[\frac{1}{2}\,a_I(2-\sigma)\right] \tag{2.22a}$$

$$v' = \sum_{I=1}^{N} d_I(x,y,t)\,\mathrm{Cos}\left[\frac{1}{2}\,a_I(2-\sigma)\right] \tag{2.22b}$$

The solution procedure is to substitute equations(2.2) into the transformed momentum and continuity equations. The expansions, however, are not exact for a finite number of terms and thus a residual results. This error is minimized by using the Galerkin technique, where the residual equations are multiplied by a weighting function and then integrated with respect to the σ-coordinate. The resulting equations, i.e. residuals, are set equal to zero and solved by finite differences for the c_I's and d_I's. The velocities are then calculated using equations(2.22).

Before expressions for velocity are substituted into the equations of motion, it is necessary to develop an expression for evaluating the coefficients a_I. The solution for these coefficients is obtained by using the bed boundary conditions (2.21). Given the expression for u', the first derivative with respect to σ is:

$$\frac{\partial u'}{\partial \sigma} = \frac{1}{2}\sum_{l=1}^{N} a_l c_l \mathrm{Sin}\left[\frac{1}{2} a_l (2 - \sigma)\right] \qquad (2.23a)$$

Substitution of u' into equation(2.23a) gives:

$$\frac{1}{2}\sum_{l=1}^{N} a_l c_l \mathrm{Sin}\left[\frac{1}{2} a_l (2 - \sigma)\right] = \frac{D\, c_b}{2\, N_V}\sum_{l=1}^{N} c_l \mathrm{Cos}\left[\frac{1}{2} a_l (2 - \sigma)\right] \qquad (2.23b)$$

This relationship will be satisfied if each term on the left-hand side of equation(2.23b) equaled the corresponding term of the series on the right-hand side of the equation. Therefore, the bed boundary condition is satisfied provided the a_l's are chosen such that:

$$a_l \tan(a_l) = \frac{D c_b}{N_v} \quad \text{at} \quad \sigma = 0 \qquad (2.23c)$$

In equation(2.23c), D is the total depth and is a function of x, y, and t. Consequently, the a_l's are also functions of x, y, and t. Figure 2.4 shows the variation of a_l as a function of c_b and N_v.

2.5.2 Momentum Equations

Since u' and v' are truncated expressions of the actual velocities and not exact, substituting these expressions into the momentum equations(2.18) will result in a

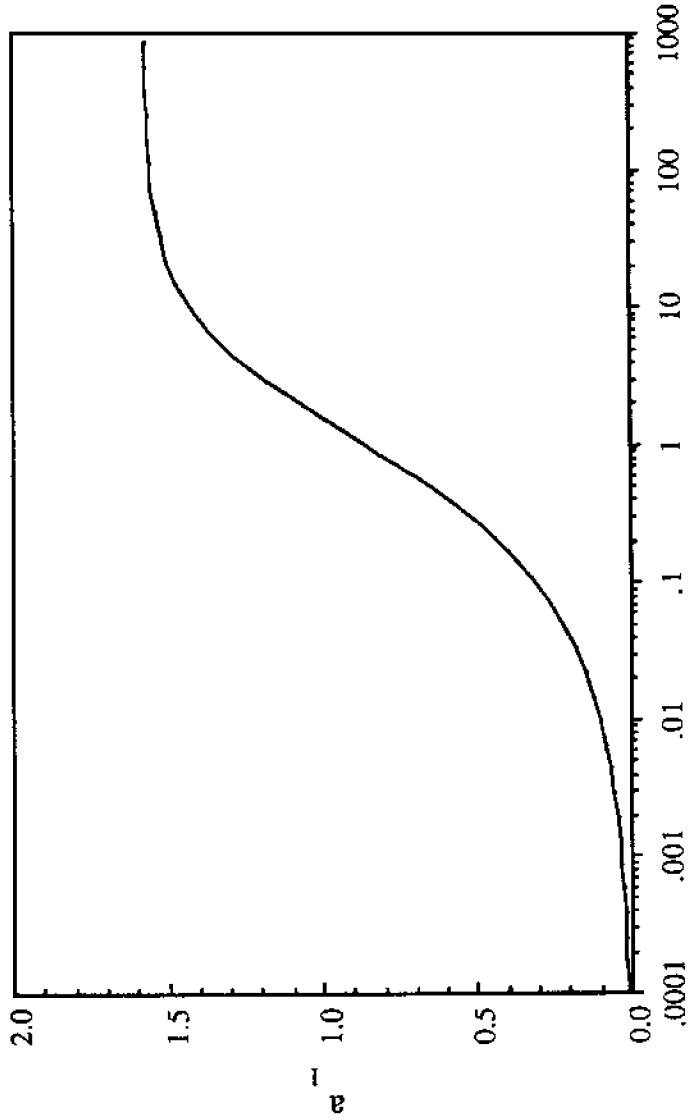

Fig.2.4: Relationship Between Slip Angle and the Ratio of Friction Coefficient to Viscosity of Fluid

residual error. The Galerkin technique minimizes this error by solving for the unknown coefficients in equations(2.22) subjected to the conditions that the integral over the depth, multiplied by a weighting function, is zero. The expressions for the residuals R_x and R_y are:

$$R_x = \frac{\partial u}{\partial t} - \frac{\sigma}{D}\frac{\partial \eta}{\partial t}\frac{\partial u}{\partial \sigma} + u\left[\frac{\partial u}{\partial x} + \Gamma_x \frac{\partial u}{\partial \sigma}\right] + v\left[\frac{\partial u}{\partial y} + \Gamma_y \frac{\partial u}{\partial \sigma}\right] + g\frac{\partial \eta}{\partial x}$$

$$- N_H\left[\frac{\partial^2 u}{\partial x^2} + \frac{\partial u}{\partial \sigma}\frac{\partial^2 u}{\partial x^2} + 2\frac{\partial \sigma}{\partial x}\frac{\partial^2 u}{\partial \sigma \partial x} + \frac{\partial u}{\partial \sigma}\frac{\partial^2 \sigma}{\partial \sigma \partial x}\frac{\partial \sigma}{\partial x} + \left(\frac{\partial \sigma}{\partial x}\right)^2 \frac{\partial^2 u}{\partial \sigma^2}\right]$$

$$- N_H\left[\frac{\partial^2 u}{\partial y^2} + \frac{\partial u}{\partial \sigma}\frac{\partial^2 u}{\partial y^2} + 2\frac{\partial \sigma}{\partial y}\frac{\partial^2 u}{\partial \sigma \partial y} + \frac{\partial u}{\partial \sigma}\frac{\partial^2 \sigma}{\partial \sigma \partial y}\frac{\partial \sigma}{\partial y} + \left(\frac{\partial \sigma}{\partial y}\right)^2 \frac{\partial^2 u}{\partial \sigma^2}\right]$$

$$- N_V\left[\frac{4}{D^2}\frac{\partial^2 u}{\partial \sigma^2}\right] \qquad (2.24a)$$

$$R_y = \frac{\partial v}{\partial t} - \frac{\sigma}{D}\frac{\partial \eta}{\partial t}\frac{\partial v}{\partial \sigma} + u\left[\frac{\partial v}{\partial x} + \Gamma_x \frac{\partial v}{\partial \sigma}\right] + v\left[\frac{\partial v}{\partial y} + \Gamma_y \frac{\partial v}{\partial \sigma}\right] + g\frac{\partial \eta}{\partial y}$$

$$- N_H\left[\frac{\partial^2 v}{\partial x^2} + \frac{\partial v}{\partial \sigma}\frac{\partial^2 v}{\partial x^2} + 2\frac{\partial \sigma}{\partial x}\frac{\partial^2 v}{\partial \sigma \partial x} + \frac{\partial v}{\partial \sigma}\frac{\partial^2 \sigma}{\partial \sigma \partial x}\frac{\partial \sigma}{\partial x} + \left(\frac{\partial \sigma}{\partial x}\right)^2 \frac{\partial^2 v}{\partial \sigma^2}\right] \qquad (2.24b)$$

$$- N_H \left[\frac{\partial^2 v}{\partial y^2} + \frac{\partial v}{\partial \sigma} \frac{\partial^2 v}{\partial y^2} + 2 \frac{\partial \sigma}{\partial y} \frac{\partial^2 v}{\partial \sigma \partial y} + \frac{\partial v}{\partial \sigma} \frac{\partial^2 \sigma}{\partial \sigma \partial y} \frac{\partial \sigma}{\partial y} + \left(\frac{\partial \sigma}{\partial y} \right)^2 \frac{\partial^2 v}{\partial \sigma^2} \right]$$

$$- N_V \left[\frac{4}{D^2} \frac{\partial^2 v}{\partial \sigma^2} \right]$$

where the prime on u and v has been dropped for convenience. The Galerkin statements for the above momentum equations are:

$$\int_0^2 R_x \, \psi(J) \, d\sigma = 0 , \quad J = 1, 2, 3, \ldots\ldots, N \tag{2.25a}$$

$$\int_0^2 R_y \, \psi(J) \, d\sigma = 0 , \quad J = 1, 2, 3, \ldots\ldots, N \tag{2.25b}$$

where

$$\psi(J) = \cos\left[\frac{1}{2} a_J (2 - \sigma) \right] \tag{2.26}$$

Applying the Galerkin technique to equations(2.24) and using the fact that the trial functions are orthogonal so that

$$\int_0^2 \psi(J) \, \psi(I) \, d\sigma = 0 \quad \text{when } I \neq J \tag{2.27}$$

the two momentum equations now become N sets of equations where the J-th equations in the x and y directions are as follows:

$$\frac{\partial c_J}{\partial t} S1_{(J)} - \frac{1}{D}\frac{\partial \eta}{\partial t}\sum_{I=1}^{N} c_I S2_{(I,J)} + \sum_{I=1}^{N}\left[c_I\frac{\partial c_I}{\partial x} + d_I\frac{\partial c_I}{\partial y}\right] S4_{(I,J)}$$

$$+\sum_{I=1}^{N}\left[c_I^2 S5_{(I,J)} + c_I d_I S6_{(I,J)}\right] + g\frac{\partial \eta}{\partial x} S3_{(J)} - N_H\left[\frac{\partial^2 c_J}{\partial x^2} + \frac{\partial^2 c_J}{\partial y^2}\right] S1_{(J)} \qquad (2.28a)$$

$$-N_H\sum_{I=1}^{N}\left[c_I\left(S7_{(I,J)} + S8_{(I,J)} + S9_{(I,J)} + S10_{(I,J)}\right)\right]$$

$$+N_H\sum_{I=1}^{N}\frac{1}{D}c_I\left[\frac{\partial D}{\partial x} S5_{(I,J)} + \frac{\partial D}{\partial y} S6_{(I,J)}\right]$$

$$+2N_H\sum_{I=1}^{N}\left[\frac{\partial c_I}{\partial x} S5_{(I,J)} + \frac{\partial c_I}{\partial y} S6_{(I,J)}\right] + \frac{a_J^2}{D^2} N_V c_J S1_{(J)} = 0$$

$$\frac{\partial d_J}{\partial t} S1_{(J)} - \frac{1}{D}\frac{\partial \eta}{\partial t}\sum_{I=1}^{N} d_I S2_{(I,J)} + \sum_{I=1}^{N}\left[c_I\frac{\partial d_I}{\partial x} + d_I\frac{\partial d_I}{\partial y}\right] S4_{(I,J)}$$

$$+\sum_{I=1}^{N}\left[d_I^2 S6_{(I,J)} + c_I d_I S5_{(I,J)}\right] + g\frac{\partial \eta}{\partial y} S3_{(J)} - N_H\left[\frac{\partial^2 d_J}{\partial x^2} + \frac{\partial^2 d_J}{\partial y^2}\right] S1_{(J)} \qquad (2.28b)$$

$$-N_H \sum_{I=1}^{N} \left[d_I \left(S7_{(I,J)} + S8_{(I,J)} + S9_{(I,J)} + S10_{(I,J)} \right] \right.$$

$$+N_H \sum_{I=1}^{N} \frac{1}{D} d_I \left[\frac{\partial D}{\partial x} S5_{(I,J)} + \frac{\partial D}{\partial y} S6_{(I,J)} \right]$$

$$+ 2\, N_H \sum_{I=1}^{N} \left[\frac{\partial d_I}{\partial x} S5_{(I,J)} + \frac{\partial d_I}{\partial y} S6_{(I,J)} \right] + \frac{a_J^2}{D^2} N_V d_J S1_{(J)} = 0$$

The integrals resulting from the Galerkin technique have been denoted by S1(J), S2(I,J), .. etc. These integrals are defined as follows:

$$S1_{(J)} = \int_0^2 \psi_J^2 \, d\sigma \tag{2.29a}$$

$$S2_{(I,J)} = \int_0^2 \sigma \, \psi'_I \psi_J \, d\sigma \tag{2.29b}$$

$$S3_{(J)} = \int_0^2 \psi_J \, d\sigma \tag{2.29c}$$

$$S4_{(I,J)} = \int_0^2 \psi_I^2 \psi_J^2 \, d\sigma \tag{2.29d}$$

$$S5_{(I,J)} = \int_0^2 \Gamma_x \psi'_I \psi_I \psi_J \, d\sigma \tag{2.29e}$$

$$S6_{(I,J)} = \int_0^2 \Gamma_y \psi'_I \psi_I \psi_J \, d\sigma \tag{2.29f}$$

$$S7_{(I,J)} = \int_0^2 \Lambda_x \psi'_I \psi_J \, d\sigma \tag{2.29g}$$

$$S8_{(I,J)} = \int_0^2 \Gamma_x^2 \psi''_I \psi_J \, d\sigma \tag{2.29h}$$

$$S9_{(I,J)} = \int_0^2 \Lambda_y \psi'_I \psi_J \, d\sigma \tag{2.29i}$$

$$S10_{(I,J)} = \int_0^2 \Gamma_y^2 \psi''_I \psi_J \, d\sigma \tag{2.29j}$$

In the above integrals Λ_x and Λ_y are given by:

$$\Lambda_x = \frac{\partial^2 \sigma}{\partial x^2} = \frac{1}{D}\left[(2-\sigma)\frac{\partial^2 H}{\partial x^2} - \sigma\frac{\partial^2 \eta}{\partial x^2} - \Gamma_x\left\{\frac{\partial H}{\partial x} + \frac{\partial \eta}{\partial x} + 1\right\}\right] \tag{2.30a}$$

$$\Lambda_y = \frac{\partial^2 \sigma}{\partial y^2} = \frac{1}{D}\left[(2-\sigma)\frac{\partial^2 H}{\partial y^2} - \sigma\frac{\partial^2 \eta}{\partial x^2} - \Gamma_y\left\{\frac{\partial H}{\partial y} + \frac{\partial \eta}{\partial y} + 1\right\}\right] \tag{2.30b}$$

The integrals $S1_{(J)}$ and $S3_{(J)}$ are simple and can be evaluated analytically. The rest of the integrals are evaluated numerically by Gaussian quadrature.

2.5.3 Continuity Equation

The momentum equations form a system of 2N differential equations with 2N+1 unknowns. The equations must be linked with the continuity equation to complete the solution. The continuity equation(2.3) can be expressed in terms of trial functions by finding expressions for U and V, the depth averaged velocities, in terms of c_I and d_I. The expressions for U and V are:

$$U = \frac{1}{2}\int_0^2 \left[\sum_{I=1}^{N} c_I \mathrm{Cos}\left\{\frac{1}{2} a_I (2 - \sigma)\right\}\right] d\sigma \qquad (2.31a)$$

$$V = \frac{1}{2}\int_0^2 \left[\sum_{I=1}^{N} d_I \mathrm{Cos}\left\{\frac{1}{2} a_I (2 - \sigma)\right\}\right] d\sigma \qquad (2.31b)$$

Upon performing the integrations, the expressions for U and V can be simplified to:

$$U = \sum_{I=1}^{N} \frac{c_I}{a_I} \sin(a_I) \quad \text{for } a_I \neq 0 \qquad (2.32a)$$

$$U = c_J \text{ for } a_J = 0$$

$$V = \sum_{I=1}^{N} \frac{d_I}{a_I} \sin(a_I) \quad \text{for } a_I \neq 0 \qquad (2.32b)$$

$$V = d_J \text{ for } a_J = 0$$

The expressions for U and V are substituted into continuity equation and solved for the surface elevation, η.

2.6.0 THE NUMERICAL SCHEME

The Galerkin statements for the momentum equations together with the continuity equation, are solved by a finite difference method. The solution algorithm is staggered in both space and time. Figure 2.5 shows the spatial locations of the η's, c_J's and d_J's. All the integrals, a_J's and D's are evaluated at η points. The continuity equation is solved explicitly and the momentum equations are solved by using a semi-implicit method. This solution algorithm significantly improves the stability of the model when compared with completely explicit schemes.

2.6.1 Discretized Momentum Equations

Let i, j and k represent the grid counters in the x and y directions and time respectively. Then the finite difference form of the terms in equation(2.28a), the x momentum equation, are as follows:

Term-1:

$$\frac{\partial c_J}{\partial t} S1_{(J)} = \frac{c_J^{i,j,k+1} - c_J^{i,j,k}}{\Delta t} \qquad (2.33a)$$

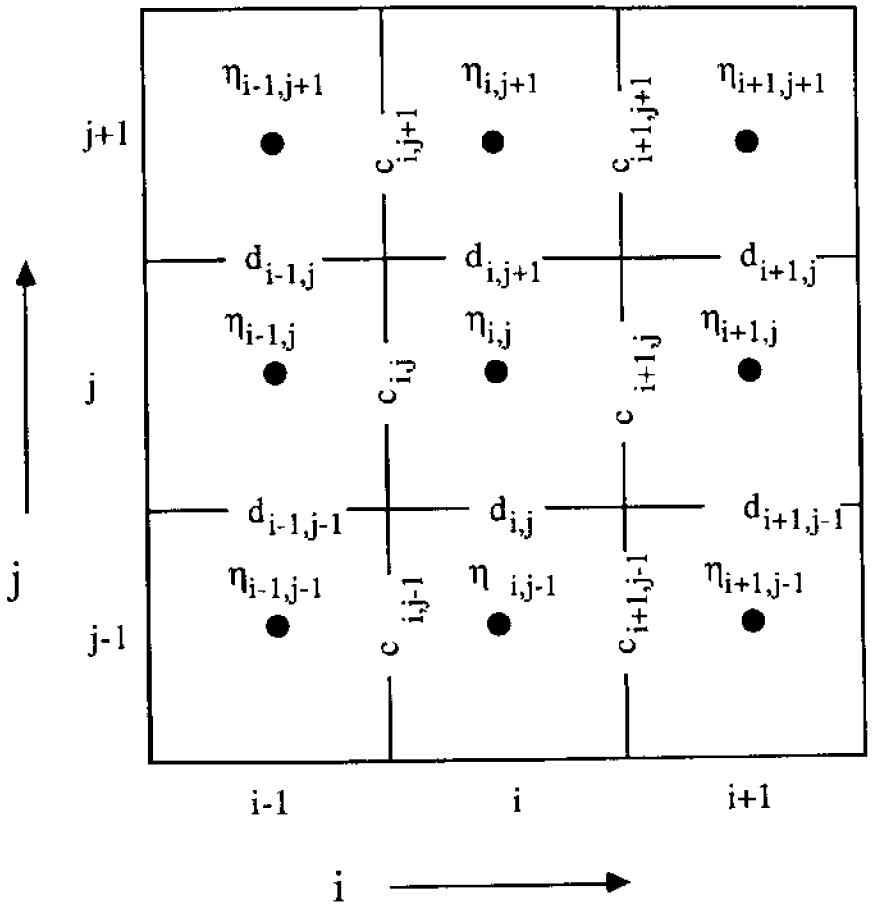

Figure 2.5: Grid Setup for Finite Difference Scheme

Term-2:

$$\frac{1}{D}\frac{\partial \eta}{\partial t}\sum_{I=1}^{N} c_I S2_{(I,J)} = \frac{1}{D}\frac{\partial \eta}{\partial t}\left[c_J S2_{(J,J)} + \sum_{I \neq J} c_I S2_{(I,J)} \right] \tag{2.33b}$$

$$= \frac{1}{D^{i,j,k+1/2}} \frac{\eta^{i,j,k+1/2} - \eta^{i,j,k-1/2}}{\Delta t} \left[c_J^{i,j,k+1} S2_{(J,J)} + \sum_{I \neq J} c_I^{i,j,k} S2_{(I,J)} \right]$$

Term-3:

$$\sum_{I=1}^{N}\left[c_I \frac{\partial c_I}{\partial x} + d_I \frac{\partial c_I}{\partial y} \right] S4_{(I,J)} =$$

$$\sum_{I=1}^{N}\left[c_I^{i,j,k} \frac{c_I^{i+1,j,k} - c_I^{i-1,j,k}}{2\Delta x} + d_I^{i,j,k} \frac{c_I^{i,j+1,k} - c_I^{i,j-1,k}}{2\Delta y} \right] S4_{(I,J)} \tag{2.33c}$$

Term-4:

$$\sum_{I=1}^{N}\left[c_I^2 S5_{(I,J)} + c_I d_I S6_{(I,J)} \right] = \sum_{I=1}^{N}\left[\left(c_I^{i,j,k} \right)^2 S5_{(I,J)} + c_I^{i,j,k} d_I^{i,j,k} S6_{(I,J)} \right] \tag{2.33d}$$

Term-5:

$$g\frac{\partial \eta}{\partial x} S3_{(J)} = g \frac{\eta^{i+1,j+1,k+1/2} - \eta^{i,j+1,k+1/2}}{\Delta x} S3_{(J)} \tag{2.33e}$$

Term-6:

$$N_H\left[\frac{\partial^2 c_J}{\partial x^2}+\frac{\partial^2 c_J}{\partial y^2}\right]S1_{(J)}=$$

$$N_H\left[\frac{c_J^{i+1,j,k}-2\,c_I^{i,j,k}+c_I^{i-1,j,k}}{\Delta x^2}+\frac{c_J^{i,j+1,k}-2\,c_I^{i,j,k}+c_I^{i,j-1,k}}{\Delta y^2}\right] \qquad (2.33f)$$

Term-7:

$$\sum_{I=1}^{N}\left[c_I\left(S7_{(I,J)}+S8_{(I,J)}+S9_{(I,J)}+S10_{(I,J)}\right)\right]=$$

$$\left[c_J^{i,j,k+1}\left(S7_{(J,J)}+S8_{(J,J)}+S9_{(J,J)}+S10_{(J,J)}\right)\right]+$$

$$\sum_{I\neq J}\left[c_I^{i,j,k}\left(S7_{(I,J)}+S8_{(I,J)}+S9_{(I,J)}+S10_{(I,J)}\right)\right] \qquad (2.33g)$$

Term-8:

$$N_H\sum_{I=1}^{N}\frac{1}{D}c_I\left[\frac{\partial D}{\partial x}S5_{(I,J)}+\frac{\partial D}{\partial y}S6_{(I,J)}\right]= \qquad (2.33h)$$

$$+N_H\frac{c_J^{i,j,k+1}}{D^{(i,j,k+1/2}}\left[\frac{D^{i+1,j,k+1/2}-D^{i-1,j,k+1/2}}{2\Delta x}S5_{(J,J)}+\frac{D^{i,j+1,k+1/2}-D^{i,j,k+1/2}}{2\Delta y}S6_{(J,J)}\right]$$

$$+N_H \sum_{I \neq J} \frac{c_I^{i,j,k+1}}{D^{(i,j,k+1/2}} \left[\frac{D^{i+1,j,k+1/2} - D^{i-1,j,k+1/2}}{2\Delta x} S5_{(I,J)} + \frac{D^{i,j+1,k+1/2} - D^{i,j,k+1/2}}{2\Delta y} S6_{(I,J)} \right]$$

Term-9:

$$2 N_H \sum_{I=1}^{N} \left[\frac{\partial c_I}{\partial x} S5_{(I,J)} + \frac{\partial c_I}{\partial y} S6_{(I,J)} \right] =$$

$$2 N_H \sum_{I=1}^{N} \left[\frac{c_I^{i+1,j,k} - c_I^{i-1,j,k}}{2\Delta x} S5_{(I,J)} + \frac{c_I^{i,j+1,k} - c_I^{i,j-1,k}}{2\Delta y} S6_{(I,J)} \right] \quad (2.33i)$$

Term-10:

$$\frac{a_J^2}{D^2} N_V c_J S1_{(J)} = N_V \left[\frac{a_J^{i,j,k}}{D^{i,k,k+1/2}} \right]^2 c_J^{i,j,k+1} S1_{(J)} \quad (2.33j)$$

In the above expressions the values of η, D, a_J and d_J are actually taken as average about the c_J location. Thus

$$\eta^{i,j,k+1/2} = \frac{1}{2} \left[\eta^{i+1,j+1,k+1/2} + \eta^{i,j+1,k+1/2} \right] \quad (2.34a)$$

$$D^{i,j,k+1/2} = \frac{1}{2} \left[D^{i+1,j+1,k+1/2} + D^{i,j+1,k+1/2} \right] \quad (2.34b)$$

$$a_J^{i,j,k+1/2} = \frac{1}{2}\left[a_J^{i+1,j+1,k+1/2} + a_J^{i,j+1,k+1/2}\right] \qquad (2.34c)$$

$$d_J^{i,j,k+1/2} = \frac{1}{4}\left[d_J^{i,j+1,k} + d_J^{i-1,j+1,k} + d_J^{i-1,j,k} + d_J^{i,j,k}\right] \qquad (2.34e)$$

The integrals involved in the solution are also taken as averages about c_J in the same way the η's are determined.

Substituting these expressions in equation(2.28a) and simplifying it gives:

$$\alpha_x c_J^{i,j,k+1} + \beta_x c_J^{i,j,k} + \gamma_x = 0 \qquad (2.35a)$$

In equation(2.35a), α_x, β_x and γ_x are known, c_J at time t= $k\Delta t$ is either known from initial condition or from the previous step of computation.

In a similar way equation(2.28b) can also be expressed as:

$$\alpha_y d_J^{i,j,k+1} + \beta_y d_J^{i,j,k} + \gamma_y = 0 \qquad (2.35b)$$

Equations(2.35) can be directly solved for c_J and d_J at t= $(k+1)\Delta t$.

2.6.2 Discretized Continuity Equation

The finite difference form of the continuity equation(2.3) is

$$\eta^{i,j,k+3/2} = \eta^{i,j,k+1/2} - \frac{\Delta t}{\Delta x}\left[(DU)^{i+1,j} - (DV)^{i,j}\right] - \frac{\Delta t}{\Delta y}\left[(DV)^{i,j+1} - (DV)^{i,j}\right] \qquad (2.36)$$

where

$$(DU)^{i+1,j} = \frac{1}{2}\left[D^{i+1,j,k+1/2} + D^{i,j,k+1/2}\right] U^{i,j,k+1} \qquad (2.37a)$$

$$(DU)^{i,j} = \frac{1}{2}\left[D^{i,j,k+1/2} + D^{i-1,j,k/2}\right] U^{i-1,j-1,k+1} \qquad (2.37b)$$

$$(DV)^{i,+1} = \frac{1}{2}\left[D^{i,j+1,k+1/2} + D^{i,j,k+1/2}\right] V^{i-1,j,k+1} \qquad (2.37c)$$

$$(DV)^{i,j} = \frac{1}{2}\left[D^{i,j,k+1/2} + D^{i,j-1,k+1/2}\right] V^{i-1,j-1,k+1} \qquad (2.37d)$$

and U and V are the depth average velocities defined by equations(2.32).

2.7.0 STABILITY ANALYSIS

The residual equations obtained by the Galerkin technique are solved by an explicit time-split finite difference scheme. The new solution process gives equal weight to some of the terms in the transformed momentum equations at advance time levels. Stability analysis of the non-linear hyperbolic system of equations is difficult analytically. For the sake of brevity and simplicity, the analysis presented in this section is based on simplified equations.

2.7..1 Effects of Friction

The Courant stability condition normally applied to explicit models (Smith, 1978 and Abbott, 1979) is based on linearized equations that neglect frictional effects. Though equation(2.2a) is a good indicator of the stability of a hydrodynamic model, it under estimates the stability of the model when high frictional resistance is involved. A high friction coefficient makes the system less dynamic and larger time steps can be used. For simplicity, the stability analysis is performed for a one-dimensional case, but includes linear friction. This analysis does not, however, include the effects of viscosity directly. The linearized one-dimensional continuity and momentum equations are:

$$\frac{\partial \eta}{\partial t} + \frac{\partial u}{\partial x} = 0 \qquad (2.38a)$$

$$\frac{\partial u}{\partial t} + c^2 \frac{\partial \eta}{\partial x} + c_b u = 0 \qquad (2.38b)$$

In equation(2.38b), $c = \sqrt{gD}$, c_b is a linear friction coefficient and the term $c_b u$ has been added to the traditional stability analysis. For the time-split finite difference scheme (figure 2.5), equations(2.38) can be discretized to the following:

$$\frac{\eta_j^{k+1} - \eta_j^{k}}{\Delta t} + \frac{u_{j+1/2}^{k+1/2} - u_{j-1/2}^{k+1/2}}{\Delta x} = 0 \qquad (2.39a)$$

$$\frac{u_{j+1/2}^{k+3/2} - u_{j+1/2}^{k+1/2}}{\Delta t} + \frac{\eta_{j+1}^{k+1} - \eta_{j-1}^{k+1}}{\Delta x} + c_b u_{j+1/2}^{k+3/2} = 0 \qquad (2.39b)$$

where j and k are counters for distance and time respectively. Following the analysis of von Neuman (Smith, 1978; Abbott, 1979) Fourier solutions of the equations(2.38) are assumed as follows:

$$\eta_j^k = \sum_{n=1}^{l} \eta_n e^{i\, j\Delta x} \tag{2.40a}$$

$$u_{j+1/2}^{k+1/2} = \sum_{n=1}^{l} u_n e^{i\,(j+1/2)\Delta x} \tag{2.40b}$$

where η_n and u_n represents the n-th Fourier component of the solution and $i = \sqrt{-1}$. As the system of equations is linear, analysis of the n-th Fourier component is sufficient to establish the propagation characteristics of the solution. Substitution of equations(2.40) into equations(2.38) and simplification gives the following equations:

$$\left(2i\,\omega\frac{\Delta t}{\Delta x}\,\mathrm{Sin}\frac{\Delta x}{2}\right)\eta^k + (\omega\text{-}1)\,u^k = 0 \tag{2.41a}$$

$$\left(\omega\text{-}1+\omega\, c_b\,\Delta t\right)\eta^k + \left(2ic^2\frac{\Delta t}{\Delta x}\,\mathrm{Sin}\,\frac{\Delta x}{2}\right)u^k = 0 \tag{2.41b}$$

where ω, known as the amplification factor, is defined as follows:

$$\omega = \frac{\eta^{k+1}}{\eta^k} \text{ or } \frac{u^{k+1}}{u^k} \tag{2.42}$$

Since η_n and u_n are non-zero, the amplification matrix, equation(2.43), must be zero for non-trivial solutions of the system of equations(2.41):

$$\Omega=\begin{pmatrix} 2\,i\,\omega\frac{\Delta t}{\Delta x}\,\mathrm{Sin}\,\Delta x/2 & \omega-1 \\ \omega-1+c_b\Delta t & 2\,i\,c^2\frac{\Delta t}{\Delta x}\,\mathrm{Sin}\,\Delta x/2 \end{pmatrix}=0 \qquad (2.43)$$

which implies that:

$$(1+c_b\Delta t)\,\omega^2+\left(4\lambda^2\,\mathrm{Sin}\,\theta-2-c_b\Delta t\right)\omega+1=0 \qquad (2.44)$$

where $\lambda = c\Delta t/\Delta x$ and $\theta = \Delta x/2$. Equation(2.44) is quadratic in ω. Solution of equation(2.44) gives a complicated expression for ω and does not provide any direct information about the stability of the solution process. Fortunately, the generalization of this problem by Cushman-Roisin(1984) allows an easier solution of the problem. In particular, if the quadratic equation is of the following form:

$$(a+ia')\,\omega^2+(b+ib')\,\omega+(c+ic')=0 \qquad (2.45a)$$

The numerical solution process is stable if $|E| \le 1$, where E is defined as:

$$E=\left[\frac{b}{a+c}\right]^2+\left[\frac{b'}{a-c}\right]^2 \qquad (2.45b)$$

Comparing equations(2.44) and (2.45a) and using equation(2.45b), the stability condition is given by:

$$-1 \le \frac{4\lambda^2 \mathrm{Sin}^2\theta}{2+c_b\Delta t} \le 1 \qquad (2.46)$$

The left hand inequality is always satisfied. The maximum value of $\mathrm{Sin}^2\theta$ is 1 so the right hand inequality results in the following stability condition:

$$c^2\left(\frac{\Delta t}{\Delta x}\right)^2 \le 1+\frac{1}{2}c_b\Delta t \qquad (2.47)$$

In the usual analysis of stability of hydrodynamic models, c_b is ignored, so equation(2.47) reduces to the conventional Courant stability condition. In glaciers $c_b >> 1$ and equation(2.47) can be simplified to the following:

$$\Delta t \le \frac{1}{2}c_b\left(\frac{\Delta x}{\sqrt{gD}}\right)^2 \qquad (2.48a)$$

This relation can be considered as a modified form of the Courant stability criterion, including the effects of linear friction. The time step, Δt, is directly proportional to friction factor, c_b. Stability analysis of two-dimensional flow models, neglecting friction, shows that Δt is smaller than the one-dimensional case by a factor of $\sqrt{2}$ (Abbott, 1979) and equation(19a) becomes:

$$\Delta t \leq \frac{1}{2} c_b \left(\frac{\Delta x}{\sqrt{2\, gD}} \right)^2 \qquad (2.48b)$$

Equation(2.48b) is based on the depth mean velocity of flow and does not allow for the deformation of the fluid within a vertical column (the model assumes the glacier as an array of vertical column of deforming ice). Thus, this analysis will over-estimate Δt for the present model, because the surface velocity can be considerably higher than the mean velocity. For linear flow and friction laws, the theoretical analysis of Nye(1960) shows that the velocity of surface wave propagation is twice the surface velocity of ice or three times the mean velocity for Couette flow. The model has been applied to the Taku Glacier with $\Delta x = \Delta y =$ 1000 m. The maximum present ice thickness is about 405 m. The lowest value of c_b is of the order of 1.0×10^7 m/s. For these conditions, equation(2.48b) gives $\Delta t \leq$ 7280 days. However, the model is found to remain stable for Δt of around 60 days and shows some numerical oscillations. To avoid these oscillations, it is necessary to use a Δt of about 30 days. The reasons for this discrepancy are discussed in the next section. Experience in using the model indicates that a reasonable estimate of Δt is given by the following semi-empirical relationship:

$$\Delta t \leq \frac{1}{2} c_b^{2/3} \left(\frac{\Delta x}{\sqrt{2\, gD}} \right)^2 \qquad (2.48c)$$

The corresponding value of Δt is 53.7 days, which is very close to the value of time step used for modelling the Taku Glacier.

2.7.2 Effects of Viscosity

In writing equation(2.35), the velocity (parameters c_J and d_J in the transformed momentum equations) were time-centered. In the hydrodynamic model these terms

are evaluated at the present time level, resulting in the stability criterion given by equation(2.2b). The following analysis illustrates how time centering of velocity makes the model stable. Neglecting horizontal viscosity, equation(2.28a) can be expressed following:

$$\frac{\partial c_J}{\partial t} S1_{(J)} - \frac{1}{2D}\frac{\partial \eta}{\partial t}\sum_{I=1}^{N} a_I c_J \; S2_{(I,J)} + g\frac{\partial \eta}{\partial x}\; S3_{(J)} + \frac{N_v}{D^2} a_J c_J \; S1_{(J)} = 0 \qquad (2.49a)$$

This equation is further simplified for the analysis of the effects of viscosity, to the following (Pearce and Cooper, 1981):

$$\frac{\partial c_J}{\partial t} + \frac{N_v a_J^2}{D^2} c_J = 0 \qquad (2.49b)$$

Equation(2.49b) is completely uncoupled from the y-momentum and continuity equations. In the conventional time-splitting scheme, used in the hydrodynamic model, c_J in the second term is taken at the present time level. The resulting stability condition, equation(2.2b), severely restricts Δt for highly viscous fluid flows. Therefore, in the present formulation, this term and also similar non-linear terms, are time centered. The finite difference form of equation(2.49b), for the present model, is as follows:

$$\frac{c_J(t+\Delta t) - c_J(t)}{\Delta t} + \left\{\frac{N_v a_J^2}{D^2}\right\} \; \frac{1}{2}\left[c_J(t+\Delta t) + c_J(t)\right] = 0 \qquad (2.50)$$

For this case the stability analysis gives the following amplification factor:

$$\omega = \frac{1- \beta}{1+ \beta} \qquad (2.51a)$$

where

$$\beta = \frac{a_J^2 N_V \Delta t}{2 D^2} \qquad (2.51b)$$

As N_V is always positive, $|\omega| \leq 1$. The plot of the amplification factor as a function of β is shown in figure 2.6. When this parameter is small, the numerical solution process is highly damped. The value of the parameter, β, in the Taku Glacier is of the order of 10^{11}, a region where the amplification factor is one. A similar analysis is also applicable to the y-momentum equation. The analysis of the individual momentum equation shows that the method of solution of the momentum equations are unconditionally stable. However, as the solution of the momentum equations are coupled to the explicit solution of the continuity equation, the model as a whole is not unconditionally stable.

While applying the model, it became apparent that the model remains stable for a certain range of viscosity values with a given friction coefficient and vise-versa. This observation, though not obvious from this analysis, represents a physically realistic situation. For a given fluid, the frictional resistance that could be generated by the interaction of the fluid and bed can vary within a certain range depending on the properties of the fluid (viscosity) and the characteristics of the bed (surface roughness parameters). Thus, if the model is run with unrealistic combinations of viscosity and friction, it blows up even for small time steps. The instability is induced by either unrealistic sliding velocity (due to friction coefficient) or shear deformation of the fluid (due to viscosity).

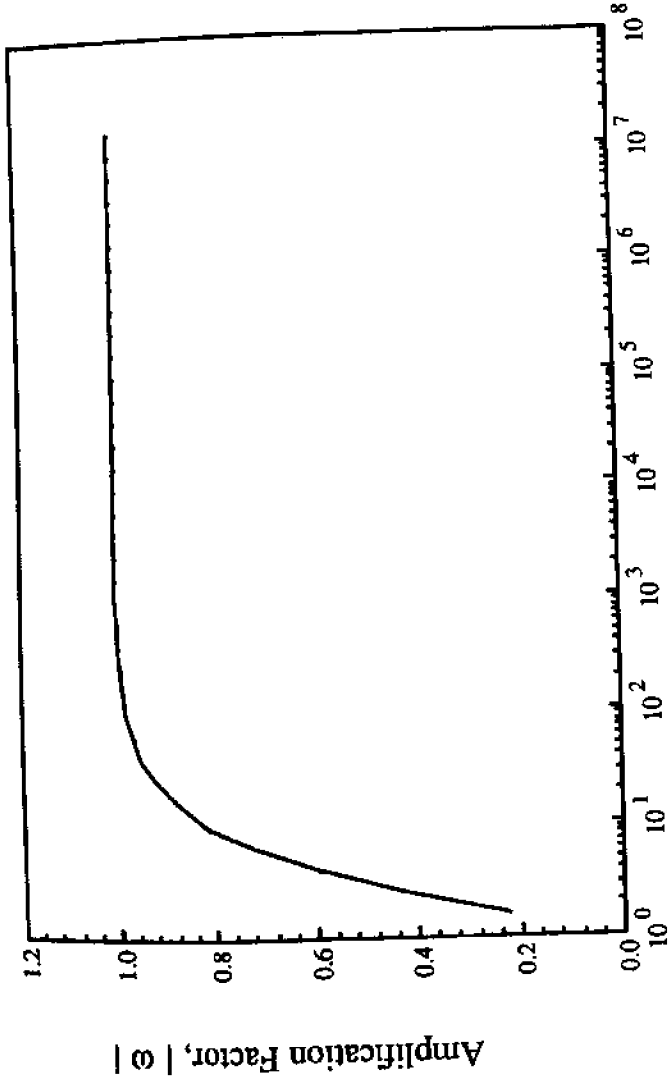

Fig.2.6: Amplification Factor as a Function of a Model Parameter

2.8.0 CHARACTERISTICS OF THE MODEL

The glacier flow model described in this paper is based on a hydrodynamic model developed by Cooper and Pearce(1977), Pearce and Cooper(1981), Pearce et al.(1978) and Sucsy and Pearce(1986). The model computes the vertical velocity distribution from functional relationships, using a Galerkin weighted residual technique. The outstanding features of this type of model (Cooper and Pearce, 1977) are:

1) a relatively simple formulation,
2) reasonable computer time requirement, and
3) a continuous functional form for the velocity profile.

The model combines the advantages of both analytical and numerical approaches (Pearce and Cooper, 1981). The advantages of using the cosine function (Pearce et al. 1978) to represent the functional form of velocity are:

1) it is well defined for all angles of flow,
2) it is well-behaved when differentiated or integrated,
3) it is able to approximate complex functions when combined together in a series, and
4) it is orthogonal with respect to other cosine functions.

The number of cosine terms needed to construct the vertical velocity profile depends on the convergence of the solution, which is a function of viscosity of the ice, bed friction and characteristics of the flow. While carrying out the numerical experiments described in Chapter-3, it was found that one cosine term is sufficient to resolve the vertical velocity profile for linear relationship between stress and strain in ice. As the model avoids the vertical discretization of the ice sheet to compute the variations of horizontal velocity components in the vertical, the

computer time and computer storage required for running the model are comparable to vertically averaged two-dimensional models (Pearce and Cooper, 1981).

The numerical flow models for glaciers and ice sheets, developed to date, can be placed into three broad categories:

i)1-D{x}: Velocity and surface elevation are averaged over the glacier cross-section and are function of longitudinal distance only (Budd 1975; Bindschadler, 1982; Fastook, 1987; Hughes, 1981).

ii)2-D{x,z}: Vertical velocity variation is considered. However, velocity and surface elevation are assumed uniform in the transverse direction (Bindschadler and Gore, 1982; Budd and Jenssen, 1975; Reeh, 1988).

iii)2-D{x,y}: Both the longitudinal and transverse variation of velocity and surface elevation are considered. However, velocity in the vertical is assumed constant (Rasmussen and Campbell,1973; Mahaffy 1976; Budd et al.,1984).

This classification is based on the spatial dimensions (x, y, z) of the model and clearly indicates the possibility of a class of models which combines the later two categories. These models will not only compute the horizontal velocity distribution, but also the variation of horizontal velocity components in the vertical. To date no such model has been reported. The vertical velocity in glaciers is so small that attempts to compute it from the solution of the z-momentum equation is not considered reasonable. Consequently, the class of models which compute the vertical variation of the horizontal velocity components can be termed as "three-dimensional models". The models reported by Rasmussen and Campbell(1973), Mahaffy(1976), Budd et al.(1984) and others are based on a vertically averaged continuity equation and velocity is a function of only two space dimensions (x,y). Therefore, these models fall into the category of two-

dimensional models in the x-y plane. It should be noted that these models are still termed "three-dimensional" by the authors. The models by Bindschadler and Gore(1982), Budd and Jenssen(1975) and Rech(1988) can take into account the vertical variations of ice properties along a flow line, but ignore transverse variations of bed and surface topographies, mass balance and horizontal velocity. These models are based on the one-dimensional continuity equation, similar to the conventional one-dimensional models by Budd(1975), Bindschadler(1982), Fastook(1987) and Hughes(1981). In hydraulics, the number of dimension refers to the space coordinates and has been adopted in this study.

3. NUMERICAL EXPERIMENTS

3.1.0 INTRODUCTION

In the last decade many numerical models have been constructed to realistically simulate the dynamics of glaciers. The major obstacle to realistic simulation of glaciers, as noted by Meier(1987) in review of glacier models, are the complexity of physical laws and the assumptions involved in formulating a model. Consequently, all numerical models of glaciers are based on some degree of parameterization of the problem. These parameters not only have different values for different glaciers, but can widely vary in different regions of the same glacier (Raymond and Harrison,1987). Therefore, extensive field data are necessary to determine the optimum values of the model parameters for the practical application of the models. Unfortunately, long-term field data to check the validity of the assumptions made in the model formulation are not available. This sparseness and limited availability of data make rigorous field verification and validation of numerical models very difficult. The alternative remaining for ascertaining the validity of model formulation is to study the simulation characteristics of a numerical model for idealized cases for which analytical solutions are available. Comparison of the results of the numerical model with analytical solutions can provide valuable insight about the validity of the assumptions made in the formulation of the numerical model.

To ascertain the simulation characteristics of a model, based on these assumptions, numerical experiments are conducted. This chapter describes several numerical experiments and their results. The model is also applied to the Fedchenko Glacier, Central Soviet Asia, to study the effects of the flow law on the computed surface profiles. To adequately simulate the flow characteristics of the Lower Taku Glacier, it is necessary to use grid sizes of the same order of

magnitude as the local ice thickness. Budd(1970) indicates that when the grid-size is less than twenty times the local ice thickness the model should include the effects of the stress-gradient terms. For practical applications of the model, the computations of the stress-gradient terms are complicated and time consuming. Therefore, an analysis of the stress-gradient terms, using the Fedchenko Glacier as a test case, is also included.

3.2.0 STEADY STATE SURFACE PROFILE

In the first numerical experiment a thin film of ice 5.0 m thick, subjected to uniform accumulation over a part of it and uniform ablation over the rest, was used to study the growth of a glacier to steady state. For this situation, analytical expressions for the steady state profile are as follows (Paterson 1972; Weertman 1961):

$$\left(\frac{\eta}{D_o}\right)^4 + \left(1 + \frac{S^+}{S^-}\right)\left(\frac{x}{L}\right)^2 = 1\ ,\ 0 \le x < L_1 \qquad (3.1a)$$

$$\left(\frac{\eta}{D_o}\right)^2 = \left(1 + \frac{S^-}{S^+}\right)\left(1 - \frac{x}{L}\right)\ ,\ L_1 \le x \le L \qquad (3.1b)$$

where η is the ice thickness at a distance x from the head of ice sheet ($x = 0$), D_o is the height of the ice sheet at the head, L is the half length of the ice sheet, S^+ is the accumulation rate over a distance L_1 from the head of the glacier and S^- is the ablation rate over the rest of the glacier.

For $S^+ = 1.0$ m/year and $S^- = 1.5$ m/year , with $L_1 = 15.0$ km, figure 3.1 shows the progressive growth of the glacier over a period of about 1170 years and

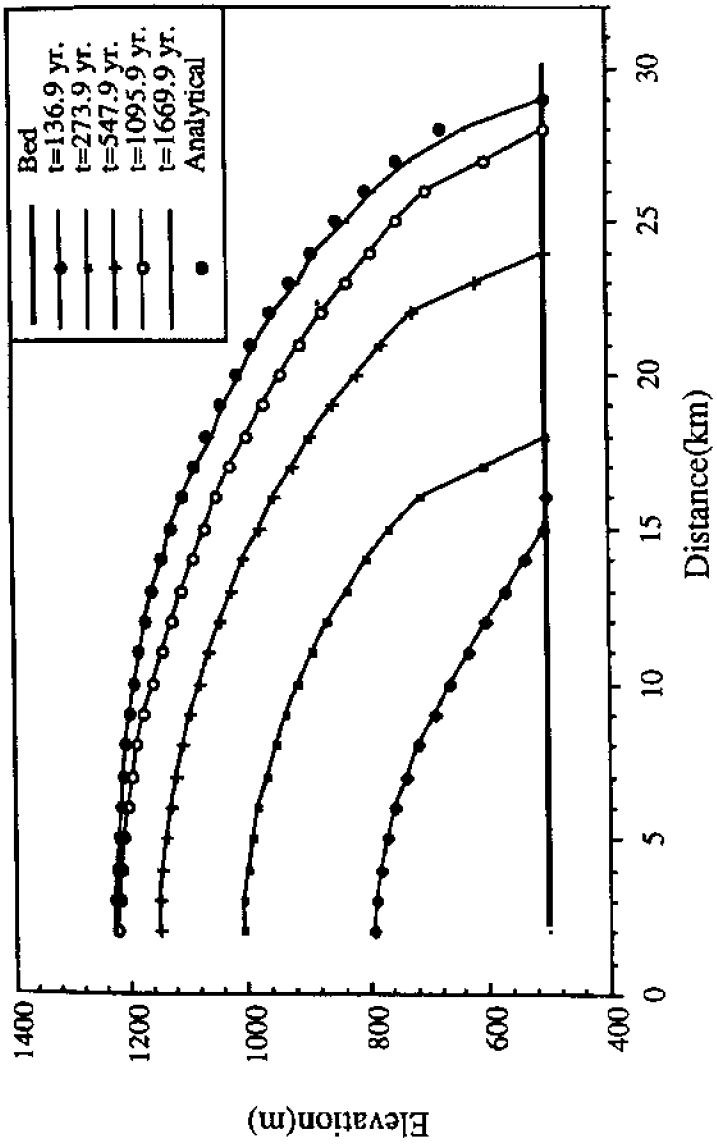

Fig. 3.1: Growth of a Glacier on a Horizontal Bed and Comparison of the Computed Surface With Analytical Solution (Paterson, 1972).

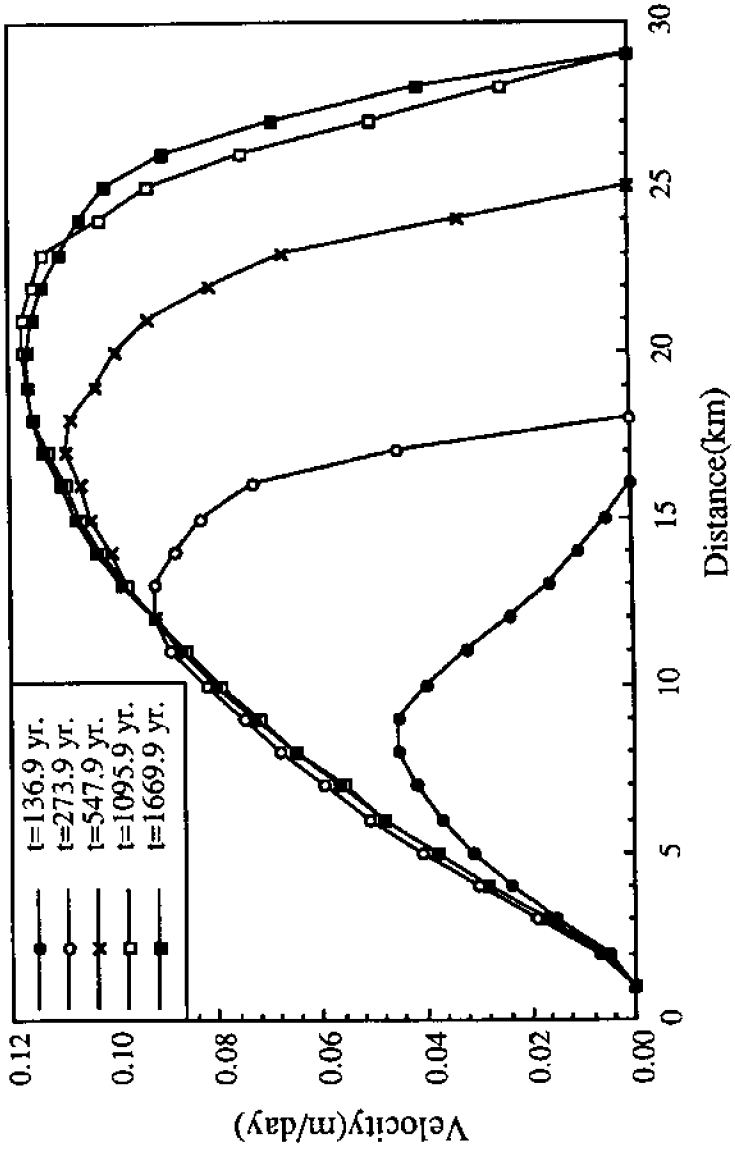

Fig. 3.2: Temporal Variation of Surface Velocity During the Growth of the Steady State Glacier

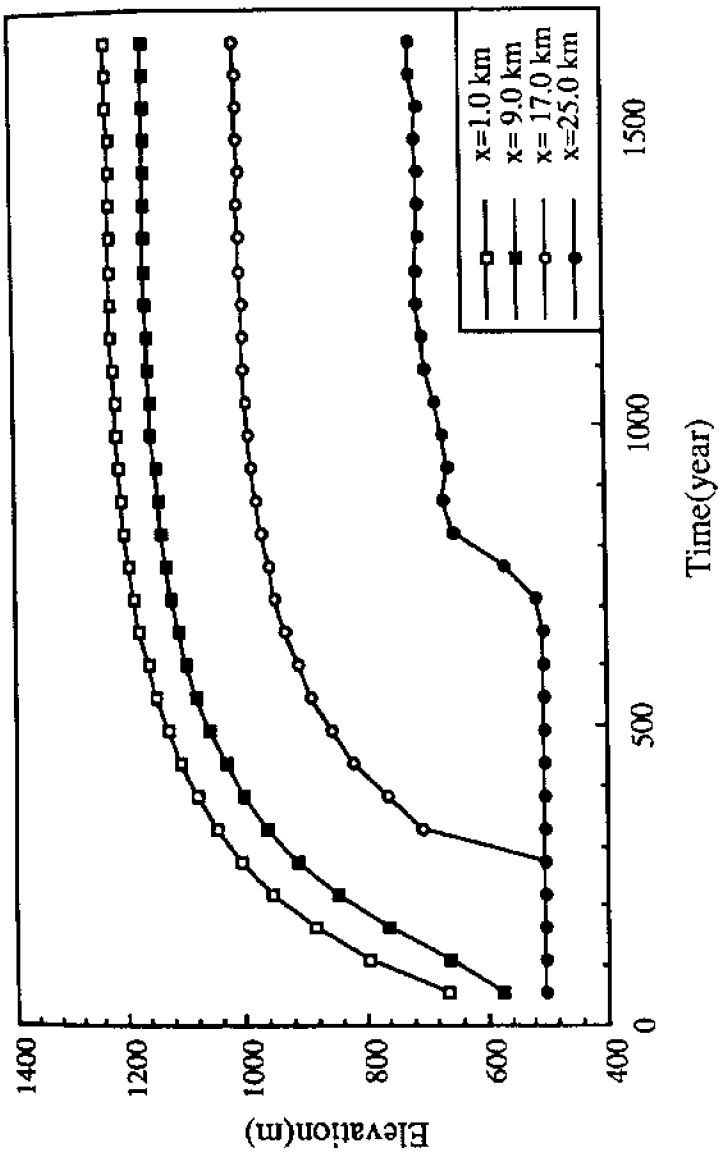

Fig. 3.3: Temporal Variation of Surface Elevation at Selected Locations

compares the numerical solution with analytical solution. The corresponding longitudinal variation of surface velocity and temporal variation of surface elevations at selected locations are shown in figures 3.2 and 3.3 respectively. Figures 3.1 and 3.3 show that as the glacier grows the rate at which it approaches steady state gradually decreases. The comparison of the analytical and numerical solution shows that over most of the glacier the two solutions coincide. However, as the terminus is approached the numerical model results depart slightly from the analytical solution. This discrepancy can be attributed to the assumption made in the development of the moving boundary conditions. As the actual length of the glacier for the given mass balance is not likely to be a multiple of grid size, which is 1.0 km, the terminus oscillates back and forth between the last two grid points as steady state is approached.

3.3.0 VERTICAL VELOCITY DISTRIBUTION

Nye(1965) has developed analytical solutions for the velocity distribution in channels of rectangular elliptic and parabolic sections. Assuming linear flow law, n= 1, the vertical velocity distribution in an infinitely wide channel of uniform depth D can be written as follows:

$$u(z) = u_b + \frac{1}{2}\rho\, g\, D^2\, A \sin\alpha \left(1 - \left\{1 - \frac{z}{D}\right\}^2\right) \qquad (3.2)$$

where α is the longitudinal surface slope. The term, u_b, has been added to Nye's solution to account for bed sliding. The second term gives the vertical velocity distribution due to internal deformation of ice.

Figure 3.4 shows the longitudinal profile of a channel with a bed slope of 0.025. The initial surface profile was assumed parallel to the bed. At the boundaries,

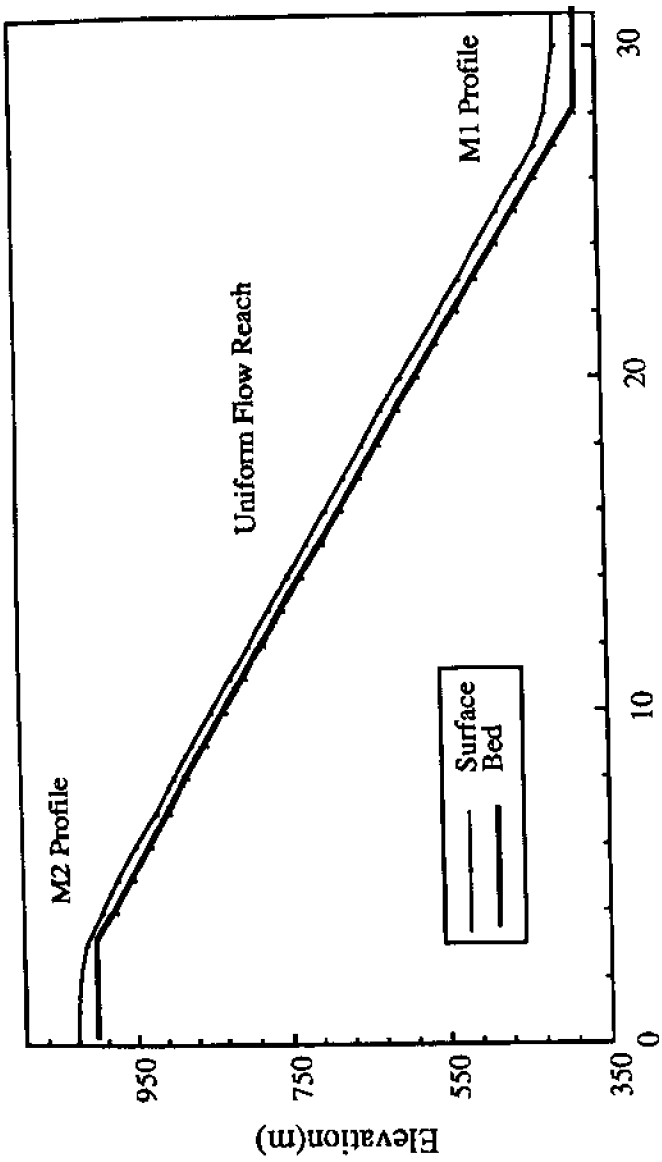

Fig. 3.4: Longitudinal Variations of Channel Bed and Steady State Surface Profile

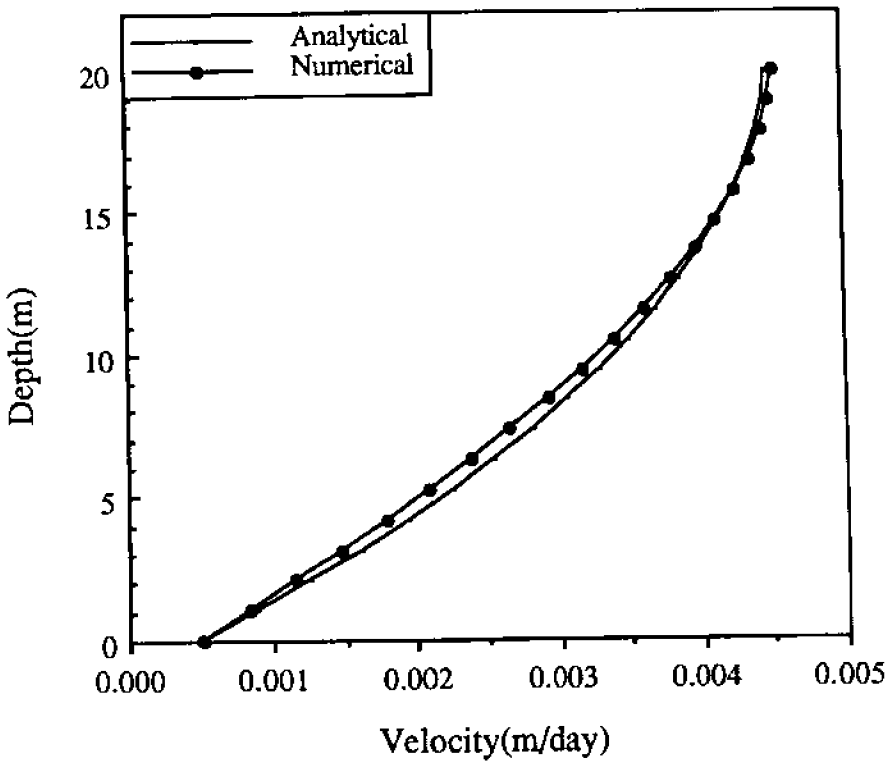

Fig. 3.5: Comparison of Vertical Velocity Profile With Analytical Solution of Nye(1965)

surface elevations were fixed to specified elevations such that difference in ice surface elevation at the entrance and exit of the channel was 750.0 m over a distance of 30.0 km. The numerical model was run for the specified boundary conditions with dynamic viscosity of 12.0 x10^9 m^2/s until steady state was reached. The figure also shows the computed longitudinal surface profile. Figure 3.5 compares the vertical velocity profile given by the numerical model with analytical solution. The bed velocity u_b for the analytical solution was set equal to the bed sliding obtained from the numerical solution. The density of ice was taken as 900 kg/m^3 and the value of A was taken as the reciprocal of kinematic viscosity. The agreement between the two solutions is good. The minor difference between the two solutions is mainly due to two different approaches used in the computation of the profiles. The analytical solution is a parabolic profile, while the model attempts to approximate the profile with a cosine function. The use of cosine functions to reproduce the vertical velocity is attractive as pointed out in Chapter-2.

3.4.0 SURFACE WAVE PROPAGATION

Nye(1960) first applied the concept of kinematic wave propagation to glaciers and derived the governing equation and its solution along characteristic curves. The analysis considers a wave as a point moving with a velocity different from the velocity of ice and does not imply a travelling 'wave train' (Hutter 1983; Paterson, 1981). When diffusion is negligible the wave velocity, c_o, can be approximated by the following equation (Nye, 1960):

$$c_o = (n+1)\,(u_s - u_b) + (m+1)\,u_b \qquad (3.3a)$$

where m and n are the flow and friction law exponents, u_s and u_b are the surface and bed velocities respectively. For linear flow and friction laws equations(3.3a) can be further simplified to the following:

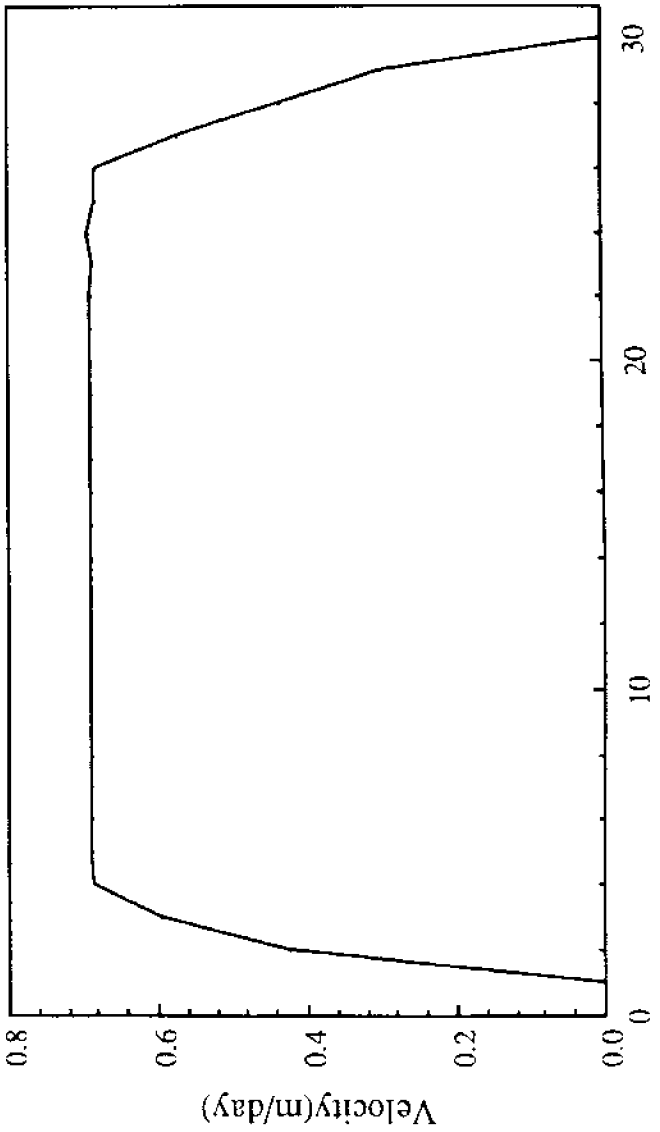

Fig.3.6: Longitudinal Variation of Surface Velocity in a Channel

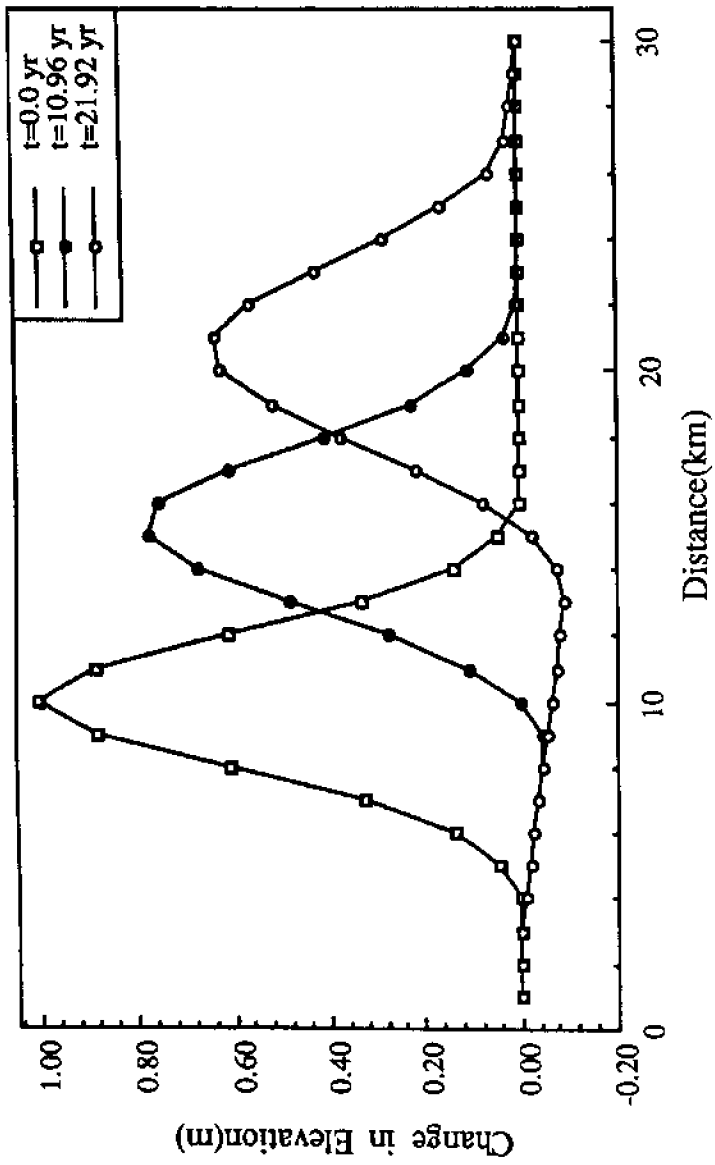

Fig. 3.7: Propagation of Surface Wave in a Channel

$$c_o = 2\,u_s \qquad (3.3b)$$

To study the propagation of surface waves, the same experimental set-up shown in figure 3.4 was used. However, viscosity of the ice was decreased to 12.0 $x10^6$ m^2/s, so that the wave propagation is reasonably fast. Figure 3.6 shows the longitudinal surface velocity distribution in the channel. The average velocity in the channel was about 0.67 m/day. At time t=0 a Gaussian hump of one meter height was introduced. Figure 3.7 shows the propagation of the hump as a function of time. In 21.92 years the hump has covered a distance of 11.5 km. Therefore, c_o is approximately 1.44 m/day. As the wave propagates downstream, its height decreases and the base of the hump increases due to diffusion. The computed ratio of wave and surface velocities is 2.15, slightly greater than the theoretical value of 2.0. The ratio is slightly higher mainly due to the local increase in flow velocity induced by the propagation of the Gaussian hump.

3.5.0 RESPONSE TO PERTURBATIONS

To study the response of a glacier to surface perturbation and mass balance change, two numerical experiments were performed on a glacier resting on a sloping bed as shown in figure 3.8. These experiments are similar to that performed by Bindschadler(1982). Altitude dependent accumulation and ablation rates were specified. For the assumed viscosity and friction coefficient, the model was run to obtain a steady state glacier. The computed steady state surface profile is shown in figure 3.8. Figure 3.9 shows the variations of surface velocity and the ice thickness. In the first experiment, a 1.0 m ice slab was added over the entire length of the glacier. Other parameters remained the same, figure 3.10 shows the temporal deviations of the surface profile from the equilibrium configuration. In the second numerical experiment, the steady state glacier was subjected to sudden increase in mass balance of 0.1 m/year. Figure 3.11 shows

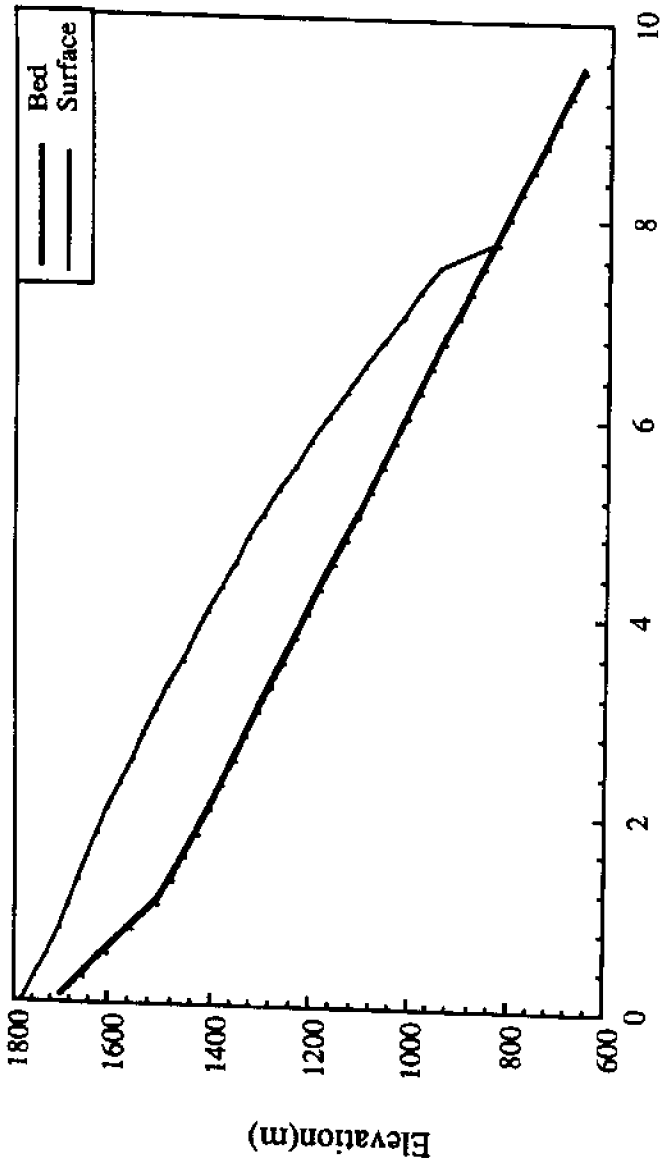

Fig. 3.8: Longitudinal Variations of Bed and Steady State Surface Profiles in a Test Glacier

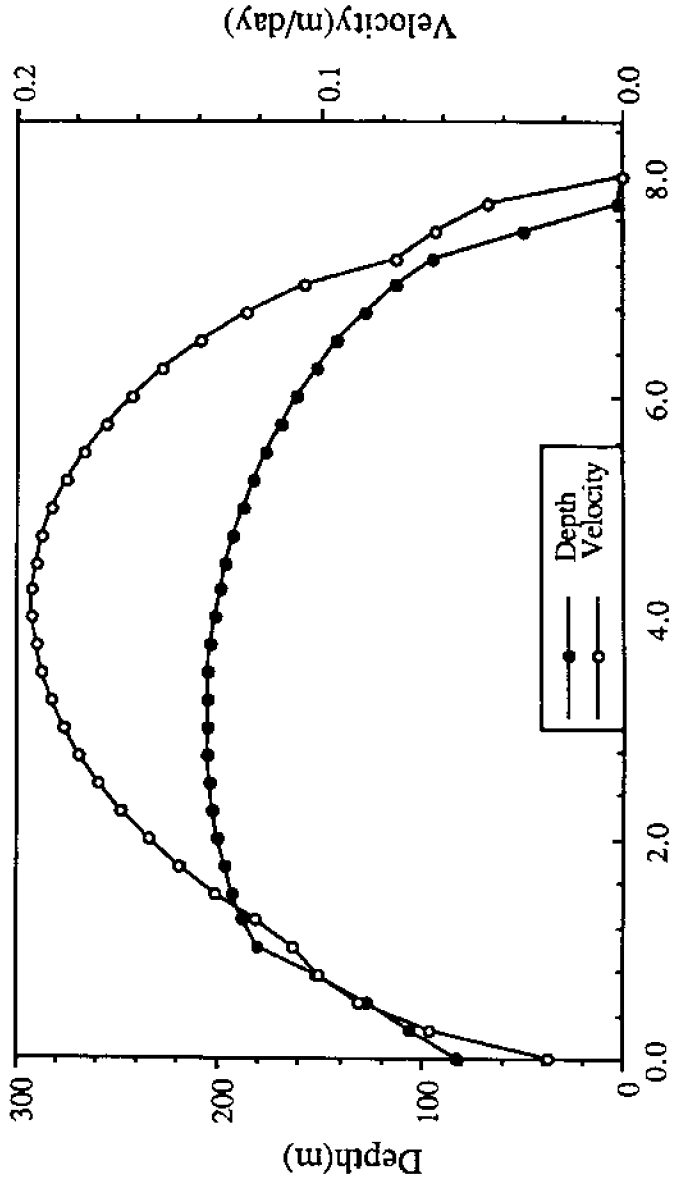

Fig. 3.9: Longitudinal Variations of Surface Velocity and Ice Theickness in the Test Glacier

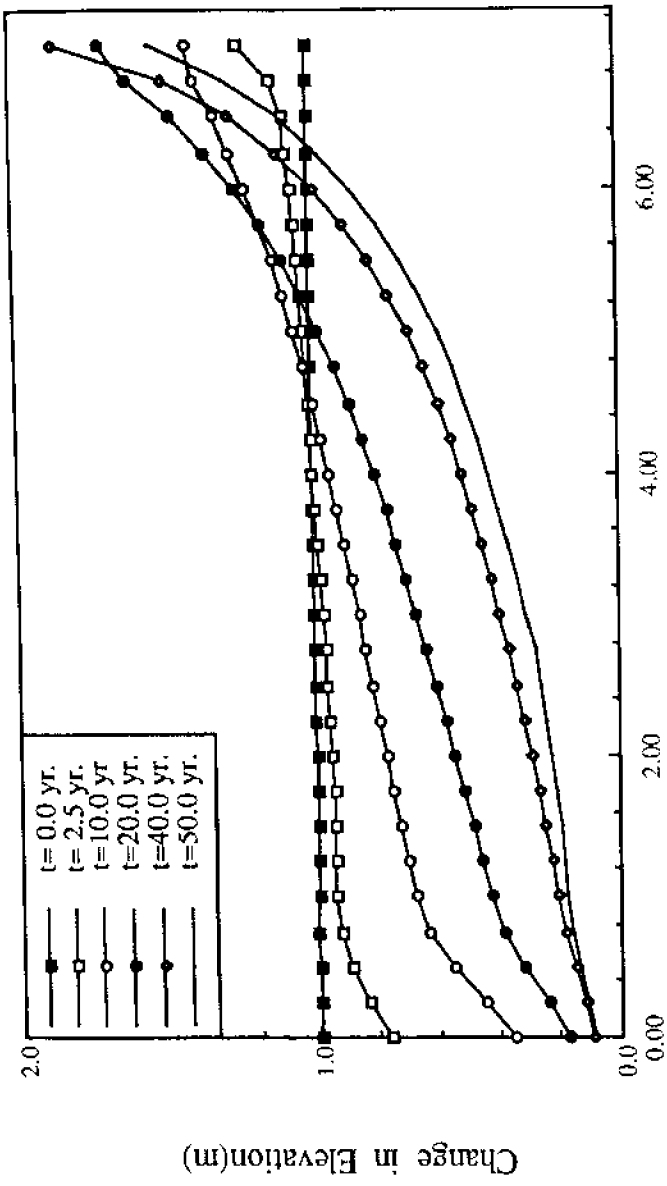

Fig. 3.10: Response of the Test Glacier to 1.0 m Increase in Ice Thickness

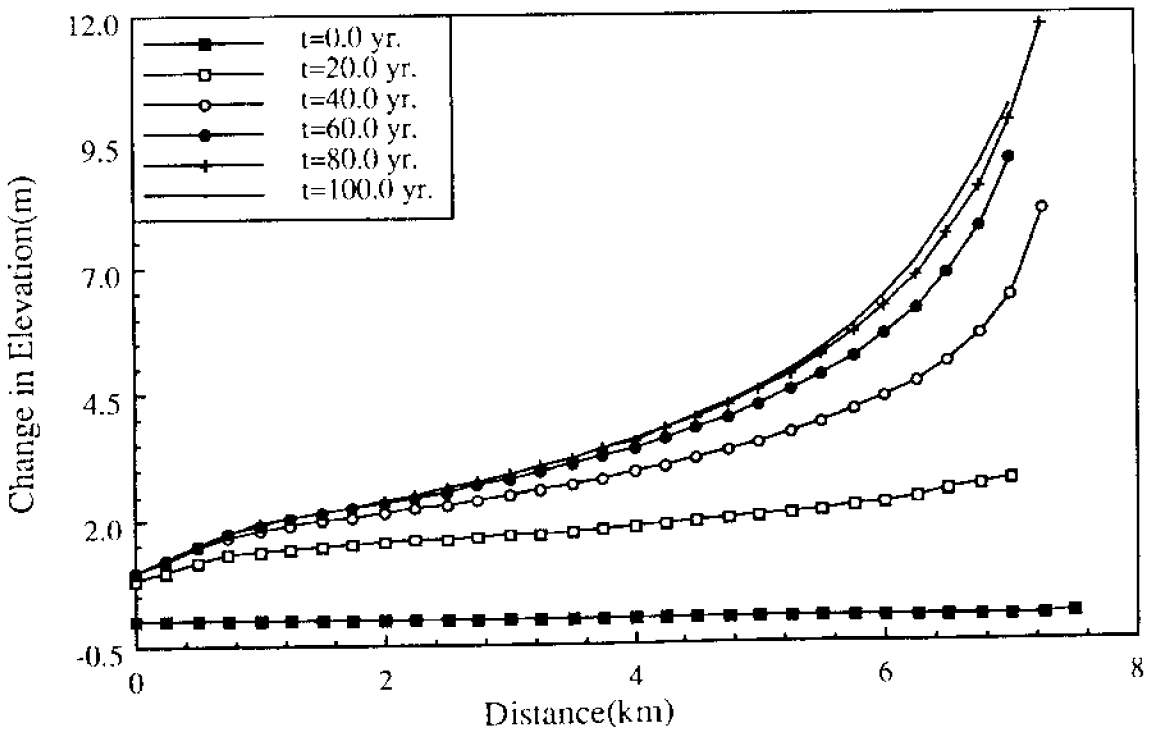

Fig.3.11: Response of the Test Glacier to an Uniform Increase in Mass Balance by 0.10 m/year.

the response of the idealized glacier with respect to the equilibrium surface profile. Qualitatively, the response curves are in good agreement with the theoretical predictions (Nye, 1960) and with the numerical results of Bindschadler(1982). Precise quantitative comparisons with the analytical solution of Nye(1960) are not possible because 1) the numerically computed response curves are not along the characteristics paths, 2) the analytical solution is function of physical parameters of glacier (field data are needed to determine these parameters) and 3) the numerical experiment represents a much more complex situation than that for which the analytical solutions are applicable.

3.6.0 APPLICATION TO THE FEDCHENKO GLACIER

To study the relative magnitudes of stress-gradient terms (Budd, 1970) and the effects of flow law on the computed surface profile, the model was applied to Fedchenko Glacier in Soviet Central Asia. The data necessary for the model application, bed topography and mass balance, were extracted from Budd(1975) at one kilometer intervals. Figures 3.12 and 3.13 show the mass balance and bed topography of the glacier. Actual field data were processed and filtered by Budd(1975) to get the smooth mass balance curve and bed profile. However, these data represent the overall geometry and characteristics of the Fedchenko Glacier. Initial ice thickness was assumed, and the model was run with different values of friction coefficient, until steady state was attained. The viscosity of ice was 12.0×10^9 m^2/s in all the runs. Figure 3.13 compares computed steady state surface profile with that obtained by Budd(1975) for $c_b = 50.0 \times 10^6$. The time required by the model to reach steady state was about 1150 years. Budd(1975) had to run his model for 700 to 1000 years to attain steady state. Figure 3.14 shows the longitudinal variations of surface and bed velocity along the glacier. The longitudinal variations of ice thickness and bed shear stress are shown in figure 3.15. The results of the two models practically coincide, except near the terminus. This discrepancy in the last few kilometers is mainly due to the difference in the

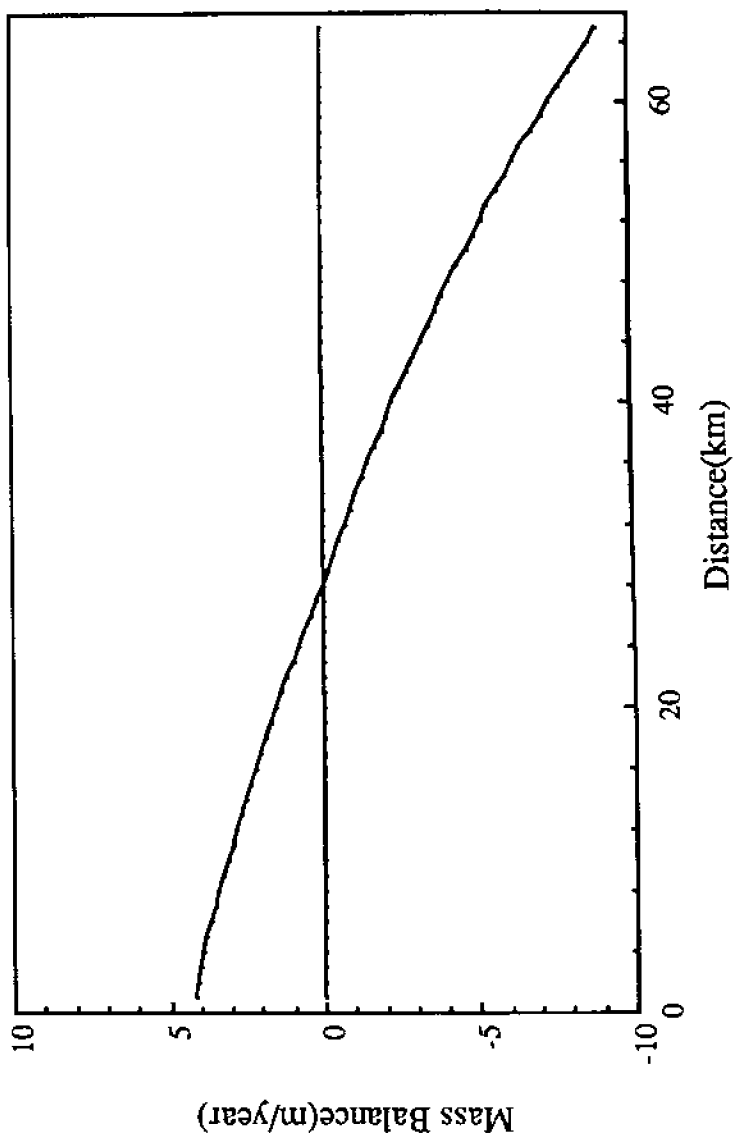

Fig. 3.12: Mass Balance Distribution of the Fedchenko Glacier (Budd, 1975)

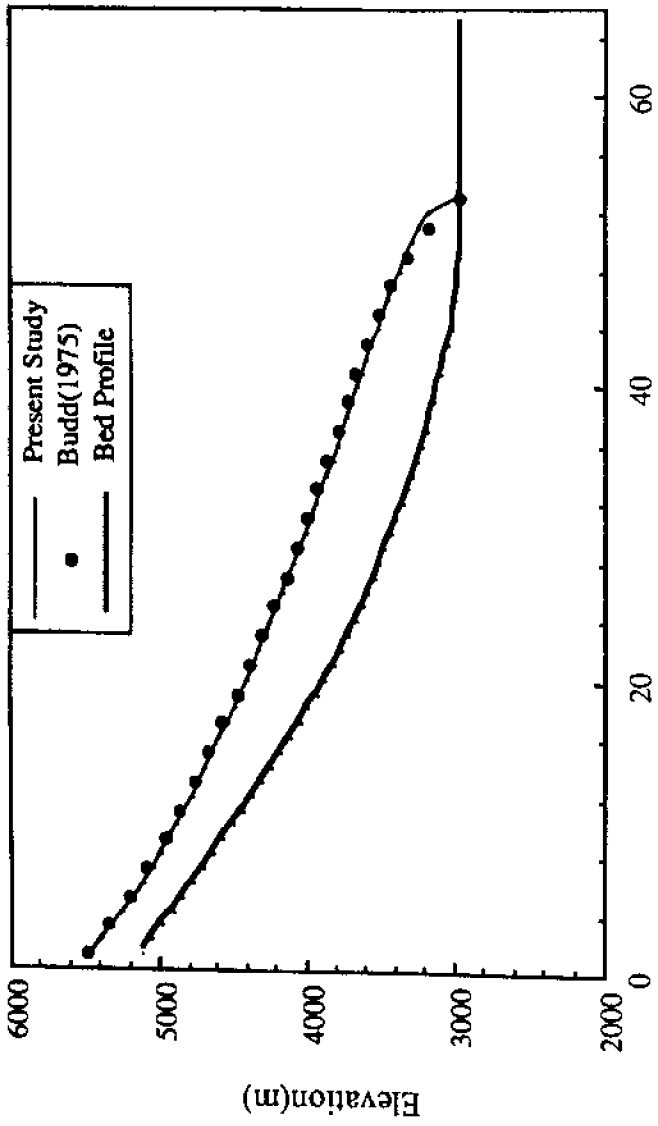

Fig. 3.13: Comparison of the Computed Steady State Surface Profile of the Fedchenko Glacier With Budd(1975)

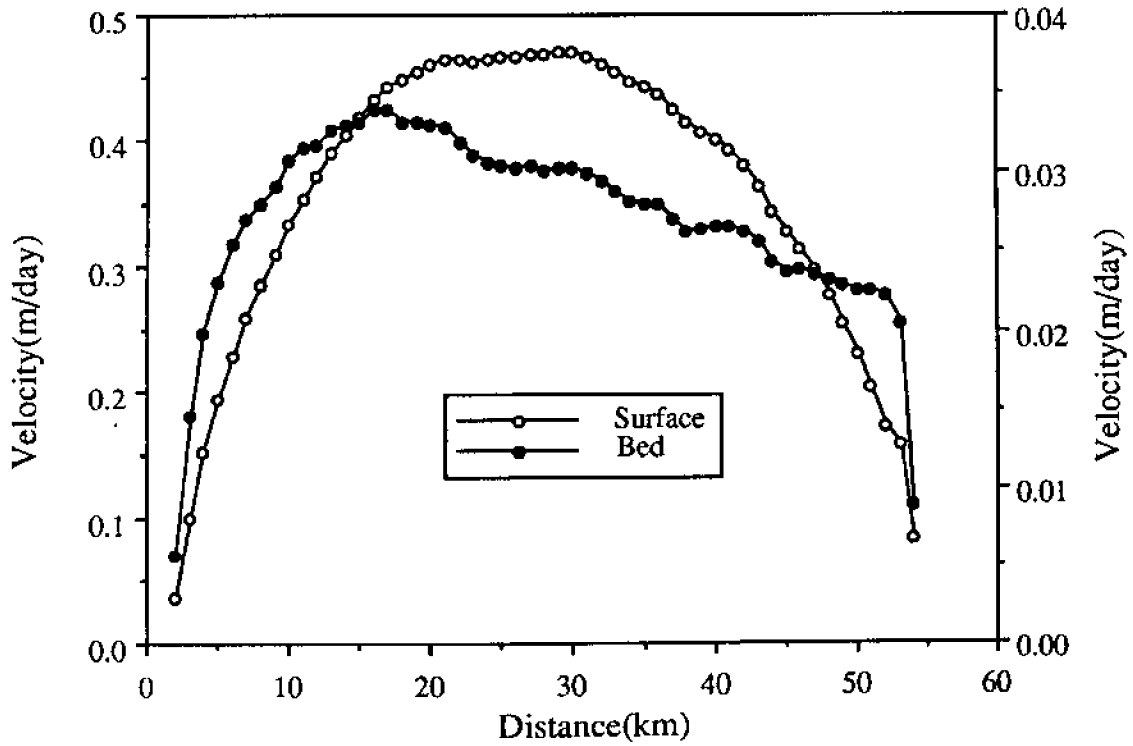

Fig. 3.14: Longitudinal Variations of Surface and Bed Velocity in the Fedchenko Glacier

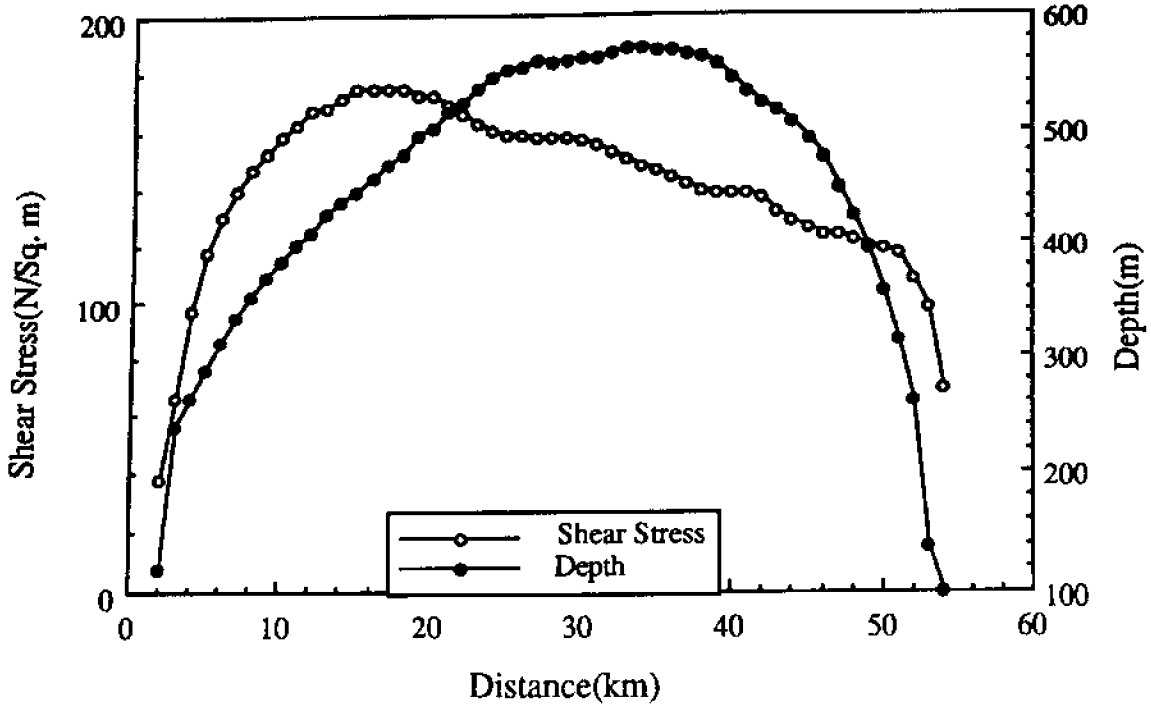

Fig. 3.15: Longitudinal Variations of Ice Thickness and Bed Shear Stress in the Fedchenko Glacier

assumptions made in the development of the moving boundary condition. This modelling exercise further indicates that the moving boundary conditions at the terminus does not significantly affect the over all computed behavior of the glacier.

3.7.0 ANALYSIS OF STRESS GRADIENTS

Studies of stress components in a flowing mass of ice by Budd(1970) indicate that if a grid spacing of less than 20 times the local ice thickness is used, the computations of stress are complicated by the presence of longitudinal stress gradients. Equations relating only the local surface slope of ice to basal shear stress are no longer appropriate. Budd(1970) suggested the following relationship for computing basal shear stress:

$$\tau_b = \rho\, g\, D\, \alpha + 2G - T \tag{3.4}$$

where

$$T = \int_H^{\eta} \int_H^{z} \frac{\partial^2 \tau_{xz}}{\partial x^2}\, dz\, dz \tag{3.5}$$

$$G = \frac{\partial}{\partial x} \int_H^{\eta} \sigma'_x\, dz \tag{3.6}$$

Assuming that ice follows Glen's flow law (visco-plastic material) and the vertical variation of velocity is small compared to the surface velocity, equation(3.6) can be expressed as follows (Paterson, 1981):

$$G = \frac{1}{A^{1/n}} \frac{\partial}{\partial x} \left\{ D \left| \frac{\partial u}{\partial x} \right|_{\eta}^{1/n} \right\} \operatorname{sgn}\left[\frac{\partial u}{\partial x}\right] \tag{3.7}$$

In equation(3.7) 'sgn' denotes 'the sign of'. The third term in equation(3.4) is called the variational stress since it represents the resistance of the ice to a changing stress gradient in the line of motion. It is usually associated with curved particle paths. Budd(1970) indicated that if D and α are averaged over twenty times the ice thickness, T becomes negligible compared to total stress. The second term is the stress-deviator gradient which represents the net longitudinal stress on the column of the ice. It determines whether the column will extend or compress in the line of motion, and is important if grid spacing is less than four times the ice thickness.

For Newtonian viscous fluids (n=1) shear stress is related to vertical velocity gradient by the following relationship (White, 1973):

$$\tau_{xz} = \frac{N_v}{\rho} \frac{\partial u}{\partial z} \tag{3.8}$$

Substituting the expression for velocity from equation(2.22) and using the σ transformation given by equation(2.14), τ_{xz} can be expressed as follows:

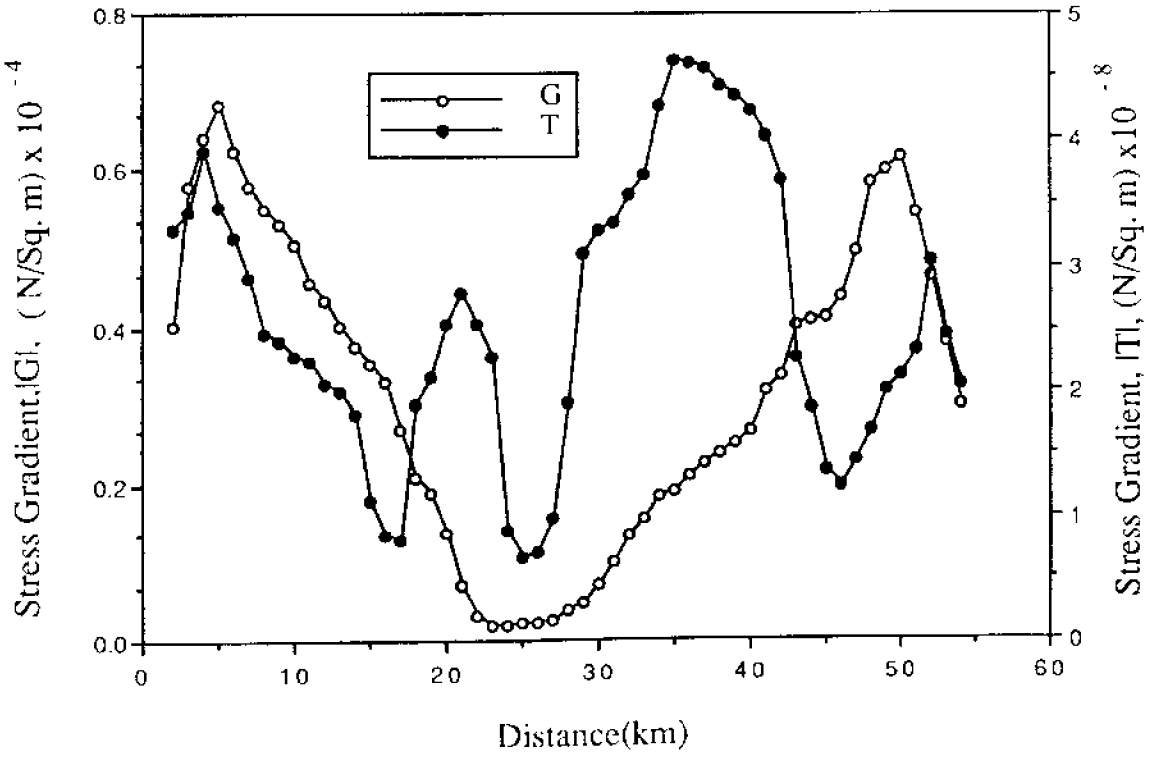

Fig. 3.16: Longitudinal Variations of the Magnitudes of Stress Gradient Components T and G

$$\tau_{xz} = \frac{N_v}{\rho D} \sum_{I=1}^{N} a_I c_I \ \mathrm{Sin}\left\{\frac{1}{2} a_I (2-\sigma)\right\} \tag{3.9}$$

and the expression for T can be written as follow:

$$T = \frac{4 N_v D}{\rho} \sum_{I=1}^{N} \frac{1}{a_I} \left\{\mathrm{Sin}\, a_I - a_I \mathrm{Cos}\, a_I\right\} \frac{\partial^2 c_I}{\partial x^2} \tag{3.10}$$

In deriving these equations a_I and D are assumed to remain constant over a distance of $2\Delta x$.

Figure 3.16 shows the distribution of the magnitudes of G and T in the Fedchenko Glacier. The grid size used for this application of the model was 1.0 km. The corresponding variations of ice thickness and bed shear stress, computed on the basis of equations(2.7), are shown in figure 3.15. The stress-gradient terms are small compared to basal shear stress, but they are highly non-linear as indicated by figure 3.16. This behavior can be attributed to the non-linearity associated with the longitudinal distributions of velocity and ice thickness as indicated in figures 3.14 and 3.15. As T and G are functions of the gradients of velocity and depth, small oscillations in velocity and ice thickness are greatly amplified. This analysis indicates that T and G are very small compared to τ_b. Therefore, in applying the model to a glacier, the grid spacing of the same order of magnitude as the ice thickness can be used without considering the effects of longitudinal stress gradients.

3.8.0 CONCLUSIONS

To ascertain the simulation characteristics and the assumptions made in the development of the model, numerical experiments were performed for simple cases where analytical solutions are available. All the comparisons were made for

n =1. The computed steady state surface profile of a glacier on a horizontal bed matches quite well with the analytical solution by Paterson(1972). The computed vertical velocity profile is consistent with the analytical solution of Nye(1965). The velocity of surface wave propagation is slightly higher than the theoretical value, because of the local increase in flow velocity. The response of a test glacier to the sudden addition of a uniform ice layer and change in accumulation and ablation rates is similar to the analytical prediction of Nye(1960) and the results of Bindschadler(1982) for similar experiments. Application of the model to Fedchenko Glacier shows that the computed steady-state profile is practically the same as that of Budd(1975). Analysis of longitudinal stress gradients shows that these stresses are small compared to total bed shear stress. Therefore, the present model can be used for simulation with grid spacing of the same order of magnitude as the ice thickness.

4. CLIMATIC PERTURBATIONS

4.1.0 INTRODUCTION

Since the turn of this century, measurements of relative sea levels suggest a global average sea level rise of 1 to 3 mm/year (Meier, 1985 and 1984). Table-4.1, based on data from U.S. Department of Commerce, National Oceanic and Atmospheric Administration (Bruun,1972), shows the yearly average rise in mean sea level along the Eastern Seaboard of the United States. During this period the atmospheric and the ocean surface temperatures appear to have increased by 0.6± 0.3 °C (Meier, 1985; Hoffert and Michael 1983). This climatic warming has been mainly attributed to the increased CO_2 concentration in the atmosphere. In 1870 global mean concentration of CO_2 was about 285 ppmv, and it has increased to about 350 ppmv in the eighties (Wallen, 1983; Lorius and Raynaud, 1983). Figure 4.1 shows the observed monthly variation of CO_2 concentration at Barrow, Alaska (World Meteorological Organization, 1985). The figure indicates that the concentration of CO_2 varies from month to month, with an average amplitude of about 16.2 ppmv. The concentration is high during warmer months and lower in the colder period. The yearly mean concentration is increasing at an annual rate of about 1.32 ppmv and this rate is expected to increase sharply until the middle of the 22-nd. century. Estimates by Bjorkstrom(1983) indicate that the concentration of CO_2 will reach a maximum value of around 700-800% of pre-industrial level in the second or third quarter of 22-nd century. The concentration of CO_2 will double by the second half of the next century. The molecular structure of CO_2 is such that it absorbs radiative energy of wave-length between 13 to 18 μm (Wallen, 1983). As the terrestrial radiation is intense in the 15 μm band of the infrared spectrum, much of the long-wave radiation from the earth is absorbed by CO_2 and re-emitted back. Thus, an

Table-4.1: Average Sea-level Rise Along the Eastern Seaboard, U.S.A.(Bruun, 1972)

Location	Period	Rise(cm/year)
Eastport, Maine	1930-69	0.338
Portsmouth, New Hampshire	1927-70	0.165
Woods Hole, Massachusetts	1933-70	0.268
Newport, Rhode Island	1931-70	0.210
New London, Connecticut	1939-70	0.229
New York, New York	1893-70	0.287
Sandy Hook, New Jersey	1933-70	0.457
Baltimore, Maryland	1903-70	0.259
Washington, D.C.	1932-70	0.244
Portsmouth, Virginia	1936-70	0.341
Charleston, South Carolina	1922-70	0.180
Fort Pulaski, Georgia	1936-70	0.198
Mayport, Florida	1929-70	0.155
Miami Beach, Florida	1932-70	0.192
Pensacola, Florida	1924-70	0.040
Eugene I., Louisiana	1940-70	0.905
Galveton, Texas	1909-70	0.430

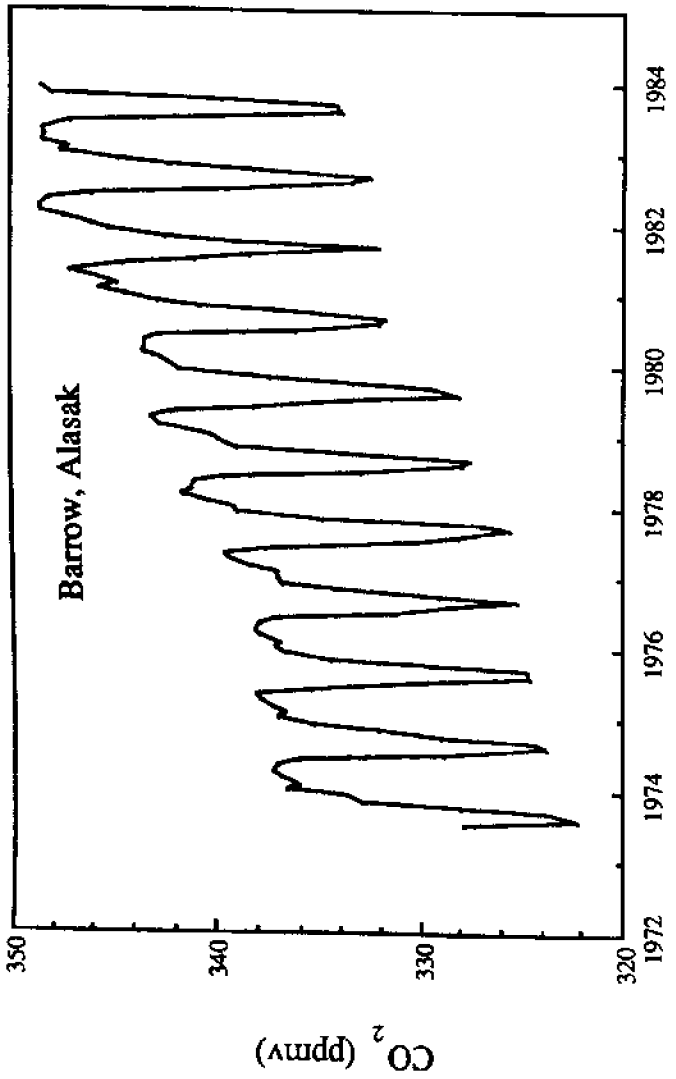

Fig. 4.1 : Variation of Monthly Mean CO_2 Concentration at Barrows, Alaska (World Meteorological Organization, 1985)

in CO_2 concentration in the atmosphere is accompanied by warming of the atmosphere, which is known as the "greenhouse effect" of the CO_2.

Calculations based on radiation models (Ramanathan, 1981; Hansen et al. 1981; Gilliland and Schneider, 1984; Kandel, 1983; Hoffert and Michael 1893), indicate that on doubling the atmospheric CO_2 content a global warming of 2 to 5 °C should be expected. The resultant temperature, however, may or may not increase in a similar proportion because many other variables are involved in the process. Figure-4.2 reproduced from Hansen et al.(1981) illustrates the effects of some of the parameters in changing the climatic temperature. The effects of atmospheric aerosols are not shown in the figure. Assuming that the solar luminosity remains constant in the next 100 years, the climatic warming could be partly compensated by increased land albedo and the low altitude clouds. The temperature rise will be amplified, by a factor of two to three, at higher altitudes especially in the northern hemisphere (Manabe and Stouffer, 1980; Gilliland and Schneider, 1984; Hansen et al. 1981; Hoffert and Michael 1893).

4.2.0 RESPONSE OF GLACIERS

The glaciers and ice caps of the world, excluding the ice sheets of Antarctica and Greenland, have in general, been shrinking during the last 100 years (Meier, 1985 and 1984). Glaciers and small ice caps thus, account for an important part of the observed sea-level rise. A third of the calculated glacier contribution to rising sea level comes from mountains bordering the Gulf of Alaska (Meier, 1985). The atmospheric warming will cause a further rise in sea level mainly by the melting of ice and by volume expansion of ocean water (Meier, 1985). The climatic warming will effect the glaciers in the following ways: 1) higher air temperatures will cause an increased rate of melting in the ablation areas, and 2) this warming will cause ablation areas to expand as equilibrium lines, which divide ablation area from accumulation area, retreat to higher elevations. Table-4.2, taken from Oerlemans(1988), lists the retreat of four European glaciers in

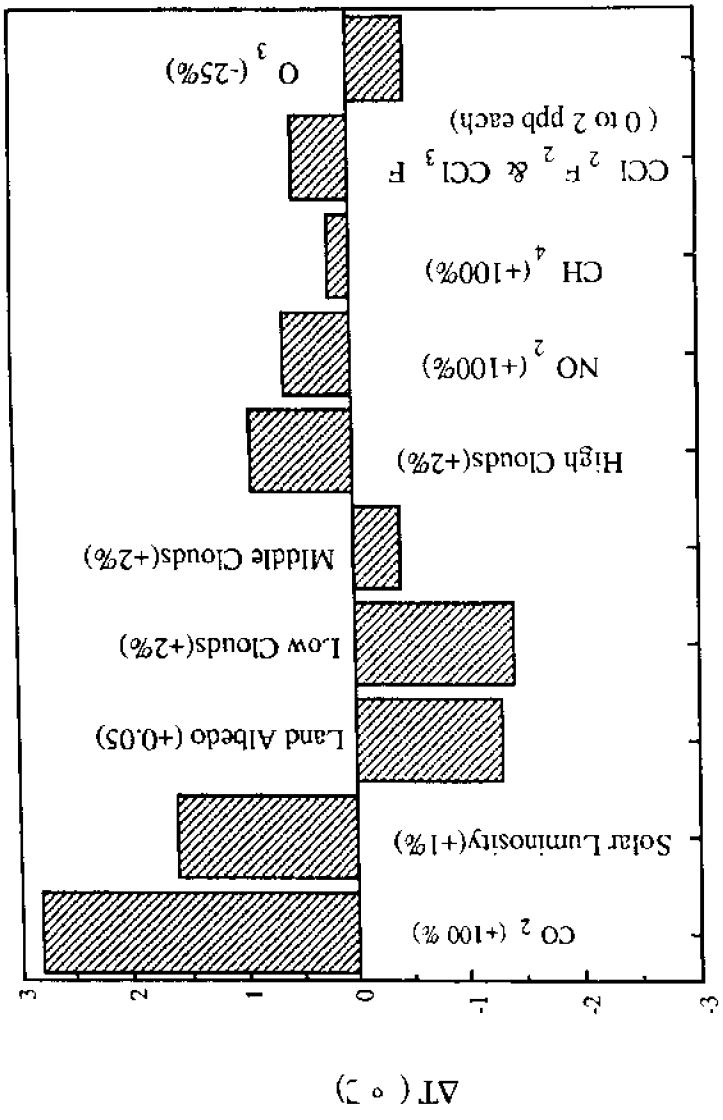

Fig. 4.2: Effects of Various Global Radiative Perturbations on the Surface Temperature (Hansen et al., 1985)

Table-4.2: Change in Equilibrium-Line Altitude Needed to Explain the Retreat of Five European Glaciers in the Last 150 Years (Oerlemans, 1988).

Glacier	Change in Length (kilometers)	Change in Equilibrium-Line Altitude(meter)
Nigardsbreen	3.90	120.0
Rhonegletscher	1.20	90.0
Glacier d' Argentiere	1.60	55.0
Hintereisferner	3.10	63.0

the last 150 years and the shift of the equilibrium line necessary to cause the retreat. The "greenhouse" warming is responsible for about 50 percent of the glacier retreat observed over the last 100 years (Oerlemans, 1988). Computations by Kuhn(1985) indicate that the equilibrium line will rise by 190 m in the European Alps for a rise of temperature by one degree. Analysis of Greenland Ice Sheet by Bindschadler(1985) indicates a rise of the equilibrium line ranging from 500 m to 1000 m corresponding to a surface temperature rise of 3 to 6 °C.

Three different methods for estimating the shift of the equilibrium line have been used in recent years. Mayo and Trabant(1984) have used statistical analysis of the available temperature and mass balance data to project the shift of equilibrium line of the Wolverine Glacier, Southern Alaska. Bindschadler(1985) has analyzed the altitudinal shift of the equilibrium line of the Greenland Icesheet, by assuming constant accumulation rate and a linear decrease of ablation with altitude. By balancing total accumulation and total ablation, the location of the equilibrium line was determined. The method which appears most promising was proposed by Kuhn(1980) and has been applied to the Greenland Icesheet (Ambach, 1985a, 1985b; Ambach and Kuhn, 1985) and mid-latitude glacier in Europe (Kuhn, 1985). Application of this method is dependent on the availability

of heat and energy balance data. Though most of this information is not directly available for the Taku Glacier, an attempt has been made to estimate the necessary parameters and study the effects of these parameters on the altitudinal shift of the equilibrium line of the Taku Glacier. This chapter describes Khun's algorithm for the computation of altitudinal shift of the equilibrium line and the methods for estimating the parameters involved in the algorithm.

4.3.0 KUHN'S ALGORITHM

The effects of climatic warming on glaciers can be parameterized by a rise in the equilibrium line and redistribution of accumulation and ablation areas and their rates. Kuhn(1980) has published a general algorithm to calculate the shift of the equilibrium line of mid-latitude glaciers in response to small climatic changes. Mid-latitude glaciers are glaciers having a mean annual ice temperature of 0 °C, with clearly distinguishable accumulation and ablation areas. Contrary to the polar-ice fields, mid-latitude mountain glaciers do not influence the general circulation or large-scale climate (Kuhn, 1985). Their existence modifies the local wind system. However, their presence or absence at the end of the summer season is of little effect compared to the interannual variability of the seasonal snow cover. Analysis of temperature data at different locations in the Taku Glacier indicates that the icefield can exert its influence on the free air temperature only in the zone 100 m immediately above it (Miller,1963). Therefore, analysis of the response of the mid-latitude glaciers are possible, without considering the effects of the glacier on the atmosphere.

Kuhn's algorithm links cumulative accumulation, S^+, with sensible heat flux, H_S, and radiation, R, as parameters of the energy balance. At the equilibrium line altitude, h, accumulation equals ablation ($S^+ = S^-$) and ablation can be parameterized as follows:

$$S^- = f(H_S, R) \qquad (4.1)$$

A climatic fluctuation in any of these variables (δS^+, δH_s and δR) is compensated by the altitudinal gradient $\partial S^+/\partial z$ measured along the glacier surface, such that an equilibrium is established at a new altitude, h+δh, where δh is given by:

$$\delta h = \frac{-\delta S^+ + \frac{\Gamma}{\Pi}\left(\delta R + \delta H_s\right)}{\frac{\partial S^+}{\partial z} - \frac{\Gamma}{\Pi}\left(\frac{\partial R}{\partial z} + \frac{\partial H_s}{\partial z}\right)} \qquad (4.2)$$

where Π is the latent heat of melting of ice, and Γ is the number of ablation days at the equilibrium line. To the first-order, the turbulent-heat flux from the atmosphere to the glacier is proportional to the temperature difference between the air and the ice surface. Therefore, for small temperature perturbations, the sensible heat flux, H_s, is related to the air temperature, by the following linearized relationship (Kuhn, 1979; Oerlemans, 1988):

$$H_s = \mu T_a \qquad (4.3)$$

where T_a is the air temperature and μ is the bulk heat transfer coefficient. According to Kuhn(1980) and Ambach(1985a), only the change in the long wave downward radiation with the air temperature (δR_o) needs to be taken into account in the change of the net radiation balance. The short wave radiation flux, the albedo and the long wave upward radiation flux of the surface remain constant. The effect of an atmospheric temperature change δTa on the long-wave downward radiation δR_o may be parameterized as follows (Ambach, 1985a, 1985b):

$$R_o = \mu' T_a \tag{4.4}$$

where μ' is the constant of proportionality and known as radiative transfer coefficient. According to Stefan-Boltzman law R_O is given by (Oerlemans and Veen, 1984; Holton, 1979):

$$R_o = \nu \varphi T_a^4 \tag{4.5}$$

with ν being the relative emissivity and φ is known as Stefan-Boltzman constant. Therefore, the change in the long-wave downward radiation with temperature is:

$$\delta R_o = 4 \nu \varphi T_a^3 \delta T_a \tag{4.6}$$

Comparison of equations(4.4) and (4.6), and noting that at the ice surface the air temperature is equal to the temperature of ice, T_S, μ' is given by (Kuhn, 1979 and Ambach, 1985b):

$$\mu' = 4 \nu \varphi T_s^3 \tag{4.7}$$

Remembering that only the change in the long wave downward radiation with the air temperature (δR_o) needs to be taken into account in the change of the net radiation balance ($\delta R_o \approx \delta R$) , the altitudinal gradient of radiation can, therefore, be written as follows:

$$\frac{\partial R}{\partial z} = \mu' \frac{\partial T_a}{\partial z} \tag{4.8}$$

and the equation for altitudinal shift of the equilibrium line becomes:

$$\delta h = \frac{-\delta S^+ + \frac{\Gamma}{\Pi}(\mu + \mu')\delta T_a}{\frac{\partial S^+}{\partial z} - \frac{\Gamma}{\Pi}(\mu + \mu')\frac{\partial T_a}{\partial z}} \tag{4.9}$$

In equation(4.9) δT_a represents the amount of global warming. The value of δh thus determined establishes the position of the new accumulation area for a given topography. Thus, knowing δh and $\partial S^+/\partial z$ and having a suitable ice-dynamics model, the transient glacier behavior to a changed climate can be predicted. The transient behavior of the Taku Glacier will be discussed in Chapter-6.

4.3.1 Assumptions

The following assumptions were made by Kuhn(1979) and Ambach (1985a, 1985b) to arrive at equation(4.9):

1. The sensible heat flux across the melting ice surface and long wave downward radiation flux are linear functions of air temperature.

2. The mass loss by evaporation is negligible.

3. Change in the latent heat flux H_L and the altitudinal gradient $\partial H_L/\partial z$ is zero.

4.The dependence of S^+, R, and T_a on the altitude is taken into account in the region of the equilibrium line by the altitudinal gradients $\partial S^+/\partial z$, $\partial R/\partial z$ and $\partial T_a/\partial z$.

5.The duration of the ablation season is assumed to be constant regardless of the disturbances in S^+, R, and T_a.

6.The specific net balance is zero at the end of the balance year in the new position of the equilibrium line regardless of the disturbances in S^+, R and T_a.

7.The parameters S^+, R, and T_a are independent variables. In nature they will most likely to be interrelated and hence a combination of their influence will prevail.

4.3.3 Estimation of Parameters

To apply equation(4.9) to a particular glacier or ice sheet it is necessary to determine μ, μ', and ν from field data. φ is taken as constant. In addition mass balance data are necessary to determine change in accumulation and altitudinal gradient of accumulation. Assuming a logarithmic wind velocity profile, the bulk heat transfer coefficient can be expressed as follows (Kuhn, 1979):

$$\mu = \frac{\rho\, c_p\, U_* \,\kappa}{\phi \ln(z_a/z_o)} \qquad (4.11)$$

where ρ is the density of air, c_p is specific heat of air at constant pressure, U_* is the friction velocity at the ice surface, κ is the von Karman's constant, ϕ is a stability function for the atmosphere, z_o is roughness height, and z_a is the height

from the surface at which air velocity is measured. The density and specific heat of air are 1.225 kg/m^3 and 1004 $J\ ^{\circ}K^{-1}\ kg^{-1}$ respectively, κ is approximately equal to 0.4, and ϕ is 1.0 for neutral stratification of the atmosphere (Gill, 1982; Holton, 1979). No information about friction velocity and surface roughness is available for the Taku Glacier. The surface roughness z_o is not a well defined parameter. Table-4.3, taken from Kuhn(1979) shows the compilation of wind velocity and friction velocity in six melting glaciers or ice sheets. Figure-4.3 shows the plot of friction velocity as a function of wind velocity, which indicates a linear relationship. The best fit linear equation is given by:

$$U_* = -0.0308 + 0.0753\ U_w \qquad (4.12)$$

where U_w is the wind velocity in meters per second at a height of 2 m from the surface and U_* is friction velocity. The coefficient of correlation, r^2, is 0.973. The surface roughness values applicable to snow and ice surfaces (Kuhn, 1979 and Morris 1989) are presented in table-4.4, and it varies from 0.091 to 0.69 cm. An increase of z_o by two orders of magnitude only doubles the value of α. Therefore, in this analysis z_o is assumed 0.338 cm, which is the mean of the values listed by Kuhn(1979) and Morris(1989). Thus from information of wind velocity over the Taku Glacier, the value of μ can be computed.

Equation(4.7) indicates that μ' is a function of emissivity and surface temperature. The Stefan-Boltzman constant φ has a value of $5.67 \times 10^{-8}\ W\ m^{-2}\ ^{\circ}K^{-4}$ (Gill,1982; Holton,1979) and temperature at the ice surface T_s is taken as 273.2 °K (Oerlemans and Veen, 1984). The emissivity, ν, is function of the long wave radiation balance and cloudiness and its value can vary from 0.5 to 1.0 (Oerlemans and Veen, 1984). Higher air temperature leads to larger atmospheric humidity and thus to increased emissivity. For the average atmospheric conditions, $\nu = 0.9$ (Oerlemans and Veen, 1984).

Table-4.3: Representative Wind Velocity and Friction Velocity (Kuhn, 1979)

Glacier	Wind Velocity (m/s at 2m)	Friction Velocity (m/s)
Saint Sorlin	6.60	0.46
	5.00	0.37
	4.20	0.31
Hornkeers	4.00	0.25
Vernagt	3.00	0.17
Camp-IV-EGIG	2.80	0.16
Zentralnyy Tuyuksu	2.00	0.12
Chogo Lungma	1.30	0.09

4.3.0 CONCLUSIONS

This chapter presents a largely accepted scenario of the global temperature rise due to greenhouse effect and the response of glaciers. Khun's algorithm for the computation of the altitudinal shift of the equilibrium line has been described. The purpose is to allow calculations of the response of the Taku Glacier to climatic changes in Chapter-6. The information necessary to apply Khun's algorithm to a particular glacier are : 1) the heat transfer coefficient of the sensible heat flux, 2) the effective emissivity of the atmosphere for the long wave downward radiation, 3) a factor relating net radiation to cloudiness, 4) the duration of the ablation season, 5) the altitudinal temperature gradient, and 6) the altitudinal accumulation

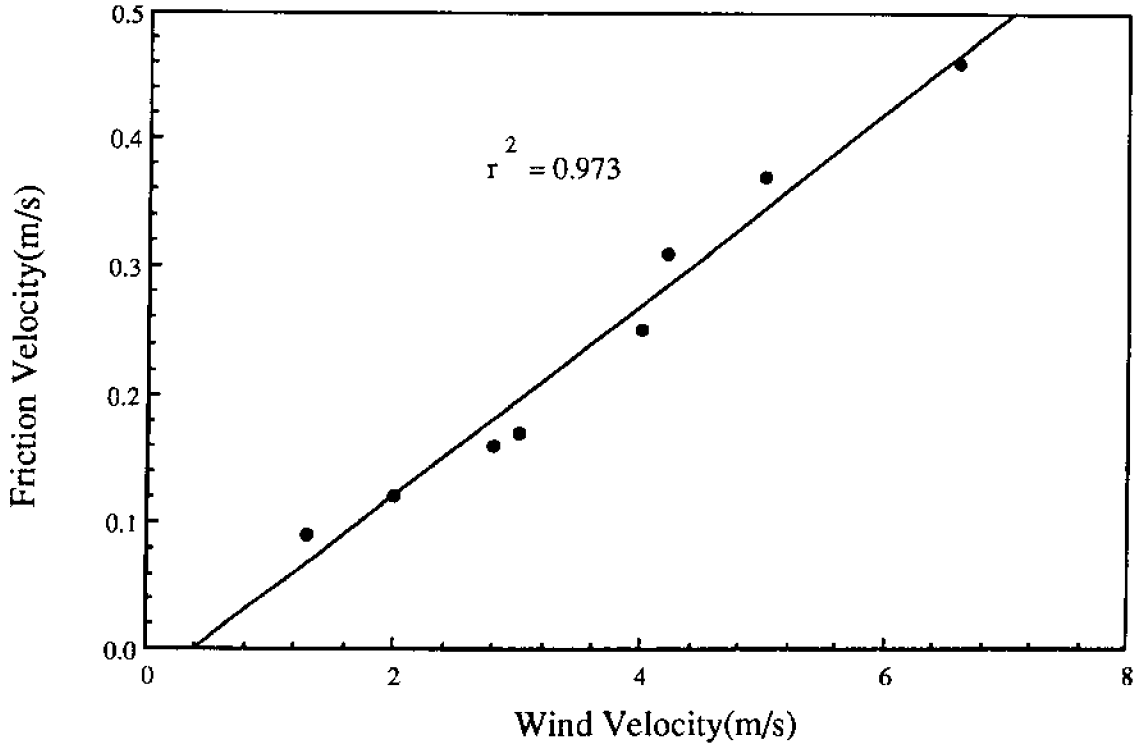

Fig. 4.3: Relationship Between Wind Velocity and Friction Velocity on Snow and Ice Surfaces (Kuhn, 1979)

Table-4.4: Roughness Heights of Snow and Ice Covered Areas
(Kuhn, 1979 and Morris 1989)

Glacier	Surface Roughness (cm)
Saint Sorlin	0.55
	0.69
	0.67
Hornkeers	0.17
Vernagt	0.15
Camp-IV-EGIG	0.18
Zentralnyy Tuyuksu	0.11
Chogo Lungma	0.20
Britannia Glacier	0.68
	0.58
Lemon Creek Glacier	0.09
McCall Glacier	0.09
	0.24

gradient. The bulk heat transfer coefficient, μ, is related to density and specific heat of air, friction velocity and surface roughness parameters by equation(4.11). The friction velocity is computed by the empirical relationship, equation(4.12), and is based on field data from Kuhn(1979). The surface roughness parameter is taken as the mean of available field data(Kuhn 1979; Morris, 1989). Equation(4.11) indicates that an error of one order of magnitude in estimating roughness parameter only doubles the value of the heat transfer coefficient. Another source of error is the computation of friction velocity by equation(4.12). It should be pointed out that extrapolation of friction velocity, based on equation(4.12), is not justified if the wind velocity exceeds 7.0 m/s or falls

below 1.5 m/s. As an illustration, if wind velocity is zero, the friction velocity should also be zero. However, equation(4.12) gives a negative friction velocity which is an absurd situation. In estimating the value of μ' the source of error is the error in the value of the emissivity, ε. Theoretically, emissivity can vary from 0.5 to 1.0 and the global mean is 0.9. Analysis of heat balance data of the Greenland Ice Cap along the International Glaciological Greenland Expedition (EGIG) profile by Ambach(1985a, 1985b) gives a value of 0.92 for 0.5 cloudiness. Therefore, the error in estimating μ' is not expected to be high.

5. THE TAKU GLACIER

5.1.0 INTRODUCTION

The Coast Range of southeast Alaska and adjacent British Columbia contains 88,000 km^2 of glacial ice. There are 750 Coast Range glaciers with an area exceeding 15 km^2. The Taku Glacier, shown in figure 5.1, is the largest glacier with an area of about 650 km^2. Because of the large size of Coast Range glaciers, the complete response to a mass balance change ranges from several decades to several centuries. For this reason, to successfully model a Coast Range glacier, a long record of mass balance and accompanying velocity fluctuations is required. The Taku Glacier has a sufficiently detailed and lengthy record to be used in a time dependent modeling study. Since 1946 the Juneau Icefield has been the site of extensive annual field measurements conducted by the Juneau Icefield Research Program (JIRP). Annual field measurements include determination of the equilibrium line altitude (ELA), balance gradient, glacier movement, glacier surface level, heat balance, surface meteorology and terminus fluctuations. The main emphasis has been on the Taku Glacier.

This chapter describes the topographic, and meteorologic conditions of the Taku Glacier, especially with respect to the application of the flow model and the computation of altitudinal shift of the equilibrium line. The input data necessary to the model the glacier include ice surface elevation, elevation of the glacier base, and surface mass balance. Surface mass balance has been monitored since 1949 using techniques described by LaChapelle(1954), Nielsen(1957), Miller(1963) and Pelto(1987). The available data allow estimates of mean annual mass balance at any given point on the glacier to within ±10%. Surface elevation is

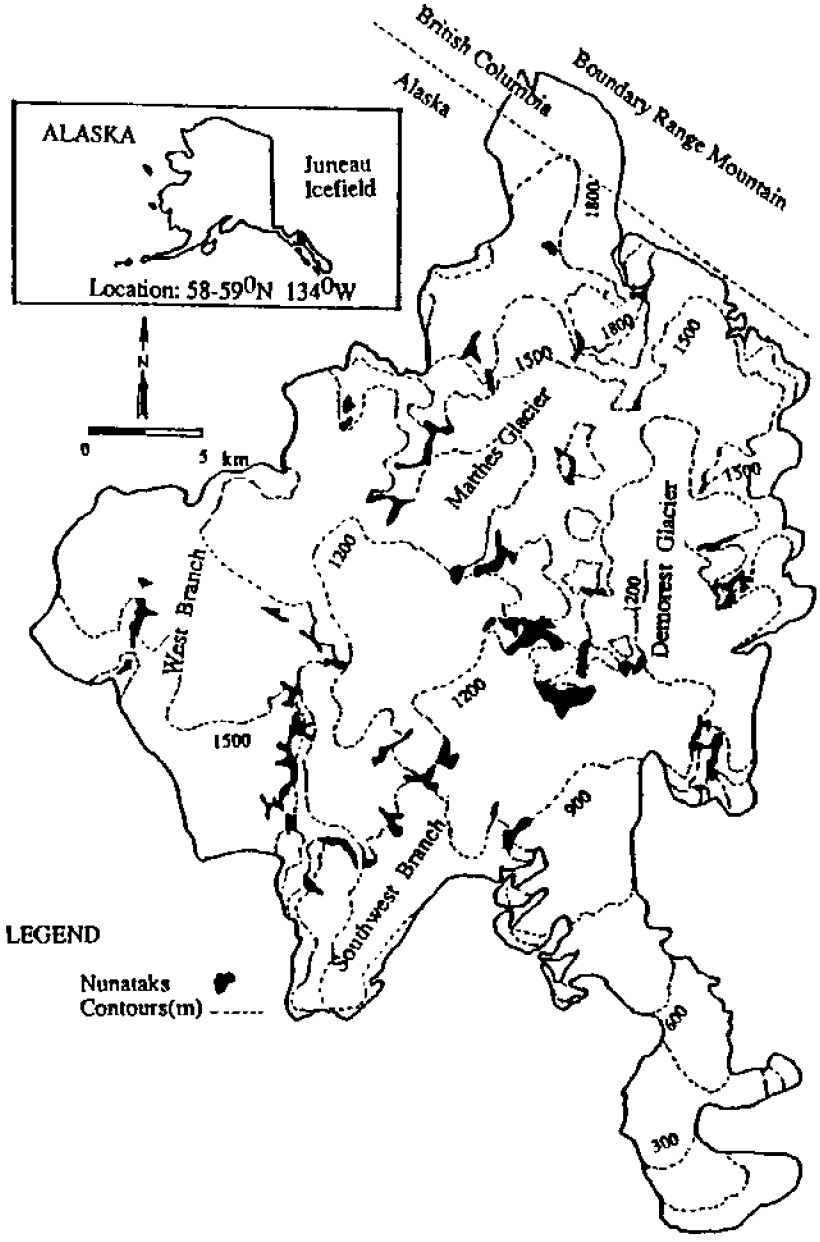

Fig.5.1: Location Map of the Taku Glacier

taken from USGS topographic maps with an accuracy of ±3m. Bedrock elevation is based on seismic and gravimmetric profiles across the glacier (Poultier, 1952; Prather, 1971; Carlson, 1987).

5.2.0 MORPHOLOGY

The Taku Glacier drains southward from the coast Range into the head of the Taku Inlet, east of Juneau. The uppermost nourishment zone of the Taku lies near the crest of the Boundary Range mountains at 58° 40' N and 134° 12' W. The terminus of the trunk branch is approximately 60 km due south. Morphologically, Taku is an interconnected network of highland valley glaciers. Its length, measured at the uppermost part of the neve, is about 55 km. In the lower 15 km. of the glacier, the width of the terminus varies from 2.5 km. to 3.0 km. Figures 5.2 and 5.3 show bed and surface topography respectively. Under the terminus lobe, the bed is below sea level and rises to more than 1600 m above sea level in the north, near Boundary Range mountain. The ice thickness of the Taku Glacier is shown in figure 5.4. At the terminus lobe the ice thickness is approximately 300 meters while its maximum value is about 550 meters. Therefore, surface topography closely resembles the bed topography.

The surface area of the Taku Glacier can be divided into three zones: the ablation (113 km^2) zone occurring below the equilibrium line altitude (ELA), the lower neve region (178 km^2) extending for 400 m in elevation above the ELA, and the upper neve region (380 km^2) occurring more than 400 m above the ELA. Figure 5.5 shows the area-elevation curve of the glacier. The glacier has eight primary tributaries and two terminus tongues, the main glacier terminus, and the Hole-in-the-Wall Glacier-a two kilometer long distributary tongue that branches off five kilometers above the main terminus. The terminus, which was tidal before 1950, is largely separated from the inlet by a frontal moraine (Miller, 1963). Since 1900 the terminus of the Taku has advanced about 6.5 km. The average rate of advance is about 37 m/year (Pelto and Miller, 1988). Figure 5.6 shows the location of the terminus of the Taku Glacier since 1880. The advance remains rapid and will probably close off Taku Inlet sometime during this century. In

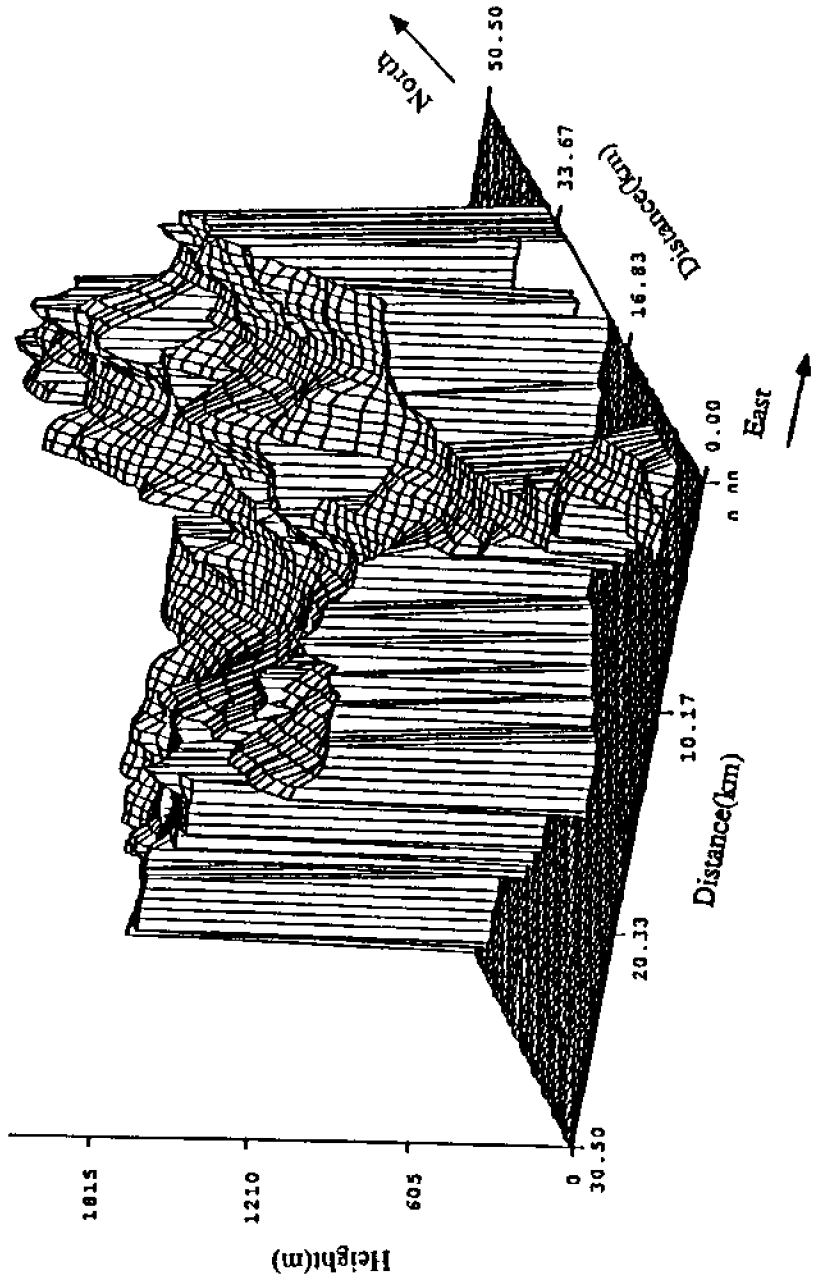

Fig.5.2: Bed Topography of the Taku Glacier

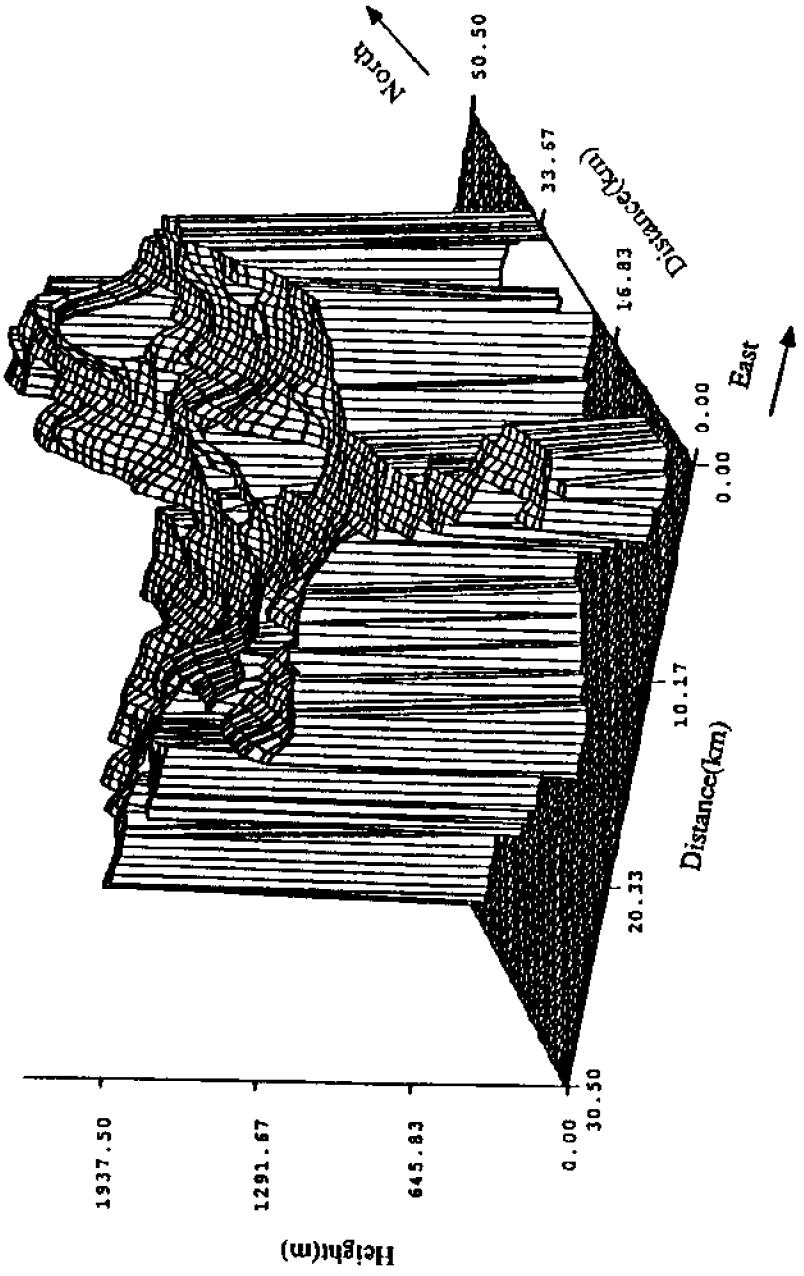

Fig.5.3: Surface Topography of the Taku Glacier

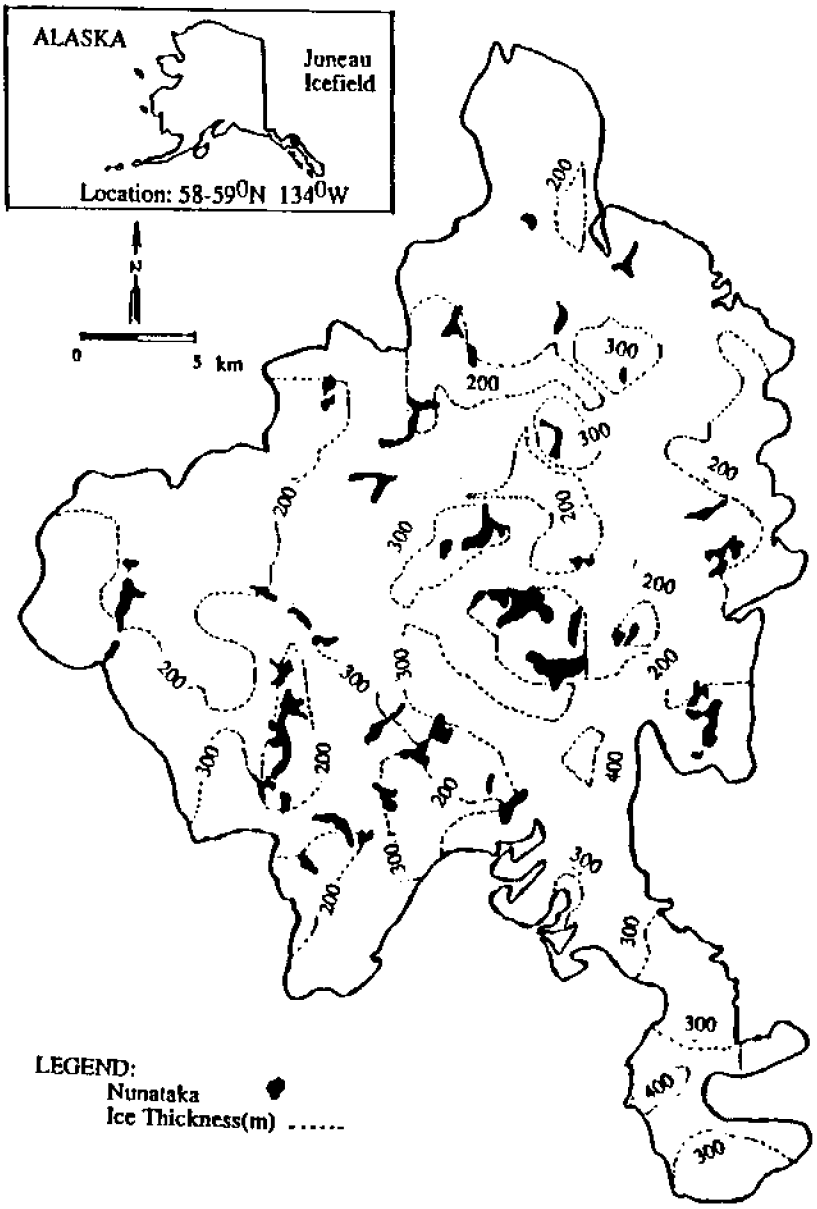

Fig.5.4: Spatial Distribution of Ice Thickness

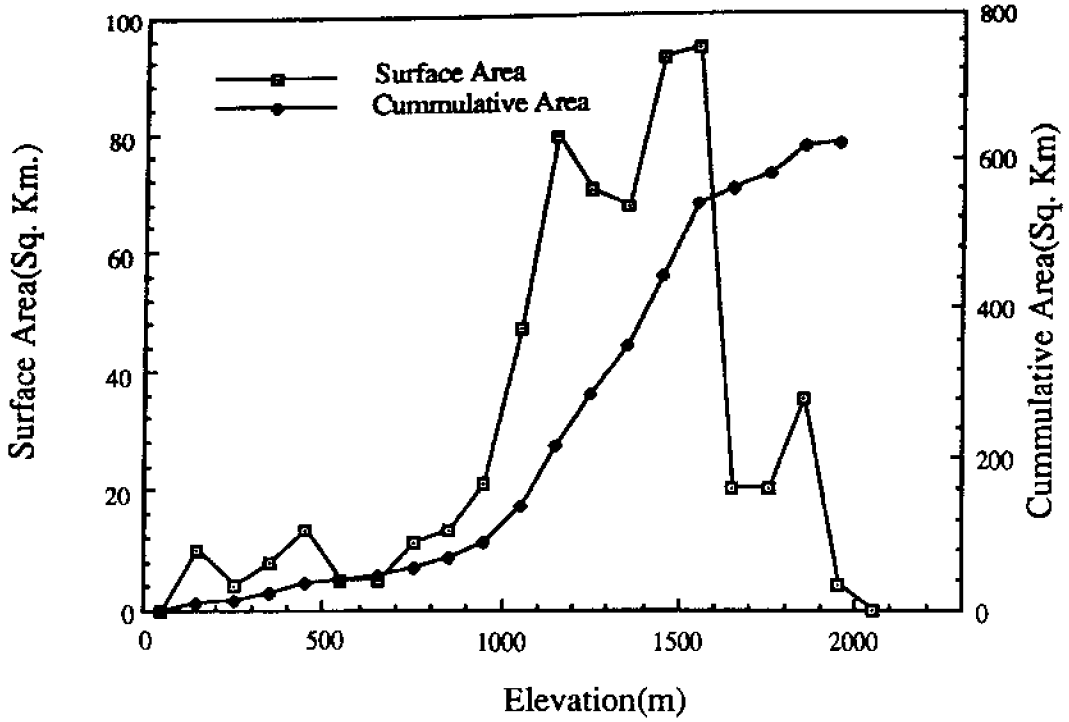

Fig. 5.5: Area-Elevation Curve of the Taku Glacier

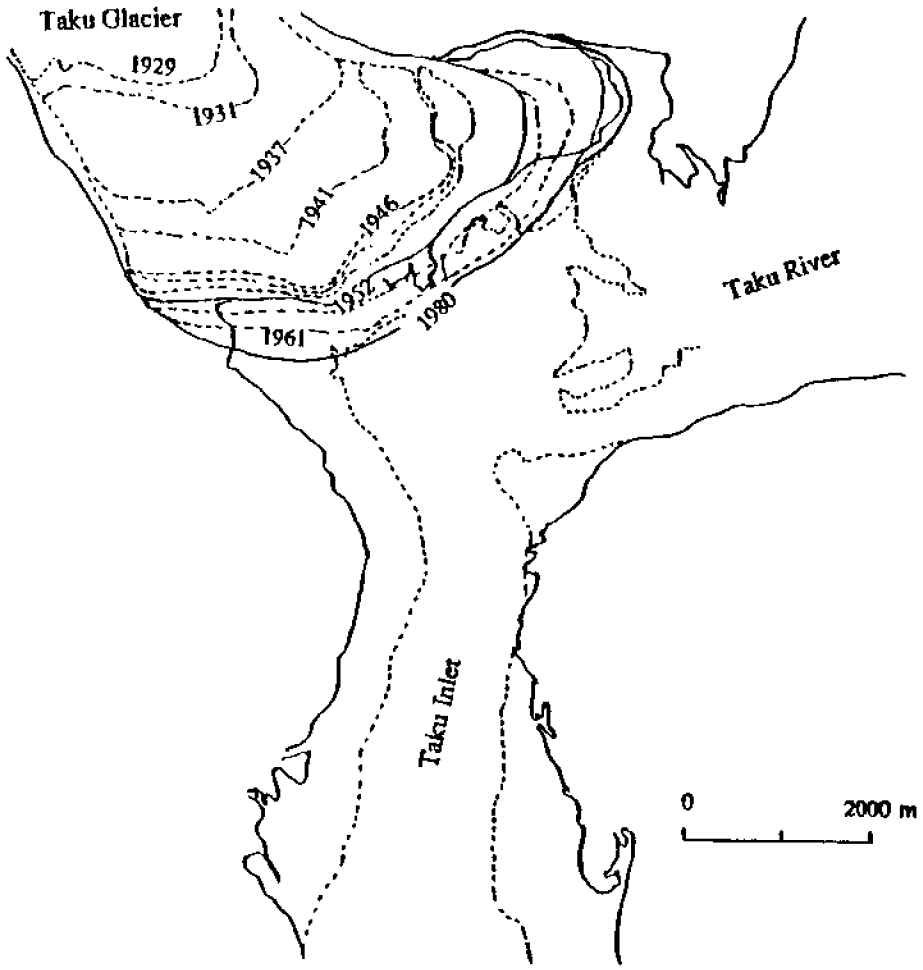

Fig.5.6: Advance of the Terminus

1960 Alaskan Department of Highways funded an investigation of the Taku Glacier to determine if the glacier would block off Taku Inlet. The conclusion was that Taku Glacier would block off the inlet, thus, the only possible route for a road into Juneau has not been utilized. This could also adversely effect to local fishery.

5.3.0 IDENTIFICATION OF BOUNDARIES

The Taku Glacier is an interconnected network of highland valley glaciers. Figure 5.7 taken from Miller(1963) shows some profiles of the Taku along different survey lines. The boundaries of Taku Glacier with Eagle Glacier and Mendenhall Glacier are clearly defined by mountains protruding through the ice. However, it is contiguous with Llewellyn, East Twin, Herbert and other glaciers as shown in the figure. The figure also indicates that at these boundaries the bed levels are much higher and the bed slopes down in both directions. Thus the bed topography along these transacts indicate the existence of flow divide lines. These ice divide lines are modeled as no flow boundaries and their positions do not change in time. Consequently, no distinction is made between boundaries defined by nunatak or ice divide.

5.4.0 MASS BALANCE

The mass balance of a glacier is the principle variable determining its present and future behavior. The surface mass balance is dictated solely by the climate and is responsible for any volume changes of non-calving. The mass balance of the Taku Glacier is dictated by the percentage of its total area within the maximum accumulation zone (MAA) and the accumulation area ratio (AAR), which is the ratio of accumulation area to the total area of glacier above the equilibrium line altitude (ELA). The threshold value for AAR and MAA, for steady state non-calving glaciers (Pelto, 1987) are 67 and 50 respectively. Present ARR and MAA values of the Taku Glacier are 82 and 62 respectively. Figure 5.8 shows the areal distribution of annual accumulation and ablation rates (Pelto and Miller,

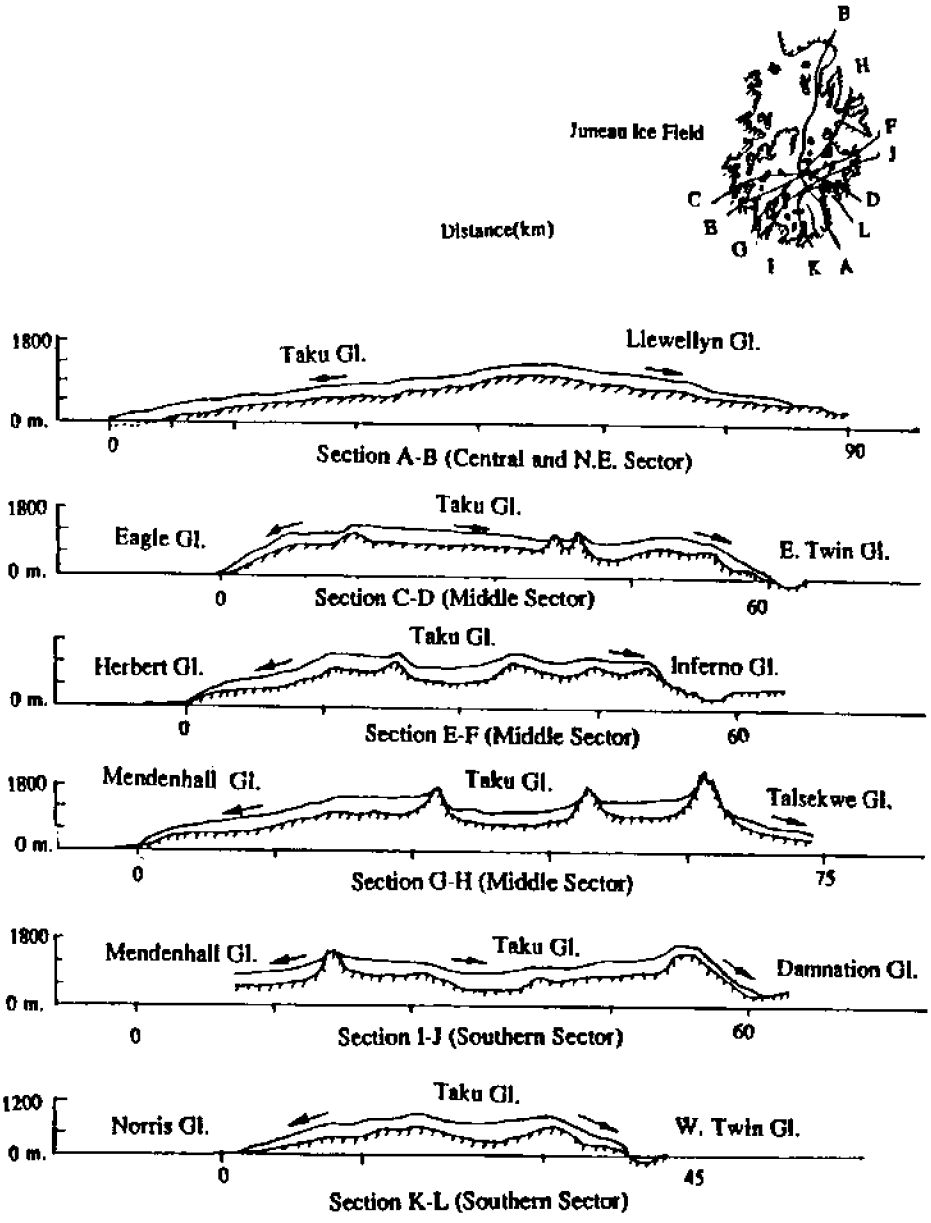

Fig.5.7: Longitudinal Profiles Through the Taku Glacier

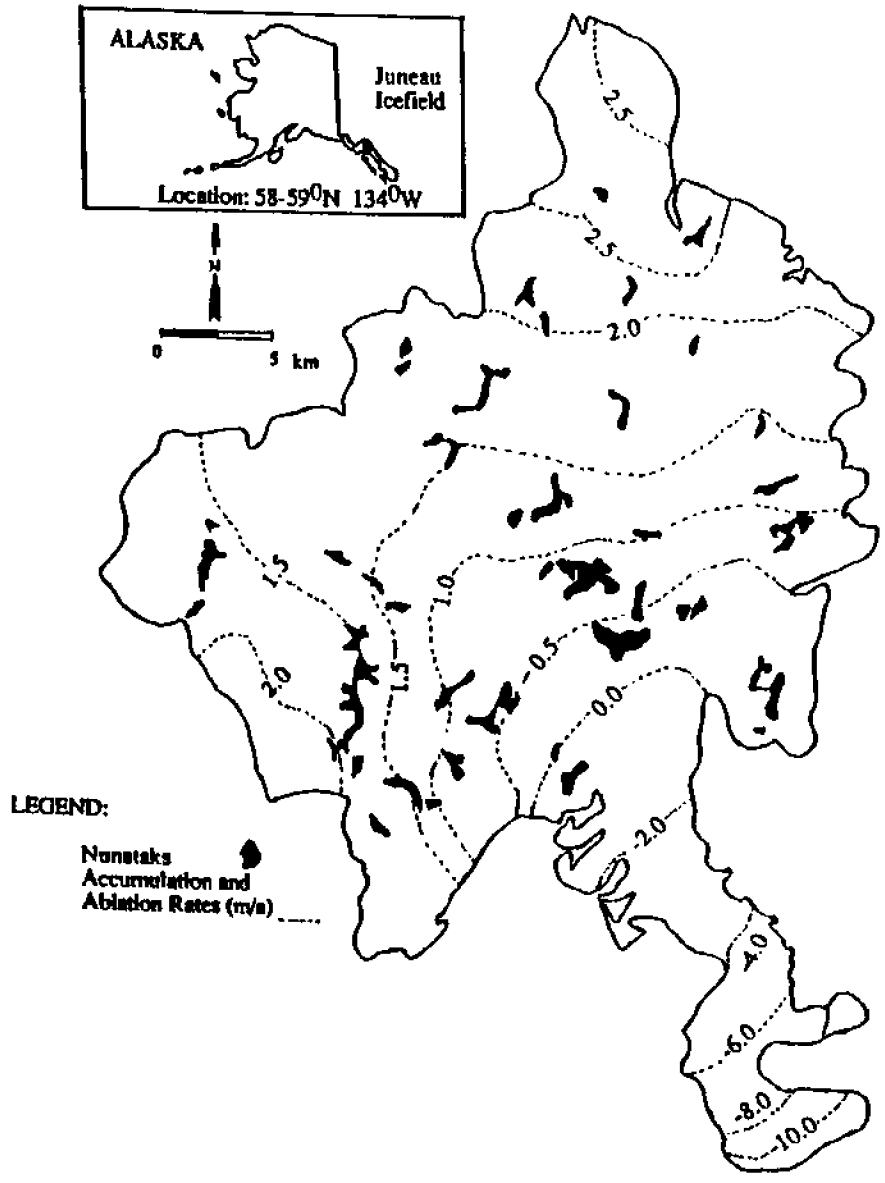

Fig.5.8: Spatial Distribution of Mass Balance

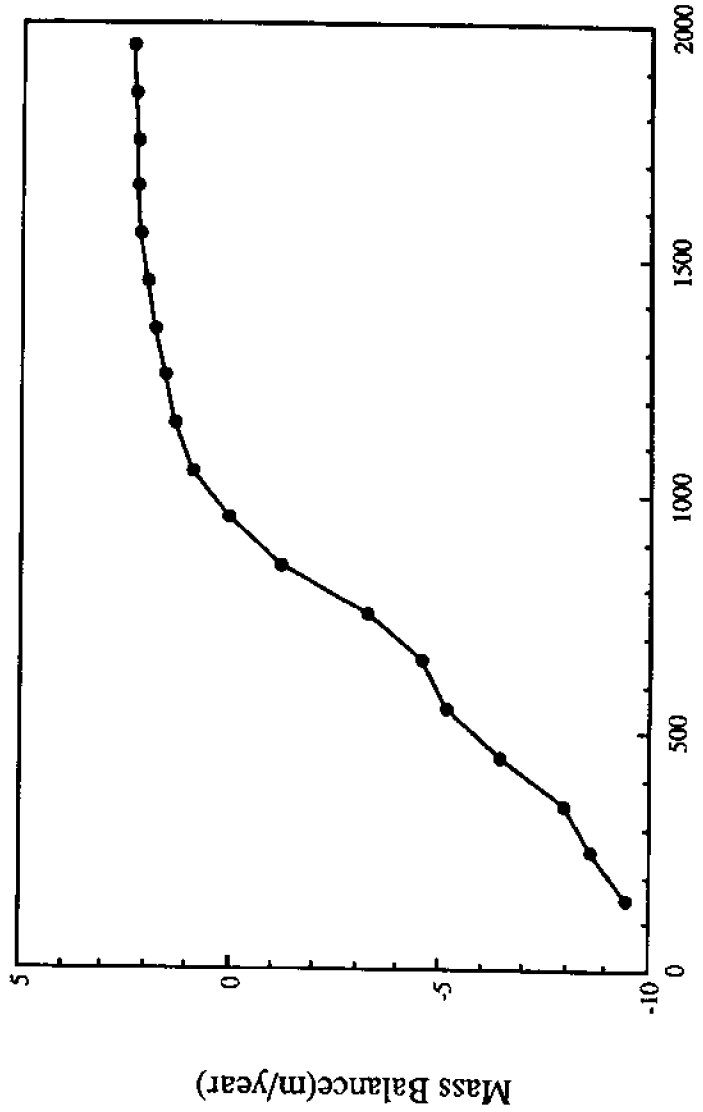

Fgi. 5.9: Altitudinal Variation of Mass Balance

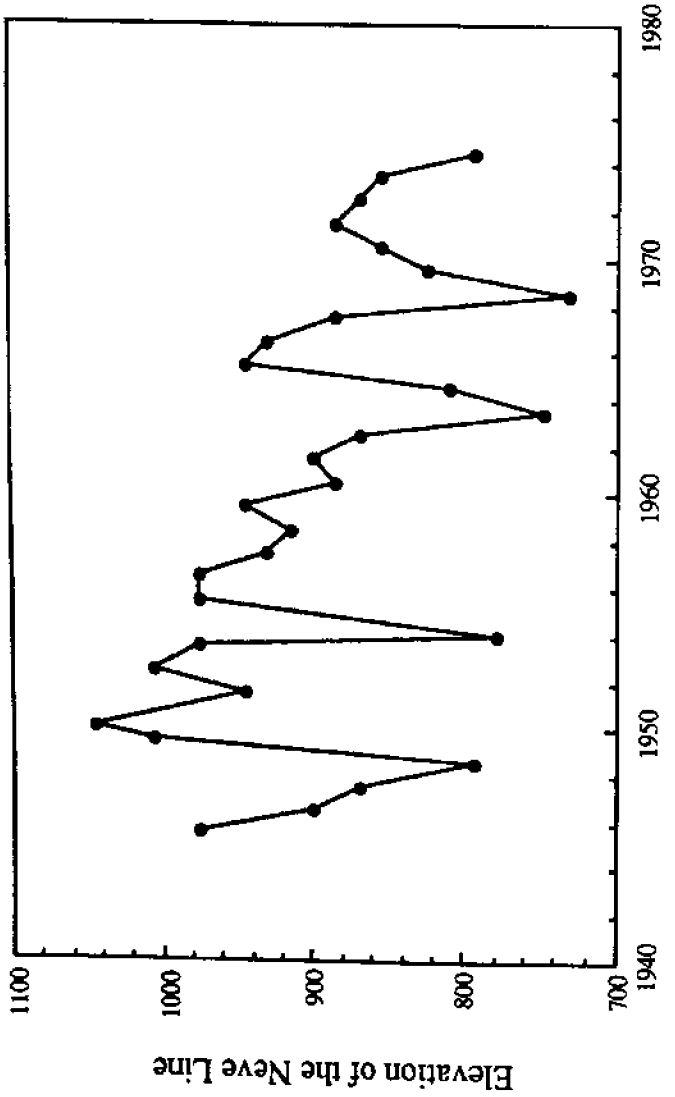

Fig. 5.10: Temporal Variation of the Neve Line

1988). Ablation reaches a maximum rate of 10.0 m/year at the terminus. Accumulation rates over most of the accumulation zone are between 2.0 and 3.0 m/year. Figure 5.9 shows the altitudinal variations of mass balance. The mass balance changes from ablation to accumulation at an elevation of about 925 m. Therefore, the altitude of the equilibrium line can be taken at 925 m above mean sea level. Analysis of mass balance data indicates that in the accumulation zone, the specific accumulation rate is 1.74 m/year and the altitudinal gradient $\partial S^{+}/\partial z$ is 1.84 kg/m^3. Figure 5.10 shows the variation of the neve line from 1944 to 1975. These data were obtained from Miller(1975). The elevation of the neve line is gradually decreasing with time, and the trend is distinct. The fluctuations of the neve line is an index of the mass balance in the glacier. A high accumulation rate in a balance year tends to rise the elevation of the neve line, while falling neve line indicates a net loss of mass by ablation.

5.5.0 SEASONAL CYCLONIC ACTIVITY

Two important climatic conditions influencing the mass balance of a maritime glaciers are the seasonal cyclonic activity and seasonal temperature (Pelto and Miller, 1989). In this study wind velocity is taken as an index of the cyclonic activity. Information about wind velocity and seasonal temperature variations are also necessary for the determination of the interaction of the glacier to climatic perturbations. Figure 5.11 shows the distribution of monthly mean wind velocity at Juneau in 1987. The yearly mean velocity is 4.14 m/s, with standard deviation of 0.62 m/s.

5.6.0 SEASONAL TEMPERATURE

Figure 5.12 shows the temporal variations of five-year running mean temperature and precipitation over a period of 45 years. The figure indicates successive warmer periods followed by relatively cold periods. During this period the mean temperature and precipitation were 4.47±0.54 °C and 1.351±0.087 m/year respectively. Out of this 36 years the annual temperature was below the mean

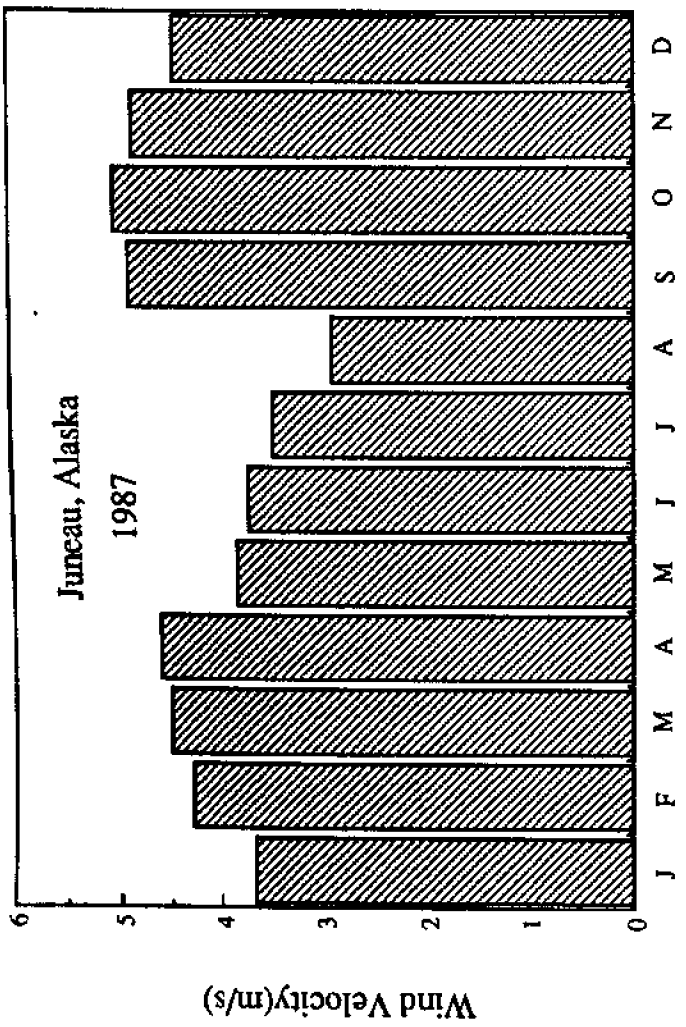

Fg.5.11: Monthly Mean Wind Velocity at Juneau

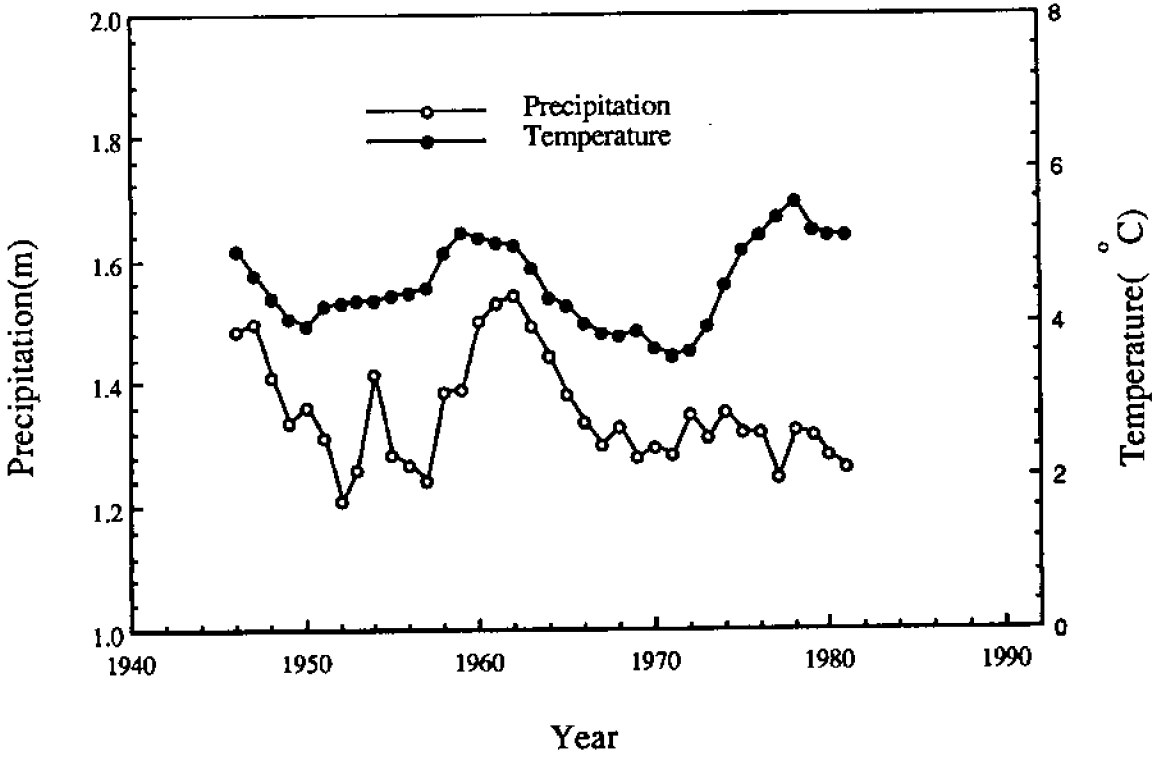

Fig.5.12: Temporal Variations of Five Year Moving Mean Temperature and Precipitation

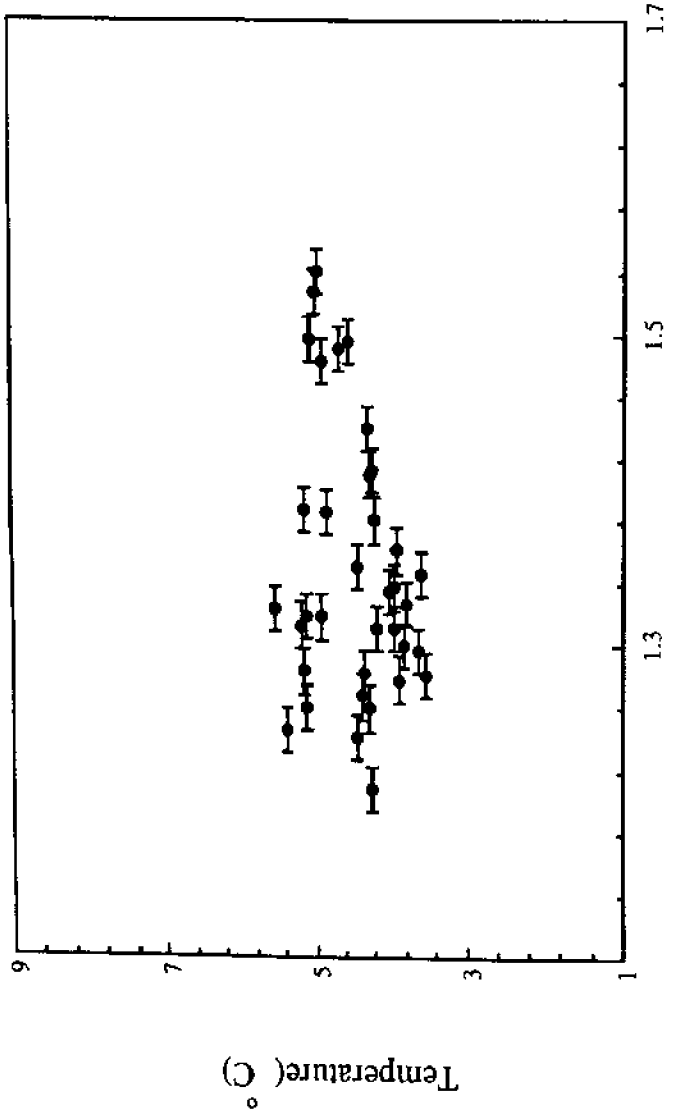

Fig.5.13: Plot of Temperature Versus Precipitation

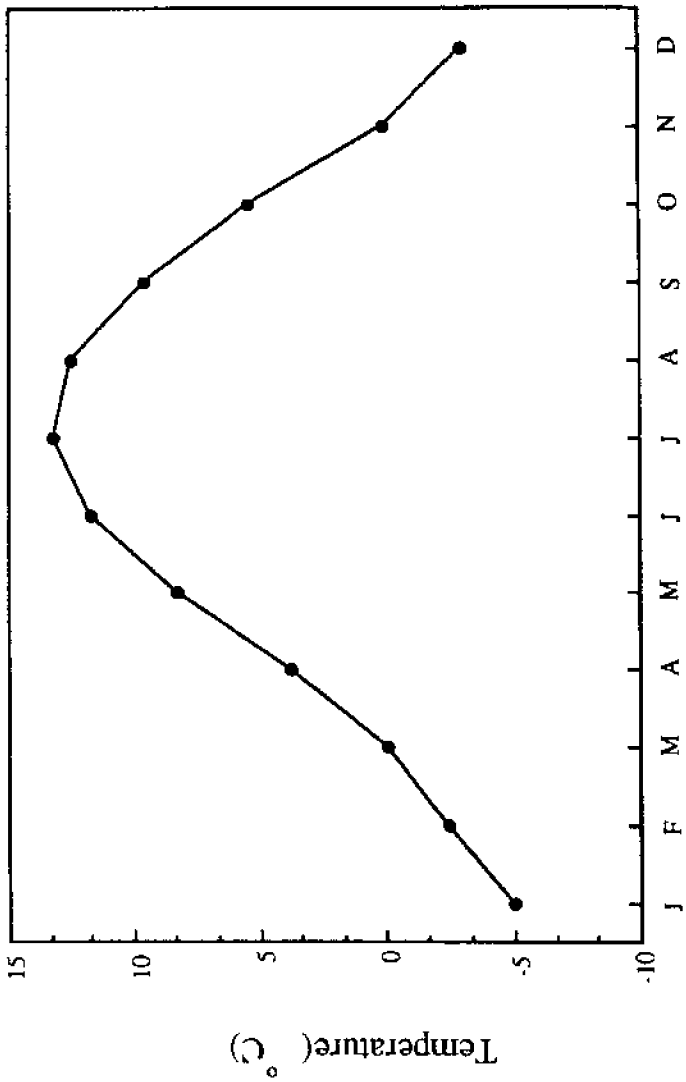

Fig.5.14: Monthly Mean Temperature at Juneau

temperature for 20 years, while it was above the mean value for 16 years. The precipitation was below normal for 21 years and above normal for rest of the 15 years. The trend in the variation of temperature and precipitation are similar, with much more noise in the precipitation curve. Comparison of both the curves shows that the variation of precipitation lags behind the fluctuation in temperature. Figure 5.13 is a plot of precipitation against temperature. The correlation between temperature and precipitation is very poor. The noise in the data is much more than the expected increase in precipitation rate due to the climatic warming.

Figure 5.14 shows the monthly mean temperature at Juneau for a 45 year record. The figure indicates that the range of temperature variation in a year is about 13.3 °C. The lowest temperature is -5 °C, while the highest temperature is around 8.3 °C. This analysis is based on the temperature and precipitation data at Juneau. Plots of temperature at Juneau and on the Taku Glacier from 1949 to 1953 (Miller, 1963) indicates a very high correlation. This is mainly because the temperature in the Taku Glacier is strongly influenced by "regional free air temperature" (Miller, 1963).

5.7.0 ALTITUDINAL TEMPERATURE GRADIENT

Table-5.1, taken from Miller(1975), shows the mean daily temperature at five locations in the Juneau ice field as a function of elevation and climatic conditions. The table shows that highest temperature is about 11.77 °C at Atlin Lake, which is located at an elevation of 670 m above mean sea level. The lowest daily mean temperature is 3.33 °C at Camp No. 8, located at an elevation of 2195 m. Figure 5.15 shows the plot of temperature as a function of elevation. Based on these data the relationship between temperature and elevation is given by:

$$T_a = 14.80 - 0.00546\, z \qquad (5.1)$$

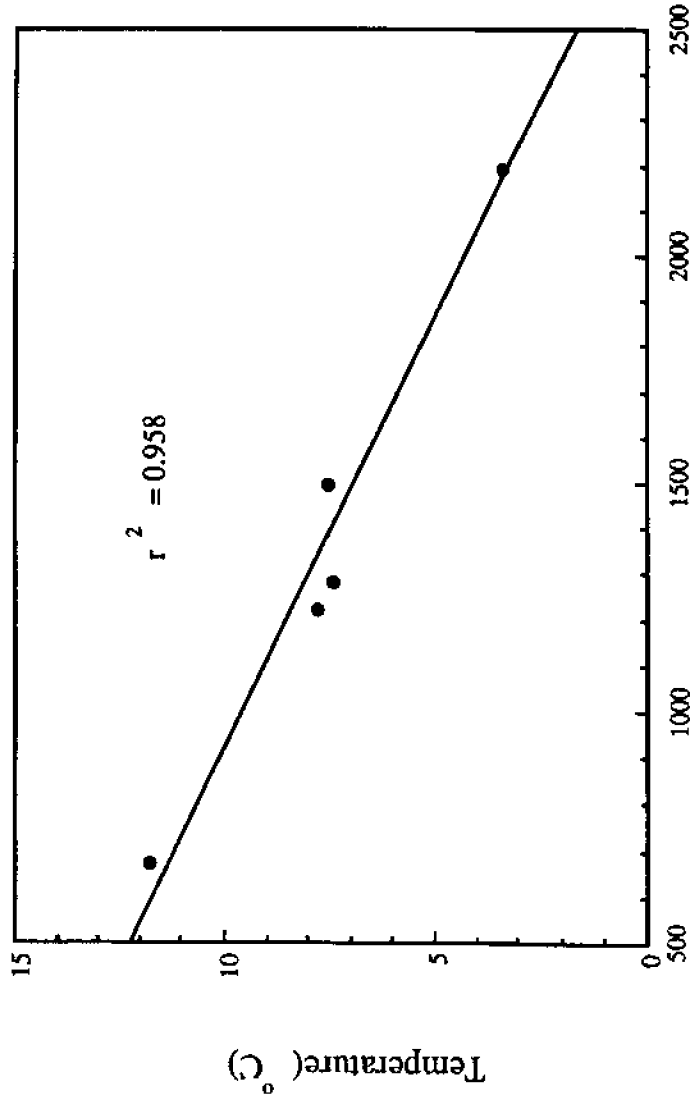

Fig.5.15: Altitudinal Temperature Gradient

Table-5: Daily Mean Temperature Data in the Juneau Ice Field
July 22 to August 31, 1971 (Miller, 1975)

Station	Location	Elevation (meter)	Meteorological Setting	Temperature (°C)
8		2195		3.38
10		1220		7.77
17	Lemon-Ptarmigan	1280	Maritime Climate	7.38
26	Llewellyn	1495	Sub-continental to Continental Climate	7.56
30	Atlin Lake	670	Continental to Semi-arid Climate	11.77

where T_a is temperature in °C and z is elevation in meter from mean sea level. The coefficient of correlation, r^2, is 0.958. The altitudinal temperature gradient $\partial T_a/\partial z$ = -0.00546 °C/m. The global mean temperature gradient is -0.006 °C/m (Oerlemans and van der Veen, 1984). This decrease in temperature gradient may be due to unstable atmospheric stratification accompanied by the convective adjustment of temperature (Oerlemans and Veen, 1984).

5.8.0 NUMBER OF ABLATION DAYS

Based on the monthly mean temperature, shown in figure 5.4 and equation(5.1), figure 5.16 shows the number of ablation days, defined as the number of days in which temperature is below 2.5 °C, as a function of altitude. The best fit polynomial is given by:

$$\Pi = 193.6 - 2.646 \times 10^{-1} z + 4.351 \times 10^{-4} z^2 - 4.472 \times 10^{-7} z^3 + 2.142 \times 10^{-10} z^4 - 3.946 \times 10^{-14} z^5 \qquad (5.2)$$

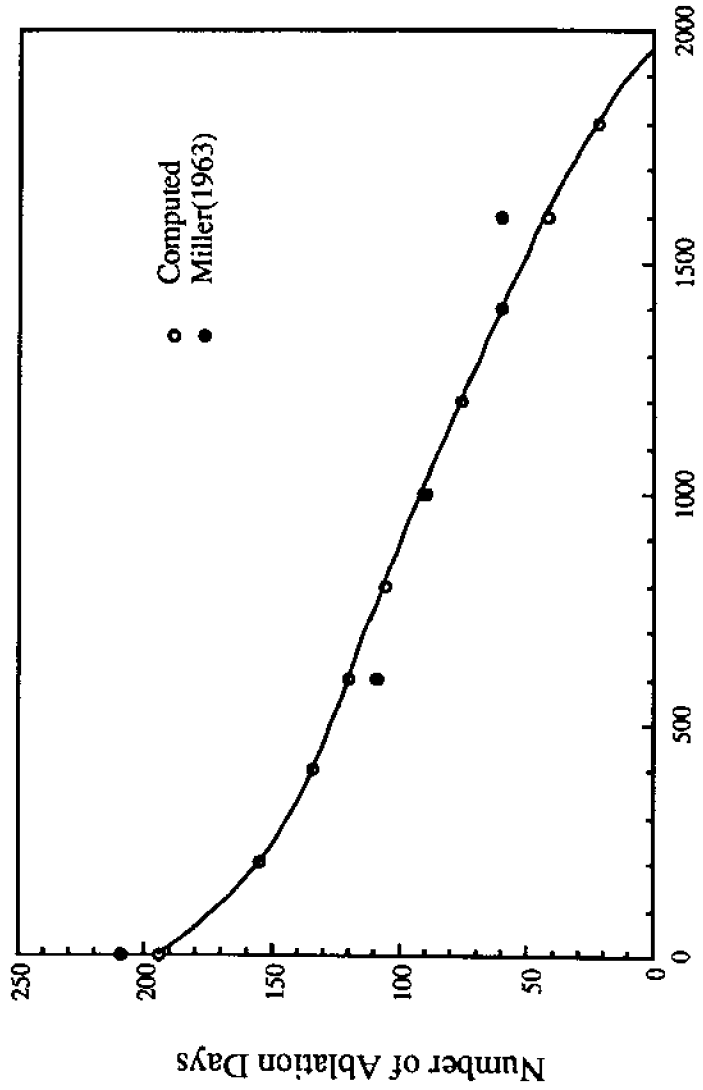

Fig.5.16: Number of Ablation Days as a Function of Elevation

where Π is the number of ablation days. Thus at the equilibrium line the number of ablation days is about 100. Generally, the ablation season is defined as the period in a year when the temperature is above 0 °C (Ambach, 1985a, 1985b). Field experience (Pelto, 1989) in the Juneau Icefield indicates that the melting of ice does not start until the air temperature exceeds 2.5 °C. Therefore, in this study the number of effective ablation days is taken as the number of days in which the air temperature is above 2.5 °C. A comparison with the observed number of ablation days (Miller, 1963) shows that the equation gives a reasonable estimate. Miller(1963) points out that the decrease in ablation period, in the Juneau Icefield, with the increase of elevation is greater in the bare ice zone below 450 m than in the intermediate areas up to 900 m. This is a common situation in most temperate glaciers. Equation(5.2) does indeed show a rapid decrease in ablation days as elevation changes from zero to 500 m and then the rate of change decreases. In analyzing the number of ablation days, it has been implicitly assumed that it is a function of free air temperature only. In general the ablation season in a glacier is a function of convective heat supply from the air, and solar radiation (Oerlemans and Veen, 1984). However, in a strongly maritime climate, meteorological factors are far more important than radiation in causing ablation. Although in some regions it would be unsafe to use a single meteorological factor for the determination of ablation, in the Taku Glacier the variation of air temperature may be trusted to provide a good approximation of the ablation trend (Miller, 1963).

6. APPLICATIONS OF THE MODEL

6.1.0 INTRODUCTION

The Taku Glacier is a large, dynamic glacier with complex surface and bed topographies. The rapidly diverging/ converging boundaries, and the presence of a large number of nunataks complicate the discretization and application of the model. To apply the model, the Taku Glacier was discretized with Δx and Δy of 1.0 km. into 625 computational cells. The features of the glacier with surface areas of 1.0 km^2 or less were neglected. At some sections the Lower Taku Glacier is less than 3.0 km. wide. To avoid the use of smaller grid size, the minimum width in the Lower Taku was taken as 3.0 km. This provides at least three computational cells at a section. Figure 6.1a and 6.1b show the grid layout and the boundaries for the present configuration of the glacier. The Taku river is located just south of the terminus. The topographic data of the river and the adjacent area is very limited. Thus the bed elevations specified in the model, south of the terminus, are essentially an extrapolation/ interpolation of available data.

The information necessary to apply the model are:

1) bed topography (figure 5.3),
2) initial surface topography (figure 5.4),
3) mass balance distribution (figure 5.8), and,
4) initial velocity.

It is not practical to obtain measured velocity data for all grid points. Therefore, the model assumes zero initial velocity at all computational cells. As the model is hyperbolic in nature, the effects of the initial conditions gradually dissipate, as

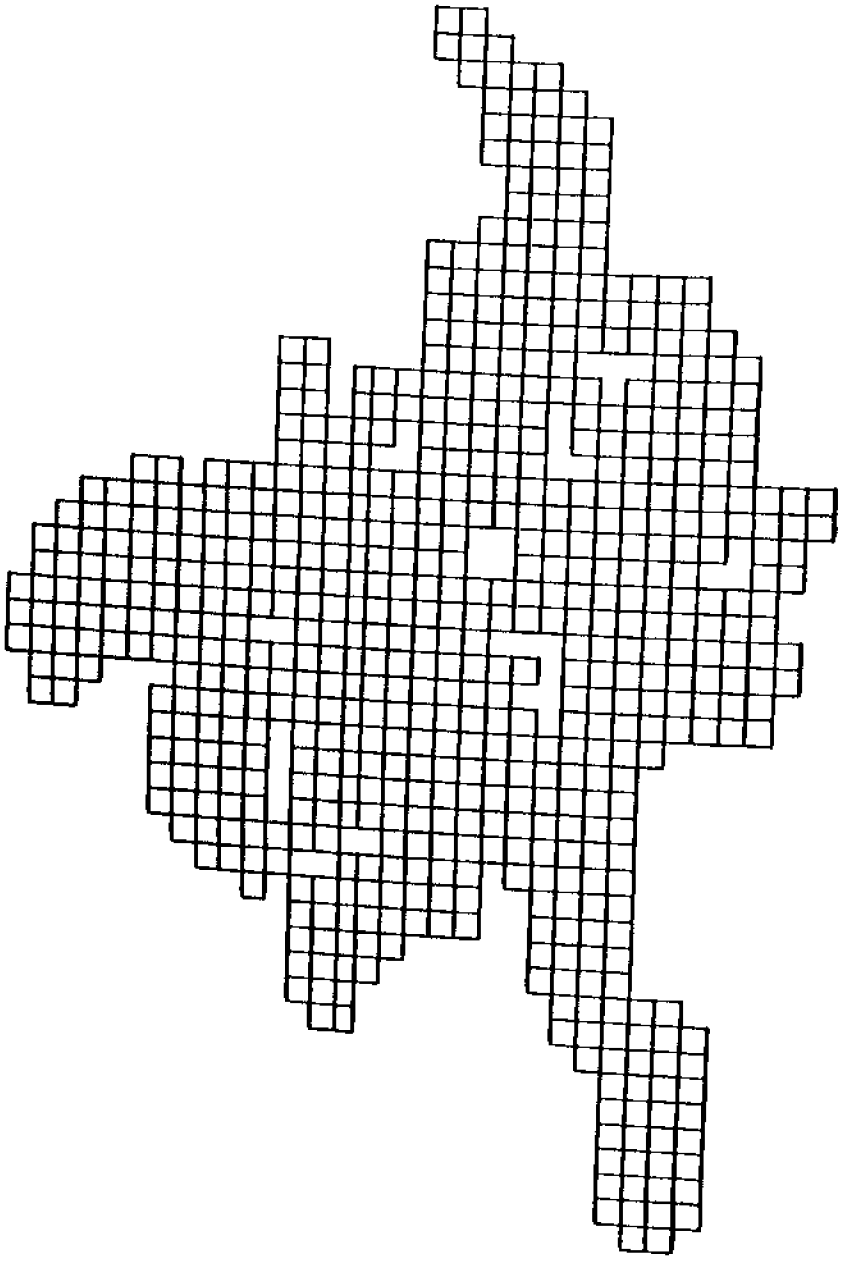

Fig.6.1a: Grid Set-up for the Taku Glacier

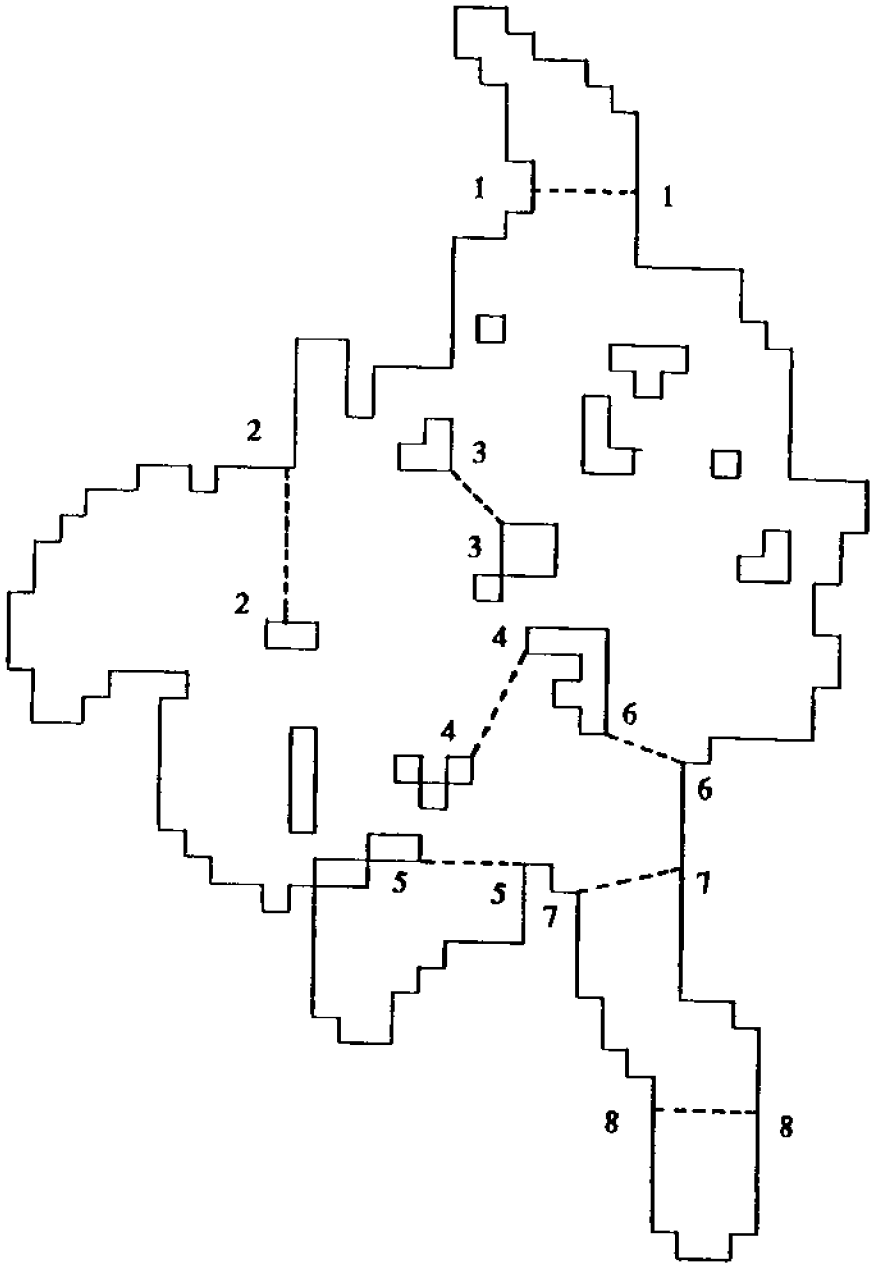

Fig.6.1b: Boundaries of the Taku Glacier and Location of Transects Where Velocity Data are Available

described in Chapter-2. The moving boundary condition was used at the main terminus of the Lower Taku Glacier only. The Hole-in-the Wall Glacier, just north of the main terminus, is generally less than 1.5 km wide, and is not included in the present application of the model. At all other boundaries and nunataks the no-flow boundary condition was used. The position of these boundaries were assumed fixed over the simulation period.

6.2.0 CALIBRATION OF THE MODEL

6.2.1 Calibration Parameters

The model has three calibration parameters that can be adjusted to match the available field data. These parameters are:

1. Horizontal viscosity of the ice, N_H,
2. Vertical viscosity of the ice, N_V, and,
3. Friction coefficient, c_b.

Both horizontal and vertical viscosities are assumed to remain constant over the model domain and the simulation period. The friction coefficient is assumed to be a function of x and y. While carrying out the numerical experiments, described in Chapter-3, it was found that the model results are not significantly influenced by horizontal viscosity, unless it is an order of magnitude greater than the vertical viscosity. There is not sufficient field data to justify the use of higher horizontal viscosity. The use of $N_H > N_V$ makes the model unstable, especially in areas of converging and diverging flows created by boundaries, nunataks and undulating bed topography. Therefore, horizontal viscosity was neglected in applying the model to the Taku Glacier. In addition this reduces the computational time considerably.

6.2.2 Available Field Data

The information available for the model calibration are:

Table-6.1: Measured and Computed Balance Velocities in m/day

Transect	1950	1952	1960	1967	1986	1987	Average	Balance
1	0.20		0.16			0.15	0.18	0.17
2		0.29	0.20			0.19	0.23	0.36
3		0.28		0.33	0.35	0.36	0.38	0.57
4	0.58	0.51	0.51	0.53	0.52	0.51	0.53	1.01
5	0.14	0.12				0.12	0.13	0.12
6	0.20	0.20				0.21	0.20	0.42
7	0.89	0.92		0.90			0.90	1.53
8	0.57	0.56	0.54	0.59			0.56	0.73

1.Surface velocity at the eight transects shown in figure 6.1b. Table 6.1, based on information obtained from Miller(1963; 1975), Nelson(1957), Blachnitzky (1987) and Kersting(1987), shows the variation of surface velocities over a period of 37 years.

2. Bed velocities are 30 to 90 present of the surface velocities in the Matthes Glacier, West Branch and Demorest Glacier (Miller, 1963). As the Lower Taku Glacier is approached, bed velocity increases. In the Lower Taku Glacier, bed sliding accounts for 80-90 percent of the total mass transport (Miller, 1963).

3.Transverse variations of surface velocities (Blachnitzky 1987; Kersting, 1987) at some sections. In the present application of the model only data at transects 3-3, 4-4 and 7-7 could be utilized because these are the transects with lengths greater than 2.0 km.

4.Field experience (Pelto, 1989) indicates that the surface of the Taku Glacier is rising in nearly all locations. In the region around Camp-10 (transect 4-4) the surface elevation has increased by 25-30 m since 1950 (Miller, 1988). The rate of rise is about 0.81 m/year.

6.2.3 Determination of Calibration Parameters

For temperate glaciers, shear viscosity (Ambach and Eisner, 1983) ranges from 7.4 x 10^9 to 15.9 x 10^9 m^2/s. The model developed by Rasmussen and Campbell(1973) treats ice as a viscous fluid. They have varied viscosity from zero to 1.0 x10^{10} m^2/s to study the propagation of surge in idealized glaciers. They indicate that a generally accepted value of viscosity is 12.0 x10^9 m^2/s. This was used as a first estimate of vertical viscosity of ice in this model.

Compared to viscosity, the friction coefficient can vary over a wide range. For glaciers with frozen bed (zero bed velocity), the friction coefficient should be high. As the glacier starts sliding, the coefficient of friction deceases and the physics of bed sliding becomes complicated. Campbell and Rasmussen(1969) and Rasmussen and Campbell(1971) have used friction coefficients similar to the present model with values ranging from 1.0 x10^6 to 5.0 x10^4 to initiate surge. As the Taku is a non-surging glacier, the friction coefficient is expected to be higher. To simplify the selection of friction coefficient in each of the 625 computational cells, the following functional form for a friction coefficient was assumed:

$$c_b = c_{b_{min}} + \frac{H - H_{min}}{H_{max} - H_{min}} \left(c_{b_{max}} - c_{b_{min}} \right) \qquad (6.1)$$

where

c_{bmin} = the minimum value of friction coefficient,

c_{bmax} = the maximum value of friction coefficient,
H_{max} = the maximum bed elevation , and,
H_{min} = the minimum bed elevation.

Equation(6.1) assumes that the friction coefficient is a linear function of bed elevation. This functional form of friction coefficient was assumed because:

1. Field data indicate that the velocity gradually decreases as one goes north, north-east, and north-west of the equilibrium line. These are the regions where the bed elevation of the Taku Glacier are higher.

2. In the southern region of the glacier more water is expected to be present at the ice-bed interface. This will provide more lubrication, thereby decreasing the bed friction. In the Taku Glacier the ratio of bed velocity to surface velocity increases south wards.

By a trial and error, the minimum and maximum values of friction coefficient, that appear to give a reasonable simulation of field data, were found to be 20.0×10^6 and 100×10^6 respectively. To obtain correct relative values of bed and surface velocities, it was necessary to increase viscosity to 14×10^9 m^2/s. Accumulation and ablation rates are kept constant over the simulation period.

6.2.4 Comparison With Field Observations

Figure 6.2 and 6.3 show the variations of surface elevation and surface velocity at the eight transects over a period of 500 years. Both surface elevation and velocity increase and the glacier appears to reach a steady state in about 450 years. The rate of approach to the steady state gradually decreases as simulation advances in time. Field data indicate that the surface elevation around transect 4-4 is increasing at an average rate of 0.81 m/year. Using 100 year intervals to

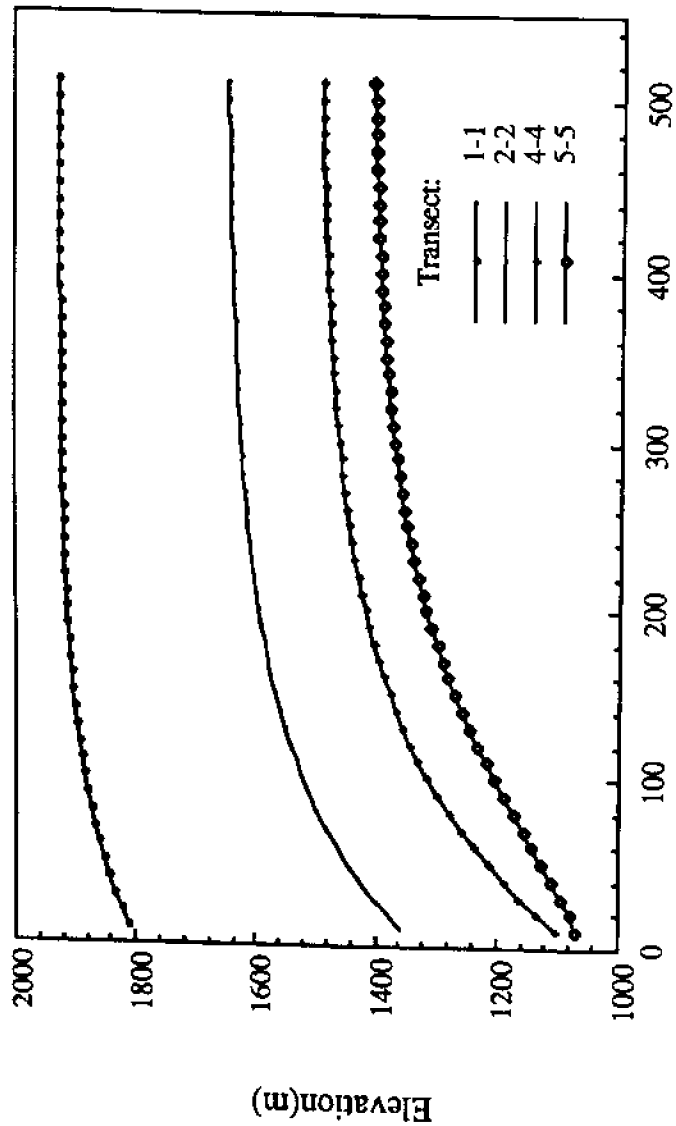

Fig.6.2: Temporal Variation of Surface Elevation at Selected Locations

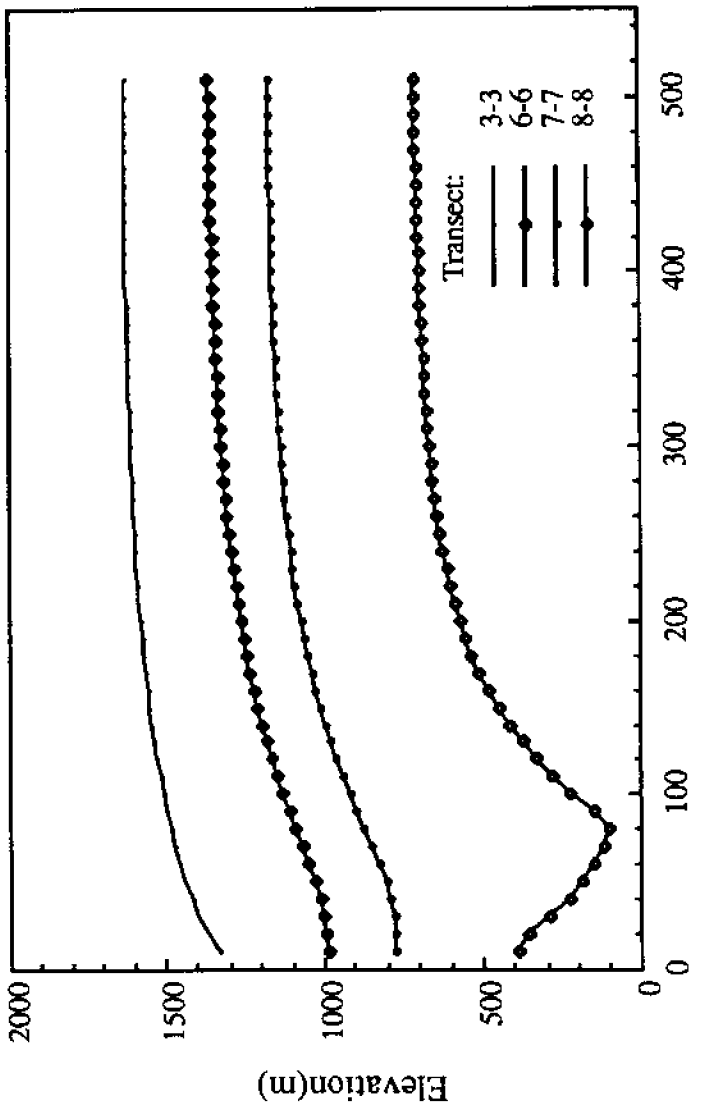

Fig.6.2: Temporal Variation of Surface Elevations at Selected Locations

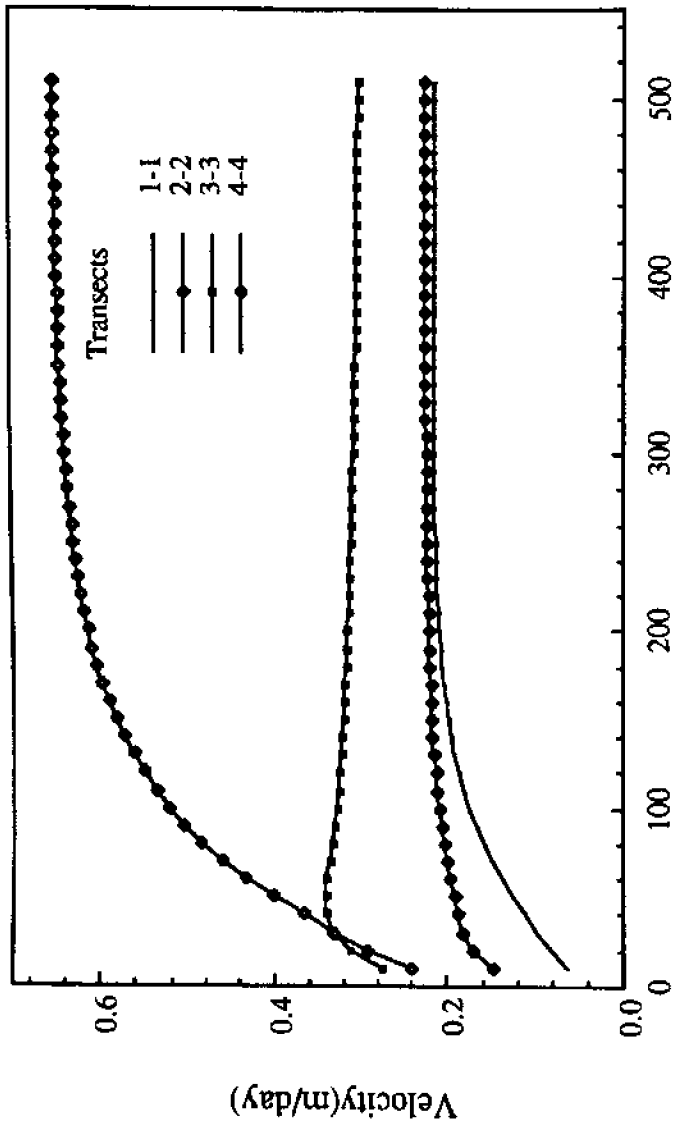

Fig.6.3: Temporal Variation of Surface Velocities at Selected Locations

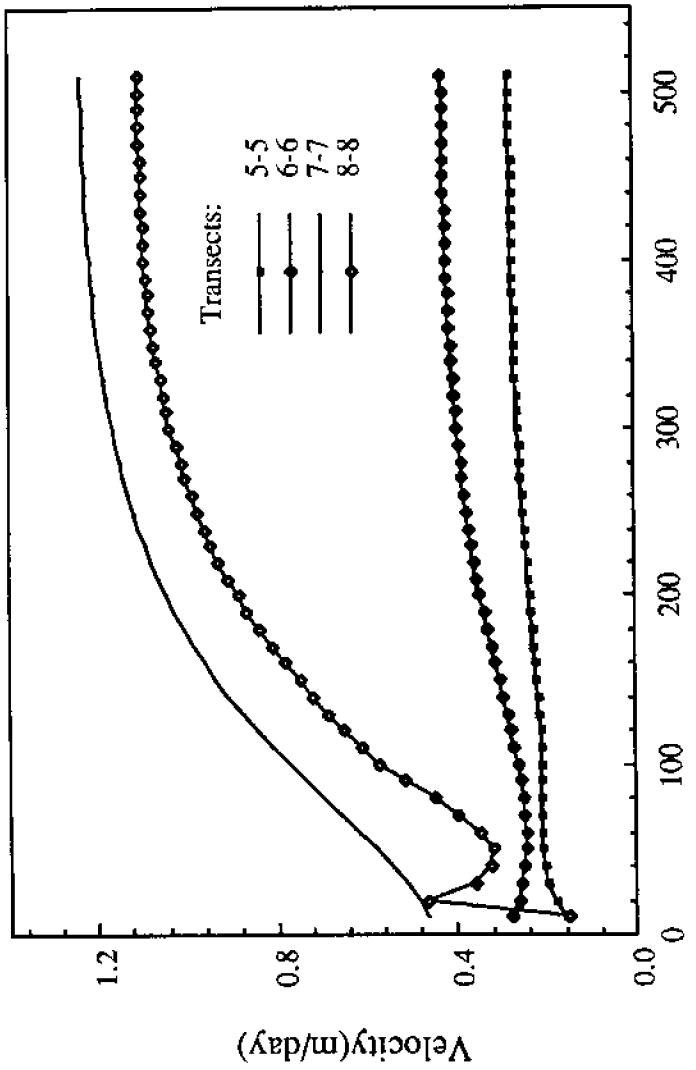

Fig.6.3: Temporal Variation of Surface Velocities at Selected Locations

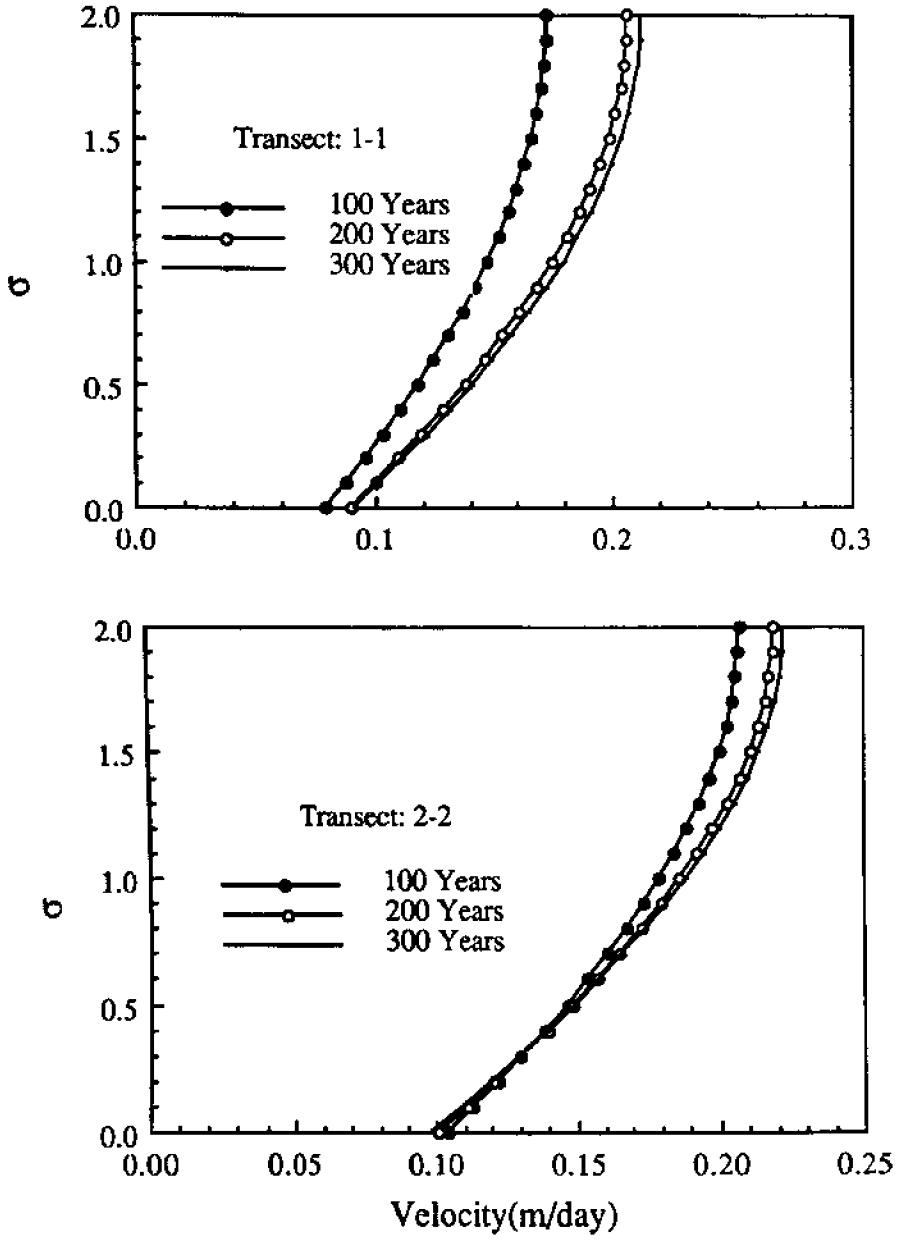

Fig.6.4: Vertical Variations of Horizontal Velocity Components at Selected Locations

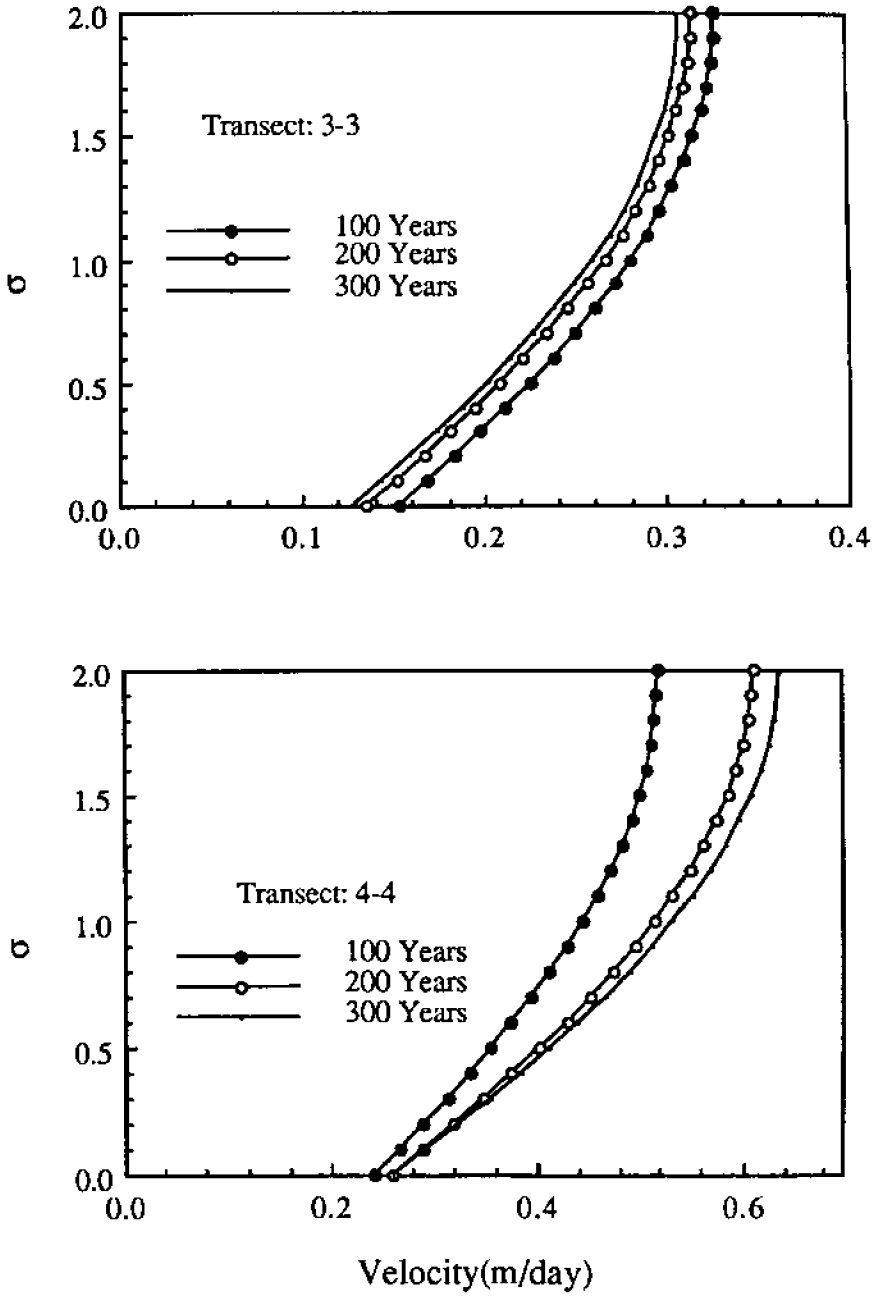

Fig.6.4: Vertical Variations of Horizontal Velocity Components at Selected Locations

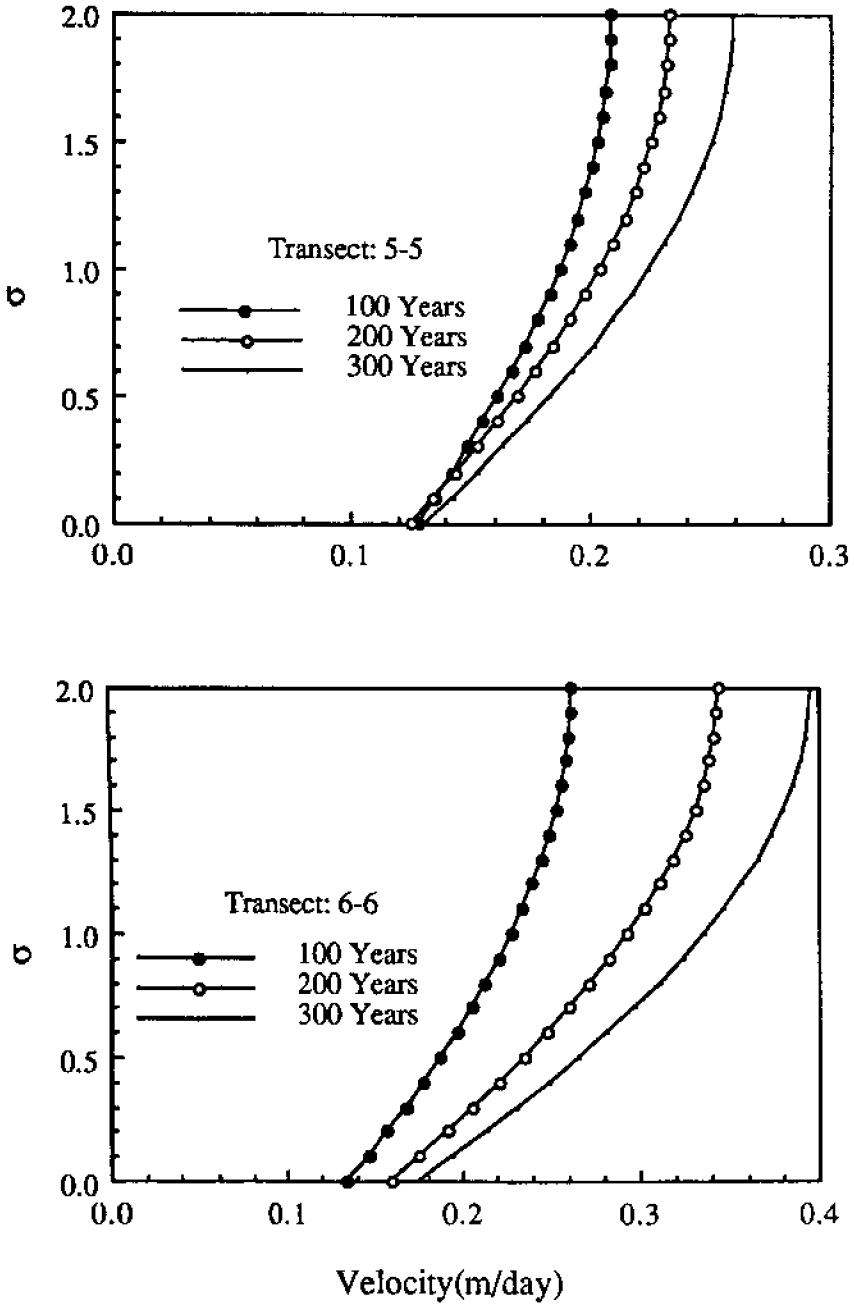

Fig.6.4: Vertical Variations of Horizontal Velocity Components at Selected Locations

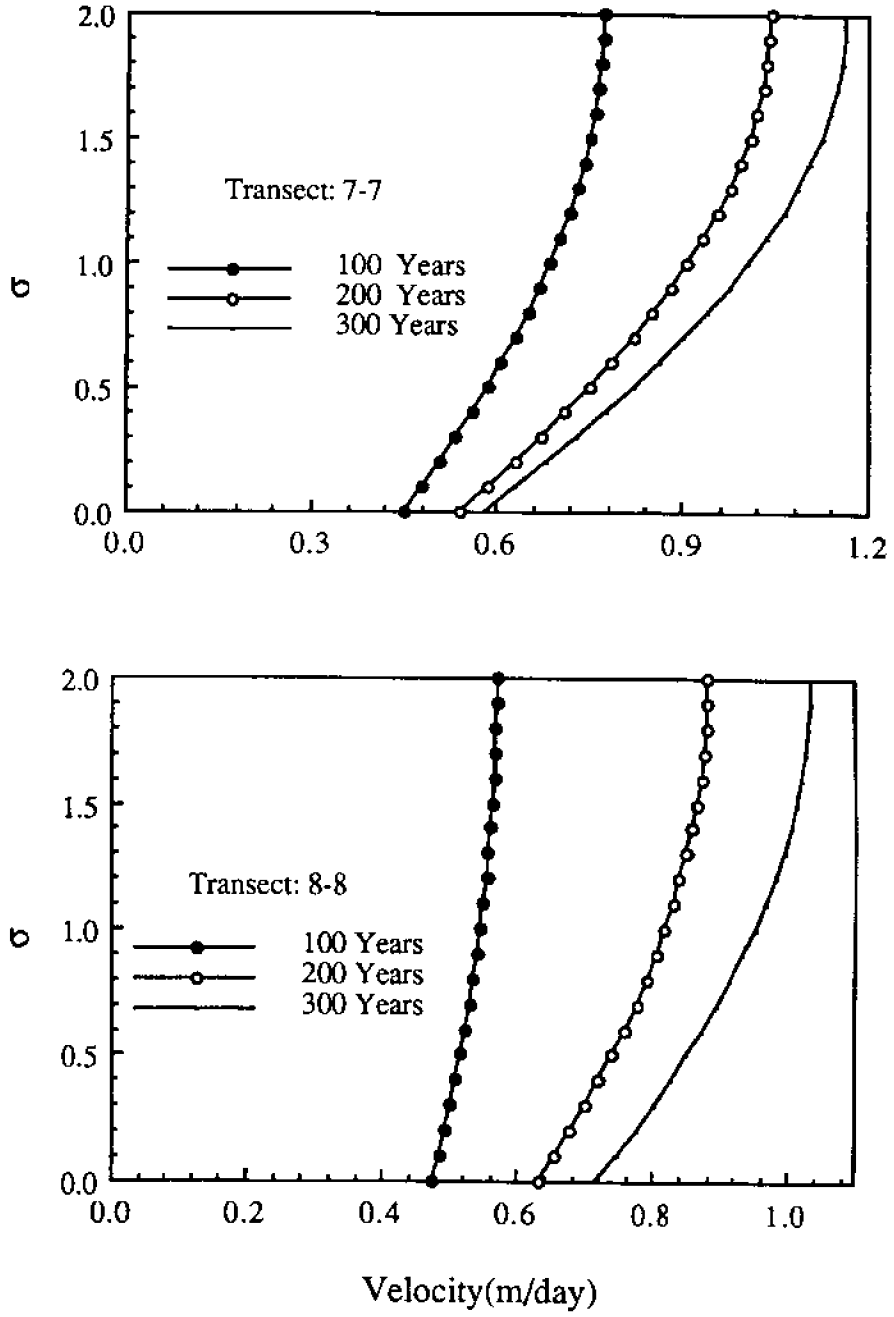

Fig.6.4: Vertical Variations of Horizontal Velocity Components at Selected Locations

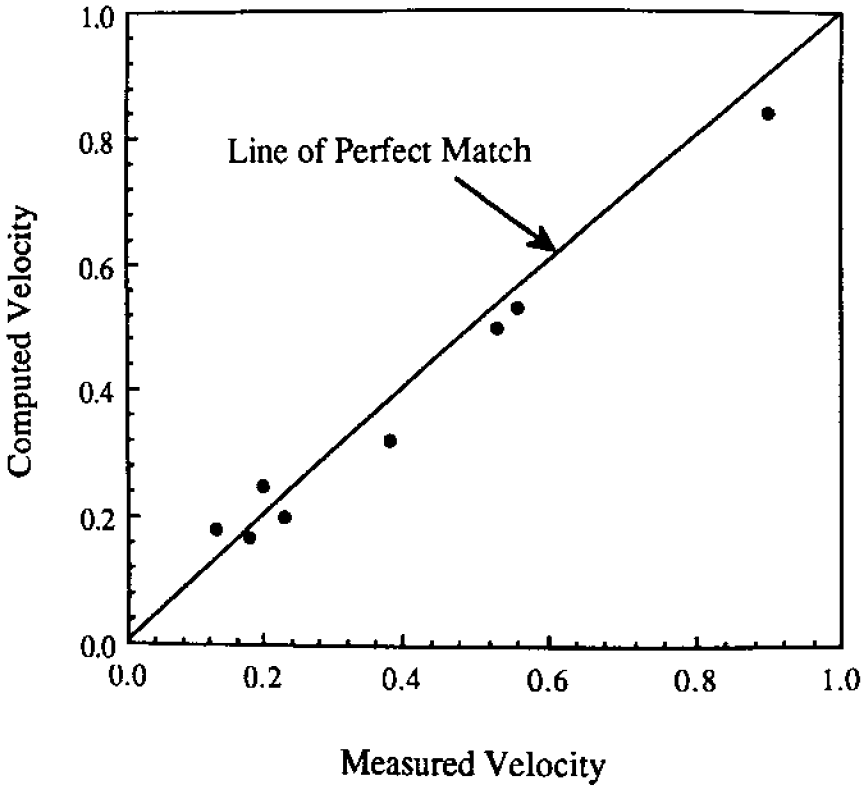

Fig.6.5: Comparison of the Computed Surface Velocity With Field Data

Table-6.2: Computed Surface and Bed Velocities at Transects

Transect	Velocity(m/day) Surface	Bed	Ratio
1	0.17	0.08	0.47
2	0.20	0.10	0.50
3	0.32	0.13	0.40
4	0.50	0.24	0.48
5	0.18	0.12	0.67
6	0.25	0.13	0.52
7	0.80	0.48	0.60
8	0.53	0.48	0.90

compute the rate of rise, figure 6.2 indicates that the computed rates of rise of surface elevation are 1.86 m/year, 0.90 m/year and 0.36 m/year in the first 300 years. The higher rate of rise in the first 100 years can be attributed to the assumed zero initial velocity. In the next 100 years, the computed rate of rise is very close to the field observations.

The vertical variation of velocities at the center of these transects are shown in figure 6.4. Figure 6.5 compares the computed surface velocities at the eight transects with the field data, presented in Table 6.1, at t= 100 years. Table 6.2 lists the numerical values of the computed surface and bed velocities shown in figure 6.4. The ratios of the two velocities, shown in table 6.2, appear to be consistent with field observations. Comparisons of the variations in transverse surface velocities at transects 3-3, 4-4 and 7-7 are shown in figure 6.6. The computed velocities follow the trend in measured velocity distribution and the velocities are of the same order of magnitudes. Measured velocity at transect 3-3

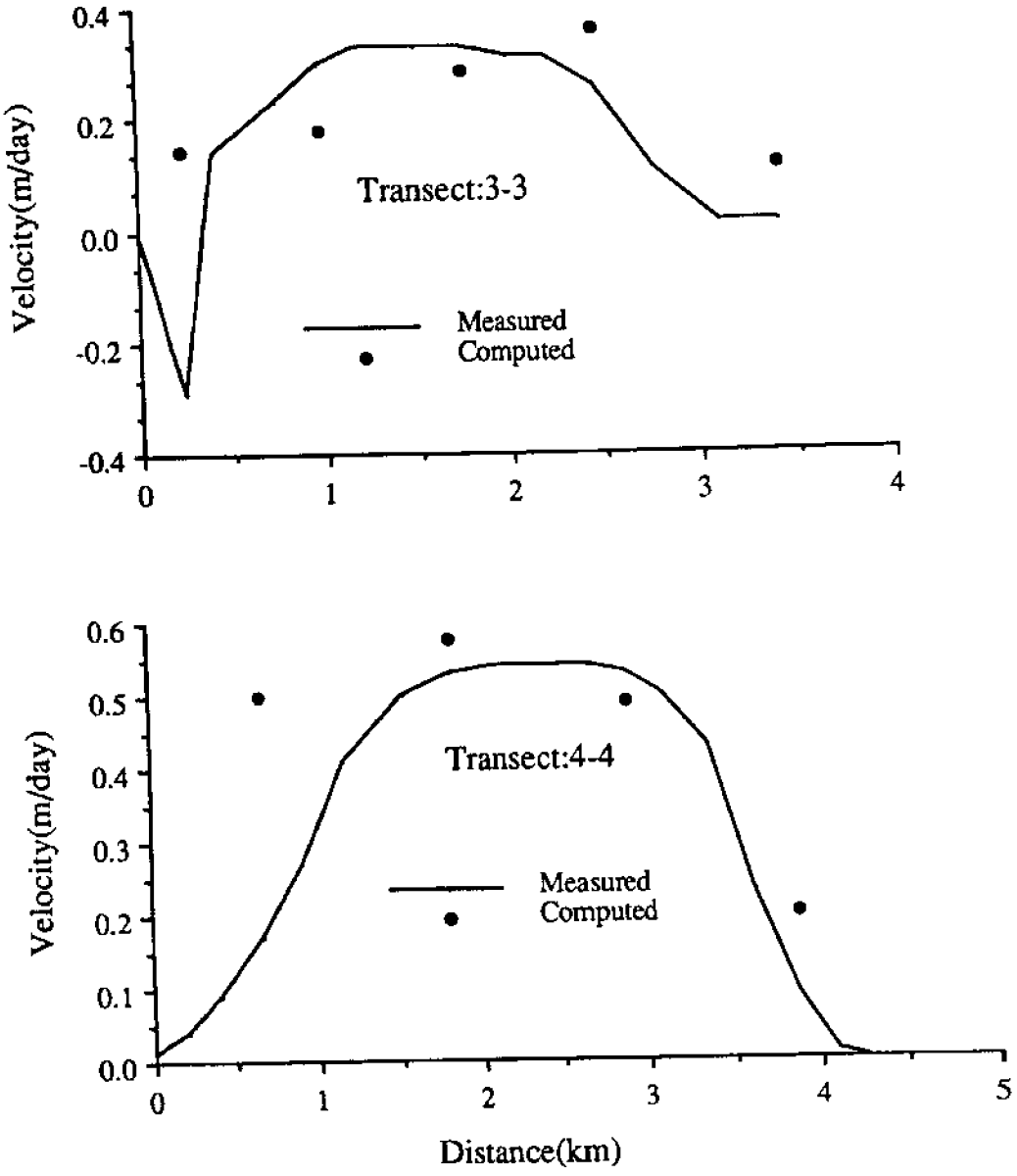

Fig.6.6: Comparison of Transverse Velocity Distributions at Selected Transects

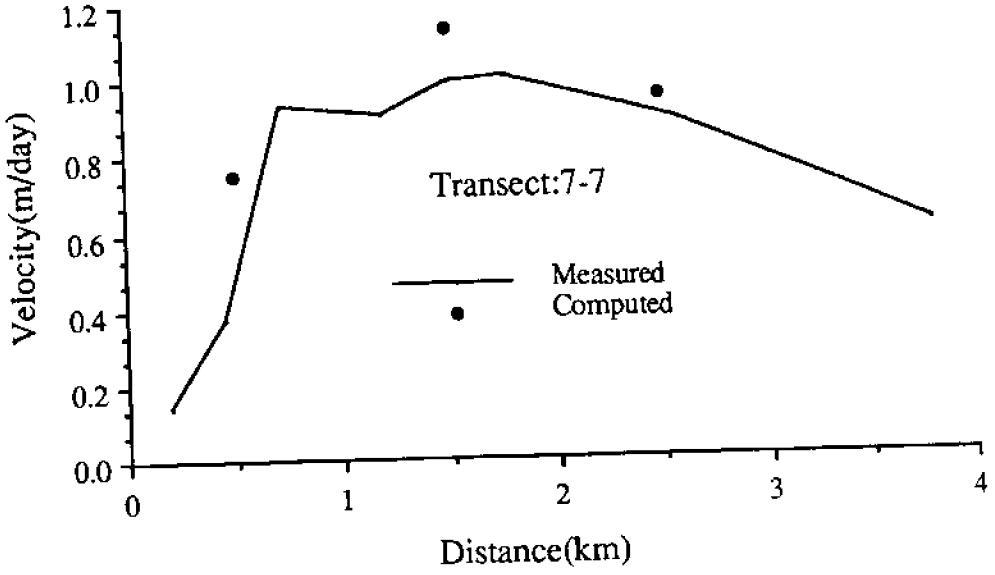

Fig.6.6: Comparison of Transverse Velocity Distributions at Selected Transects

shows an abrupt change in direction a short distance from a nunatak. The discrepancies between the computed and measured velocities in this region are significant. It is not possible for the model to reproduce such an abrupt change in velocity. In addition, such an abrupt change in velocity is not consistent with other observations. In general glaciers do not respond to local surface and bed topographies (Paterson, 1981). The match of the field velocities at the end of 100 years of simulations indicates that the effects of the assumed initial conditions have dissipated.

6.3.0 SIMULATIONS WITH THE PRESENT CLIMATIC CONDITIONS

As pointed out earlier, the glacier approaches steady state as the computations advance in time for the given accumulation and ablation rates. Figure 6.2 indicates that after 300 years the rates of change in velocity and surface elevations are small. Therefore, this section presents an analysis of the flow characteristics of the Taku Glacier over a period of 300 years.

6.3.1 Transient Velocity Distributions

Figure 6.7 shows the computed surface velocity field in the Taku at time, t= 50, 100, 200 and 300 years. The corresponding bed velocity fields are shown in figure 6.8. These figures show the major channels conveying most of the ice from the Matthes Glacier and West Branch to the Lower Taku Glacier. Flows form the Matthes Glacier and the West Branch converge to a single channel, north-west of Camp-10 (transect 4-4) and the combined flow advance towards the Lower Taku Glacier with increasing velocity. Contribution to the flow from the Demorest Glacier and the South Branch are small compared to the total volume of ice flow. The velocity of flow continues to increase some distance north of transect 8-8 and then it starts decreasing.

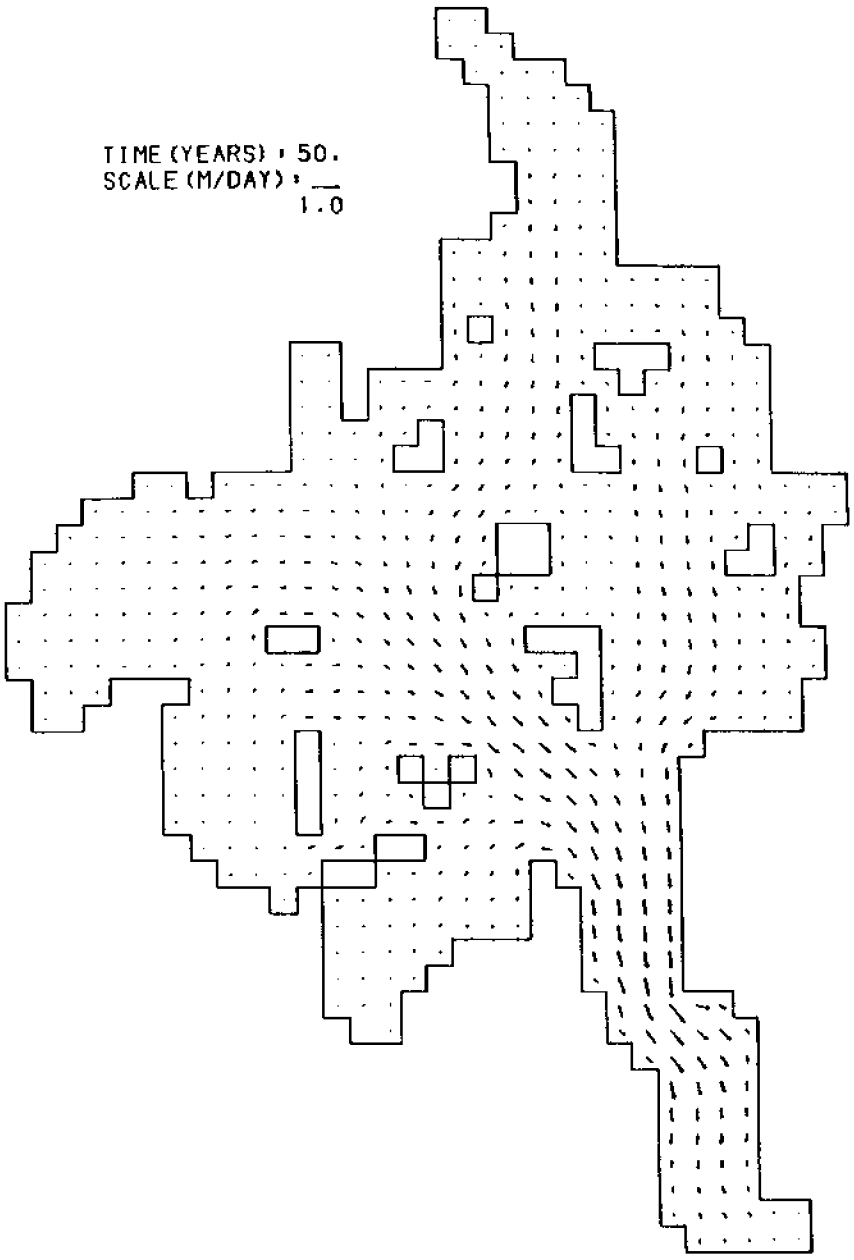

Fig.6.7a: Surface Velocity Field in the Taku Glacier at t= 50 Years

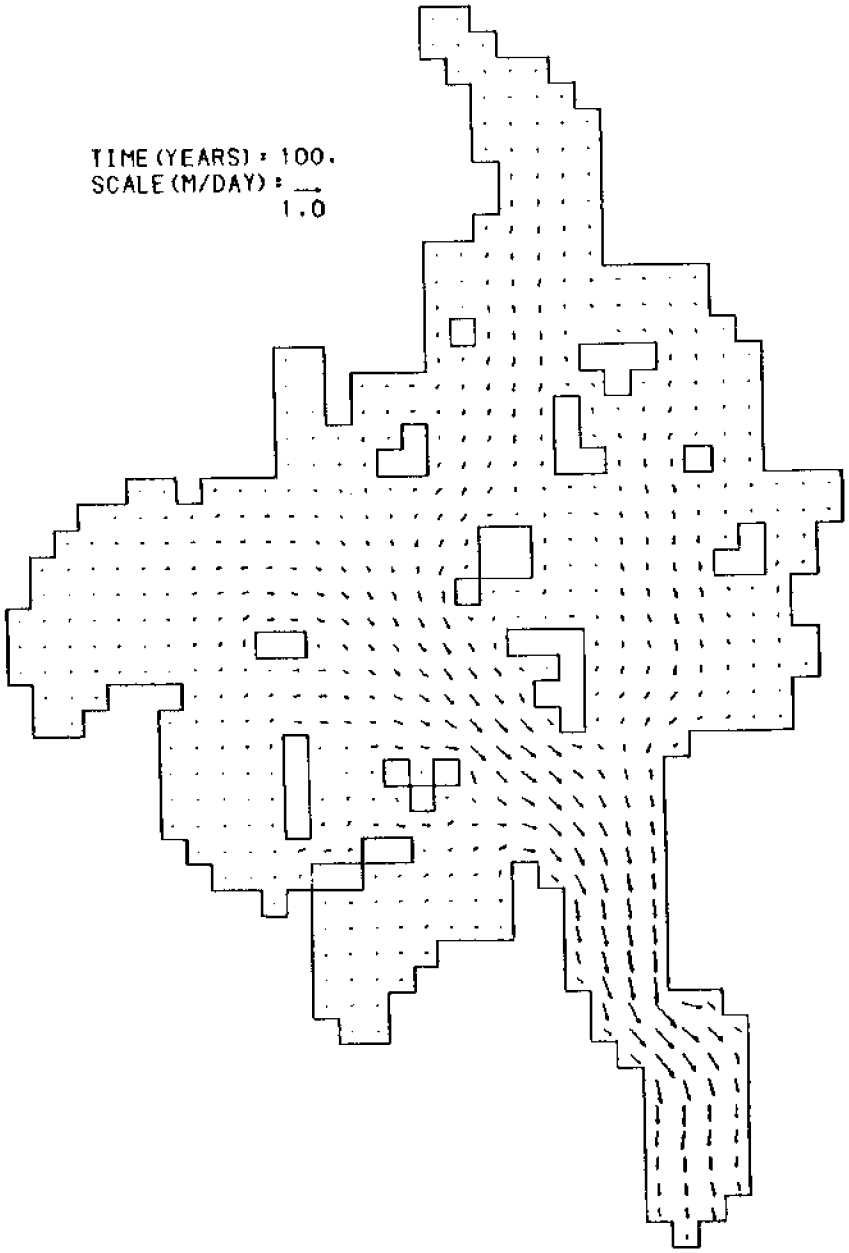

Fig.6.7b: Surface Velocity Field in the Taku Glacier
at t= 100 Years

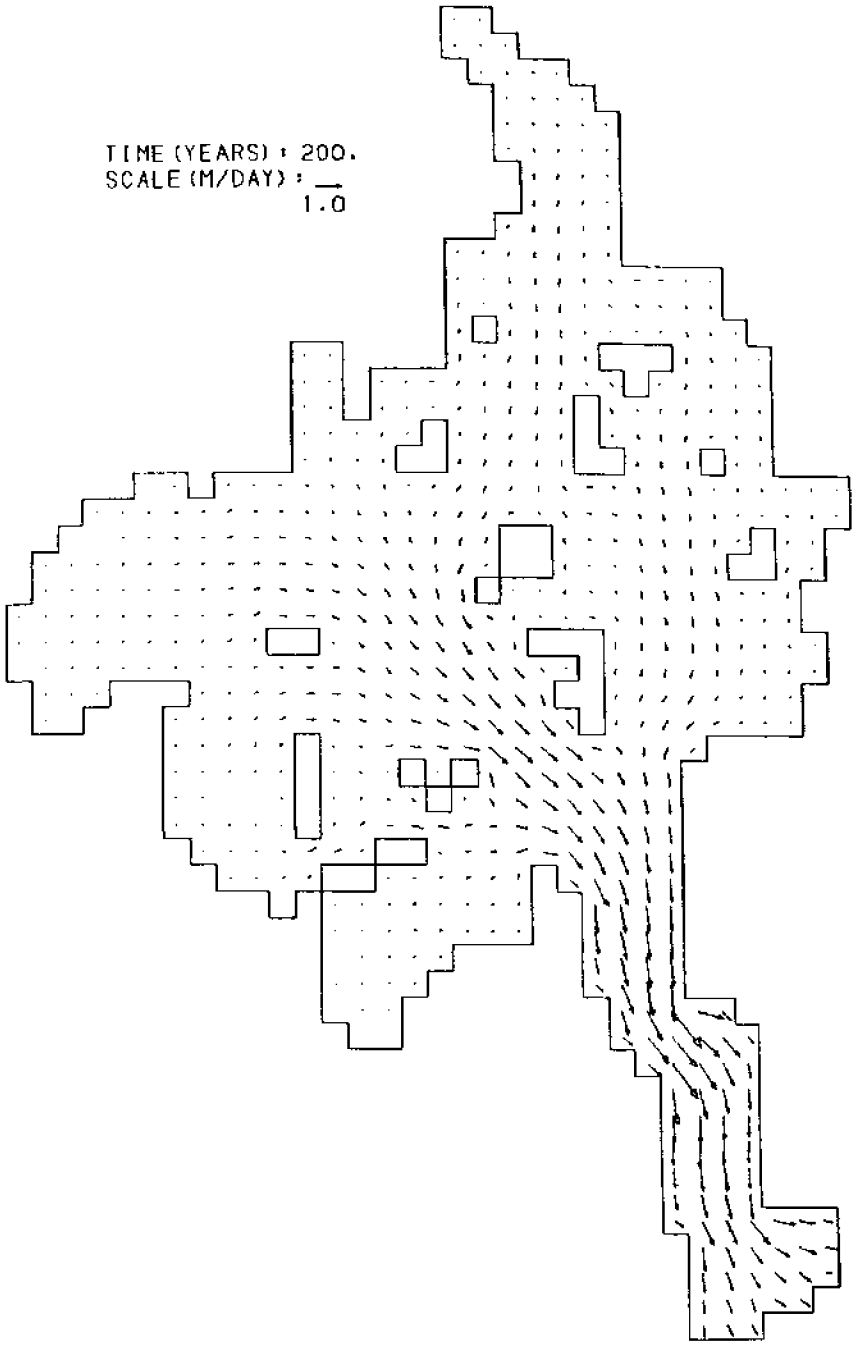

Fig.6.7c: Surface Velocity Field in the Taku Glacier
at t= 200 Years

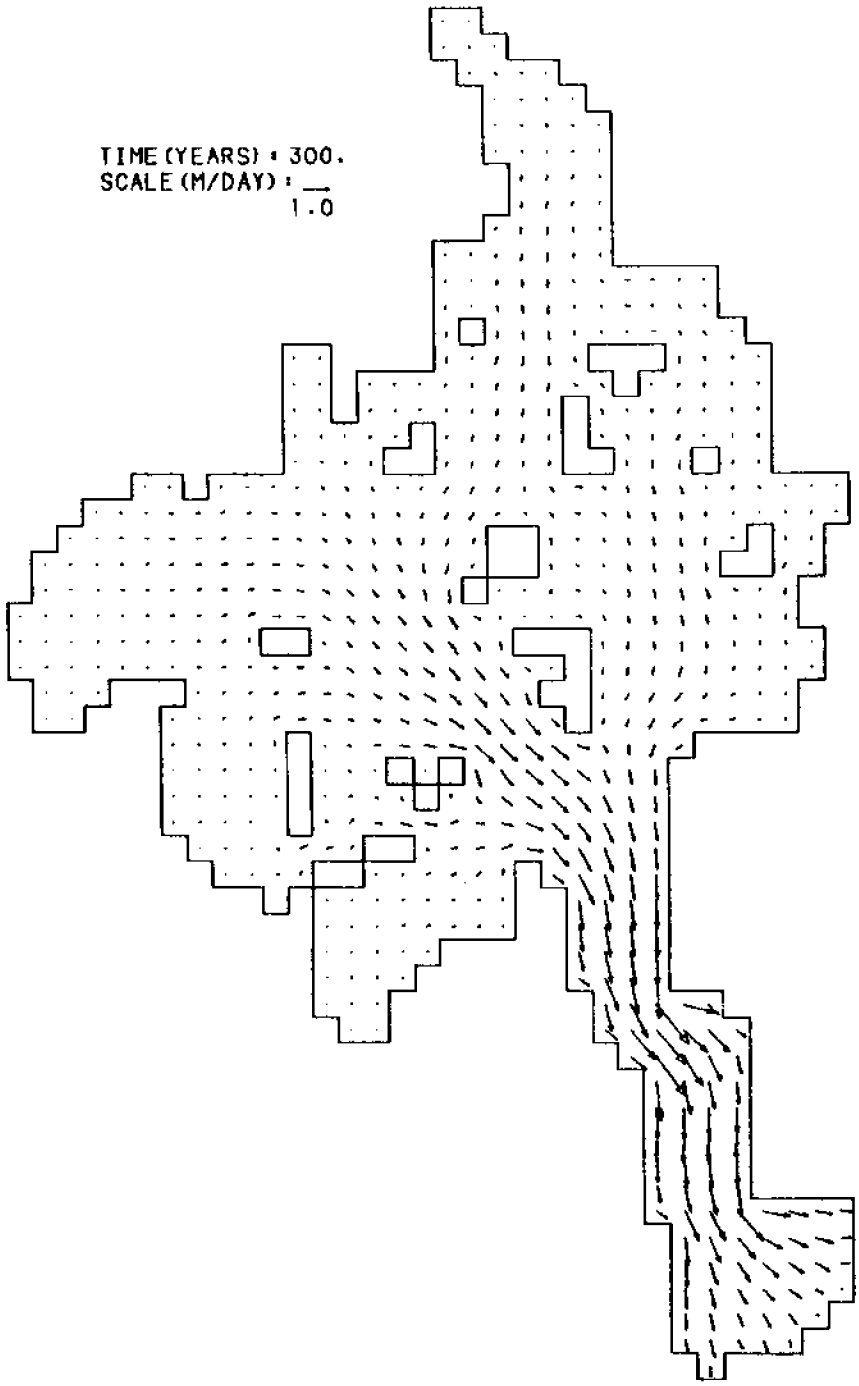

Fig.6.7d: Surface Velocity Field in the Taku Glacier at t=300 Years

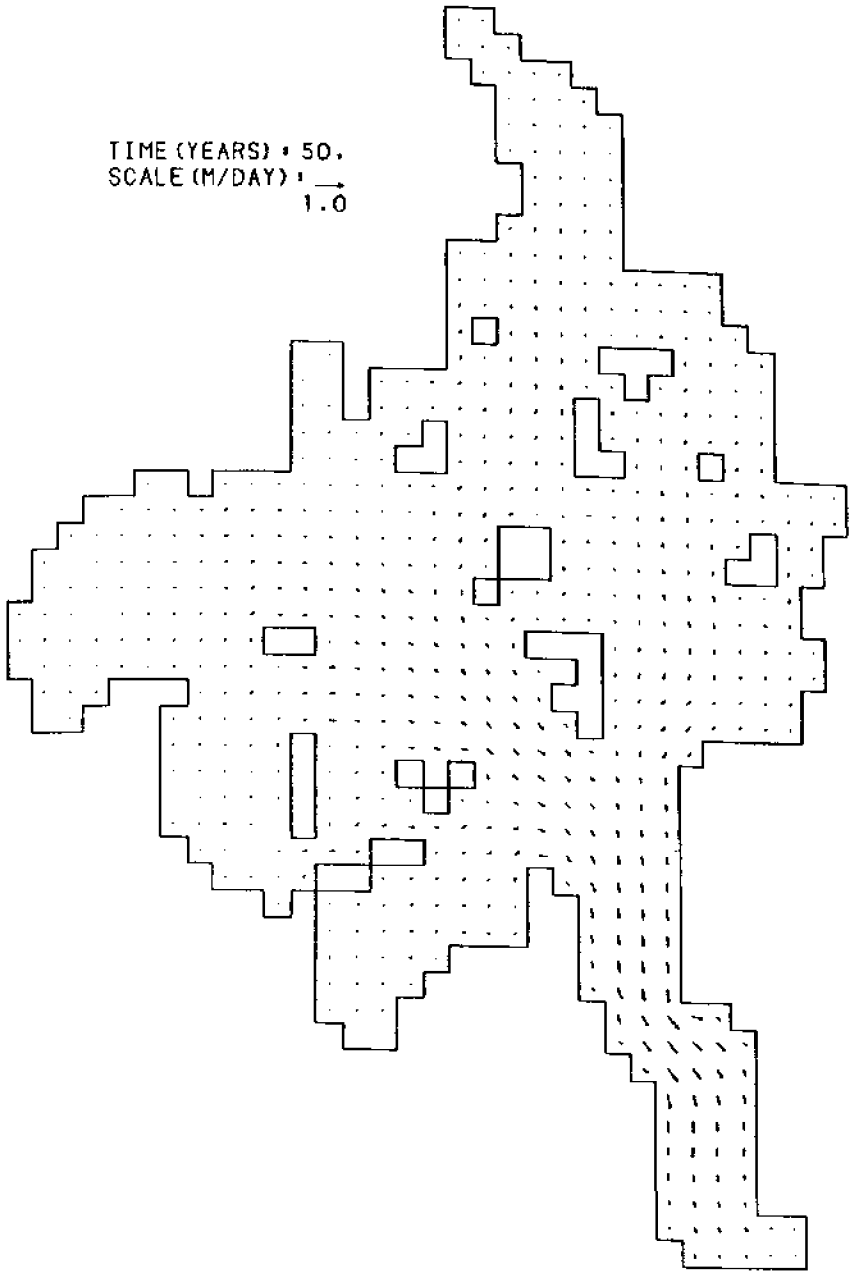

Fig.6.8a: Bed Velocity Field in the Taku Glacier at t= 50 Years

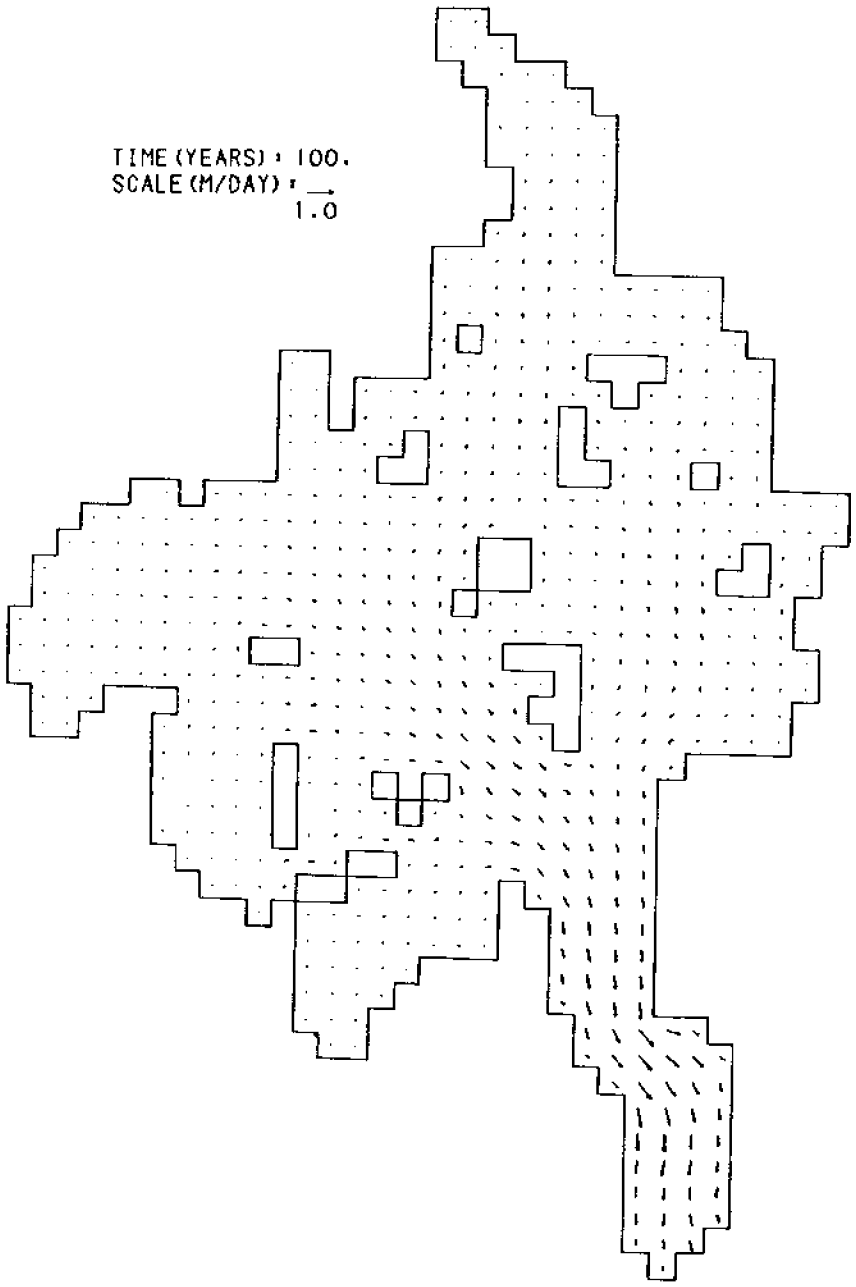

Fig.6.8b: Bed Velocity Field in the Taku Glacier at t= 100 Years

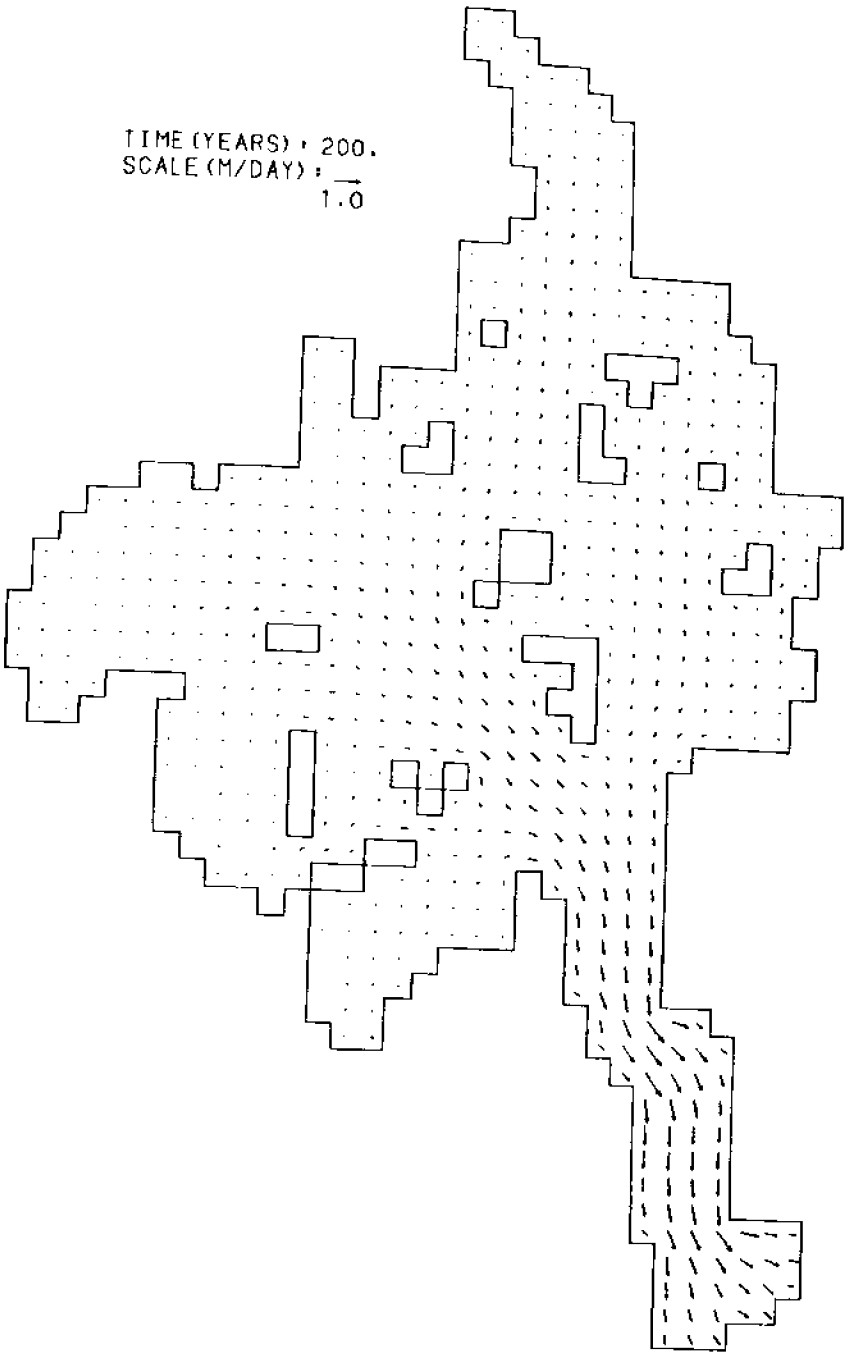

Fig.6.8c: Bed Velocity Field in the Taku Glacier at t= 200 Years

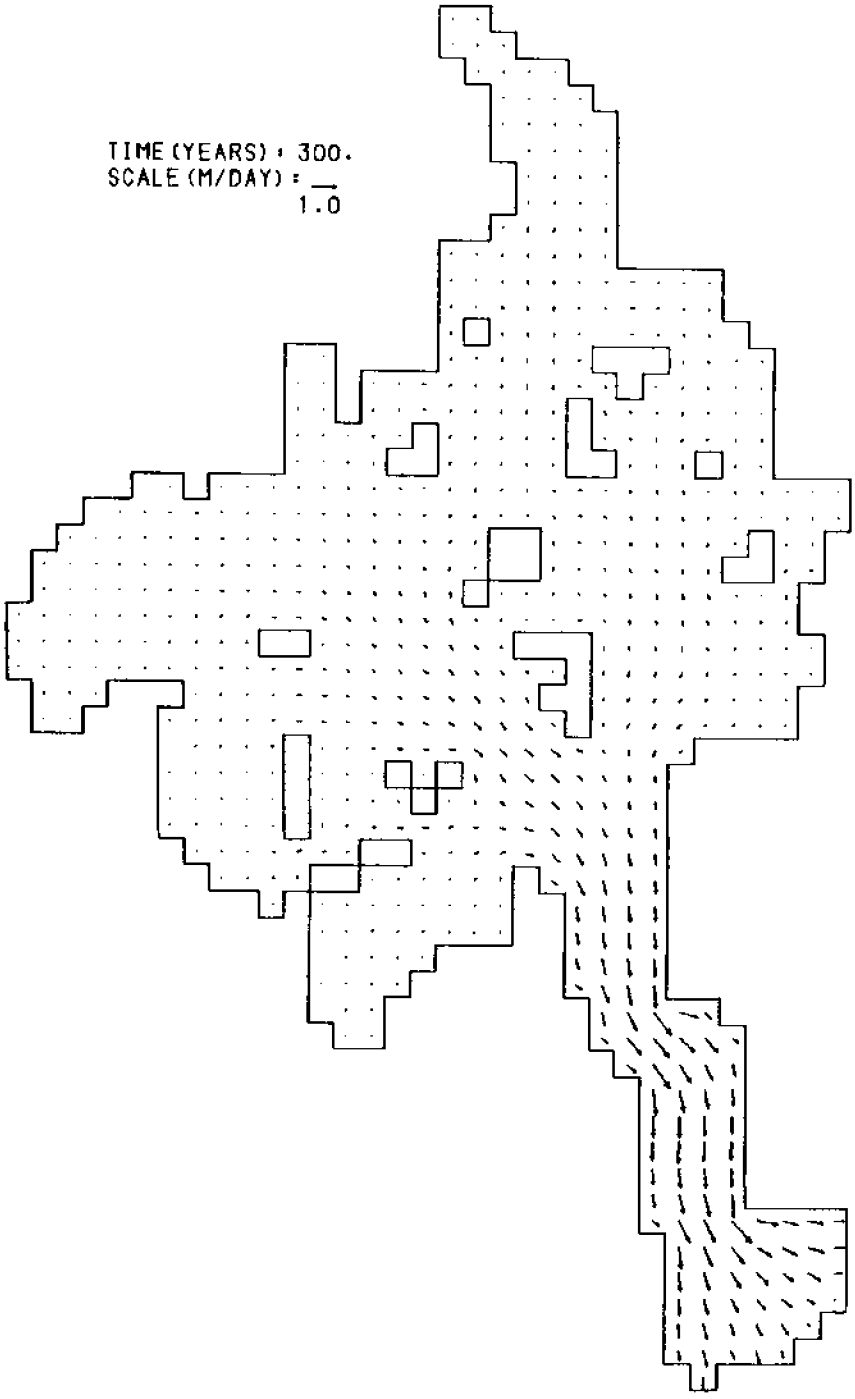

Fig.6.8d: Bed Velocity Field in the Taku Glacier at t=300 Years

6.3.2 Advance of the Terminus

Figure 6.9 shows a three-dimensional view of the computed surface topography of the Taku Glacier at t= 300 years. Figure 6.10 shows the variation of ablation area and the volume of the glacier during this period. The initial ablation area and the volume of the glacier are about 73 km^2 and 150 km^3 respectively. In this period ablation area and the volume of the glacier increase to 1.62 and 1.83 times their present values. The accumulation area remains constant at 552 km^2. The increase in the ablation area is due to the advance of the terminus of the Lower Taku Glacier, as indicated by the plots of velocity fields in figures 6.7 and 6.8. The surface topography of the Taku Glacier shown in figure 6.9 also indicates the same information. Figure 6.11 shows the plot of the leading edge of the terminus at t= 0, 50, 100, 200 and 300 years. The corresponding surface topographies of the terminus are shown in figure 6.12. In the first 50 years the terminus advances by 2.0 km and then retreats 3.0 km in the next 50 years. This rapid advance and then retreat of the terminus is mainly the results of the assumed initial conditions. It takes about 100 years to establish sufficient flow so that the supply of ice from the accumulation area exceeds the ablation. The hump in the temporal variation of surface elevation, and velocity at transect 8-8 in figures 6.2 and 6.3, and accumulation area shown in figure 6.10 are caused by the rapid oscillation of the terminus in the first 100 years of simulation.

6.3.3 Quasi-Steady State Characteristics

Numerical simulations indicate that the Taku Glacier reaches a quasi-steady state in about 300 years. Thereafter, the growth of the glacier is very slow. The configuration of the glacier at t= 300 years can therefore, be assumed to represent a situation very close to steady-state. Figure 6.13 show the contour of the increase in ice thickness in the glacier. The increase in ice thickness varies from about 100 m to about 400 m. The 400 m increase occurs in a small reach of the Lower Taku Glacier just north of transect 8-8. A 100 m change in elevation takes place in two small regions near the Boundary Range Mountains and north-eastern

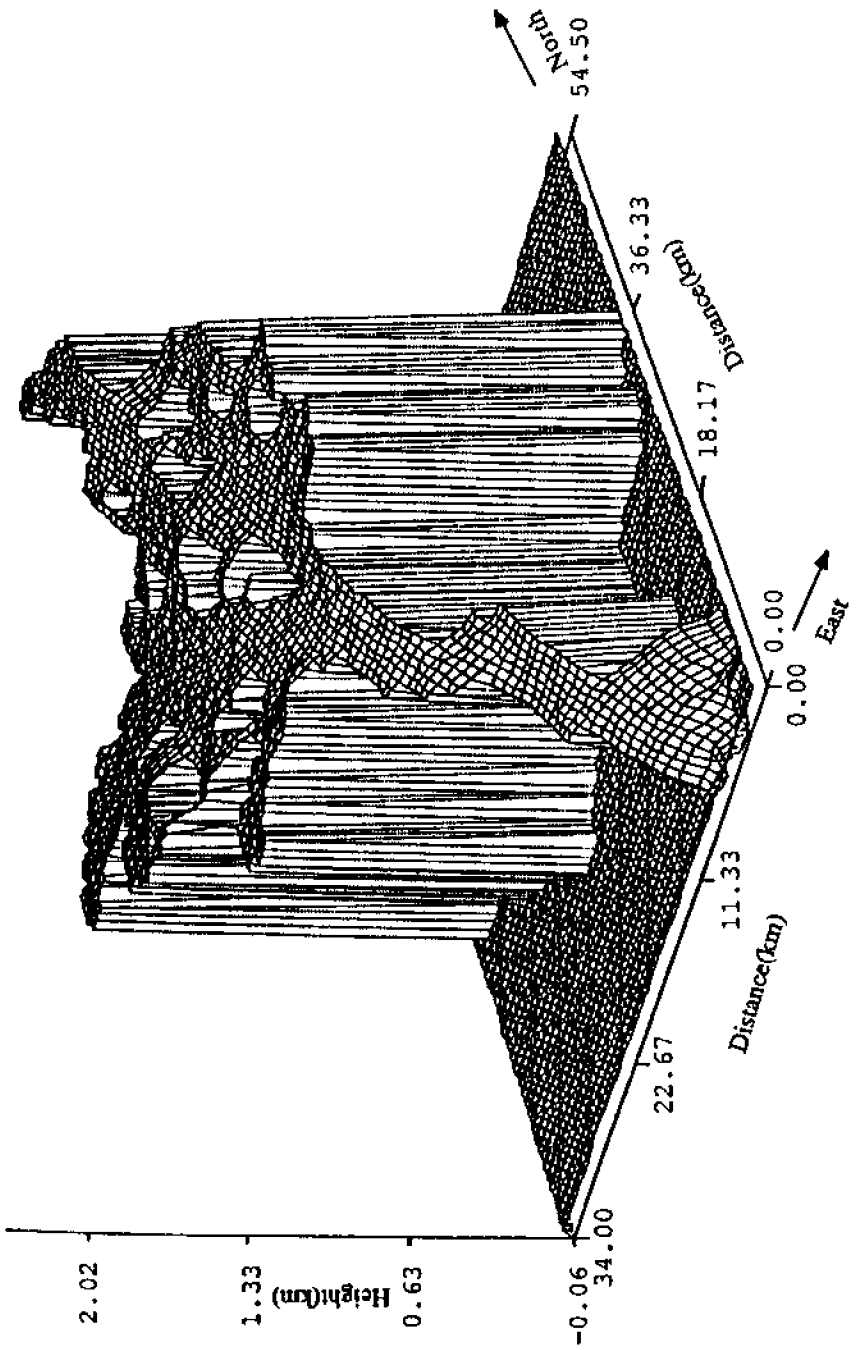

Fig.6.9: Surface Topography of the Taku Glacier at t=300 Years

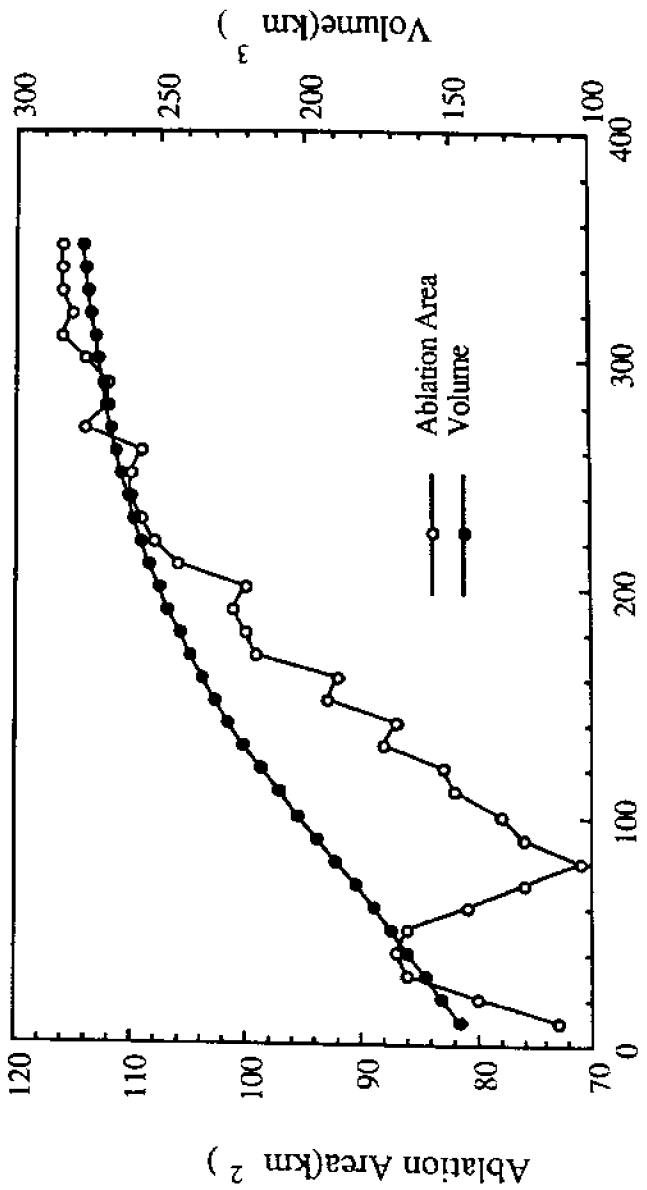

Fig.6.10: Temporal Variations of Ablation Area and Volume of the Taku Glacier

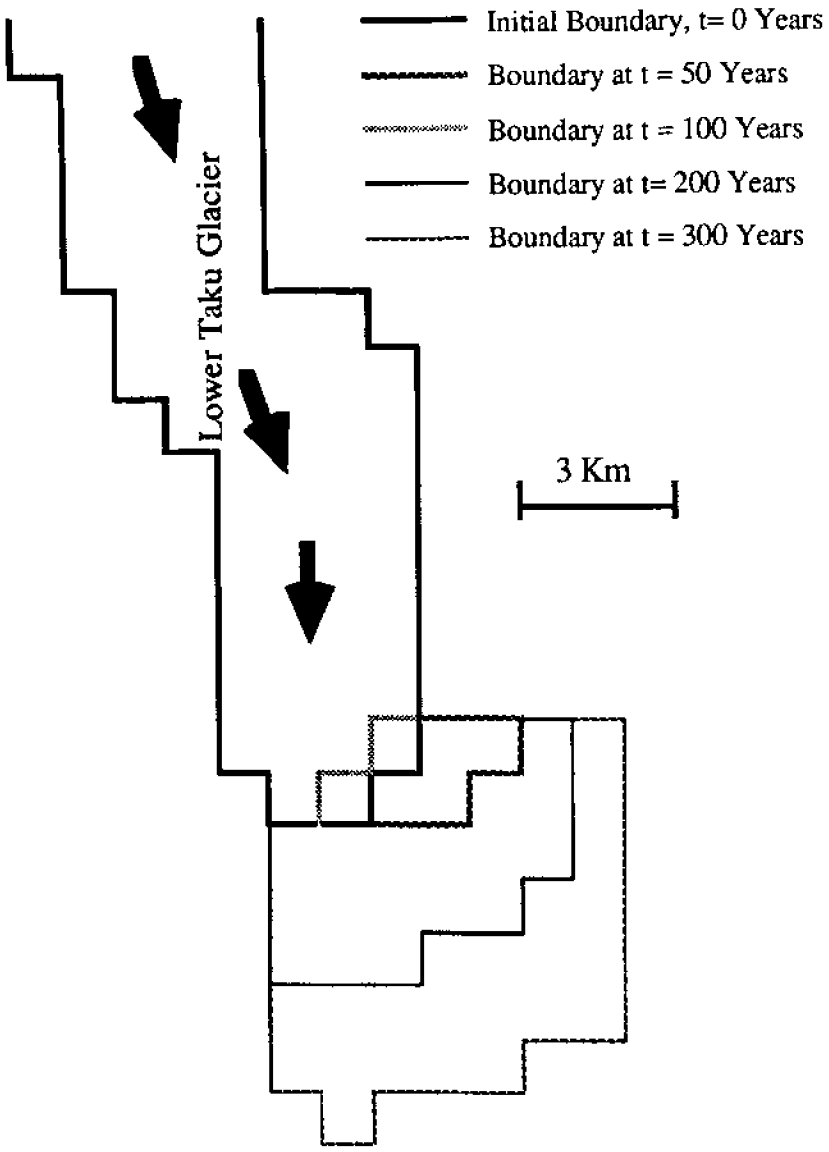

Fig.6.11: Advance of the Terminus of the Taku Glacier in Time

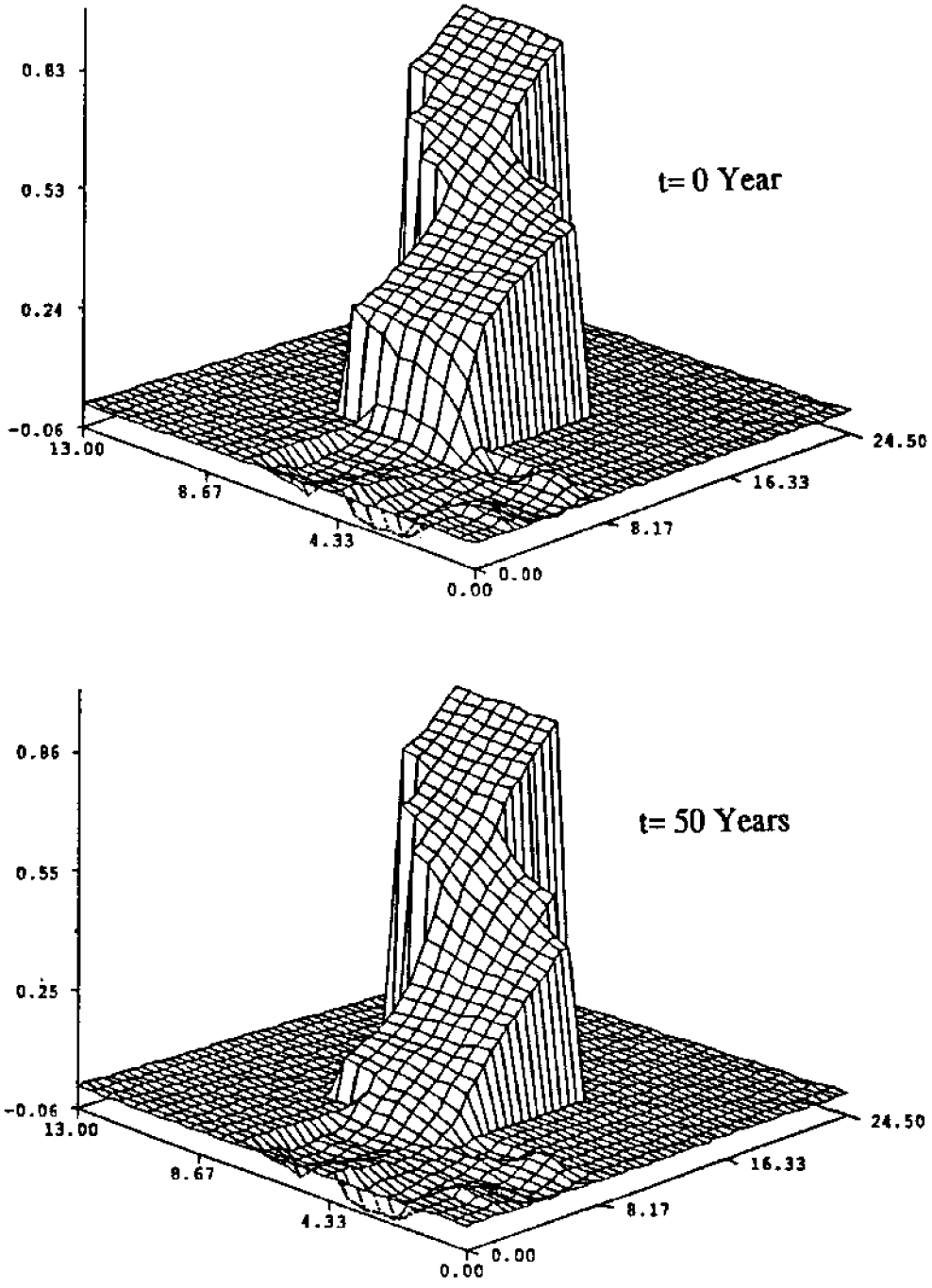

Fig.6.12: Surface Topography of the Terminus at Selected Time (Height and Lengths in Km)

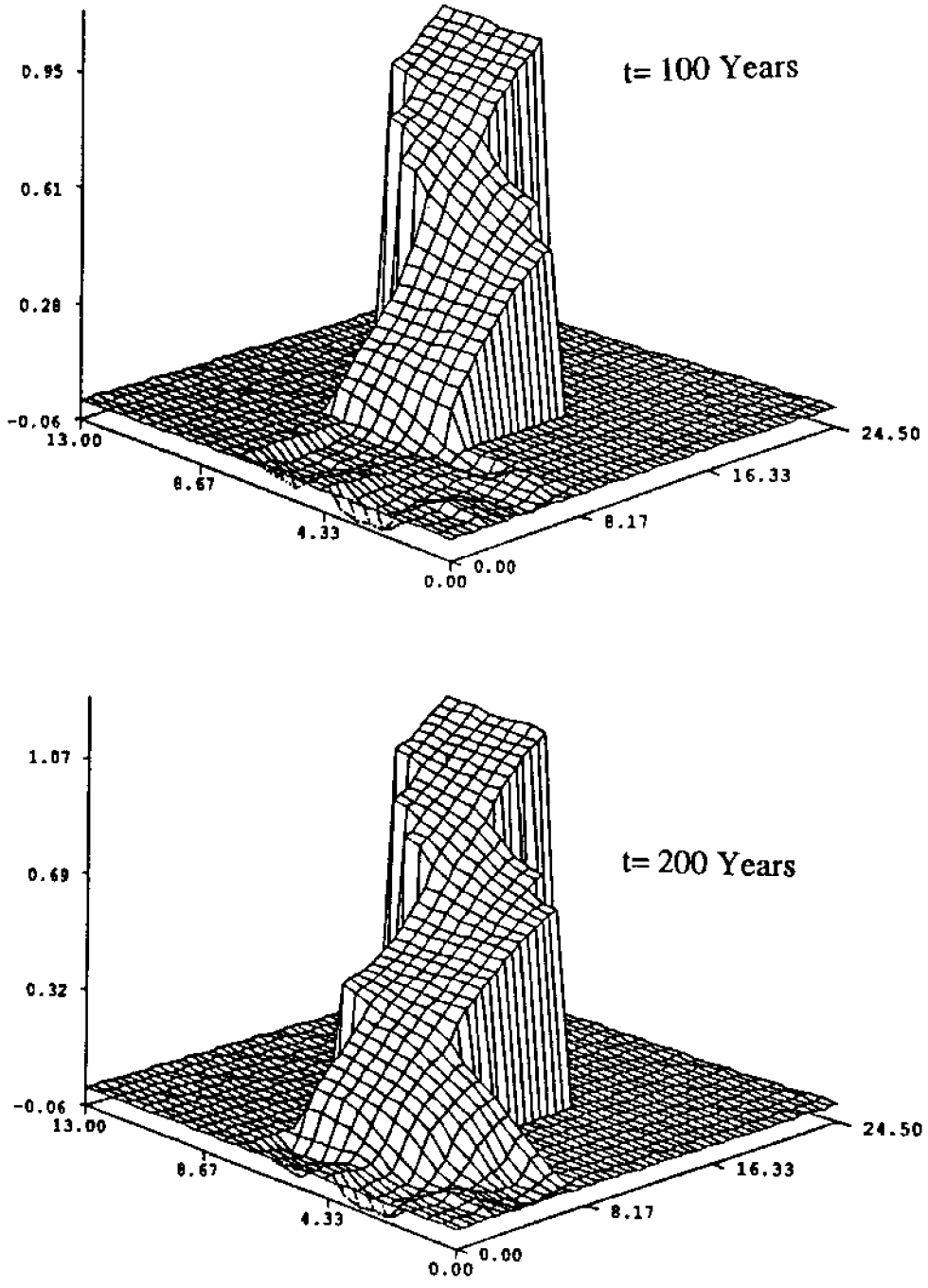

Fig.6.12: Surface Topography of the Terminus at Selected Time (Height and Lengths in Km)

t=300 Years

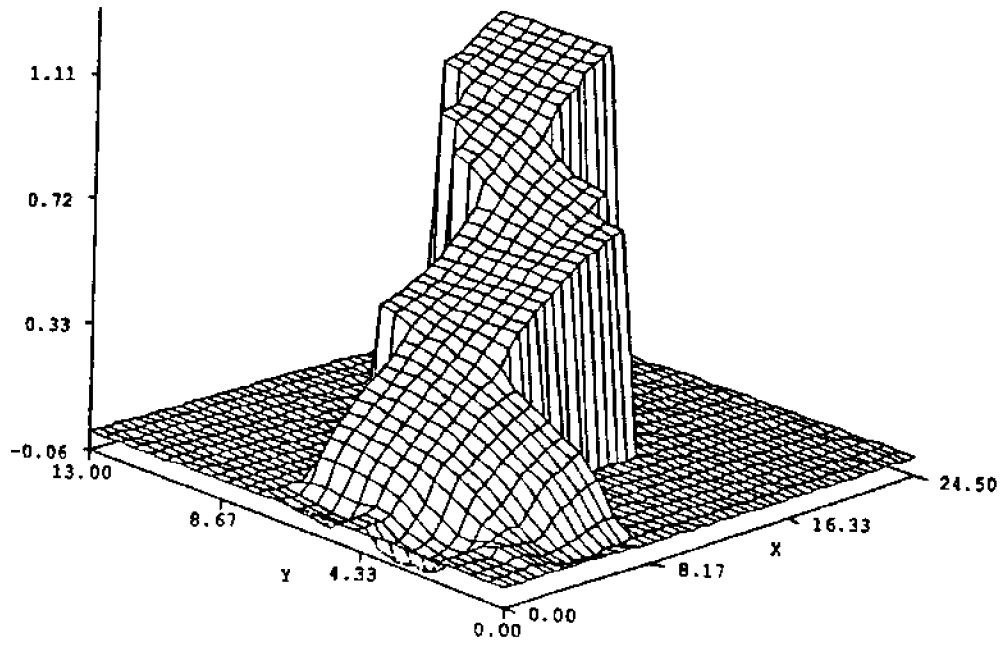

Fig.6.12: Surface Topography of the Terminus at
Selected Time (Height and Lengths in Km)

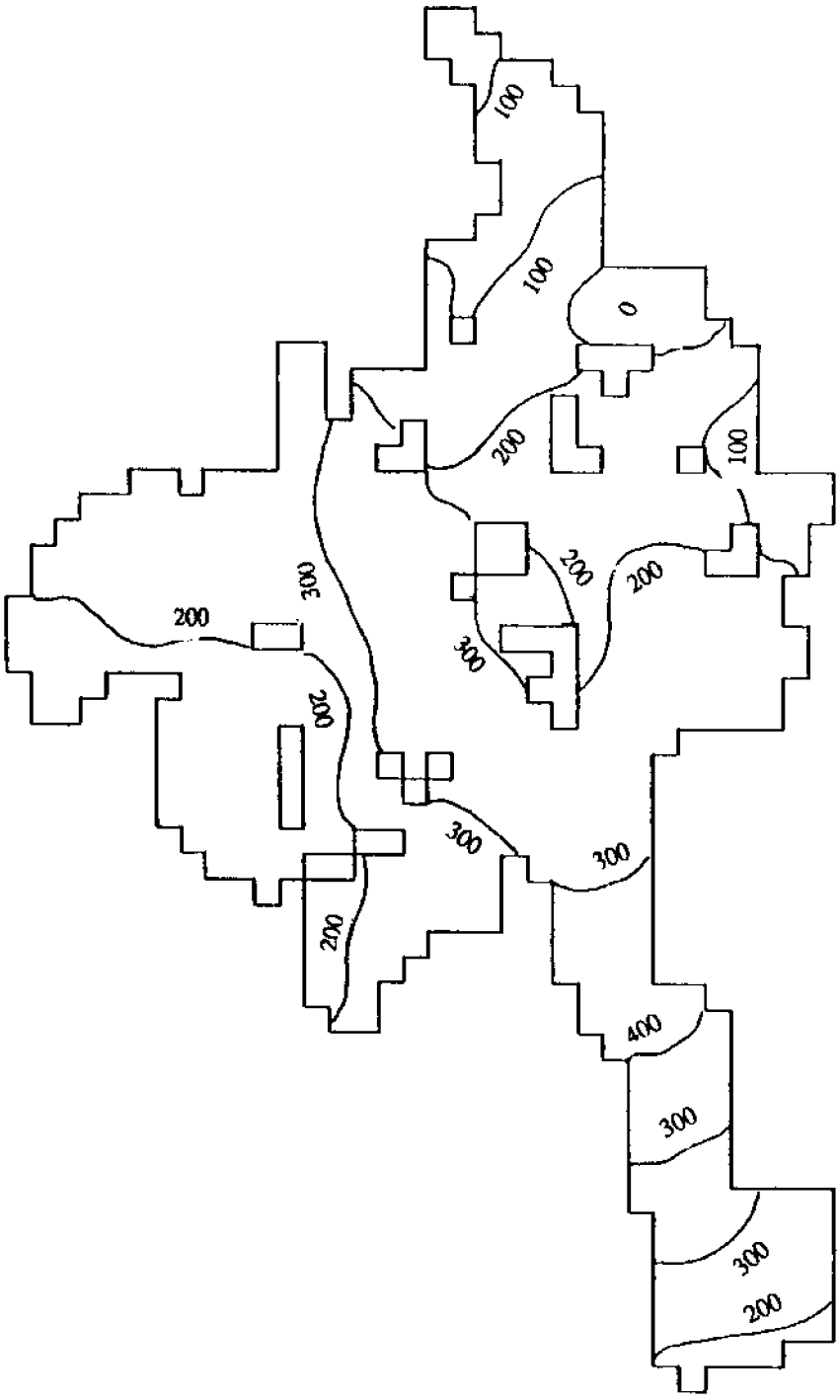

Fig.6.13: Change in Ice Thickness (m) in 300 Years

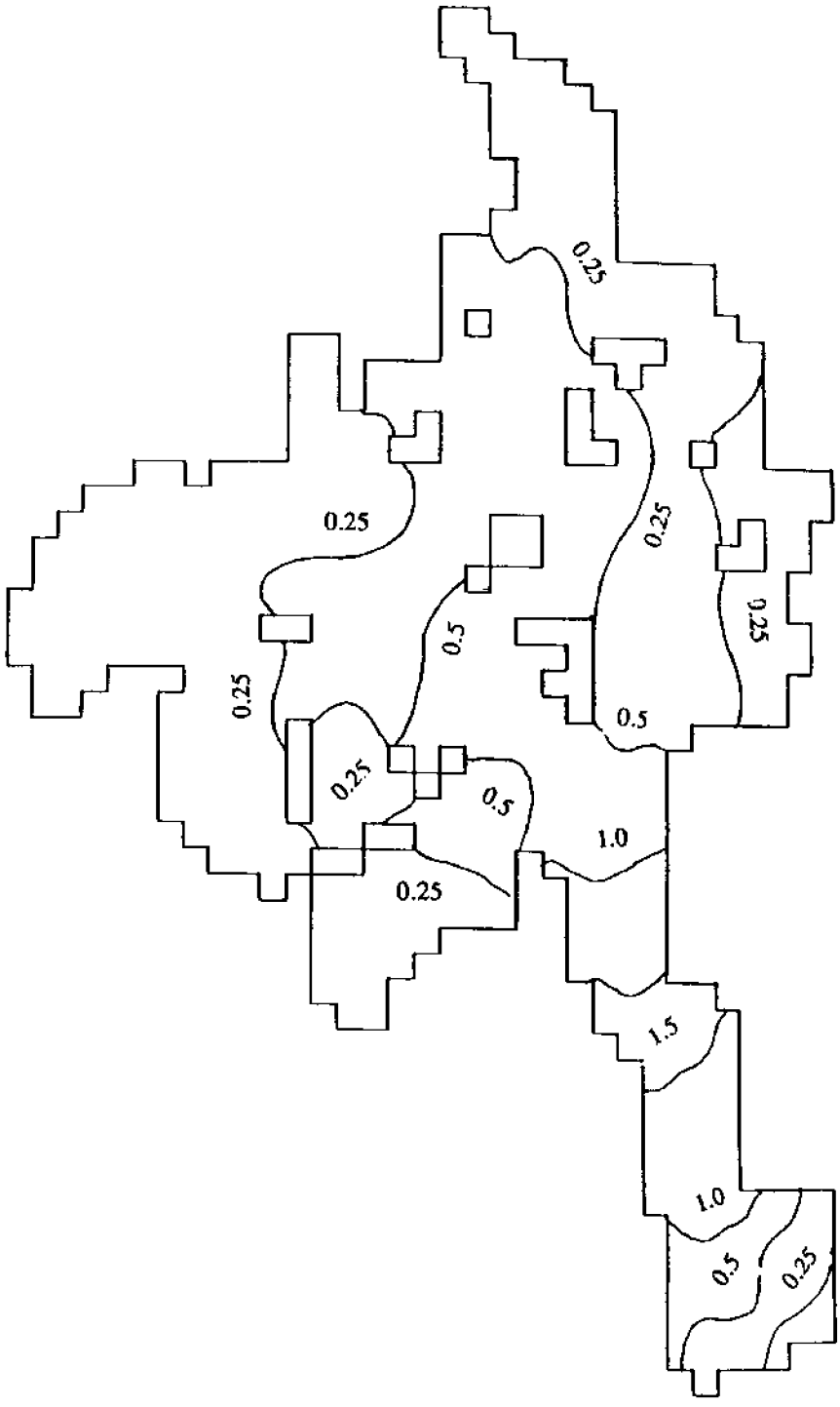

Fig.6.14: Surface Velocity (m/day) at t= 300 Years

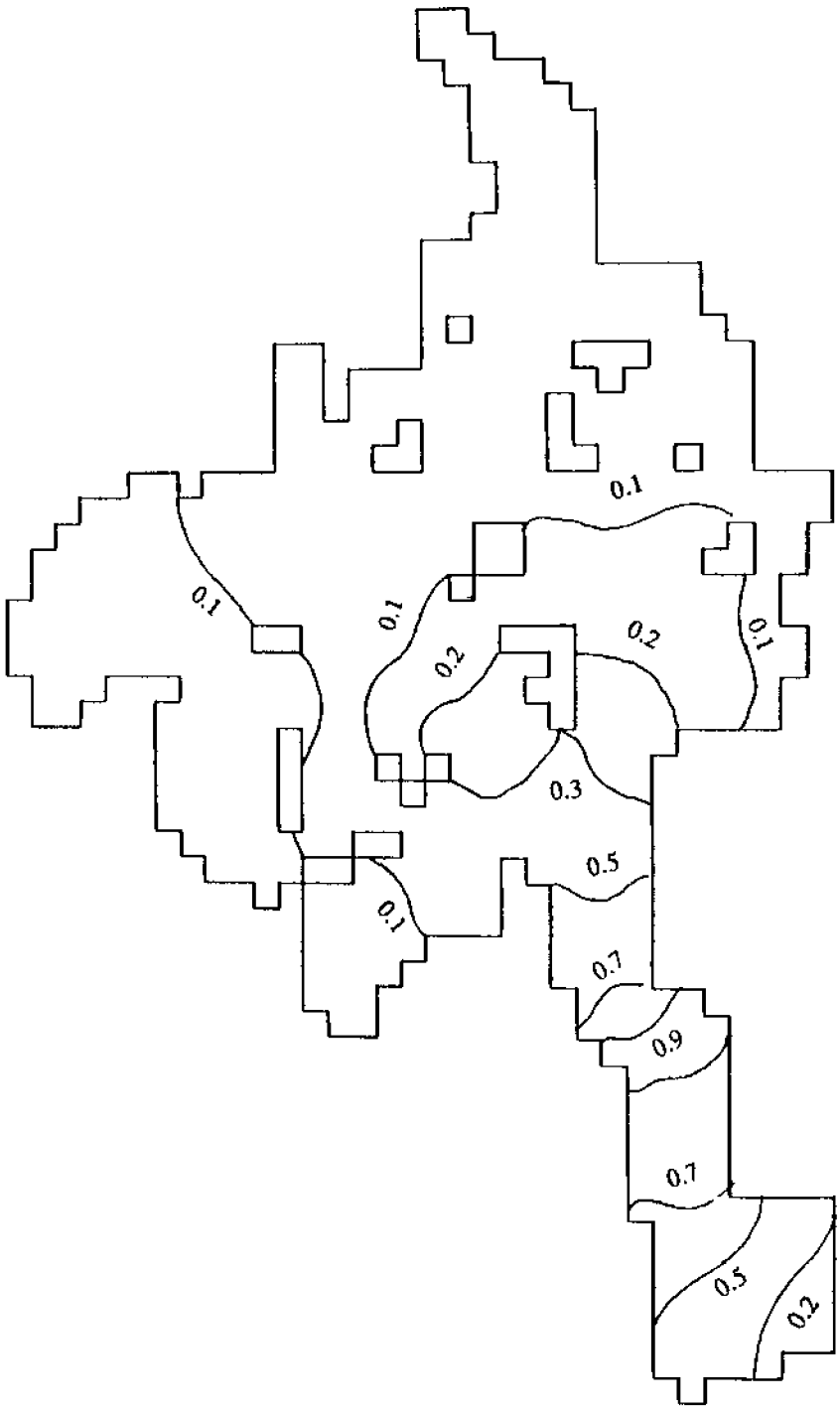

Fig.6.15: Bed Velocity (m/day) at t= 300 Years

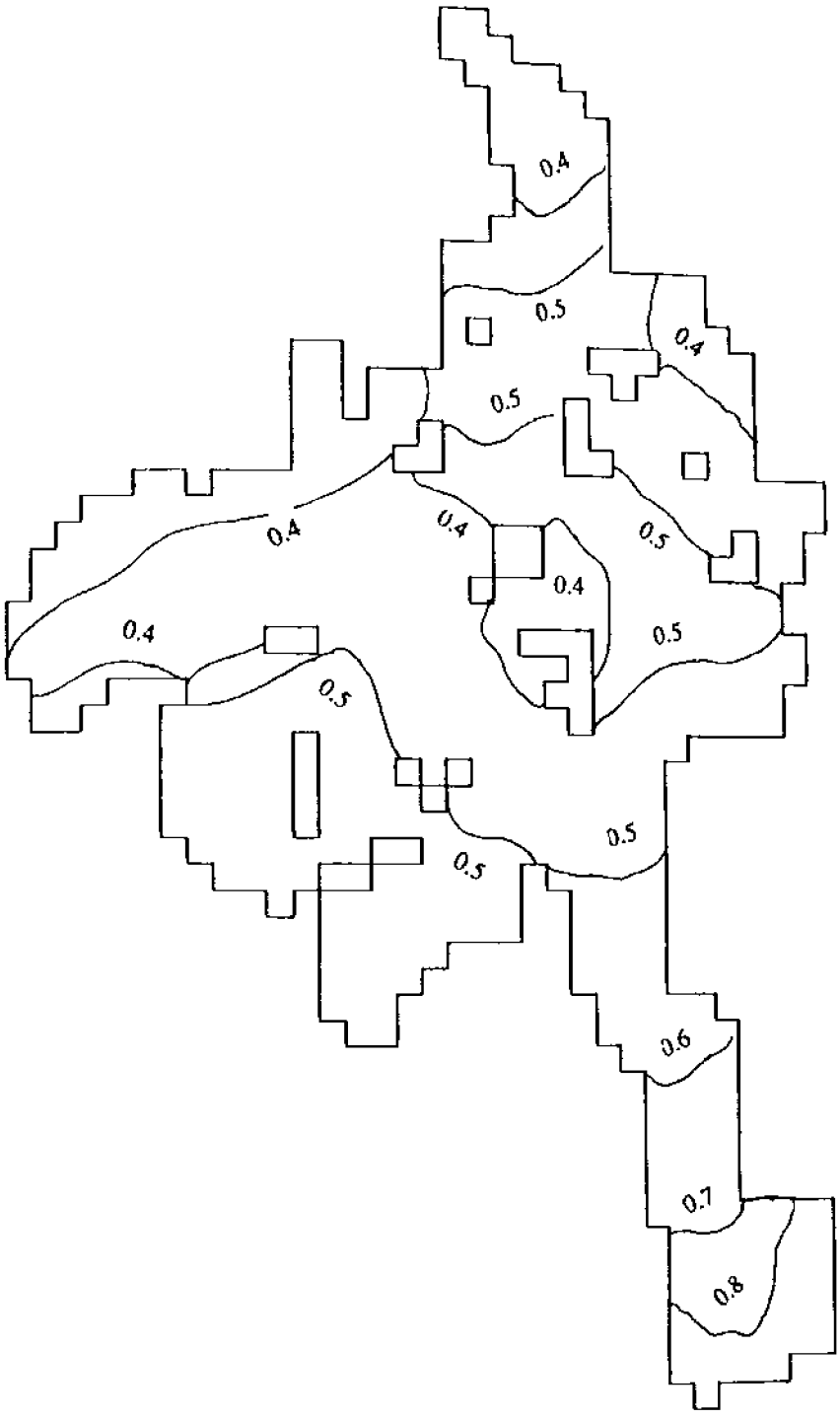

Fig.6.16: Ratio of Bed to Surface Velocity at t= 300 Years

region of the Demorest Glacier. In the central region, covering a major part of the Taku Glacier, the change in ice thickness varies from 200 to 300 m. The average rate of increase of ice thickness in this region varies from 0.67 to 1.0 m/year. The figure also shows that the ice thickness along the leading edge of the terminus is close to 200 m. This is also indicated in the three-dimensional topographies of the terminus, shown in figure 6.12.

Figures 6.14 and 6.15 show the spatial variations of surface and bed velocities in the Taku Glacier. The surface and velocities over most of the glacier are below 0.25 m/day and 0.1 m/day respectively. The velocities start increasing only after the flow from the Matthes Glacier, the West Branch, and the Domorest Glacier converges to a single flow channel. The surface velocity exceeds 1.0 m/day over most of the Lower Taku Glacier, with a maximum velocity occurring north of the transect 8-8. The maximum bed velocity occurs in the same region and its value is about 0.9 m/day. The maximum increase in ice thickness and maximum surface and bed velocities occur in the same region of the Taku Glacier. Figure 6.16 shows the distribution of the ratio of bed velocity to surface velocity in the Taku Glacier. The ratio varies from 0.4 to 0.8. Except for the Lower Taku Glacier, this ratio is smaller near the boundaries of the Glacier. In the Lower Taku Glacier it follows a pattern similar to the bed velocity. This figure also shows that in the upper reaches of the Taku Glacier, the major part of the ice flow is due to the internal deformation of ice. In most of the central region, bed sliding and deformation of ice have roughly equal contributions. In the Lower Taku Glacier, bed sliding is the dominant mode of mass transport. These results are comparable to the present field observations.

Figure 6.17 shows the distribution of bed shear stress. The computation is based on equation(2.7) with $\rho = 900$ kg/m^3. Bed shear stress varies from 50 kN/m^2 to 300 kN/m^2. In temperate glaciers, maximum bed shear stress varies from 100 to 200 kN/m^2 (Paterson, 1981). Over most of the glacier, the value of the computed bed shear stress are within acceptable limits. However, it exceeds 200 kN/m^2 in a small region north of transect 8-8 in the Lower Taku Glacier. This is the region

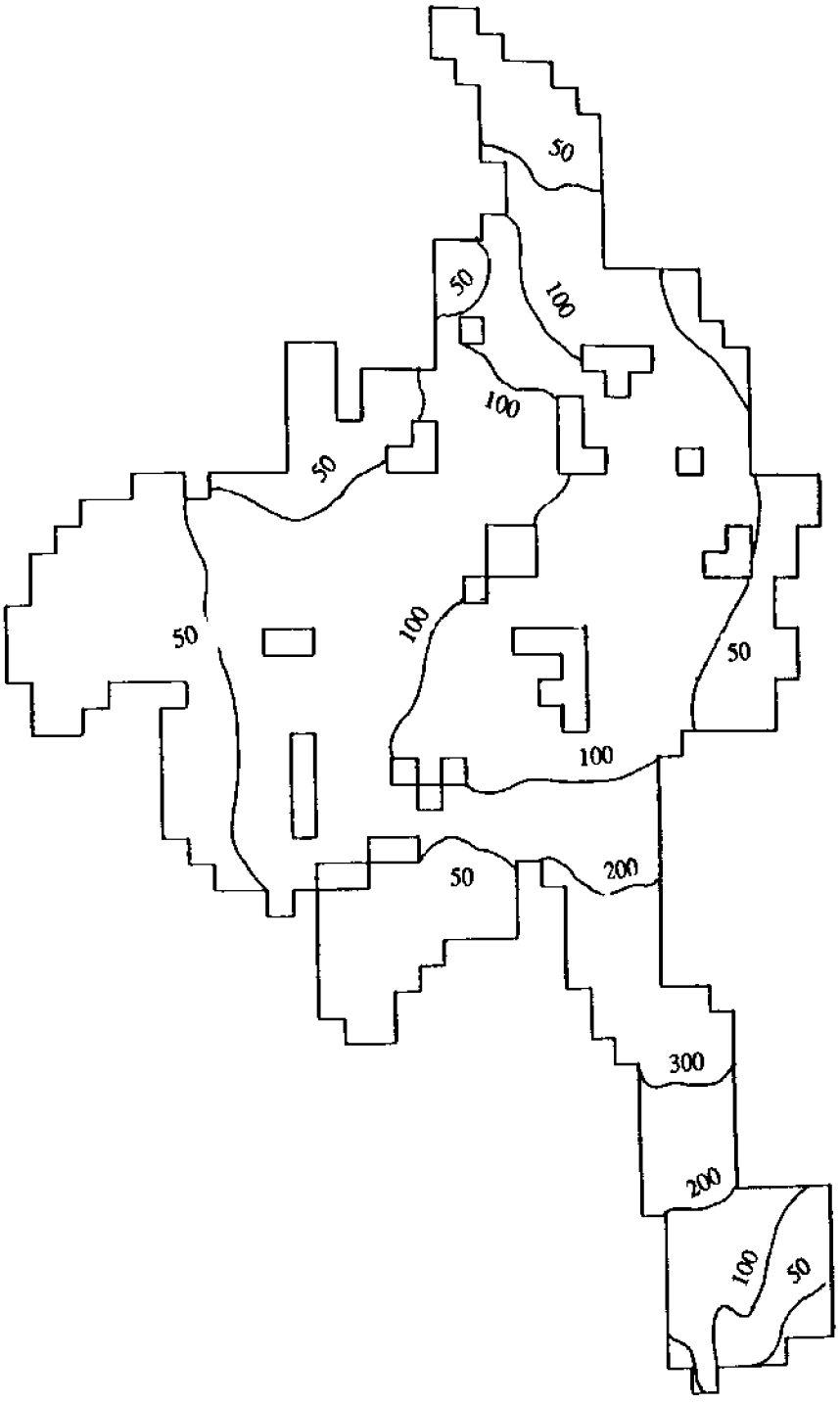

Fig.6.17: Bed Shear Stress (kN/m^2) at t= 300 Years

where both the surface and bed velocities are highest. Bed velocity accounts for more than 70 percent of the total velocity and the increase in ice thickness over time is highest.

6.4.0 RESPONSE TO CLIMATIC WARMING

6.4.1 Altitudinal Shift of the Equilibrium Line

Table-4.4 lists surface roughness in glaciers in widely different environmental, geographical and, climatic regions. The value of surface roughness varies from 0.09 to 0.69 cm. In estimating μ, z_o was taken as 0.338 cm. Based on information presented in Chapter-4 the value of μ is about 1.82×10^6 J m^{-2} d^{-1} °C^{-1} and μ' is 3.60×10^5 J m^{-2} d^{-1} °C^{-1}. The altitudinal temperature gradient $\partial T_a/\partial z$ = -0.00546 °C/m. At the equilibrium line the number of ablation days is about 100. Analysis of mass balance data indicates that, in the accumulation zone, the specific accumulation rate is 1.74 m/year and the altitudinal gradient $\partial c/\partial z$ is 1.84 kg/m^3. As no information about the change in accumulation rates are available, δS^+ is assumed zero. Figures-6.18 to 6.20 show the effects of different values of μ, change in accumulation rate, and the increase in accumulation and the number of ablation days on the altitudinal shift of the equilibrium line respectively. Using the present configuration of the Taku Glacier, figure-6.21 indicates the variations of accumulation and ablation areas as a function of the altitudinal shift of the equilibrium line. The configuration of the glacier is assumed to remain unchanged.

The results, shown in figures 6.18 through 6.20, can be partially summarized as follows ($\mu' = 3.60 \times 10^5$ and $\mu = 1.82 \times 10^6$ J m^{-2} d^{-1} °C^{-1}):

$\partial h/\partial T_a$= 61.20 m °C^{-1} (δS^+=0)

$\partial h/\partial S^+$ =-19.10 m per 100 kg/m^2 (δT_a= 0)

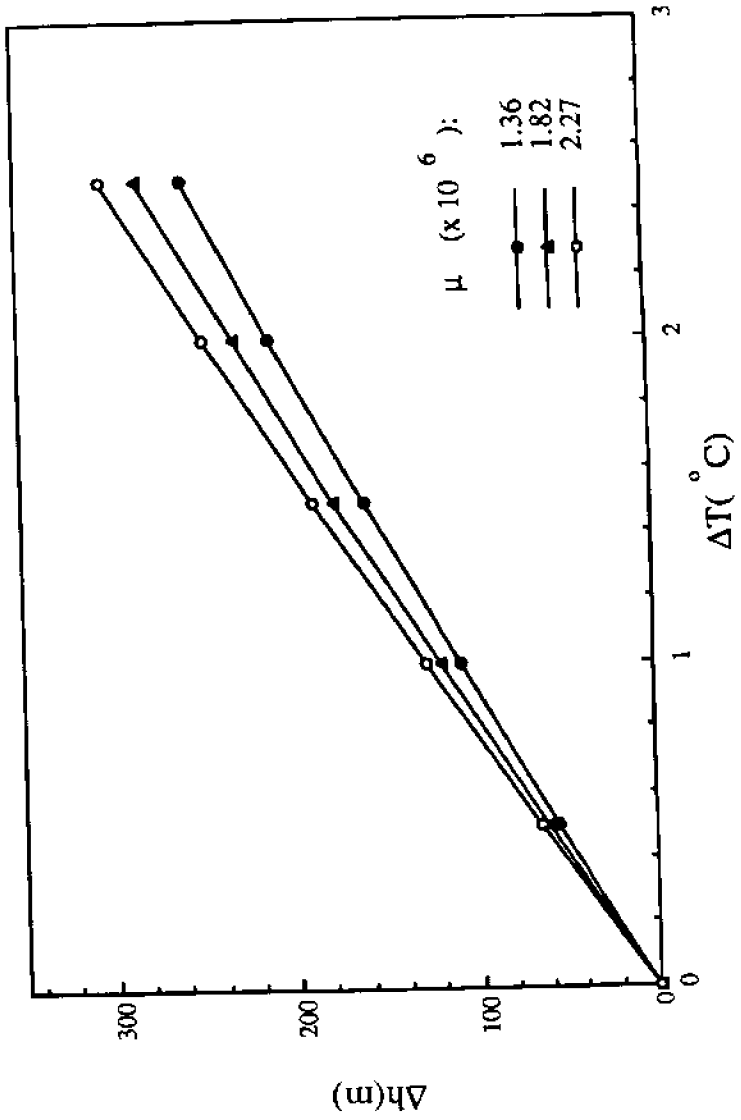

Fig.6.18: Altitudinal Shift of the Equilibrium Line as a Function of Climatic Warming

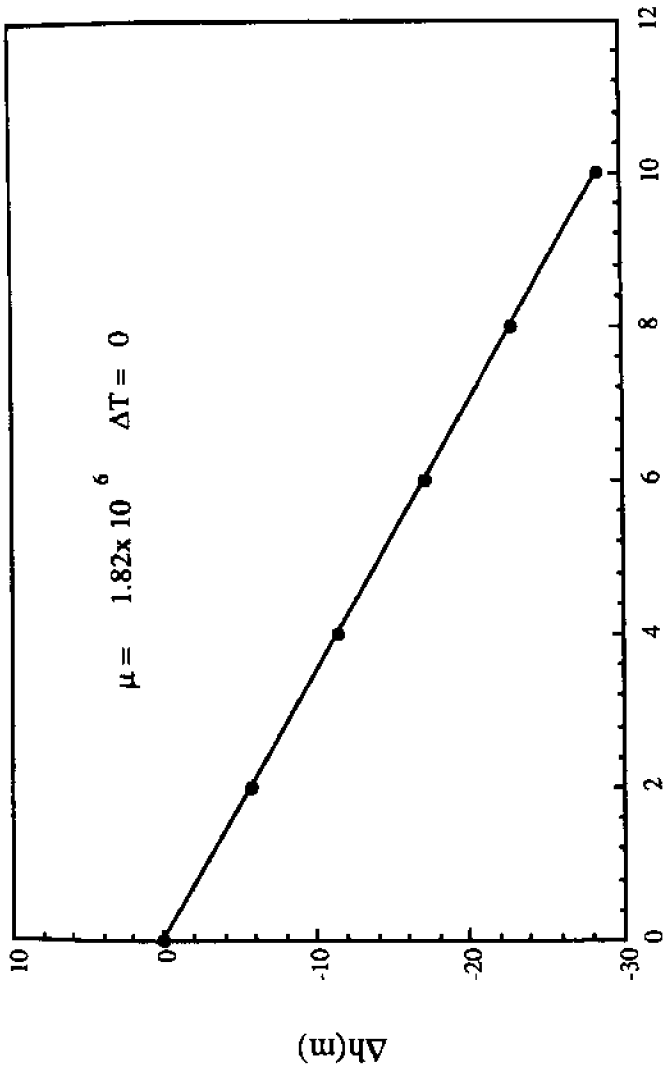

Fig.6.19: Altitudinal Shift of the Equilibrium Line as a Function of the Increase in the Accumulation Rate

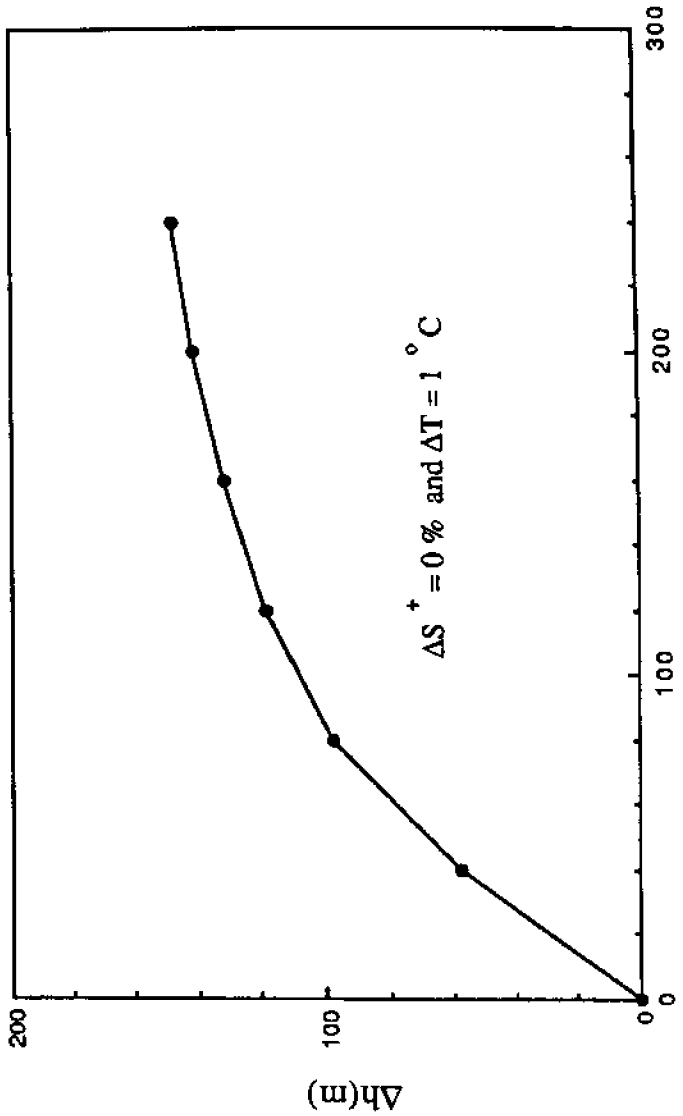

Fig.6.20: Effect of Number of the Number of Ablation Days on the Altitudinal Shift of the Equilibrium Line

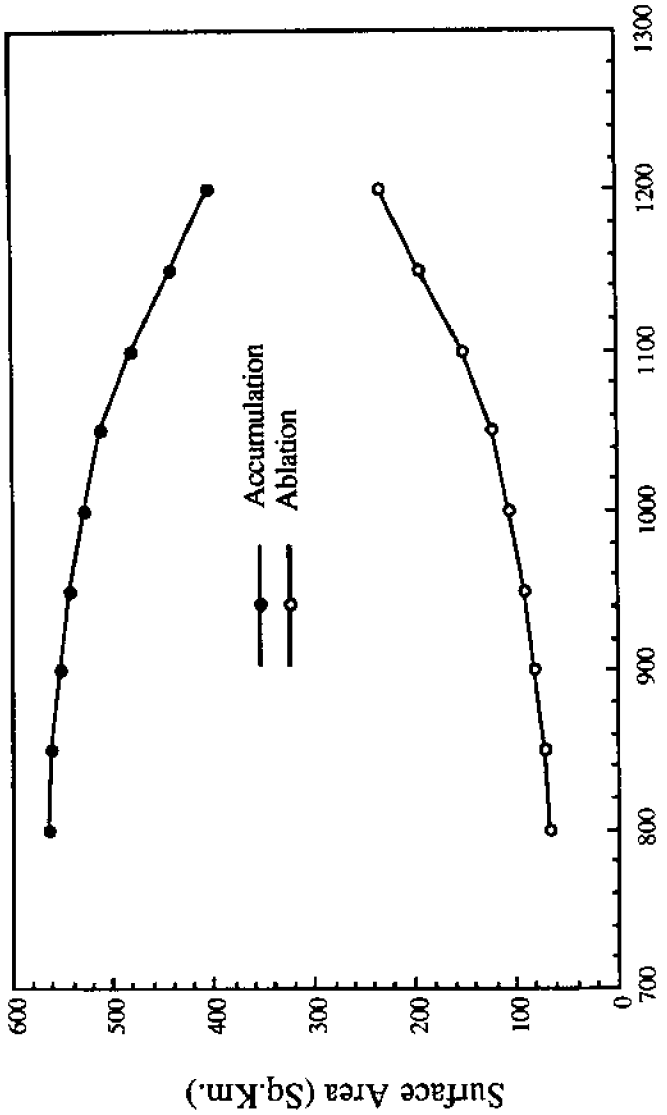

Fig.6.21: Accumulation and Ablation Areas as Function of the Altitude of the Equilibrium Line

The effects of wind velocity, surface roughness and other parameters on the altitudinal shift of the equilibrium line were not considered individually, because the variation of μ combines their individual effects. As μ' is one order of magnitude smaller than μ, its effect on the computed change in elevation is small. Figure 6.18 shows that an error in the estimation of μ by 50 percent introduces an error in the computed shift of altitude of about 9.3 m for a 1 °C rise in temperature. This error is small compared to the altitudinal shift of the equilibrium line for a 1 °C change .

A close look at figure 6.18 shows that the slope of the Δh vs ΔT curve is not actually constant. As the temperature increases, the rate of change of elevation decreases slightly. The non-linear effect is mainly due to the change in number of ablation days introduced into equation(4.9) by equation(5.2). Kuhn(1980) and Ambach(1985b) appear to have used a constant value of ablation days even though the altitudinal shift of the equilibrium lines were considerable. The effect of the number of ablation days on the altitudinal shift is shown in figure 6.20. When the number of ablation days is small, a change in its value has a significant effect on the result. As the number of ablation days increases, the effect of the change progressively decreases. The effects of cloudiness was not studied because of the lack of field data. However, its effect is considered negligible (Kuhn, 1983; Ambach and Kuhn, 1983).

In this analysis δS^+ was assumed zero. The Taku Glacier has sufficient records of mass balance data so that the computed balance gradient is reasonably good. A comparison of the effects of δS^+ and δTa on δh indicates that the effect of δS^+ is small. A change is accumulation rate by 100 kg/m^2, which corresponds to about 6.67 percent of the present mean accumulation rate, causes the equilibrium line to fall by 19.1 m. The amount of increase in precipitation in the next hundred years is uncertain but generally assumed to be not more than ten percent of the present accumulation rate (Bindschadler, 1985; Kuhn, 1985; Kandel, 1983). Therefore, an increase in temperature by 2.5 °C will cause the equilibrium line to rise by 250 to 300 m, which could be offset by only 30 m by an increase in the accumulation rate of ten percent.

6.4.2 Response of the Taku Glacier With Climatic Warming

To incorporate the influence of the climatic warming in the flow model, the following assumptions are made:

1. The temperature increase is a linear function of time and the rate of increase is 2.5 °C per century.
2. The heat and energy balance parameters involved in the Kuhn's algorithm are independent of time and the increase in temperature.
3. Ablation at and below mean sea level remains constant over the simulation period.
4. The ablation rate between the equilibrium line the mean sea level is a linear function of surface elevation. However, the computed ablation rate can not be less than the present ablation rate.
5. There is no increase in precipitation due to the climatic warming. As indicted above, this has a small effect.

Based on these assumptions, figure 6.22 shows the variations of accumulation and ablation areas over a period of 200 years. The accumulation area decreases from 545 km^2 to about 324 km^2, while the ablation area increases by 210 km^2 from only 73 km^2. Therefore, the ratio of the ablation area to accumulation area changes from 0.137 to 0.648. The increase in the ablation area is mainly due to the upward shift of the equilibrium line, rather than the advance of the terminus. During this period the variations of total accumulation and total ablation in the Taku Glacier are shown in figure 6.23. The ablation curve exhibits rapid changes in the first 75 years with no corresponding rapid changes in the accumulation curve. This is mainly due to the tendency of the Taku Glacier to advance for the present climatic conditions. In the first 50 years the effects of climatic warming is not significantly felt by the glacier. The figure also indicates that total accumulation in the glacier equal to total ablation in about 175 years. By this time the equilibrium line has reached an elevation of about 1400 m and the glacier has

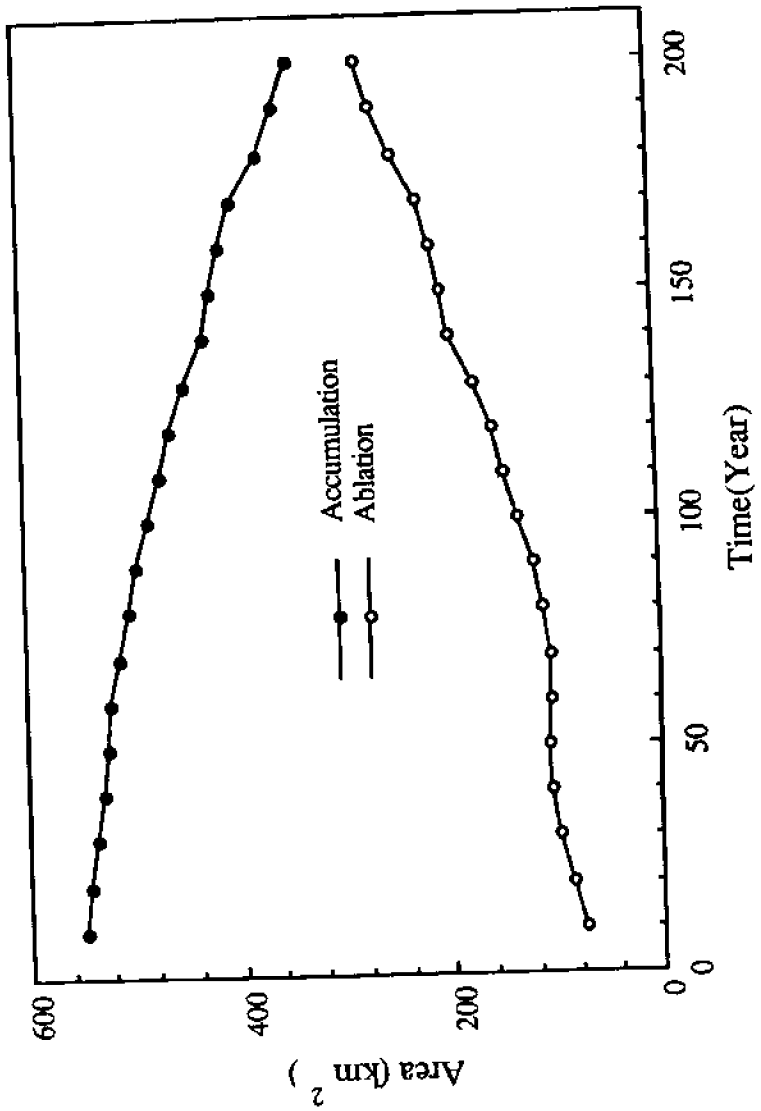

Fig.6.22: Temporal Variations of Accumulation and Ablation Areas Due to Climatic Warming

attained it maximum volume of about 210 km^3 as indicated in figure 6.24. Thereafter, the volume of the glacier starts decreasing. This decrease is the result of the retreat of the glacier, and the gradual thinning of ice below the equilibrium line. The retreat of the glacier at 100 year intervals is shown in figure 6.25. The figure also indicates the locations of the terminus for the present climatic conditions. At t= 100 years, the positions of the leading edges of the terminus for the two climatic conditions are quite close. The climatic warming causes a small retreat of the glacier, but more importantly, its unhindered advance has been arrested. The next 100 years is responsible for significant retreat of the terminus, and shrinking of the glacier. At the end of 200 years of climatic warming, the boundaries of the Taku Glacier and its surface velocity field are shown in figure 6.26.

The climatic warming is expected to influence the whole glacier if the simulations are carried over a long period. Tables 6.3 and 6.4 compares the relative changes in surface elevations, velocities, ice thickness, volume of the glacier and specific accumulation and ablation rates at t=200 years for the two climatic conditions with respect to the present glacier parameters. Figure 6.27 and 6.28 compare the temporal variations of the volume of the glacier, and the accumulation and ablation areas respectively. The decrease in the volume of the glacier due to climatic warming is about 33.7 percent. The relative changes in the accumulation and ablation areas and specific accumulation and ablation are appreciable. As the equilibrium line shifts upward it increases the ablation area and decreases the accumulation area. The present specific ablation at t= 200 years with climatic warming is about the same as its present value. However, it is about 1.7 times the present value when climatic warming is not included. For this situation the glacier advances south, where the maximum ablation rate is about 10.0 m/year. The ablation rate in this region makes specific ablation significantly high. The ice thickness in the upper Taku Glacier remains practically uneffected. However, the increase in surface velocity in this region is considerable. This increase in velocity is mainly due to increase in the surface slope caused by the thinning of ice below the equilibrium line. Below the equilibrium line the highest relative decrease in ice thickness occurs at transect 5-5, which is accompanied by a 69.2

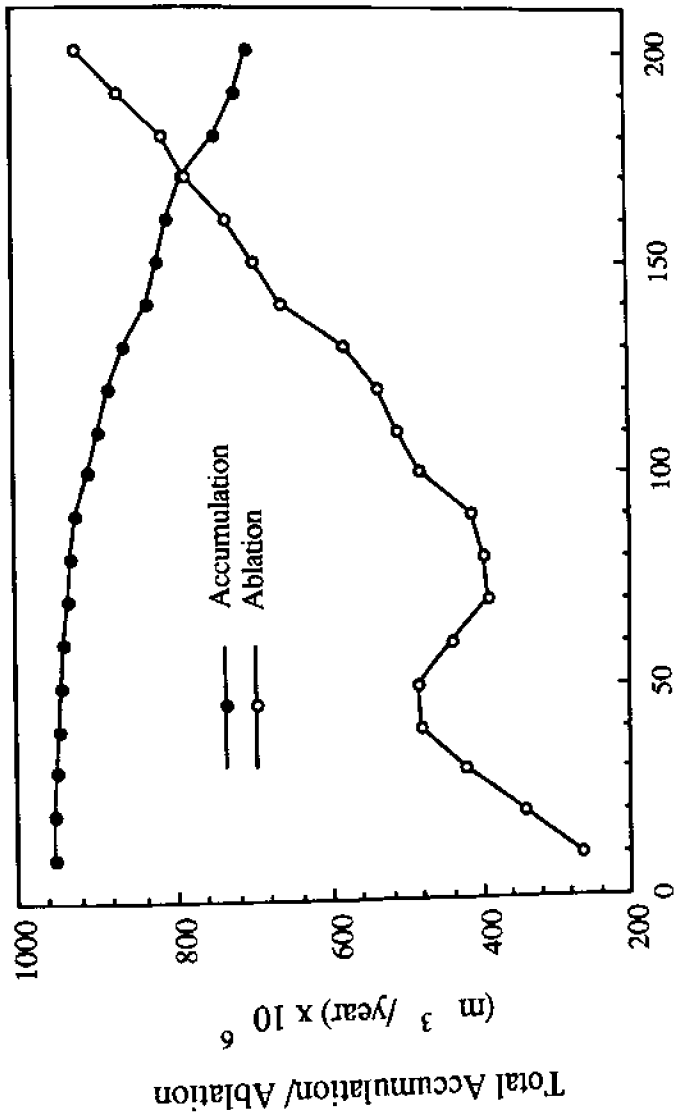

Fig.6.23: Temporal Variations of Total Accumulation and Ablation Due to Climatic Warming Over a Period of 200 Years

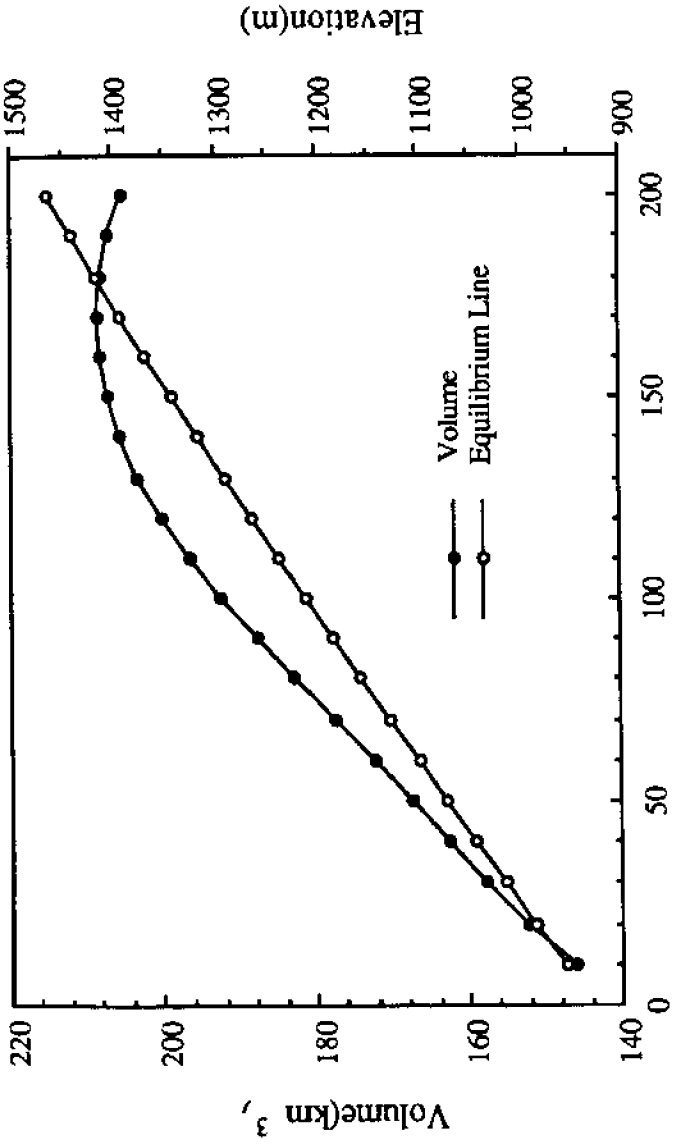

Fig.6.24: Temporal Variations of the Volume of the Glacier and the Altitude of the Equilibrium Line

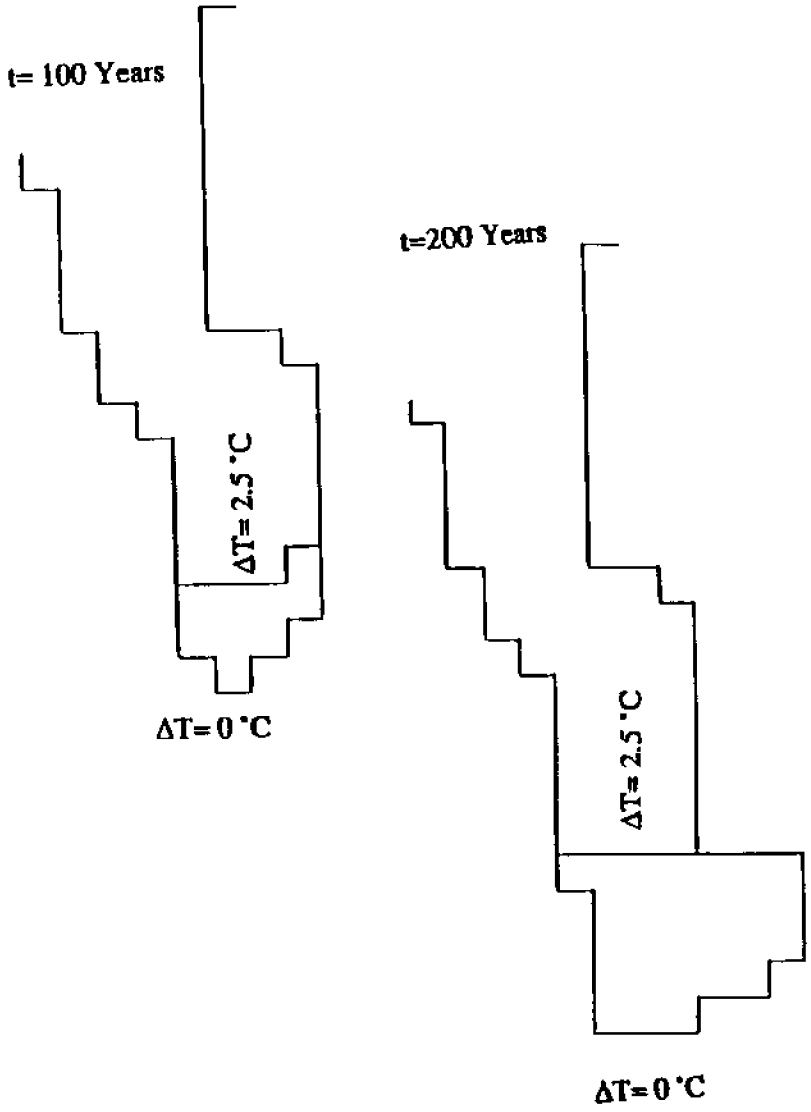

Fig.6.25: Locations of the Terminus for the
Two Climatic Conditions

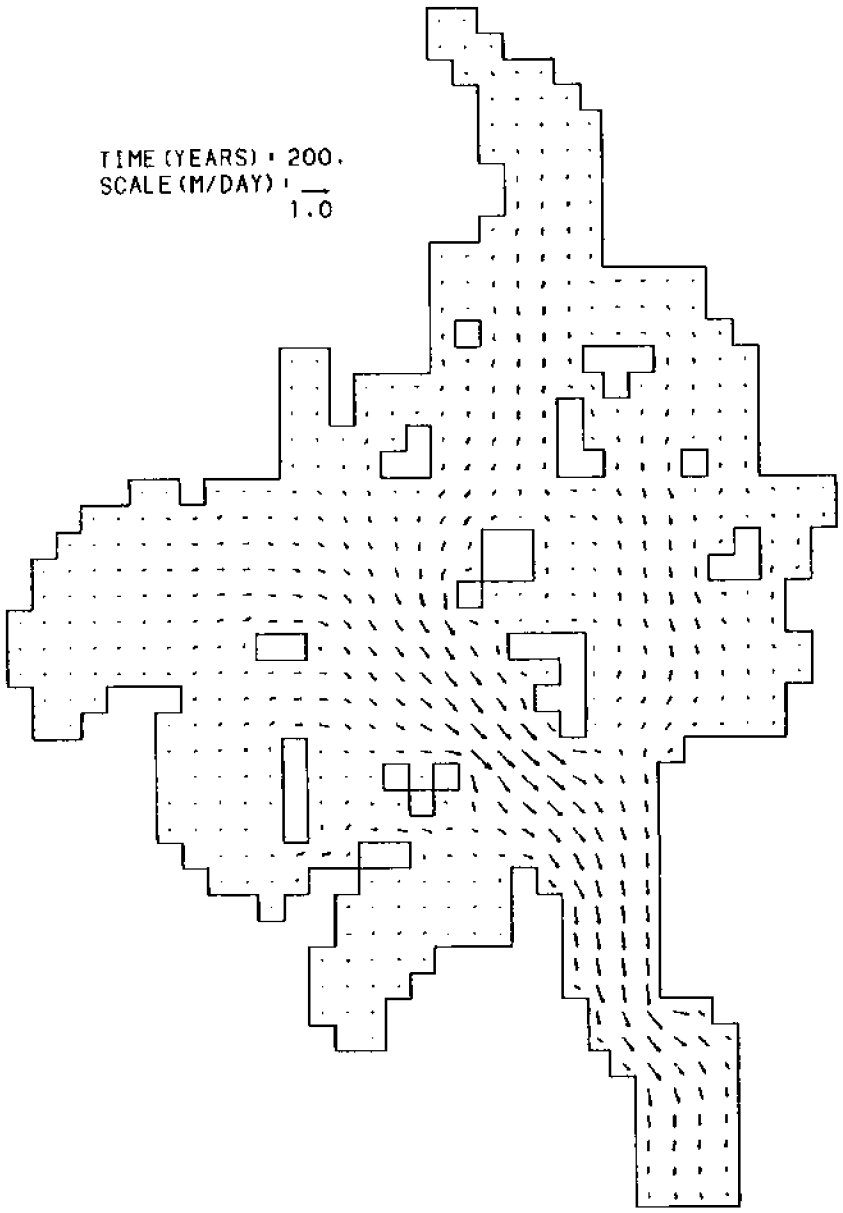

Fig.6.26: Surface Velocity Field at t= 200 Years
With Climatic Warming

Table 6.3 : Comparisons of Different Parameters of Glacier for Two Climatic Conditions at t= 200 Years.

Parameters	Present	ΔT= 0 °C	ΔT= 5°C	% Change
1. Volume(km^3)	146.2	250.3	205.4	-33.7
2. Accumulation Area(km^2)	545.0	545.0	342.0	-37.0
3. Ablation Area(km^2)	73.0	100.0	278.0	+243.8
4. Specific Accumulation(m/year)	1.73	1.73	2.05	+17.0
5. Specific Ablation(m/year)	3.30	5.67	3.30	-71.8

percent decrease in surface velocity. The climatic warming significantly alters the flow characteristics of the Lower Taku Glacier. The temporal variations of surface elevation and surface velocity at transects 7-7 and 8-8 are compared in figures 6.29 and 6.30. In this region climatic warming, in general, causes lower elevation and velocity compared to the situation when no climatic warming is assumed.

Table 6.4a: Comparison of Ice Thickness for Two Climatic Conditions at t= 200 Years

Transect	Ice Thickness(m) Present	ΔT=0°C	ΔT= 5.0 °C	% Change from Present
1-1	240.0	401.1	400.8	-0.1
2-2	160.0	418.2	405.6	-7.9
3-3	260.0	505.6	489.3	-6.3
4-4	320.0	639.4	571.5	-21.2
5-5	180.0	690.1	498.7	-106.6
6-6	370.0	623.8	447.6	-47.6
7-7	370.0	584.1	389.5	-52.6
8-8	350.0	400.4	107.7	-83.6

Table 6.4b: Comparison of Surface Velocity for Two Climatic Conditions at t= 200 Years

Transect from	Present (Field Data)	Velocity(m/day) ΔT=0°C	ΔT= 5.0 °C	% Change Present
1-1	0.18	0.207	0.207	0.0
2-2	0.23	0.218	0.241	+10.0
3-3	0.38	0.314	0.354	+10.5
4-4	0.53	0.613	0.691	+14.7
5-5	0.13	0.233	0.143	-69.2
6-6	0.20	0.343	0.195	-74.0
7-7	0.90	1.043	0.642	-44.6
8-8	0.56	0.883	0.310	-102.3

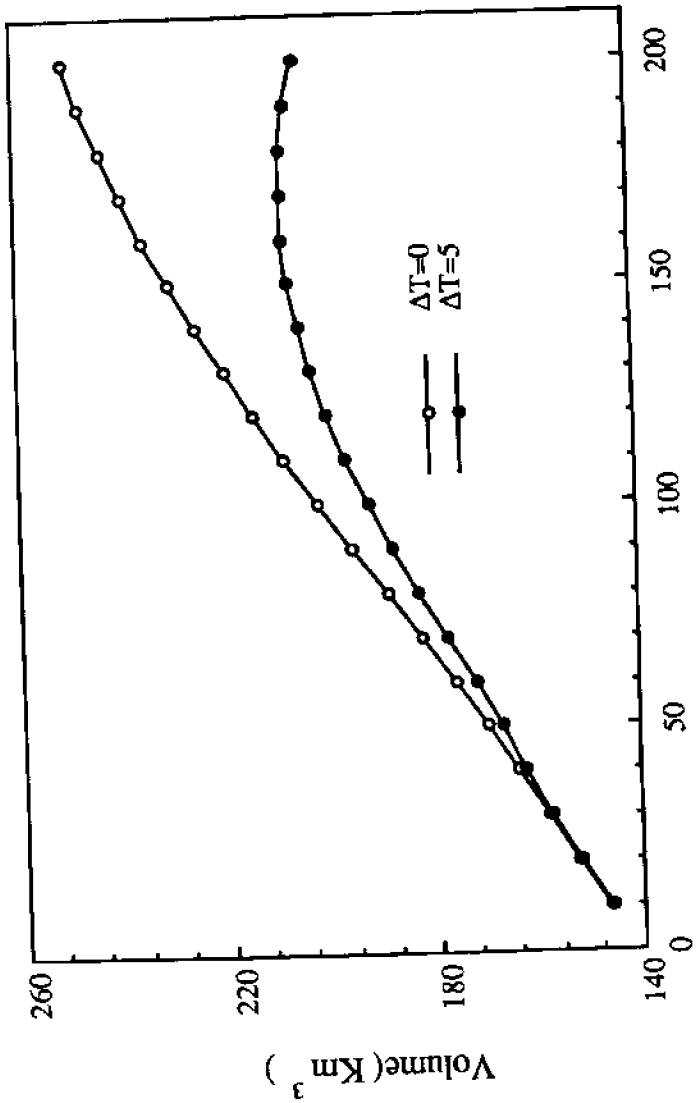

Fig.6.27: Comparison of the Temporal Variations of the Volume of the Glacier for Two Climatic Conditions

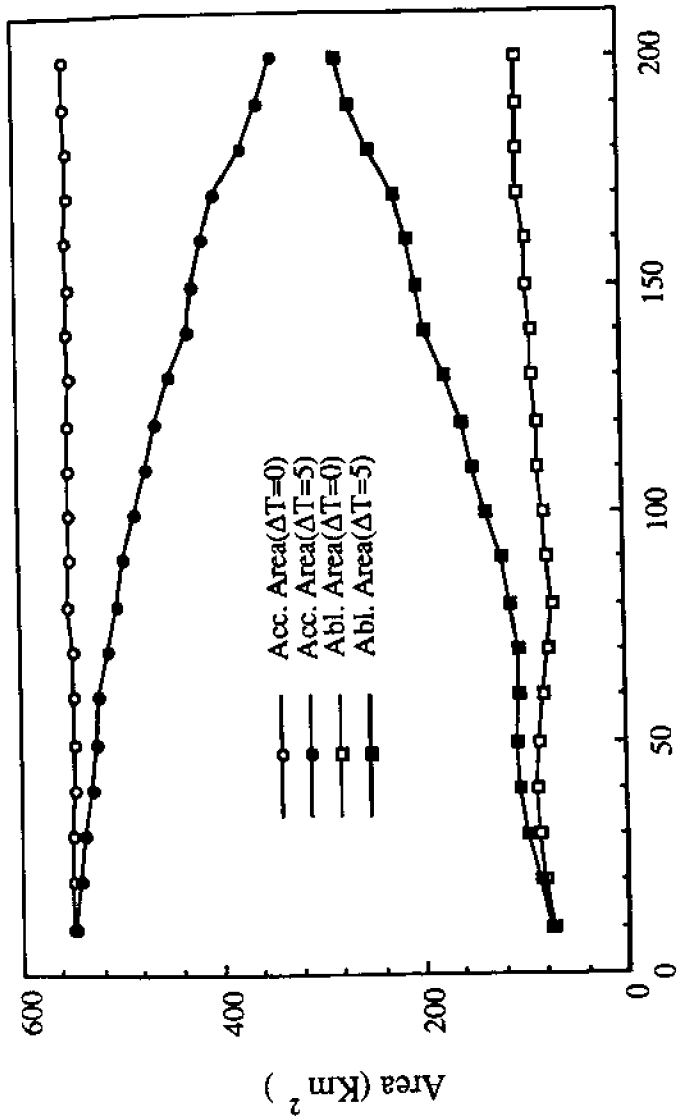

Fig.6.28: Comparisons of the Temporal Variations of the Accumulation and Ablation Areas for Two Climatic Conditions

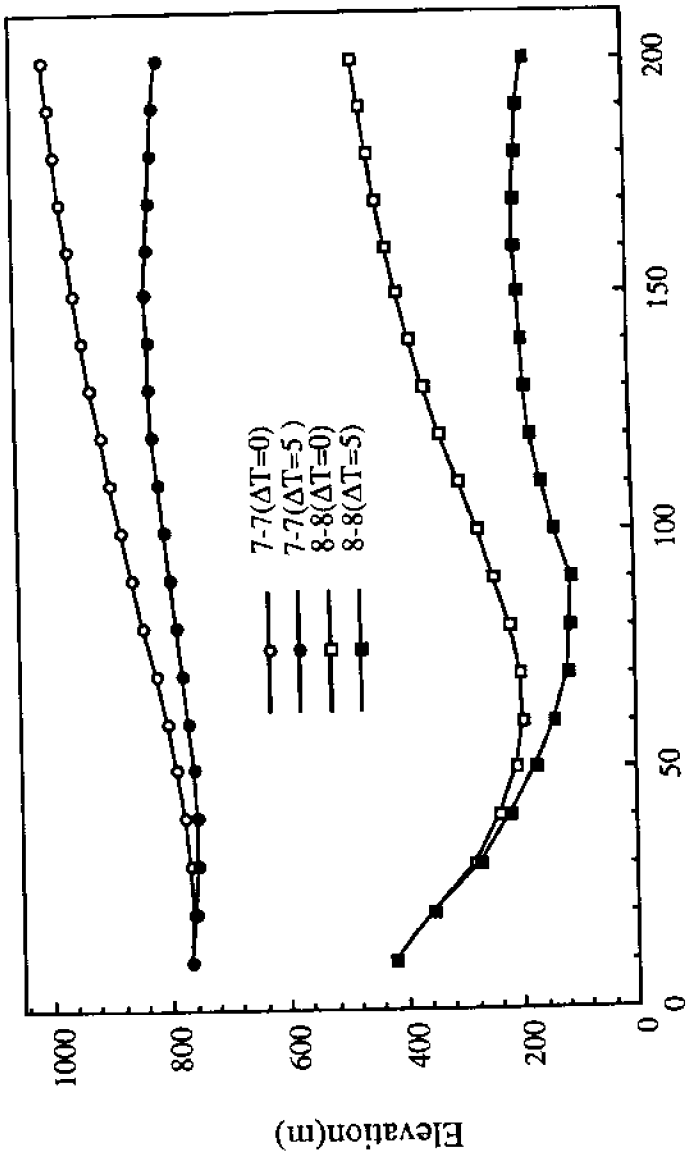

Fig.6.29: Comparisons of the Temporal Variations of Surface Elevations at Selected Locations for Two Climatic Conditions

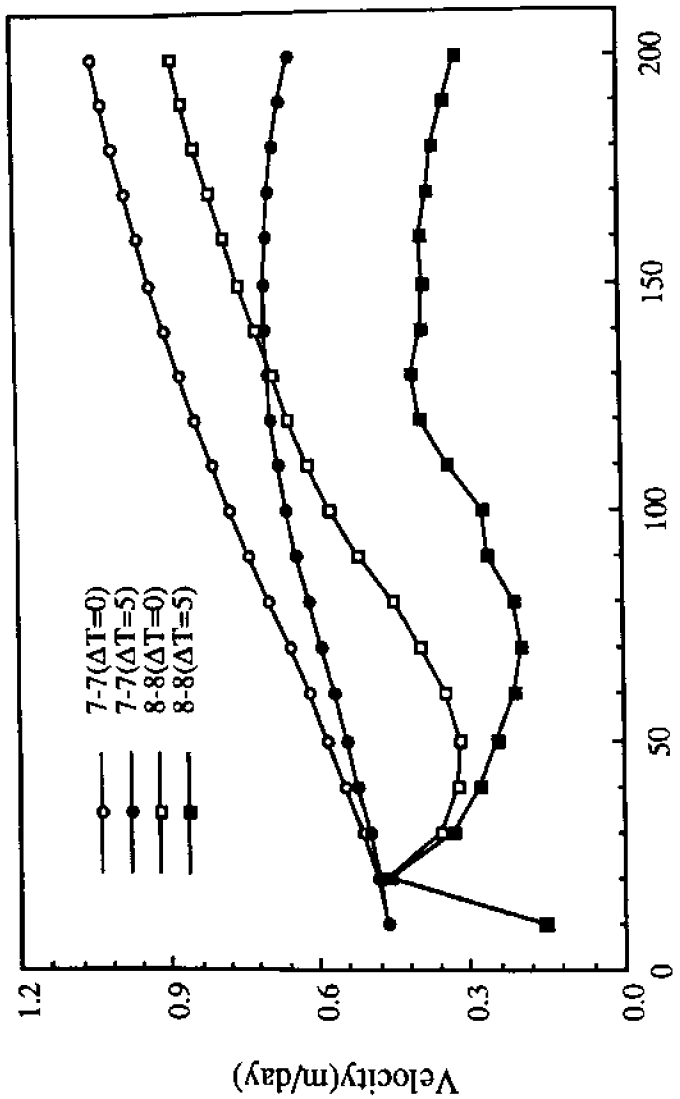

Fig.6.30: Comparisons of the Temporal Variations of Surface Velocities at Selected Locations for Two Climatic Conditions

7. DISCUSSIONS

7.1.0 INTRODUCTION

Models of ice sheets and glaciers dynamics are of interest in their own right (Meier, 1987), but most often they are constructed to understand the past or deduce what is likely to happen in the future. Verifiable models are needed in order to exploit the climatic information found in ice cores and to help interpret geological evidence of former glaciations. These models are also needed to supplement ocean and atmospheric models for predicting changes in climate and sea level and to answer questions, such as, whether a "greenhouse" warming will cause melting of sufficient ice to cause a significant rise in global sea level.

In the last decade many numerical models have been constructed to realistically simulate the dynamics of glaciers. The major obstacles to realistic simulation of glaciers, as noted by Meier(1987) in his review of glacier models, are the complexity of physical laws and assumptions involved in formulating the model. Flow of ice consists of bed sliding and internal deformation of ice. Though many models are based on a non-linear flow law, considerable controversy exists. The physics of the basal boundary condition (at the ice-bed interface) is very complex (Meier, 1987). The boundary condition at the terminus is another uncertain factor in modeling time-dependent flows (Meier, 1987). Therefore, it is impossible to construct numerical flow models without introducing certain degree of empirical or semi-empirical parameters. These parameters not only have different values for different glaciers, but can widely vary in different regions of the same glacier, requiring extensive amount of field data for model calibration. Unfortunately, sufficient field data is rarely available. It is important to keep in mind the limitations of the model while using the model and interpreting the model results.

7.2.0 FLOW LAW

To determine the internal deformation of ice, a relationship between stress and the corresponding strain rate is needed. Conventionally, ice is treated in flow models as a visco-plastic material (Paterson, 1981) and the relationship between stress and ice deformation is given by Glen's law (equation 2.1). A frequently used value of n is 3. For n=1 this relation represents Newton's law of viscosity. Many recent studies suggest the applicability of a linear flow law for the range of stresses found in glaciers. For the power law type flow law, Colbeck and Evans(1973) found that n = 1.30 for Blue glacier, Washington. Analysis of data from polar ice sheets by Doake and Wolff(1985) shows that n varied from 0.8 to 1.04 and that n = 1 provides a better simulation of horizontal velocity, while n = 3 gives better results for vertical velocity (Doake and Wolff, 1986). If changes in τ are comparable to the average value of τ over the time span when ε' is being measured, ice deforms in regimens of transient creep. Under these conditions, n = 1 gives a better fit to creep data (Weertman, 1985).

The application of the model to the Fedchenko Glacier, indicates an interesting phenomenon. Though the present model is based on a linear flow law, while the model developed by Budd(1975) is based on non-linear flow law (n=2) the two computed profiles practically coincide, except near the terminus (figure 3.13). This discrepancy in the last few kilometers is mainly due to the difference in the assumptions made in the development of the moving boundary condition. During the model application it was found that 5 to 10 percent changes in the ice viscosity and bed friction do not result in significant change in the computed surface profile. This indicates that small velocities, the surface profile is strongly dependent on mass balance and conservation of mass governs the development and growth of the glacier. Consequently, it is not surprising that models based on different flow laws compute similar surface profiles. Application of the model to the Taku Glacier indicates that the model is capable of reproducing the surface velocity field very well (figure 6.5 and 6.6). The ratio of bed velocity to surface velocity at the transects (table 6.2) and after 300 years of simulation (figure 6.16) varies from 0.47 to 0.90. Field estimates of the ratio varies from 0.30 to over 0.9 (Miller, 1963). Therefore, the model computes not only surface

velocities, but also bed velocity consistent with field observations. These observations strongly suggest the applicability of a linear flow law to glaciers, at least for the class of glaciers considered in this study.

The applicability of the linear flow law leads to a parabolic vertical velocity distribution given by equation(3.2). Figure 3.5 shows the comparison of vertical velocity profile with an analytical solution. The agreement between the two solutions is good. The minor difference between the two solutions is mainly due to two different approaches used in the computation of the profiles. The analytical solution is a parabolic profile, while the model attempts to approximate the profile by using a cosine function. The use of cosine functions to reproduce the vertical velocity is attractive as pointed out in Chapter-2. Consequently, it is expected that the mass flux computed by the model is also correct.

7.3.0 FRICTION LAW

The resistance to flow due to bed topography is an area of extensive research (Kamb, 1970; Nye 1970; Budd et al. 1979; Weertman 1979; Fowler, 1982; and Lliboutry, 1987), and is not well understood, especially when appreciable bed sliding is involved. In many cases of special interest because of fast flow, the flow is by sliding over the bed or on a layer of deforming till. It is impossible to state a basal boundary condition without introducing many poorly defined, tunable parameters. The present model assumes a linear friction law, and the friction coefficient is function of bed velocity (equation 2.7). Because of the uncertainty involved in specifying bed friction, it appears reasonable to use a simple parameterization of the problem. The applications of the model to the Taku Glacier, and correct simulation of the ratio of bed to surface velocities over the model domain, indicates that the assumption is acceptable for temperate glaciers.

7.4.0 BOUNDARY CONDITION AT TERMINUS

The boundary condition at the terminus is another uncertain factor in modeling time-dependent flows (Meier, 1987). The fact that the geometry of the terminus depends on the dynamics of the glacier complicates the solution of the flow equations, and no adequate theory has been developed to date for flow of ice in the neighborhood of the leading edge (Hutter, 1983). Generally, the advance or retreat of the terminus is computed by conserving mass and assuming the depth and flux of ice at the leading edge of the terminus are zero (Nye, 1960; Budd and Jenssen, 1975; Bindschadler, 1982; Rasmussen and Campbell,1973). In this study a different formulation of the boundary conditions was attempted. The formulation is such that it is not necessary to assume zero depth at the leading edge of the terminus. If the velocity of flow near the leading edge is sufficiently high, this formulation can maintain finite depth at the edge. However, as the glacier reaches steady state (ablation rate and vertical motion of the terminus cancel one other) the depth of ice approaches zero, similar to the boundary condition generally used in glacier dynamics.

Figure 3.1 shows the progressive growth of a glacier on a horizontal bed, and subjected to the mass balance distribution described in Chapter-3. The comparison of the analytical and numerical solutions show that over most of the glacier the two solutions coincide. However, as the terminus is approached the numerical model results depart slightly from the analytical solution. A similar situation is also found in applying the model to the Fedchenko Glacier (figure 3.13). These discrepancies can be attributed to the assumption made in the development of the moving boundary conditions. For a assumed mass balance, it is very unlikely that the length of a glacier will be an exact multiple of the grid size. Therefore, as the glacier approaches steady state, the terminus is found to oscillate between two grid points. The results of numerical simulation, including the shape of the leading edge of the ice sheet, are similar to that presented by Oerlemans and Veen(1984). As the ice sheet edge "jumps" from grid-point to grid-point, the slope of the leading edge is not as steep as it should be. Analysis of truncation error, due to the finite size of the grid spacing, shows that the size of the ice sheet is determined by "large-scale mechanics and mass balance, not by

the small scale mechanics" of the leading edge (Oerlemans and van der Veen, 1984). Therefore, the moving boundary conditions applied at the terminus is not expected to significantly affect the overall computed behavior of the glaciers.

The results of the model application to the Taku Glacier are shown in figures 6.11 and 6.12. Field data indicates that the terminus is advancing at an average rate of about 37.0 m/year (Pelto and Miller, 1988). Neglecting the first 100 years of simulations, the computed rates of advance of the terminus in the next two centuries are 40.0 m/year and 20.0 m/year respectively. The rate of advance of the terminus is very sensitive to the bed topography, supply of ice from upstream, and ablation rate. Considering the reliability of the bed topographic data (described in Chapter-6) in this region, the computed rates of advance appear reasonably good.

7.5.0 FEATURES OF THE MODEL

7.5.1 Calibration Parameters

The calibration parameters of the present model are the viscosity of ice and the friction coefficient. The viscosity of ice can vary from 7.4 to 15.9 x 10^9 m^2/s (Ambach and Eisner, 1983) in temperate glaciers. Campbell and Rasmussen(1969) and Rasmussen and Campbell(1971) have varied viscosity from zero to 1.0 x10^{10} m^2/s to study the propagation of surge in idealized glaciers. A generally accepted value of viscosity is 12.0 x10^9 m^2/s. In all the numerical experiments, described in Chapter-3, viscosity was assumed to be 12.0 x10^9 m^2/s. In the Taku Glacier, it was necessary to use a higher viscosity of 14.0 x10^9 m^2/s. This was done to obtain surface and bed velocity distributions consistent with field data.

Compared to viscosity, the friction coefficient can vary over a wide range. For glaciers with frozen bed (zero bed velocity), the friction coefficient should be very high. Campbell and Rasmussen(1969) and Rasmussen and Campbell(1971) have used friction coefficients similar to the present model, and they varied it from 1.0 x10^6 to 5.0 x10^4 to initiate surge. In the numerical experiments

conducted in Chapter-3 constant friction was used. The maximum value of the coefficient in these experiments was 50 $x10^6$. In the Taku Glacier, a functional form of friction coefficient is assumed. The maximum and the minimum values of the friction coefficients are 20 $x10^6$ and 100 $x10^6$ respectively. Compared to Campbell and Rasmussen(1969) the friction coefficients are relatively high. However, it should be pointed out that the Taku Glacier in a non-surging glacier and friction is expected to be higher.

7.5.2 Computational Time Steps

The stability analysis presented in Chapter-2 is based on simplified equations and provides an estimate of Δt. In the analysis of the influence of viscosity on the model stability, the effects of horizontal viscosity, N_H, has been ignored. The analysis implicitly assumes that $\partial^2u/\partial x^2$, $\partial^2u/\partial y^2 << \partial^2u/\partial z^2$ in equation(2.4). These terms are evaluated at the present time level, to keep the model explicit. Time centering of $\partial^2u/\partial x^2$, $\partial^2u/\partial y^2$ makes the model implicit, requiring the solution of a system of coupled simultaneous equations. The corresponding computer code and application of moving boundary conditions are rather complicated. In applying the model to the Taku Glacier, it was found that $\partial^2u/\partial x^2$ and $\partial^2u/\partial y^2$ are small compared to $\partial^2u/\partial z^2$, but may not always be negligible. Flows from the upper Taku Glacier, with a maximum width of about 55 km, converge into the Lower Taku Glacier where the width of the glacier reduces to less than 3 km at many locations. This converging flow creates appreciable transverse velocity gradients. In the Lower Taku Glacier a substantial volume of mass leaves the system as ablation. The maximum rate of ablation is 10 m/year or 0.822 m per time step for Δt = 30 days. When larger time steps are used, the model starts to oscillates in a region close to the equilibrium line, where the precipitation changes from positive (accumulation) to negative (ablation). The accumulation or ablation throughout the model domain and over the simulation period act as a source of noise. The amplitude of this noise becomes larger per time step as Δt increases. The large values of positive and negative precipitation over a short distance, about the equilibrium line, is a source of model instability.

The computational time step used by different numerical models varies over a wide range. Generally, time steps of the order of days have been used for simulating the dynamics of temperate glaciers with a relatively high velocity of flow. These temperate glaciers are much more dynamic than icesheets (Paterson, 1981), where time steps of years have been used (Mahaffy, 1976; Budd et al., 1984). A comparison of Δt used by other models, for simulating flow in the temperate or surging glaciers, indicates that the time step for which the present model remains stable and consistent appears quite reasonable. Rasmussen and Campbell(1971) have used an iterative technique to solve the two-dimensional (x-y plane) flow equations and applied the model to idealized glaciers. Their time step, Δt, varied from 10 to 40 days for steady-state solutions and 2.0 to 0.5 days for surge simulations. The one-dimensional model by Bindschadler(1982) was applied to Variegated Glacier, Alaska, with a time step of as small as 0.10 days. The present numerical model is based on a modified version of an explicit time-split finite difference scheme and retains the advantages of an explicit model.

7.5.3 Grid Spacing

The flow model has been applied to the Taku Glacier with grid a spacing of 1.0 km. Generally, the grid size is a compromise between the details of the flow and the computational time. The lower Taku Glacier in only a few kilometer wide, so it is necessary to use grid spacing of the same order of magnitude as the local ice thickness. The present ice thickness in the lower Taku Glacier is of the order of 300 to 400 meters. As the glacier approaches a steady state, the glacier grows and the ice thickness increases by another 300 m , on average. Therefore, if the criteria for the lower limit of grid size suggested by Budd(1968,1970) is followed, the minimum grid spacing would be about 5.0 to 6.0 km. ,which is greater than the width of the Lower Taku Glacier. Therefore, an analysis of stress gradient terms on the basis of linear flow was performed, using the idealized Fedchenko Glacier as a test case The analysis (figure 3.15 and 3.16) shows that T and G (equation 3.4) are very small compared to τ_b. Therefore, the grid spacing of 1.0 km or appreciably less could be used without considering the effects of longitudinal stress gradients. This is possible because the model is

based on a linear flow law and treats ice as viscous fluid rather than as a visco-plastic material.

7.5.4 Vertical Velocity Profile

Using one cosine term in the trial function for vertical velocity variation (equation 2.22), figure 3.5 shows that the computed velocity profile matches with the analytical solution very well. The number of cosine terms needed to construct the vertical velocity profile depends on the convergence of the solution, which is a function of viscosity of the material, bed friction and characteristics of the flow. In the initial stage of model application two or more cosine terms were tried. It was found that model parameters corresponding to second and third terms were so small that their effects on the resultant velocity were hardly noticeable. The computer time required for the solution of the governing equation is proportional to the number of cosine terms used. Therefore, in all subsequent runs only one cosine term was used.

7.6.0 RESULTS OF NUMERICAL EXPERIMENTS

The limited availability of field data makes the verification and validation of flow models for glaciers difficult. To address questions concerning convergence, stability, and verification of the computer coding, numerical experiments were performed and comparison were made with analytical solutions. The problems for which closed form analytical solutions can be found tend to be for simplified geometry and flow situations. Nevertheless, this aspect of the process is valuable since it provides the only situation where nearly perfect agreement can be expected.

7.6.1 Surface Waves Propagation

Waves in glaciers are undulations on the surface profile which travel down glaciers at a speed higher than the flow velocity of ice and are analogous to ordinary flood waves in rivers (Fowler, 1982). These waves are known as kinematic waves and are a consequence of conservation laws. Dynamic waves, encountered in rivers and oceans, do not occur in glaciers because velocity of flow is so low that the inertia terms in the equation of motion are negligible compared to gravity and viscous terms (Paterson, 1981). Kinematic waves are of fundamental importance in studying the dynamics of glaciers, because they are the means by which the effects of mass balance changes, due to climatic fluctuations, are propagated down the glacier. For linear flow and friction laws, the ratio of wave propagation velocity to surface velocity is 2.0 (equation 3.3). In the numerical experiment (figure 3.7), the ratio of wave and flow velocities is 2.15, slightly greater than the theoretical value. The ratio is slightly higher mainly due to the local increase in flow velocity induced by the propagation of a Gaussian hump.

7.6.2 Response to Surface Perturbations

To study the response of a glacier to perturbations, two numerical experiments were conducted. The response curves of the glacier for both the experiments follow a trend predicted by the theoretical analysis of Nye(1963). Qualitatively, the curves are also in good agreement with the numerical results of Bindschadler(1982). For time-dependent accumulation rates and boundary conditions, the model will reach a steady state configuration independent of the initial geometry of the glacier (Bindschadler 1982). This steady state configuration corresponds to the situation where the volume of flux at any point is equal to the total accumulation received by the glacier upstream of the point, so that no additional thickness change occur. A knowledge of this particular configuration is important in studying the behavior of glaciers, because at any particular time the geometry of the glacier will be adjusting to reach steady state for the current climate. If the climate changes before steady state is achieved, the

behavior of the glacier will alter accordingly and begin approaching the new steady state. Model experiments of perturbations from a known steady state configuration are an excellent way of measuring the response time scales of the modelled glacier (Nye, 1960; and Bindschadler, 1982).

7.7.0 KUHN'S ALGORITHM

In this study the effects of climatic warming on the Taku Glacier is based in the theory presented by Kuhn(1980). As most of the information necessary for the application of the theory are not available directly, various indirect methods were used to estimate the heat and energy transfer coefficients (equation 4.9). The computed value of μ and μ' are 1.82 $x10^6$ and 3.60 $x10^5$ $Jm^{-2}d^{-1}{}^oC^{-1}$ respectively. For the Greenland Icesheet (Ambach,1985a: 1985b) the corresponding values are 1.72 $x10^6$ and 3.7 $x10^5$ $Jm^{-2}d^{-1}{}^oC^{-1}$. As μ' is one order of magnitude smaller than μ, its effect on the computed change in elevation is very small. Figure 6.18 shows that an error in the estimation of μ by 50 percent introduces an error in the computed shift of altitude of about 9.3 m for 1 °C rise in temperature. This error is small compared to the altitudinal shift of the equilibrium line for 1 °C . The effects of cloudiness was not studied because of the lack of field data. However, its effect is considered negligible (Kuhn, 1983; Ambach and Kuhn, 1983). In the analysis δS^+ was assumed zero. Analysis of bore hole data of the Greenland Icesheet by Ambach(1985a) indicates that the averaged water equivalent of the annual net accumulation to have been constant since 600 AD. The coupled climate-glacier model of Oerlemans(1988) indicates that the parameterization of mass balance gradient is a more important link between climatic and glacier flow model. The Taku Glacier has sufficient records of mass balance data so that the computed balance gradient is reasonable good. A comparison of the effects of δS^+ and δT_a to δh indicates that the effect of δS^+ is very small. A change is accumulation rate by 100 km/m^2, which corresponds to about 6.67 percent of the present mean accumulation rate, causes the equilibrium line to fall by 19.1 m. The amount of increase in precipitation in the next hundred years is very uncertain but generally assumed to be not more than ten percent of the present accumulation rate (Bindschadler, 1985; Kuhn, 1985;

Kandel, 1983). Therefore, an increase in temperature by 2.5 °C will cause equilibrium line to rise by 250 to 300 m, which could be offset by only 30 m by increase in the accumulation rate by ten percent.

The analysis presented here is applicable to long term climatic warming, where the glaciers have time to respond to climatic perturbations. Bindschadler(1983) and Ambach and Kuhn(1983) have assumed that the glacier reaches a steady state after each climatic perturbation. Over a short period, an increase in temperature does not necessarily mean a corresponding shrinking of the glaciers. Measurements in Wolverine Glacier, Alaska, from 1967 to 1981, indicate that a rapid glacier growth can accompany climatic warming primarily because larger amounts of precipitation occurs during the warm winter (Mayo and Trabant, 1984). An increase in winter precipitation with temperature is expected because warm temperature is associated with more air flow from the ocean and also because warm air is capable of carrying more moisture. In studying the influence of climatic warming on the Taku Glacier, it was observed that the volume of the glacier keeps growing in the first 150 years (figure 6.27), while the terminus keeps advancing for about 50 years. This is mainly due to the large response time to the glacier, so that the climatic perturbations have a delayed action on the dynamics of the glacier.

7.8.0 FLOW CHARACTERISTICS OF THE TAKU GLACIER

7.8.1 Simulations With Present Climatic Conditions

The temporal variations of surface elevations and surface velocities at eight transects (figures 6.2 and 6.3), the volume of the glacier (figure 6.10) indicate that the Taku Glacier reaches steady state in about 400 years. By the time it reaches steady state, its volume increases by about 70 percent and the ablation area by about 40 percent. The surface elevations and velocities at all the transects increase continuously during this period. This is the result of a surplus mass balance in the Taku Glacier. In most of the glacier the rate of increase in surface elevation (figure 6.13) exceeds 0.67 m/year. South of transect 4-4 the rate of rise is 1.0 m/year. In a small area, in the center of the Lower Taku Glacier, the rate of

rise approaches 1.33 m/year. The Taku Glacier appears to be transporting approximately half of the total accumulation to the ablation zone. The other half is increasing the glacier thickness. As the glacier approaches the steady state, surface velocities also increase. The maximum surface velocity is about 1.2 m/day. Figure 6.4 indicates a corresponding increase in bed velocities. In general, both the surface and bed velocities increase toward the terminus. The ratio of bed to surface velocity (figure 6.16) also follows a similar trend. Consequently, the relative contribution to total velocity by the internal deformation of ice decreases accordingly. Below transect 4-4, bed sliding is the dominant mode of mass transport.

The numerical simulations indicate that in the first hundred years the glacier terminus advances by 2.0 km (figure 6.11) and then retreats by 3.0 km. This is the result of the initial conditions used in applying the model. The rate of advance in the east is higher than in the south during this period. The model takes about 100 years to build up velocities that are of same order of magnitudes as the present velocities (figure 6.5). Thereafter, the glacier takes only 50 years to reaches the northern bank of the Taku River. The inlet is blocked in the next 50 years. Further advance of the terminus is restricted by steep mountains on the southern bank of the Taku River. The Taku Inlet is tidal, so as the glacier crosses the inlet, it will start calving. As the present version of the model does not incorporate calving of the glacier, the rate of advance of the terminus might be considerably different.

7.9.2 Simulations With Global Warming

In these simulations, rate of climatic warming as assumed to be 2.5 °C per century. As the simulations are carried over a period of 200 years, the total increase in temperature is 5.0 °C. The altitudinal shift of the equilibrium line is about 600 m. As discussed in the previous section, the model takes about 100 years to 'get-started', and that the response time to the Taku Glacier is large, the resultant shrinking of the glacier is more likely due to the global warming of 2.5 °C in the first 100 years. To determine the response to the additional 2.5 °C

increase in temperature, it would be necessary to run the model for another century. As the coupling of the climatic perturbations with the flow model is based on very simplified assumptions, and because the trend of the climatic warming over such a long period is uncertain, it is not reasonable to go for very long term predictions.

The results of the model simulations indicate that the climatic warming over the next 200 years will significantly alter flow characteristics of the Lower Taku Glacier and the Southwest Branch (figures 6.28 and 6.29). However, its effect on the West Branch, and Matthes Glacier are negligible (Table 6.3 and 6.4). Figure 6.27 indicates that for the assumed scenario of global warming, the glacier continues to increase in volume in the next 150 years. Thereafter, it starts shrinking, and the volume loss is about 59.2 km^3. The melt water, due to this loss in volume, will flow into the Taku river, and eventually contribute to global sea level rise.

8. SUMMARY AND CONCLUSIONS

Glacial ice is generally treated as a visco-plastic material, and the flow models are based on Glen's law (Paterson, 1981). At stresses normally found in temperate glaciers, the Newtonian viscous law is a good approximation (Doake and Wolff, 1985; Colbeck and Evans, 1973), and the equations of motion correspond to the Navier-Stokes equations. In this study a three-dimensional time-dependent flow model for glaciers has been developed. The starting point of this modelling effort is the hydrodynamic model by Pearce and Cooper(1981). The model is three-dimensional in the sense that it computes the horizontal velocity variations in the vertical direction as well as in the horizontal. The stability criteria of this hydrodynamic model prevents its application to a highly damped and viscous system, like glaciers and ice sheets. A partial time centering of velocity in the conventional time-split finite difference scheme of Pearce and Cooper(1981) circumvents the stability criterion arising due to the fluid viscosity. The use of high viscosity and linear friction makes the hydrodynamic model significantly less dynamic. With these changes, the model remains stable with time steps of 30 days or more for the flow conditions in the Taku Glacier. The ice-to-ice friction is controlled by viscosity and ice-to-bed friction is controlled separately by a linear friction coefficient. An algorithm for the advance and retreat of the terminus has been developed to simulate the response of glaciers to climatic perturbations.

To study the simulation characteristics of the model, numerical experiments were performed. The first experiment compares the computed steady-state surface profile with the analytical solution of Paterson(1972). In the second experiment the vertical velocity profile is compared with an analytical solution of Nye(1965).

Kinematic wave propagation in a channel is studied in the third simulation. The computed ratio of wave propagation velocity to surface velocity of ice is 2.15, which is slightly greater than the theoretical value. The final experiment consists of studying the response of a test glacier to sudden increase in surface elevation by 1.0 m and change in mass balance by 0.1 m/year. The response of the test glacier is qualitatively similar to the analytical predictions of Nye(1960) and the results of Bindschadler(1982). As a simple application, the model was then applied to the Fedchenko glacier in the Soviet Union. By adjusting friction, the steady-state profile obtained by Budd(1975) was simulated. Using the Fedchenko glacier as a test glacier, an analysis of the stress gradient terms (Budd,1970) has been carried out. The results indicate that these stresses are negligible for models based on linear flow law and grid size of the same order of magnitude as the local ice thickness can be used without incorporating the stress gradient terms in the model.

To study the long term response of glaciers, it is necessary to include the effect of global warming in the flow model. In the last one hundred years the atmospheric and ocean surface temperatures have increased by about 0.6 °C (Meire,1984), mainly due to the CO_2 induced "greenhouse effect". Recent studies (Hansen et al, 1981; Schneider, 1984) indicate that this trend will accelerate and the global mean temperature will increase by 2 to 5 °C in the second half of the 21-st. century. This climatic warming will result in the altitudinal shift of the equilibrium line of glaciers and redistribution of accumulation and ablation areas. Kuhn's algorithm (Kuhn, 1979), based on the balance of energy at the equilibrium line has been used to study, the effect of climatic warming on the altitudinal shift of the equilibrium line of the Taku Glacier. The analysis indicates that the altitude of the equilibrium line of the Taku Glacier moves up by about 61.2 m per °C rise in temperature. This shift could be off-set by about 19.1 m by an increase of accumulation rate by 100 kg/m^2. The increase in the number of ablation days moves the equilibrium line upward. The effects of the climatic warming is incorporated in the flow model by raising the altitude of the equilibrium line and redistributing accumulation and ablation areas. The temperature is assumed to increase linearly in time at a rate of 2.5 °C per century.

The ablation below the equilibrium line is assumed inversely proportional to the elevation of the glacier surface.

The Taku Glacier, located in south-east Alaska, is a dynamic, temperate glacier, covering about 625 km^2 in the Juneau Ice Field. It was selected for the field application of the model because of the availability of data. The Taku Glacier has 40 years of mass balance data, a considerable amount of surface velocity data to selected transects. In addition no numerical model has been applied to it. The model application to the Taku Glacier consists of calibrating the model, calculating the flow characteristics for the present climatic condition, and calculating the response to climatic warming. The model calibration consists of selecting proper values of the friction coefficient and viscosity to match the field data. To simplify the calibration process, the friction coefficient was assumed to increase linearly with bed elevation. The calibrated friction coefficients varies from 20 $x10^6$ in the Lower Taku Glacier to 100 $x10^6$ in the northern zone. Field data (Ambach and Eisner, 1983) indicates that viscosity of glacial ice varies from 7.4 to 15.9 $x10^9$ m^2/s. For the assumed distribution of friction coefficient it was necessary to use a viscosity of 14.0 $x10^9$ m^2/s to reproduce a) surface velocities varying from 0.13 to 0.90 m/day at eight transects, b) correct relative values of bed sliding varying from 30 to 90 percent of surface velocity, c) transverse velocity distribution at three transects, and d) the rate of rise of surface which is about 0.81 m/year in the central zone of the Taku Glacier.

After calibrating the model, it was used to simulate the flow characteristics of the Taku Glacier, for the present climatic conditions, over a period of 500 years. The glacier appears to approach a steady state in about 450 years. The glacier continues advancing in the next 300 years with an average rate of 20 m/year, and completely blocks the Taku Inlet. The volume of the glacier increases 71 percent, while the ablation area increases by 42 percent of its present size mainly due to the advance of the terminus. As it approaches a quasi-steady state in 300 years, the change is ice thickness varies from zero to 400 m, surface velocity reaches a maximum value of about 1.2 m/day. Except in a small area in the Lower Taku Glacier, bed shear stress varies from 50 to 200 kN/m^2. When climatic warming of 2.5 °C per hundred years is assumed, the advance of the Taku Glacier is

arrested in about 50 years and it starts retreating in about 100 years. In the next 100 years the terminus retreats by about 3.0 km from its present position. Compared to the location of the terminus for the present climatic conditions, the retreat is about 8.0 km. This climatic warming will be responsible for a 33.7 percent decrease in the volume of the glacier, significant thinning of the ice and velocity below the equilibrium line.

REFERENCES

Abbott, M.B.,1979, *Computational Hydraulics: Elements of the Theory of Free Surface Flows*, Pitman, London, U.K.

Abbott, M.B., McCowan, A. and Warren, I.R., 1981, Numerical Modelling of Free-Surface Flows that are Two-Dimensional in Plan, *Predictive Abilities of Surface Water Flow and Transport Models*, Edited by Fisher, H.B., Academic Press, Inc., N.Y, U.S.A, pp.222-83.

Ambach, W.,1985a, Characteristics of the Heat Balance of the Greenland Ice Sheet for Modelling, J. of Glaciol., Vol.31, pp.3-12.

Ambach, W.,1985b, Climatic Shift of the Equilibrium Line: Kuhn's Concept Applied to the Greenland Ice Cap, Ann. of Glaciol., Vol.6, pp.76-78.

Ambach, W. and Eisner, H., 1983, Effective Shear Viscosity and Effective Bulk Viscosity of Firn of a Temperate Glacier, Ann. of Glaciol., Vol. 4, p.10-12.

Ambach, W. and Kuhn, M.,1985, The Shift of Equilibrium-Line Altitude on the Greenland Ice Sheet Following Climatic Changes, In Proc. of Workshop on *Glaciers, Ice Sheets, and Sea Level: Effects of a CO_2-Induced Climatic Changes*, Seattle, Washington, pp.255-257.

Barnet, T.P., 1983, Recent Change in Sea Level and Their Possible Causes, Climatic Changes, Vol. 5, pp.15-38.

Bindschadler, R.A.,1985, Contribution of the Greenland Ice Cap to Changing Sea Level: Present and Future, In Proc. of Workshop on *Glaciers, Ice Sheets, and Sea Level: Effects of a CO_2-Induced Climatic Changes*, Seattle, Washington, pp.258-266.

Bindschadler, R.,1982, A Numerical Model of Temperate Glacier Flow Applied to the Quiescent Phase of a Surge-type Glacier, J. of Glaciol., Vol. 28, 239-65.

Bindschadler, R.A. and Gore, R.,1982, A Time-Dependent Ice sheet Model: Preliminary Results, J. of Geophys. Res., Vol. 87, 9675-85.

Bindschadler, R.a., 1978, A Time-Dependent Model of Temperate Glacier Flow and its Application to Predict Changes in the Surge-Type Varegated Glacier During its Quiescent Phase, Unpublished Ph.D Thesis, University of Washington, Seattle, U.S.A.

Bjorkstrom, A., 1983, Modelling the Oceanic CO_2 Uptake and Future CO_2 Levels, In *Carbon Dioxide: Current Views and Developments in Energy/ Climate Research*, Edited by Bach, W., Crane, A.J., Berger, A.L., Longhetto, A., D. Reidel Publishing Company, Dordrecht, Holland, pp.57-92.

Blachnitzky, K., 1987, Report on the Geodetic Activities During the 1987 JIRP Campaign, Geodetic Institute, University of the Bundeswehr, Neubiberg, F.R.G.

Boulton, G.S. and Jones, A.S., 1979, Stability of Temperate Ice Caps and Ice Sheets Resting on Beds of Deformable Sediment, J. Glaciol., Vol. 24, pp.29-43.

Bryan, K. and Manabe, S., 1985, A Coupled Ocean-Atmosphere and the Response to Increasing Atmospheric CO_2, *Coupled Ocean-Atmosphere Models*, Edited by Nihoul, J.C.J, Elsevier Science Publisher, Amsterdam, the Netherlands, pp.1-6.

Budd, W.F., McInnes, B.J., Jenssen, D. and Smith, D., 1987, Modelling the Response of the West Antarctic Ice Sheet to a Climatic Warming, In *Dynamics of the West Antarctic Ice Sheet*, Edited by van der Veen, C.J. and Oerlemans, J., D. Reidel Publishing Company, Dordrecht, Holland, pp.321-58.

Budd, W.F., Jenssen, D. and Smith, I.N.,1984, A Three-Dimensional Time-Dependent Model of the West Antarctic Ice Sheet, Ann.of Glaciol., Vol. 5, pp.42-49.

Budd, W.F. and Smith, I.N.,1982, Large-Scale Numerical Modelling of the Antarctic Ice Sheet, Ann. of Glaciol., Vol. 3, pp. 42-49.

Budd, W.F., Keage, P.L. and Blundy, N.A.,1979, Empirical Studies of Ice Sliding, J. of Glaciol., Vol. 23, pp. 157-69.

Budd, W.F. and Carter, D.B.,1971, An Analysis of the Relationship Between the Surface and Bed profiles of Ice Caps, J. of Glaciol., Vol. 10, pp. 197-209.

Budd, W.F.,1970a, The Longitudinal Stress and Strain-Rate Gradients in Ice Masses, J. of Glaciol., Vol. 9, pp. 19-27.

Budd, W.F., 1970b, Ice Flow Over Bed rock Perturbations, J. of Glaciol., Vol. 9, pp. 29-47.

Budd, W.F.,1968, The Longitudinal Velocity Profile of Large Ice Mass, IAHS, Publ. No. 79, pp.58-75.

Campbell, W.J. and Rasmussen, L.A.,1969, Three-Dimensional Surges and Recoveries in a Numerical Model, Canadian J. of Earth Sci., Vol. 6, pp. 679-86.

Carlson, R.C., 1987, Seismic and Gravimmetric Depth Measurements on the Taku Glacier, Alaska, Juneau Icefield Research Program, Res. Rept. 127.

Colbeck, S.C. and Evans, R.J.,1973, A Flow Law for Temperate Glacier Ice, J. of Glaciol., Vol. 12, pp. 71-83.

Colbeck, S.C. and Evans, R.J.,1973, A Flow Law for Temperate Glacier Ice, J. of Glaciol., Vol. 12, pp.71-83.

Cooper, C.K. and Pearce, B.R, 1977, Development of a Simple Numerical Model to Calculate the 3-D Structure of Currents in Coastal Areas Using a Depth Varying Eddy Viscosity, Proc. of IAHR, Vol. 2, pp.141-48.

Cushman-Roisin, B.,1984, Analytical, Linear Stability Criteria for the Leap-Frog, Dufort-Frankel Method, J. of Comp. Phys., Vol.53, pp. 227-39.

Doake, C.S.M. and Wolff, E.W.,1985, Flow Law for Ice in Polar Ice Sheets, Nature, Vol. 314, pp. 255-57.

Fastook, J.L, 1987, The Finite-Element Method Applied to a Time-Dependent Flowband Model, In *Dynamics of the West Antarctic Ice Sheet*, Edited by van der Veen, C.J. and Oerlemans, J., D. Reidel Publishing Company, Dordrecht, Holland, pp.203-21.

Fastook, J.L.,1984, West Antarctic, The Sea-Level Controlled Marine Instability: Past and Future, In *Climate Processes and Climate Sensitivity*, Geophysics Monograph 29, Edited by Hansen, J.E. and Takahashi, T., American Geophysical Union, Washington, D.C., pp.275-87.

Fowler, A.C.,1982, Waves in Glaciers, J. of Fluid Mech.,Vol. 120, pp. 283-321.

French, R.H.,1985, *Open-channel Hydraulics*, McGraw-Hill Book Company, N.Y., U.S.A.

Gill,A.E.,1982, *Atmosphere-Ocean Dynamics*, Academy Press, N.Y., U.S.A.

Gilliland, R.L. and Schneider, S.H.,1984, Volcanic, CO_2 and Solar Forcing of Northern and Southern Hemisphere Surface Air Temperatures, Nature, Vol. 319, pp.39-41.

Hansen, J. et al.,1981, Climatic Impact of Increasing Atmospheric Carbon Dioxide, Vol. 213, Science, pp.957-66.

Hodge, S.M.,1985, Two-Dimensional, Time-Dependent Modeling of an Arbitrary Shaped Ice Mass With the Finite-Element Technique, J. of Glaciol., 31.

Hoffert, M.I. and Michael, P.A.,1983, Increasing Carbon Dioxide Concentrations and Climate: The Transient Response, In *Carbon Dioxide: Current Views and Developments in Energy/ Climate Research*, Edited by Bach, W., Crane, A.J., Berger, A.L., Longhetto, A., D. Reidel Publishing Company, Dordrecht, Holland, pp.259-79.

Holton, J.R.,1979, *An Introduction to Dynamic Meteorology*, Academic Press, London, U.K.

Hughes, T.,1987, Ice Dynamics and Deglaciation Model When Ice Sheet Collapsed, Ruddiman, W.F. and Wright, H.E., Jr. Eds. *North America and Adjacent Oceans During the Last Deglaciation*, Vol.K-3, Geological Society of America, Boulder Colorado, 183-220.

Hughes, T., 1981, Numerical Reconstruction of Paleo Ice Sheets, In *The Last Great Ice Sheets*, Edited by Denton, G.H and Hughes, T., Wiley-Interscience, New York, U.S..A., pp.221-61.

Hutter,K.,1983, *Theoretical Glaciology*, D. Reidel Publishing Company, Dordrecht, Holland.

Kandel, R.S.,1983, Simple Climate Model and the Greenhouse Effects, In *Carbon Dioxide: Current Views and Developments in Energy/ Climate Research*, Edited by Bach, W., Crane, A.J., Berger, A.L., Longhetto, A., D. Reidel Publishing Company, Dordrecht, Holland, pp.179-218.

Kamb, W.B.,1970, Sliding Motion of Glaciers: Theory and Observation, Rev. in Geophys. and Space Phys., Vol. 8, pp. 673-728.

Kamb, W.B., 1970, Sliding Motion of Glaciers: Theory and Observation, Rev. in Geophys. and Space Phys., Vol. 8, p.673-728.

Kersting, N., 1987, Determination of the Taku Glacier Movement Juneau Ice Field, Alaska, 1986, Geodetic Institute, University of the Bundeswehr, Neubiberg, F.R.G.

Kuhn, M., 1985, Reaction of Mid-Latitude Glacier Mass Balance to Predicted Climatic Changes, In Proc. of Workshop on *Glaciers, Ice Sheets, and Sea Level: Effects of a CO_2-Induced Climatic Changes*, Seattle, Washington, pp.248-254.

Kuhn, M.,1980, Climate and Glaciers, In Proc. of Symp. on *Sea Level, Ice and Climatic Changes*, IAHS Publ. No. 131, pp.3-20.

Kuhn, M.,1979, On the Computation of Heat Transfer Coefficients From Energy-Balance Gradients on a Glacier, J. of Glaciol., Vol.22, pp.263-272.

LaChapell, E.R., 1957, Snow Studies of the Juneau Icefield, Juneau Icefiled Research Program, Rept. 9, American Geophysical Society, N.Y., U.S.A.

Llibourty, L.,1987, Realistic, Yet Simple Bottom Boundary Conditions for Glaciers and Ice Sheets, J. of Geophys. Res., Vol. 92, pp. 9101-9.

Lorius, C. and Raynaud, D.,1983, Record of Past Atmospheric CO_2 from Tree-Ring and Ice Core Studies, In *Carbon Dioxide: Current Views and Developments in Energy/ Climate Research*, Edited by Bach, W., Crane, A.J., Berger, A.L., Longhetto, A., D. Reidel Publishing Company, Dordrecht, Holland, pp.145- 76.

Mahaffy, M.W.,1975, A Three-Dimensional Numerical Model of Ice Sheets: Tests on the Barnes Ice Cap, Northwest Territories, J. of Geophys. Res., Vol. 81, pp. 1059-66.

Manabe, S. and Stouffer, R.J.,1980, Sensitivity of a Global Climatic Model to an Increase of CO_2 Concentration in the Atmosphere, J. of Geophy. Res., Vol. 85, pp. 5529-54.

Mayo, L.R.,1986, Annual Runoff Rate From Glaciers in Alaska: A Model Using the Altitude of Glacier Mass Balance Equilibrium, In Proc. of Symp. on *Cold Region Hydrology*, AWRS , Bethesda, Maryland, pp.509-17.

Mayo, L.R. and Trabant, D.C.,1984, Observed and Predicted Effects of Climate Change on Wolverine Glacier, Southern Alaska, In Proc. of *The Potential Effects of Carbon Dioxide-Induced Climatic Changes in Alaska*, University of Alaska, Fairbanks, pp.114-123.

Meier, M.F., 1987, Ice-Sheet Models- an Overview, *The Physical Basis of Ice Sheet Modelling*, IASH Publ. No. 170, pp.1-4.

Meier, F.M.,1985, Mass Balance of the Glaciers and Small Ice Caps of the World, In Proc. of Workshop on *Glaciers, Ice Sheets, and Sea Level: Effects of a CO_2-Induced Climatic Changes*, Seattle, Washington, pp.139-144.

Meier, F.M.,1984, Contribution of Small Glaciers to Global Sea Level, Science, Vol. 266, pp.1418-21.

Meier, F.M.,1983, Snow and Ice in a Changing Hydrological World, Hyd.Sci. J., Vol.28, pp.3-21.

Miller, M.M.,1988, Private Communications.

Miller, M.M.,1975, Mountain and Glacier Terrain Study and Related Investigations in the Juneau Icefield Region, Alaska-Canada, Foundation for Glacier and Environmental Research, Seattle, Washington, U.S.A.

Miller, M.M.,1963, The Taku Glacier Evaluation Study, Foundation of Glacier Research, Department of Highways, Alaska, U.S.A.

Miller, M.M and Field, W.O., 1951, Studies of the Taku Glacier, Alaska, Geological Notes, J. of Geol., Vol. 59, p.622-23.

Morris, E.M.,1989, Turbulent Transfer Over Snow and Ice, J. of Hydr., Vol. 105, pp.205-23.

National Research Council, 1983, Snow and Ice Research: An Assessment, National Academy Press, Washington, D.C., U.S.A.

Neilson, L.E., 1957, Preliminary Study on the Regimen and Movement of the Taku Glacier, Alaska, Bulletin of the Geological Society of America, Vol. 68, No. 2, pp.171-80.

Nye, J.F., 1970, Glacier Sliding Without Cavitation in a Linear Viscous Approximation, Poc. Royal Soc. of London, Ser. A, Vol. 239, pp.381-402.

Nye, J.F.,1965, The Flow of a Glacier in a Channel of Rectangular, Elliptic and Parabolic Cross-Section, J. of Glaciol., Vol. 5, pp. 661-90.

Nye, J.F.,1963, The Response of a Glacier to Changes in the rate of Nourishment and Wastage, Proc. R. Soc. London, Ser. A, Vol. 275, pp. 87-112.

Nye, J.F., 1960, The Response of Glaciers and Ice Sheets to Seasonal and Climatic Changes, Proc. R. Soc. of London, Ser. A, Vol. 257, pp. 559-83.

Nye, J.F.,1959, The Motion of Ice Sheets and Glaciers, J.. of Glaciol., Vol 3, pp. 493-507.

Oerlemans, J.,1988, Simulation of Historic Glacier Variations With a Simple Climatic-Glacier Model, J. of Glaciol., Vol. 34, pp.333-41.

Oerlemans, J.,1986, Glaciers as Indicators of a Carbon Dioxide Warming, Nature, Vol. 320, pp. 607-09.

Oerlemans, J. and van der Veen, C.J.,1984, *Ice Sheets and Climate*, D. Reidel Publishing Company, Dordrecht, Holland.

Paterson, W.S.B, 1980, *The Physics of Glaciers*, Pergamon Press, N.Y., U.S.A.

Paterson, W.S.B,1972, Laurentide Ice Sheet: Estimated Volumes During Late Wisconsin, Rev. Geophys. and Space Phys., Vol. 10, pp.885-917.

Pearce, B.R. and Cooper, C.K.,1981, Numerical Circulation Model for Wind Induced Flow, J. of Hyd. Div., ASCE, 107, HY3, pp. 285-302.

Pearce, B., Cooper, C. and Nelson, S.,1978, GAL: A 3-Dimensional Numerical Model to Calculate Currents With a Depth Varying Vertical Eddy Viscosity, Tech. Rept., Department of Civil Engr., Univ. of Maine, Orono, U.S.A.

Pelto, M.S.,1989, Private Communication.

Pelto, M.S. and Miller, M.M.,1988, Mass Balance of the Taku Glacier, Alaska From 1946 to 1985, Northwest Science.

Pelto, M.S.,1987, Mass Balance of Southeast Alaska and Northwest British Columbia Glacier from 1976-1984: Methods and Results, Ann. of Glaciol., Vol. 9, pp.111-17.

Ramanathan, V., 1981, The Role of Ocean-Atmosphere Interactions in the CO_2 Climate Problem, J. of Atmosph. Sci., Vol. 38, pp.918-930.

Rasmussen, L.A. and Campbell , W.J.,1973, Comparison of Three Flow Contemporary Flow Laws in a Three-Dimensional, Time-Dependent Glacier Model, J. of Glaciol., Vol. 12, pp.361-73.

Raymond, C.F. and Harrison, W.D.,1988, Evolution of Varigated Glacier, Alaska, U.S.A., Prior to its Surge, J. of Glaciol., Vol. 34, pp. 154-69.

Raymond, C.F. and Harrison, W.D.,1987, Fit of Ice Motion Model to Observations from Variegated Glacier, Alaska, IAHS Publ. No. 170, pp. 153-66.

Schlessinger, M.E., 1984, Climate Model Simulations of CO2-induced Climatic Change, Edited by Saltzman, B., *Advances in Geophysics*, Vol. 26, Academic Press, New York, U.S.A, pp.141-235.

Smith, G.D.,1978, *Numerical Solution of Partial Differential Equations: Finite Difference Methods*, Oxford University Press, Oxford, U.K.

Sucsy, P. and Pearce, B.,1986, TIDE: A Three-dimensional Hydrodynamic Model, Tech. Rept. Department of Civil Engr., Univ. fo Maine, Orono, U.S.A.

van der Veen, C.J., 1987, Longitudinal Stresses and Basal Sliding: A Comparative Study, *Dynamics of the West Antarctic Ice Sheet*, Edited by van der Veen,

C.J. and Oerlemans, J., D. Reidel Publishing Company, Dordrecht, Holland, pp.223-48.

Wallen, C-C.,1983, Monitoring the Atmospheric CO_2 Concentration, In *Carbon Dioxide: Current Views and Developments in Energy/ Climate Research*, Edited by Bach, W., Crane, A.J., Berger, A.L., Longhetto, A., D. Reidel Publishing Company, Dordrecht, Holland, pp.3-29.

White, F.M.,1973, *Viscous Fluid Flow*, McGraw Hill, Inc., N.Y., U.S.A.

Weertman, J., 1985, Unsolved Problems of Creep, Nature, Vol. 314, pp.227.

Weertman, J., 1983, Creep Deformation of Ice Sheet, Annual Rev. of Earth and Planetary Sci., Vol. 11, p.215-240.

Weertman, J.,9161, Equilibrium Profile of Ice Caps, J. of Glaciol, Vol. 3, pp. 953-64.

Wolff, E.W. and Doake, C.S.M.,1986, Implications of the Form of the Flow Law for Vertical Velocity and Age-Depth Profiles in Polar Ice, J. of Glaciol., Vol.32, pp.366-70.

World Meteorological Organization, 1985, Atmospheric Ozone 1985, *Global Ozone Research and Monitoring Project* Rept. No. 16, Geneva, Switzerland.